

**Phosphoinositides modulate auxin-dependent transcription
by controlling the histone acetyltransferase GCN5
in Arabidopsis**

Dissertation

zur Erlangung des
Doktorgrades der Naturwissenschaften
(Dr. rer. nat.)

der
Naturwissenschaftlichen Fakultät I
– Biowissenschaften –

der Martin-Luther-Universität
Halle-Wittenberg,

vorgelegt von
Frau Franziska Daamen

geb. am 16. Oktober 1992
in Kleve

Gutachter: Prof. Dr. Ingo Heilmann
Prof. Dr. Klaus Humbeck
Prof. Dr. Wolfgang Dröge-Laser

Die vorliegende Dissertation wurde unter Anleitung von Dr. Mareike Heilmann in der Abteilung für Pflanzenbiochemie (Prof. Dr. Ingo Heilmann, Martin-Luther-Universität Halle-Wittenberg) angefertigt.

Eingereicht am: 25.08.2021
Tag der Verteidigung: 23.02.2022

Table of Contents

Abbreviations	VII
Summary / Zusammenfassung	XII
1. Introduction.....	1
1.1. The plant PI system.....	1
1.2. Enzymes of PI biosynthesis	2
1.3. Physiological functions of PtdIns3P and VPS34.....	5
1.4. Physiological functions of PtdIns(4,5)P ₂ and PI4P 5-kinases	6
1.5. Evidence for physiological functions of nuclear PIs	10
1.6. Histone modification and the control of gene activation	11
1.7. The histone acetyltransferase GCN5.....	14
1.8. Physiological roles of GCN5 in phytohormone signaling and the control of growth .	17
1.9. Aims of this thesis	20
2. Results	21
2.1. Histone H3 acetylation is influenced in Arabidopsis by expression level of the intrinsic PI4P 5-kinases PIP5K1 and PIP5K2.....	21
2.2. PIP5K1 and PIP5K2 interact with the histone acetyltransferase GCN5	23
2.2.1. Arabidopsis PIP5K1 and PIP5K2 and GCN5 interact with ING1 and ING2.....	26
2.3. Overexpression of PIP5K1 or PIP5K2 attenuates GCN5-dependent activation of the <i>GH3.3</i> gene	27
2.4. PtdIns(4,5)P ₂ and other PIs inhibit histone acetyltransferase activity of recombinant GCN5 protein <i>in vitro</i>	32
2.5. Recombinant MBP-GCN5 protein binds PIs	37
2.5.1. Identification of the putative lipid binding site in GCN5	40
2.6. PI 3-kinase VPS34 has no impact on the GCN5-dependent activation of <i>GH3.3</i>	44
2.7. PI binding contributes to nuclear localization of GCN5	49
3. Discussion	53
3.1. PI4P 5-kinases interact with GCN5 and putative components of the histone acetylation machinery.....	54
3.2. PIP5K2 activity markedly affects auxin-induced <i>GH3.3</i> transcription.....	55
3.3. Inhibition of GCN5 and lipid binding	57
3.4. Possible modes of GCN5 inhibition by PIs.....	58
3.5. PI binding contributes to nuclear localization of GCN5	59
4. Material and Methods.....	62
4.1. Equipment and devices	62
4.2. Chemicals.....	62
4.2.1. Antibiotics used for the selection of bacteria.....	62
4.2.2. Phospholipids	62

4.3. Consumables and Kits.....	62
4.4. Enzymes, proteins, peptides and molecular size markers	62
4.5. Microorganisms.....	62
4.6. Plants	63
4.7. Culture media	63
4.7.1. Media for <i>E. coli</i>	63
4.7.2. Media for yeast	64
4.7.3. Plant medium.....	64
4.8. Growth conditions	65
4.8.1. Growth conditions for Arabidopsis plants.....	65
4.8.2. Maintenance of yeast strain NMY51.....	65
4.9. Vectors used in this study	65
4.9.1. Vectors for recombinant protein expression in <i>E. coli</i>	65
4.9.2. Vectors for yeast-two-hybrid studies	66
4.9.3. Vectors for transient protein expression in Arabidopsis protoplasts	66
4.10. Molecular biology methods	67
4.10.1. DNA isolation.....	67
4.10.2. RNA isolation.....	67
4.10.3. cDNA synthesis	68
4.11. Separation of DNA and RNA in agarose gels.....	68
4.11.1. Extraction of DNA from gels	68
4.12. PCR strategies.....	69
4.12.1. Genotyping of Arabidopsis plants.....	69
4.12.2. Quantitative real-time RT PCR (qPCR)	69
4.12.3. Amplification of DNA fragments by PCR.....	69
4.12.4. Introduction of amino acid substitutions: fusion PCR.....	70
4.13. Restriction.....	70
4.14. Ligation.....	71
4.15. Amplification of plasmid- and vector DNA in <i>E. coli</i>	71
4.15.1. Preparation of chemo-competent <i>E. coli</i>	71
4.15.2. Transformation of chemo-competent <i>E. coli</i>	71
4.15.3. Plasmid isolation from <i>E. coli</i>	72
4.16. Sequencing.....	72
4.17. Cloning strategies	72
4.17.1. Constructs for recombinant protein expression.....	72
4.17.2. Constructs for split-ubiquitin-based yeast-two-hybrid	73
4.17.3. Constructs for transformation of Arabidopsis protoplasts.....	74
4.18. Recombinant expression and enrichment of fusion proteins	75

4.18.1. Recombinant expression of fusion proteins in <i>E. coli</i>	75
4.18.2. Lysis of cells expressing recombinant fusion proteins	75
4.18.3. Enrichment of recombinant fusion proteins	76
4.18.4. Determination of protein concentrations via Bradford assay	76
4.19. Sodium dodecyl sulfate polyacrylamide gel electrophoresis (SDS-PAGE).....	76
4.20. Immunodetection of proteins (Western blotting)	77
4.20.1. Characterization of antibody specificity	78
4.21. Examining protein secondary structure using circular dichroism (CD) spectroscopy.....	78
4.22. Studies of protein-protein interactions	79
4.22.1. Split-ubiquitin-based yeast-two-hybrid (YTH).....	79
4.22.1.1. Preparation of chemo-competent <i>S. cerevisiae</i> cells	79
4.22.1.2. Transformation of chemo-competent <i>S. cerevisiae</i> NMY51 cells	80
4.22.1.3. Analysis of protein-protein interactions by yeast-two-hybrid tests.....	80
4.22.2. Analysis of protein-protein interactions by <i>in vitro</i> immuno pull-down assays ..	80
4.22.3. Analysis of protein-protein interactions by dot-blot analyses.....	81
4.23. Analysis of protein-lipid interactions	81
4.23.1. Lipid overlay assay	82
4.23.2. Liposome sedimentation assay.....	82
4.24. Histone acetyltransferase assay	83
4.25. <i>In vitro</i> lipid kinase activity assay with VPS34.....	84
4.26. Isolation and transformation of Arabidopsis leaf protoplasts	84
4.26.1. Auxin treatment of Arabidopsis leaf protoplasts	86
4.26.2. Treatment of Arabidopsis leaf protoplasts with a proteasome inhibitor	86
4.27. Microscopy	86
4.28. Isolation of nuclei and histones	87
4.28.1. Isolation of nuclei for histone analysis	87
4.28.2. Isolation of histones using a histone extraction kit.....	87
4.29. Computer-based analyses: software and online tools	88
4.29.1. Prediction of protein domains	88
4.29.2. Identification of basic hydrophobic stretches in protein sequences	88
4.29.3. Identification of putative NLS sequences.....	88
4.30. Statistics and data management	89
5. Literature	XIV
6. Appendix	XXIX
6.1. Additional information to the obtained results.....	XXIX
6.2. Additional information to Material and Methods.....	XLVII
6.2.1. Specification of equipment and devices	XLVII

6.2.2.	Specification of chemicals	XLVIII
6.2.3.	Used consumables and kits.....	L
6.2.4.	Used enzymes, proteins, peptides and molecular size markers.....	LII
6.2.5.	Oligonucleotides used in this thesis	LIII
6.2.6.	Cell lysates and enriched protein fractions	LX
6.2.7.	Composition of self-cast polyacrylamide gels	LXIII
6.2.8.	Primary and secondary antibodies	LXIV
6.2.9.	Specification of software and online tools.....	LXV
Figures	LXVIII
Tables	LXX
Acknowledgements / Danksagung	LXXI
Curriculum Vitae.....	LXXIII
Erklärung.....	LXXIV

Abbreviations

3-AT	3-amino-1,2,4-triazole
aa	amino acid
acetyl-CoA	acetyl coenzyme A
ADA2A	homolog of yeast ADA2, transcriptional adaptor
ADA2B	homolog of yeast ADA2, transcriptional adaptor
Alg5	dolichyl-phosphate beta-glucosyltransferase
AP	alkaline phosphatase
APS	ammonium persulfate
Arabidopsis	<i>Arabidopsis thaliana</i>
ARF	auxin response transcription factor
ATP	adenosine triphosphate
<i>A. tumefaciens</i>	<i>Agrobacterium tumefaciens</i>
AU	arbitrary units
AuxRE	auxin-responsive element
BCIP	5-bromo-4-chloro-3-indolyl phosphate disodium salt
BD	bromodomain (of GCN5)
BH	basic-hydrophobic
bp	DNA base pairs
BSA	bovine serum albumin, Albumin fraction V
bZIP	transcription factor of the basic leucine zipper family
C2	calcium-dependent lipid binding domain
CBP	p300/CREB-binding protein
CD	circular dichroism
cDNA	copy DNA
Col-0	<i>Arabidopsis</i> wild type, ecotype Columbia-0
CTAB	cetyltrimethylammonium bromide
Cub	C-terminal part of ubiquitin, aa 34 – 76
DMSO	dimethyl sulfoxide
DNA	deoxyribonucleic acid
DsRed	red fluorescent protein from <i>Discosoma sp.</i>
DTT	1,4-dithiothreitol
DUB	deubiquitination
<i>E. coli</i>	<i>Escherichia coli</i>
EDTA	ethylenediaminetetraacetic acid
ER	endoplasmic reticulum

EYFP	enhanced yellow fluorescent protein
Fib	fibrillarin
Fig.	figure
<i>g</i>	gravitational force equivalent
GCN5	general control non-repressible 5
GCN5 ^{EDD}	GCN5 _{R260E,K261D,K263D}
GCN5 ^{ILL}	GCN5 _{R260I,K261L,K263L}
GDI	guanidine nucleotide dissociation inhibitor
GFP	green fluorescent protein
GH3.3	auxin-responsive GH3 family protein, an auxin-conjugase
GNAT	GCN5-related N-terminal acetyltransferases
GRE	G-box-related element
GST	glutathione S-transferase
H3	histone H3
H3_Ct	histone H3 from calf thymus
H3Kac	histone H3, acetylated at lysine residues
H3K4me2	histone H3, dimethylated at lysine residue 4
H3K4me3	histone H3, trimethylated at lysine residue 4
H3K9	lysine residue 9 of histone H3
H3K9ac	histone H3, acetylated at lysine residue 9
H3K14	lysine residue 14 of histone H3
H3K14ac	histone H3, acetylated at lysine residue 14
HAM2	histone acetyltransferase of the MYST family 2
HAT	histone acetyltransferase (domain)
HDAC	histone deacetylase
HDAC6	histone deacetylase 6
HDAC19	histone deacetylase 19
HRP	horse radish peroxidase
HsH3.1	human histone H3.1
HsPIP5K1 α	human PI4P 5-kinase isoform PIP5K1 α
HsPIP5K2 α	human PI4P 5-kinase isoform PIP5K2 α
HsPIP5K2 β	human PI4P 5-kinase isoform PIP5K2 β
IAA2	indole-3-acetic acid inducible 2
IAA5	indole-3-acetic acid inducible 5
IAA19	indole-3-acetic acid inducible 19
ING1	inhibitor of growth 1
ING2	inhibitor of growth 2

IPTG	isopropyl β -D-1-thiogalactopyranoside
kb	kilo bases
kDa	kilo Dalton
LPA	lysophosphatidic acid
LPC	lysophosphocholine
-LW	without leucine and tryptophane
-LWH	without leucine, tryptophane and histidine
MBP	maltose-binding protein
mcs	multiple cloning site
MORN	membrane occupation and recognition nexus-repeat domain
MRW	mean residue weight
MS	Murashige & Skoog (medium)
MYST	MOZ, Ybf2/Sas3, Sas2 and Tip60-related
NAA	1-naphthaleneacetic acid
NBT	p-nitrotetrazolium blue chloride
NLI	nuclear lipid island
NLS	nuclear localization sequence
NuA4	nucleosome acetyltransferase of H4
Nub	N-terminal part of ubiquitin, aa 1 – 38
NubG	N-terminal part of ubiquitin, aa 1 – 38, I13 mutated to G
OCS	octopine synthase
OD ₆₀₀	absorbance at 600 nm
OE	overexpression
OsPIP5K1	PIP5K1/PIP5K2 homolog from rice
OST4	oligosaccharyltransferase 4
PCR	polymerase chain reaction
PH	Pleckstrin homology domain
PHD	plant homeodomain
PI	phosphoinositide
PI-kinase	phosphoinositide kinase
PI 3-kinase	phosphatidylinositol 3-kinase
PI 4-kinase	phosphatidylinositol 4-kinase
PI4K α	subfamily of phosphatidylinositol 4-kinases
PI4K β	subfamily of phosphatidylinositol 4-kinases
PI3P 5-kinase	phosphatidylinositol 3-phosphate 5-kinase
PI4P 5-kinase	phosphatidylinositol 4-phosphate 5-kinase
PIKK	PI 3-kinase-like kinase

PIN	pin-formed
PIP-kinase	phosphatidylinositol-monophosphate-kinase
PIP5K1	phosphatidylinositol 4-phosphate 5-kinase 1
PIP5K2	phosphatidylinositol 4-phosphate 5-kinase 2
PIP5K2 _{AAA}	PIP5K2 variant with inefficient nuclear import and reduced nuclear localization
PIP5K2 K470A	phosphatidylinositol 4-phosphate 5-kinase 2, K470 mutated to A
PIP5K3	phosphatidylinositol 4-phosphate 5-kinase 3
PIP5K4	phosphatidylinositol 4-phosphate 5-kinase 4
PIP5K5	phosphatidylinositol 4-phosphate 5-kinase 5
PIP5K6	phosphatidylinositol 4-phosphate 5-kinase 6
PIP5K7	phosphatidylinositol 4-phosphate 5-kinase 7
PIP5K8	phosphatidylinositol 4-phosphate 5-kinase 8
PIP5K9	phosphatidylinositol 4-phosphate 5-kinase 9
PIP5K10	phosphatidylinositol 4-phosphate 5-kinase 10
PIP5K11	phosphatidylinositol 4-phosphate 5-kinase 11
PEG	polyethylene glycol
PLT	PLETHORA transcription factor
PMSF	phenylmethylsulfonyl fluoride
Pol	polymerase
PtdCho	phosphatidylcholine
PtdEtn	phosphatidylethanolamine
PtdIns	phosphatidylinositol
PtdIns3P	phosphatidylinositol 3-phosphate
PtdIns4P	phosphatidylinositol 4-phosphate
PtdIns5P	phosphatidylinositol 5-phosphate
PtdIns(3,4)P ₂	phosphatidylinositol 3,4-bisphosphate
PtdIns(3,5)P ₂	phosphatidylinositol 3,5-bisphosphate
PtdIns(4,5)P ₂	phosphatidylinositol 4,5-bisphosphate
PtdIns(3,4,5)P ₃	phosphatidylinositol 3,4,5-trisphosphate
PtdOH	phosphatidic acid
PtdSer	phosphatidylserine
RAN-GTP	Ras-related GTPase
RCC1	regulator of chromosome condensation 1
RNA	ribonucleic acid
ROP	Rho of plants

qPCR	quantitative real-time RT PCR
rpm	revolutions per minute
rRNA	ribosomal RNA
RT	room temperature
S1P	sphingosine 1-phosphate
SAGA	Spt-Ada-GCN5-acetyltransferase-transcriptional co-activator
<i>S. cerevisiae</i>	<i>Saccharomyces cerevisiae</i>
ScGCN5	GCN5 homolog in <i>S. cerevisiae</i>
SD	standard deviation
SDG	SET domain group
SDS	sodium dodecyl sulfate
SDS-PAGE	sodium dodecyl sulfate polyacrylamide gel electrophoresis
SWC4	myb-like transcription factor family protein
Tab.	table
TAF1	TATA-binding protein-associated factor
T-DNA	transfer DNA of <i>A. tumefaciens</i>
TEMED	N,N,N',N'-tetramethyl-ethylenediamine
Ti	tumor-inducing
TRA1	transcription-associated protein 1
TLC	thin layer chromatography
TPL	TOPLESS
<i>UBC10</i>	<i>ubiquitin-conjugating enzyme 10</i> , a housekeeping gene
UBF	upstream binding factor
VPS34	vacuolar protein sorting 34
WOX	wuschel related homeobox transcription factor
WUS	WUSCHEL transcription factor
w/o	without
YTH	yeast-two-hybrid screen

Summary / Zusammenfassung

Phosphoinositides (PIs) occur in small amounts in eukaryotic membranes. The temporal and spatial distribution of PIs is regulated by PI-kinases. In plants, PIs are important regulators of cytoplasmic membrane trafficking and cytoskeleton. In addition to their functions in the cytoplasm, PIs are also found in the nucleus of plants, to date with unclear function. The phosphatidylinositol 4-phosphate 5-kinase (PI4P 5-kinase) PIP5K2 from *Arabidopsis* contains a functional nuclear localization sequence and shows dual localization in the nucleus and at the plasma membrane. Upon overexpression or underexpression of PIP5K2 and its sister enzyme PIP5K1, reduced and increased degrees of histone acetylation, respectively, were detected in adult *Arabidopsis* plants. Systematic interaction assays between PIP5K1 or PIP5K2 and histone-modifying enzymes revealed an interaction with the histone acetyltransferase general control non-repressible 5 (GCN5), known to regulate auxin-mediated gene activation. PIP5K1 and PIP5K2 further interact with histone H3 and the "epigenetic reader protein" inhibitor of growth (ING). Overexpression of PIP5K2, and to some extent PIP5K1, in protoplasts attenuated auxin-mediated activation of GCN5-dependent genes such as *GH3.3*, consistent with decreased histone acetylation. Overexpression of an inactive PIP5K2 K470A variant or the functionally divergent PIP5K6 isoform had no effect on gene regulation. In *in vitro* assays, PIs inhibited histone acetylation by recombinant GCN5 protein, indicating a direct effect of PIs on GCN5 function. Lipid binding studies confirmed that GCN5 binds to PIs, specifically phosphatidylinositol 3-phosphate (PtdIns3P), via basic amino acid residues. GCN5 interacted with the phosphatidylinositol 3-kinase VPS34, which is also localized in the nucleus. While expression of VPS34 did not affect GCN5-dependent gene activation, as shown for PIP5K2, PtdIns3P binding was required for nuclear localization of GCN5. Substitution variants of GCN5 (GCN5_{ILL} and GCN5_{EDD}) in which the potential PtdIns3P binding site was modified were no longer able to bind to PIs and showed significantly more cytosolic localization than wild type GCN5, which was almost exclusively detectable in the nucleus. Overall, the data suggest that GCN5 and ING, and possibly other components of histone acetylation, may be recruited by PtdIns3P to active transcription sites in the nucleus, as has previously been proposed. PI4P 5-kinases may remove PtdIns-monophosphates from this interaction and thus affect transcription. PIs such as PtdIns(4,5)P₂ could establish contact sites between chromatin with the inner nuclear membrane, which conditions the recruitment of additional protein components. Thus, nuclear PIs may influence auxin-dependent gene expression by modulating activity and recruitment of GCN5, in addition to and independent of the cytoplasmic influence of PIs on vectorial auxin transport.

Phosphoinositide (PIs) kommen in geringen Mengen in eukaryotischen Membranen vor. Die zeitliche und räumliche Verteilung von PIs wird durch PI-Kinasen reguliert. In Pflanzen sind PIs wichtige Regulatoren des zytoplasmatischen Membranverkehrs und des Zytoskeletts. Neben ihren Funktionen im Zytoplasma sind PIs auch im Zellkern von Pflanzen zu finden, allerdings mit bislang unklarer Funktion. Die Phosphatidylinositol 4-phosphat 5-Kinase PIP5K2 aus *Arabidopsis* enthält ein funktionales Kernlokalisierungssignal und zeigt duale Lokalisierung im Zellkern und an der Plasmamembran. Bei Über- oder Unterexpression von PIP5K2 und des Schwesterenzym PIP5K1 wurden in adulten *Arabidopsis*-Pflanzen reduzierte bzw. erhöhte Histon-Acetylierung detektiert. Systematische Interaktionstests zwischen PIP5K1 bzw. PIP5K2 und Histon-modifizierenden Enzymen zeigten eine Interaktion mit der Histon-Acetyltransferase *general control non-repressible 5* (GCN5), die unter anderem die Auxin-vermittelte Genaktivierung reguliert. PIP5K1 und PIP5K2 interagieren weiterhin mit Histon H3 und dem „epigenetischen Leseprotein“ *inhibitor of growth* (ING). Überexpression von PIP5K2, zum Teil auch von PIP5K1, in Protoplasten schwächte die Auxin-vermittelte Aktivierung GCN5-abhängiger Gene wie *GH3.3* ab, was mit verminderter Histon-Acetylierung konsistent ist. Überexpression einer inaktiven PIP5K2 K470A-Variante oder der funktional divergenten Isoform PIP5K6 hatten dabei keinen Einfluss auf die Genregulation. In *in vitro* Tests hemmten PIs die Histon-Acetylierung durch rekombinantes GCN5-Protein, was auf einen direkten Einfluss von PIs auf die GCN5-Funktion hinweist. Lipidbindestudien bestätigten, dass GCN5 über basische Aminosäurereste an PIs, speziell an Phosphatidylinositol 3-Phosphat (PtdIns3P), bindet. GCN5 interagiert mit der auch im Kern lokalisierten Phosphatidylinositol 3-Kinase VPS34. Die Expression von VPS34 beeinflusste die GCN5-abhängige Genaktivierung, wie für PIP5K2 gezeigt, nicht. Hingegen schien die PtdIns3P-Bindung für die nukleäre Lokalisierung von GCN5 erforderlich. Substitutionsvarianten von GCN5 (GCN5_{ILL} und GCN5_{EDD}), in denen die mögliche PtdIns3P-Bindestelle modifiziert wurde, konnten nicht mehr an PIs binden und zeigten deutlich mehr zytosolische Lokalisation als Wildtyp-GCN5, das fast ausschließlich im Zellkern zu detektieren war. Insgesamt weisen die Daten darauf hin, dass GCN5 und ING und möglicherweise auch weitere Komponenten der Histon-Acetylierung durch PtdIns3P an aktive Transkriptionsstellen im Zellkern rekrutiert werden könnten. PI4P 5-Kinasen entfernen möglicherweise PtdIns-monophosphate aus dieser Interaktion und beeinflussen so die Transkription. PIs wie PtdIns(4,5)P₂ könnten Kontaktstellen zwischen Chromatin und der inneren Kernmembran herstellen, was die Rekrutierung weiterer Proteinkomponenten bedingt. Nukleäre PIs können also die Auxin-abhängige Genexpression beeinflussen, indem sie Aktivität und Rekrutierung von GCN5 modulieren, und zwar zusätzlich und unabhängig vom zytoplasmatischen Einfluss von PIs auf den vektorialen Auxin-Transport.

1. Introduction

As sessile organisms, plants are inherently dependent on adapting to their environment. To this end, plants can respond to changing environmental conditions with altered development and growth. These reactions are regulated by complex signaling processes. External stimuli, but also signal transduction from cell to cell, are usually first perceived by receptors and transmitted to the interior of the cell. Signal transduction can be achieved by a variety of signaling pathways involving successive protein phosphorylation, phytohormone signaling or signaling lipids such as phosphoinositides (PIs). In most cases signal transduction events represent an interplay of different signaling cascades. Many signals are transmitted up to the nucleus where they lead to changes in gene expression so that physiological processes and functions in the cell can be adapted to the developmental or environmental requirements.

Nuclear-localized processes regulated by PIs are already known from animals (Yu et al., 1998; Zhao et al., 1998; Osborne et al., 2001; Irvine, 2003; Barlow et al., 2010), including DNA replication, modeling of chromatin structure and regulation of transcription factor localization. Since many processes of gene regulation and the structure of the nucleus are very similar in animals and plants, it was a key assumption of this thesis that PIs may also play a role in the regulation of nuclear-localized processes in plants.

1.1. The plant PI system

PIs are phospholipids in the membranes of eukaryotic cells (Heilmann, 2016a, 2016b) where they represent only a small fraction of membrane lipids and exert regulatory functions (Heilmann, 2009; Viaud et al., 2016; Gerth et al., 2017b; Colin and Jaillais, 2020; Jaillais and Ott, 2020). PIs are not uniformly distributed in membranes, but rather are organized in micro- or nanodomains where PIs can distinctively define membrane properties and initiate protein recruitment by mediating precise and local signaling (Ischebeck et al., 2008, 2011; Heilmann, 2016a; Gerth et al., 2017b; Fratini et al., 2021). In *Arabidopsis thaliana* (Arabidopsis), several phosphoinositide kinases (PI-kinases) can form different PIs by sequential phosphorylation of the inositol head group of phosphatidylinositol (PtdIns) (Mueller-Roeber and Pical, 2002; Boss and Im, 2012; Heilmann and Heilmann, 2015; Heilmann, 2016a, 2016b; Gerth et al., 2017b). The resulting PtdIns-monophosphates phosphatidylinositol 3-phosphate (PtdIns3P), phosphatidylinositol 4-phosphate (PtdIns4P), phosphatidylinositol 5-phosphate (PtdIns5P) and the PtdIns-bisphosphates phosphatidylinositol 3,5-bisphosphate (PtdIns(3,5)P₂) and phosphatidylinositol 4,5-bisphosphate (PtdIns(4,5)P₂) exert numerous regulatory effects on membrane-associated cytoplasmic processes in plants (Boss and Im, 2012; Heilmann and Heilmann, 2015; Heilmann, 2016a).

The formation of phosphatidylinositol 5-phosphate (PtdIns5P) remains unclear in plants (Heilmann and Heilmann, 2015). While PtdIns5P has been detected in plant material (Meijer et al., 2001), the enzymes leading to the formation of PtdIns5P have not yet been clearly identified. It is possible that PtdIns5P is not formed directly from PtdIns but is generated by dephosphorylation of the PtdIns-bisphosphates, PtdIns(3,5)P₂ or PtdIns(4,5)P₂. The biosynthesis of phosphatidylinositol 3,4-bisphosphate (PtdIns(3,4)P₂) and phosphatidylinositol 3,4,5-trisphosphate (PtdIns(3,4,5)P₃), which occur in mammalian cells, has not yet been demonstrated. Corresponding PI-kinases have not been identified in plants. (Mueller-Roeber and Pical, 2002; Heilmann, 2016a).

1.2. Enzymes of PI biosynthesis

The various PIs found in plants are synthesized by PI-kinases, some of them are represented by several isoforms. The numerous regulatory effects regulated by PIs and their subcellular distribution require a precise spatiotemporal distribution of PIs which is determined by the activities of PI-kinases (Heilmann and Heilmann, 2015; Gerth et al., 2017b). Synthesis of PIs begins with the structural lipid PtdIns. Phosphatidylinositol 3-kinase (PI 3-kinase) phosphorylates the D3 position of the inositol in PtdIns to form PtdIns3P. PI 3-kinase is represented only by a single gene in Arabidopsis. It is named after the well-characterized yeast PI 3-kinase homolog, which plays a role in vacuolar sorting and is therefore called vacuolar protein sorting 34 (VPS34, AT1G60490) (Schu et al., 1993; Welters et al., 1994; Dove et al., 1994; Heilmann and Heilmann, 2015) (Fig. 1.1 A). PI 3-kinases can be divided into three distinct classes according to their substrate specificity. Arabidopsis VPS34 is a class III enzyme using only PtdIns as substrate, whereas class I PI 3-kinases phosphorylate PtdIns4P and PtdIns(4,5)P₂. They play a central role in PI metabolism in mammals but have not yet been identified in plants (Vanhaesebroeck et al., 2001; Lee et al., 2010). Class II PI 3-kinases phosphorylate PtdIns and PtdIns4P (Vanhaesebroeck et al., 2001; Lee et al., 2010). PtdIns can alternatively be phosphorylated in the D4 position of the inositol by phosphatidylinositol 4-kinases (PI 4-kinases). The Arabidopsis genome encodes four isoforms of PI 4-kinases (Mueller-Roeber and Pical, 2002; Heilmann and Heilmann, 2015; Heilmann, 2016a), which can be divided into the subfamilies PI4K α and PI4K β , each with two members (Fig. 1.1 B).

The PtdIns-monophosphates can be further phosphorylated; PtdIns3P can be substrate for type III PtdIns-monophosphate-kinases (PIP-kinases), phosphatidylinositol 3-phosphate 5-kinases or also called PI3P 5-kinases (FAB1a – FAB1d, Fig. 1.1 C) (Mueller-Roeber and Pical, 2002; Meijer and Munnik, 2003; Heilmann and Heilmann, 2015; Heilmann, 2016a), giving rise to PtdIns(3,5)P₂. PtdIns4P can be phosphorylated to PtdIns(4,5)P₂ by eleven different isoforms of the type I PIP-kinases, phosphatidylinositol 4-phosphate 5-kinases (PI4P 5-kinases)

(Fig. 1.1 D) (Mueller-Roeber and Pical, 2002; Meijer and Munnik, 2003; Heilmann and Heilmann, 2015; Heilmann, 2016a). In addition, PI4P 5-kinases also have the ability to use PtdIns3P as a substrate and convert this substrate to PtdIns(3,5)P₂ (Stenzel et al., 2008; Ischebeck et al., 2008, 2011).

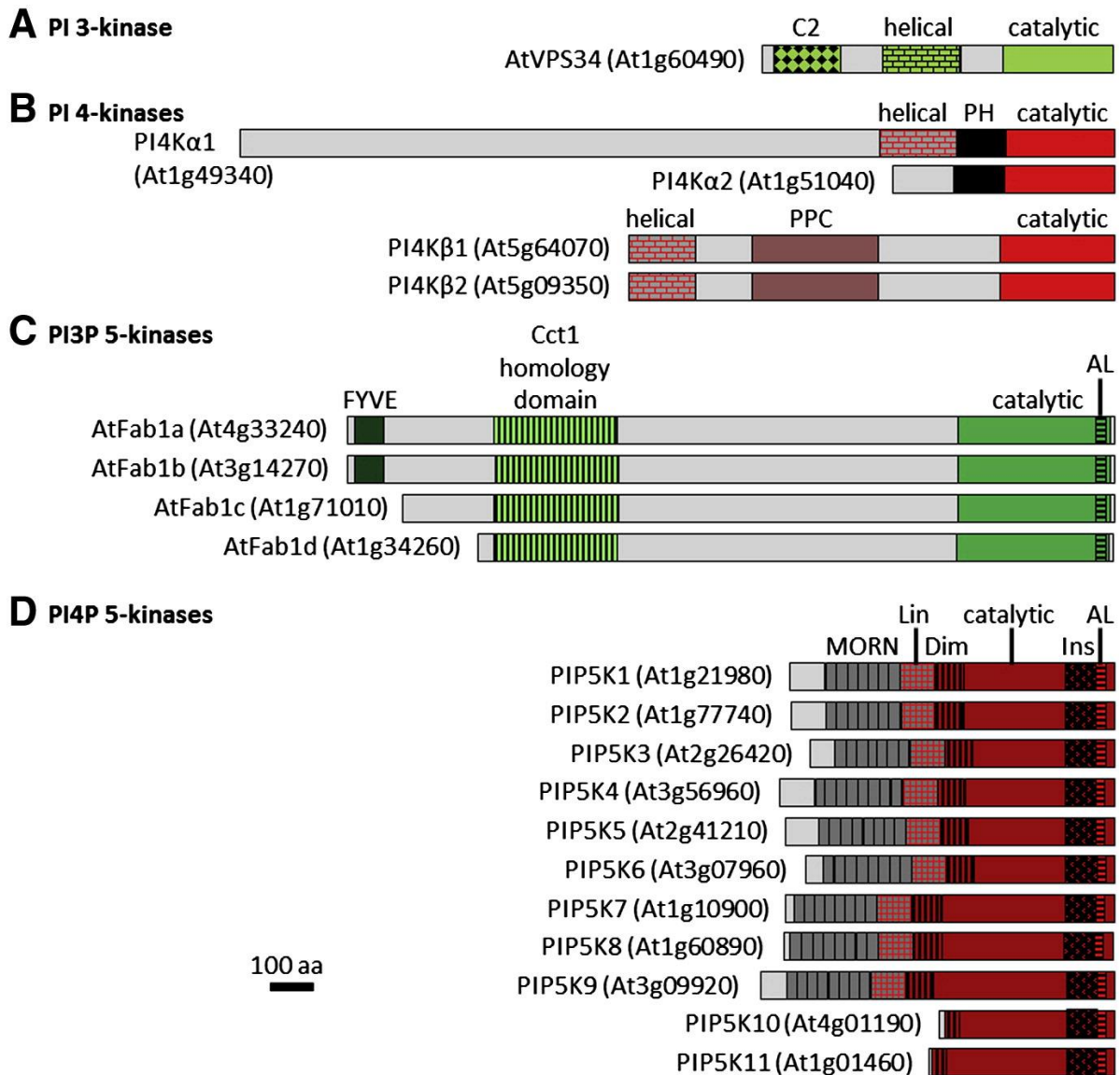


Fig. 1.1: Arabidopsis PI-kinases. The Arabidopsis genome encodes several PI-kinases. **A**, Class III PI 3-kinase, VPS34; encoded by a single gene in Arabidopsis. **B**, Four PI 4-kinase isoforms; two subfamilies consistent of the alpha subfamily PI4Kα1 and PI4Kα2 and the beta subfamily PI4Kβ1 and PI4Kβ2. **C**, Four isoforms of PI3P 5-kinases forming PtdIns(3,5)P₂. **D**, Eleven PI4P 5-kinase isoforms. The domain structure of the PI-kinases is depicted approximately to scale. The scale for 100 amino acids is indicated as well as the corresponding AGI locus identifiers for the corresponding genes. Domains with documented functions are indicated. Abbreviations stand for, AL, activation loop; C2, Ca²⁺-dependent lipid binding domain; catalytic, catalytic domain; Cct1 homology, chaperonine-containing t-complex protein 1-homology domain; Dim, dimerization domain; FYVE, Fab1 YOTB Vac1 EEA1-domain; helical, helical domain; Ins, variable insert domain; Lin, variable linker domain; MORN, membrane occupation and recognition nexus-repeat domain; PH, Pleckstrin homology-domain; PPC, plant PI4K charged region-domain. The figure was adopted from (Heilmann and Heilmann, 2015).

The Arabidopsis genome encodes eleven isoforms of PI4P 5-kinases (PIP5K1 – PIP5K11). Depending on their domain structure, PI4P 5-kinases can be categorized into subfamily A and subfamily B (Mueller-Roeber and Pical, 2002). Subfamily A includes PI4P 5-kinase isoforms PIP5K10 and PIP5K11 which consist of a dimerization domain and a catalytic domain. The latter domain contains a variable insert and an activation loop (Fig. 1.1 D) (Mueller-Roeber and Pical, 2002; Stenzel et al., 2012; Heilmann and Heilmann, 2015). These domains are conserved in their sequence between animals, yeasts, and plants (Mueller-Roeber and Pical, 2002; Stenzel et al., 2012). PI4P 5-kinase isoforms PIP5K1 to PIP5K9 belong to subfamily B and additionally contain a membrane occupation and recognition nexus (MORN)-repeat domain and a variable linker domain, positioned N-terminal of the dimerization domain and specific for plant PI4P 5-kinases (Fig. 1.1 D) (Mueller-Roeber and Pical, 2002; Stenzel et al., 2012; Heilmann and Heilmann, 2015). The linker domains are highly variable domains and differ greatly between the different PI4P-5 kinase isoforms. They contribute to the distinct subcellular localization and are most likely responsible for protein-protein interaction between the isoforms and further proteins (Stenzel et al., 2012; Gerth et al., 2017b; Fratini et al., 2021). The PIP5K1/PIP5K2/PIP5K3, PIP5K4/PIP5K5/PIP5K6 and PIP5K7/PIP5K8/PIP5K9 isoforms each form distinct phylogenetic clades within subfamily B (Mueller-Roeber and Pical, 2002; Stenzel et al., 2012). The members of the type A subfamily, PIP5K10 and PIP5K11, form a fourth and separate phylogenetic group.

The eleven PI4P 5-kinase isoenzymes differ markedly in their expression patterns and their functions. The isoforms PIP5K1 (AT1G21980), PIP5K2 (AT1G77740) (Ischebeck et al., 2013), PIP5K6 (AT3G07960) (Zhao et al., 2010; Heilmann, 2016a), PIP5K7 (AT1G10900), PIP5K8 (AT1G60890) and PIP5K9 (AT3G09920) (Heilmann, 2016a; Kuroda et al., 2021) are ubiquitously expressed. Besides those, there are isoforms, whose expression is restricted to pollen or pollen tubes, like PIP5K4 (AT3G56960), PIP5K5 (AT2G41210) (Ischebeck et al., 2008; Sousa et al., 2008; Heilmann, 2016a) and the two type A isoforms, PIP5K10 (AT4G01190) and PIP5K11 (AT1G01460) (Ischebeck et al., 2011; Heilmann, 2016a). The expression of isoform PIP5K3 (AT2G26420) is restricted to epidermal and cortical root cells and to root hairs (Kusano et al., 2008; Stenzel et al., 2008; Heilmann, 2016a). PI4P 5-kinase expression patterns are not only spatially divergent but also depend on developmental stage (Elge et al., 2001; Kusano et al., 2008; Stenzel et al., 2008; Ischebeck et al., 2008, 2013; Tejos et al., 2014; Kuroda et al., 2021) or are auxin-induced like the expression of PIP5K1 and PIP5K2 (Mei et al., 2012; Tejos et al., 2014). Together, the particular expression patterns of different PI4P 5-kinases enable a multifaceted and dynamic landscape of PtdIns(4,5)P₂ biosynthesis in plants.

Of all the enzymes mentioned, this study is mostly concerned with the elucidation of novel roles of PI 3-kinase and of PI4P 5-kinases in the nucleus. Therefore, the following paragraphs

provide an overview of what is known to date about the physiological effects of these enzymes and their reaction products, PtdIns3P and PtdIns(4,5)P₂, respectively.

1.3. Physiological functions of PtdIns3P and VPS34

Molecular genetic studies indicate that the functionality of PI 3-kinase is important for plant development, both in vegetative and reproductive organs (Welters et al., 1994). Studies using T-DNA insertion mutants have shown that the *vps34* mutant is impaired in pollen development and the homozygous T-DNA insertion is lethal (Lee et al., 2008). By down-regulating *VPS34* expression in Arabidopsis using antisense strategies, it was found that plants suffer from impaired leaf and stem development (Welters et al., 1994). The subcellular distribution of PtdIns3P was analyzed by genetically encoded biosensors. For this purpose, the biosensor 2xFYVE-GFP can be used, consisting of two FYVE domains (from Fab1, YOTB, Vac1 and EEA1) in tandem, which specifically bind PtdIns3P. Using this biosensor, PtdIns3P was detected in different Arabidopsis tissues primarily at the endomembranes (Gillooly et al., 2000; Simon et al., 2014). Consistent with this, PtdIns3P appears to play a role in different phases of vesicle transport, as salt stress in combination with inhibitors against PI 3-kinases reduced the internalization of FM4-64 dyes (Emans et al., 2002; Leshem et al., 2007). PI 3-kinase appears to be generally involved in vesicle transport and membrane biogenesis in plants (Lee et al., 2010; Simon et al., 2014). In addition, treatment of cells with wortmannin, which inhibits VPS34 among others, resulted in re-localization of pin-formed 2 (PIN2)-GFP to wortmannin-induced compartments, and PI 3-kinase may have a role in controlling the subcellular distribution of the auxin efflux carrier PIN2 (Jaillais et al., 2006).

Beside to cytoplasmic/endomembrane-localized functions, an alternative localization of VPS34 in the nucleus of plant cells was shown (Bunney et al., 2000). The observation at that time indicated that plant PI 3-kinase is involved in nuclear functions. Beside PtdIns4P, PtdIns3P was synthesized in fractions of isolated nuclei from carrot cell culture and soybean PI 3-kinase was detected at active sites of transcription by using a specific antiserum raised against a truncated variant of the PI 3-kinase (Bunney et al., 2000). Interestingly, the specific binding domain for PtdIns3P, the FYVE domain, is structurally very similar to the zinc finger domains, RING-like domains, and plant homeodomains (PHD). Zinc finger domains bind to DNA or RNA templates, and PHDs mediate binding to methylated histones. Furthermore, it is interesting to note that many FYVE domain-containing proteins in Arabidopsis also contain so-called tandem repeats of the regulator of chromosome condensation 1 (RCC1)-like domain (Burd and Emr, 1998; Misra and Hurley, 1999; van Leeuwen et al., 2004; Lee et al., 2010). RCC1 is present in mammalian cells and functions as a nuclear-localized Ras-related GTPase (RAN-GTP) exchange factor and, among other things, maintains the nuclear RAN-GTP gradient and is thereby also responsible for the disassembly of protein-nuclear import protein complexes

(Dasso, 2002). However, the FYVE/RCC1-domain-containing proteins identified in *Arabidopsis* are mostly not well-characterized or not characterized at all. Overall, the data available so far indicate a well-established role for VPS34 in cytoplasmic trafficking, and a much less well-understood alternative role in the plant nucleus.

1.4. Physiological functions of PtdIns(4,5)P₂ and PI4P 5-kinases

The most studied PI is PtdIns(4,5)P₂, formed by PI4P 5-kinases (Mueller-Roeber and Pical, 2002; Meijer and Munnik, 2003; Heilmann and Heilmann, 2015; Heilmann, 2016a). In several studies, PtdIns(4,5)P₂ has been shown to be involved in plant signal transduction, in the regulation of ion transport across the plasma membrane (Ma et al., 2009), in the control of cytoskeletal stability, protein recruitment to the plasma membrane, exocytosis and clathrin-mediated endocytosis (Fig. 1.2) (Ischebeck et al., 2008; Sousa et al., 2008; Zhao et al., 2010; Ischebeck et al., 2011; Mei et al., 2012; Ischebeck et al., 2013; Heilmann, 2016a; Fratini et al., 2021), and in vesicle transport between Golgi apparatus and plasma membrane (König et al., 2008; Camacho et al., 2009).

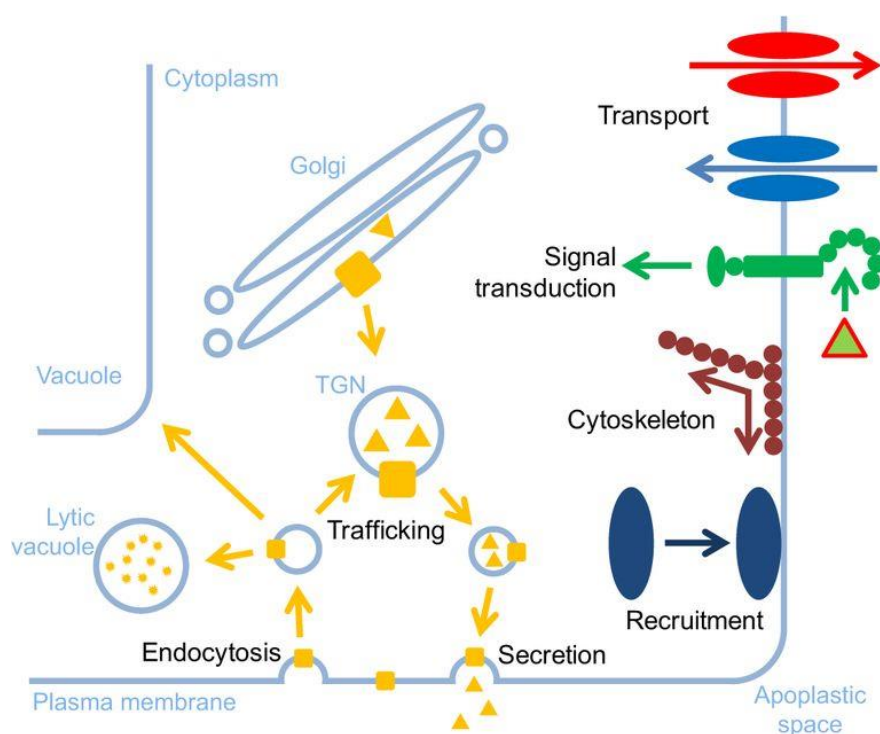


Fig. 1.2: PIs contribute to several plasma membrane-associated processes. PIs are involved in numerous plasma membrane-associated processes that take place in the cytosolic space, including vesicle trafficking, endocytosis, signal transduction, protein recruitment or cytoskeleton attachment. Figure from (Heilmann, 2016a).

By regulating these processes, PI4P-5 kinases and PtdIns(4,5)P₂ influence the polar orientation and thus the cell morphology of eukaryotic cells (Mei et al., 2012; Stenzel et al.,

2012; Ischebeck et al., 2013; Tejos et al., 2014). Polar tip growth of root hairs (Kusano et al., 2008; Vincent et al., 2005; Stenzel et al., 2008) or pollen tubes is affected by PI4P-5 kinases and PtdIns(4,5)P₂ (Kost et al., 1999; Ischebeck et al., 2008, 2011; Stenzel et al., 2012). Thus, different members of the PI4P 5-kinase subfamily B exert isoform-specific regulatory effects and therefore, when overexpressed in, e.g. tobacco pollen tubes, have different effects on phenotypes. Overexpression of either PIP5K4, PIP5K5 (Ischebeck et al., 2008; Sousa et al., 2008), and PIP5K6 (Zhao et al., 2010) affects vesicle/membrane trafficking and leads to branched pollen tubes, whereas expression of PIP5K2 in pollen tubes affects cytoskeleton stabilization and leads to a swelling phenotype in the corresponding cells (Stenzel et al., 2012). PI4P 5-kinases of the different phylogenetic groups, such as PIP5K2 and PIP5K6, have divergent regulatory functions and effects, although they form the same lipid product and localize very similarly at the subcellular level (Stenzel et al., 2012; Fratini et al., 2021). These observations indicate that the precise subcellular localization of PI4P 5-kinases determines a specific regulatory effect of PtdIns(4,5)P₂ formed.

A very well-studied example of the influence on cell polarity is the functionality of PIP5K1 and PIP5K2 PI4P 5-kinases from Arabidopsis. Both PI4P 5-kinases, PIP5K1 and PIP5K2, as well as their product PtdIns(4,5)P₂, showed polar localization in Arabidopsis root cells (Ischebeck et al., 2013; Tejos et al., 2014; Gerth et al., 2017a). Alterations in the amounts of PtdIns(4,5)P₂ produced at the plasma membrane by PIP5K1 and PIP5K2 in *pip5k1 pip5k2* double mutants resulted in decreased endocytosis and, consequently, mislocalization of the normally polar distributed auxin transport proteins PIN1 and PIN2, leading to impaired auxin distribution in these plants (Ischebeck et al., 2013). The data indicate that PI4P 5-kinases have numerous functions in the control of cytoplasmic processes and in the control of cell polarity. Interestingly, the transcription of *PIP5K1* and *PIP5K2* is by itself induced by exogenously applied auxin (Tejos et al., 2014), suggesting that PI4P 5-kinases are part of the complex regulatory networks mediating auxin-dependent effects in plants.

In addition to the well-described localization in the plasma membrane, fluorescently labeled fusions of PI-kinases were frequently observed in the nucleus of plant cells of different species and tissues (Lou et al., 2007; Ischebeck et al., 2011, 2013; Tejos et al., 2014). Moreover, PIP5K2 from Arabidopsis has been shown to interact with alpha-importins (Fig. 1.3 A) and contains a nuclear localization sequence (NLS) in the linker domain that is necessary and sufficient for active nuclear import of PIP5K2 (Gerth et al., 2017a). Replacement of the NLS in the PIP5K2 variant PIP5K2_{AAA} with alanines led to inefficient nuclear import and reduced nuclear observation of PIP5K2_{AAA} in onion epidermal cells (Fig. 1.3 B). Importantly, nuclear localization of PIP5K2 is found mainly in meristematic cells and is not observed at all times, suggesting that PIP5K2 shuttles between cytoplasm and nucleus (Gerth et al., 2017a). In addition to PIP5K2, the lipids PtdIns4P and PtdIns(4,5)P₂ have also been identified in plant

nuclei by biochemical analysis via specific antibodies in immunostainings (Gerth et al., 2017a), and by fluorescent reporters such as the Pleckstrin homology (PH) domain of PLC δ 1 fused to fluorescent proteins, which specifically binds PtdIns(4,5)P₂ (Mishkind et al., 2009). Furthermore, lipid analyses of isolated or enriched Arabidopsis organelles indicate that PIs are not only found in the membranes of plant nuclei, but also that nuclear PIs have a characteristic pattern of associated fatty acids (König et al., 2008).

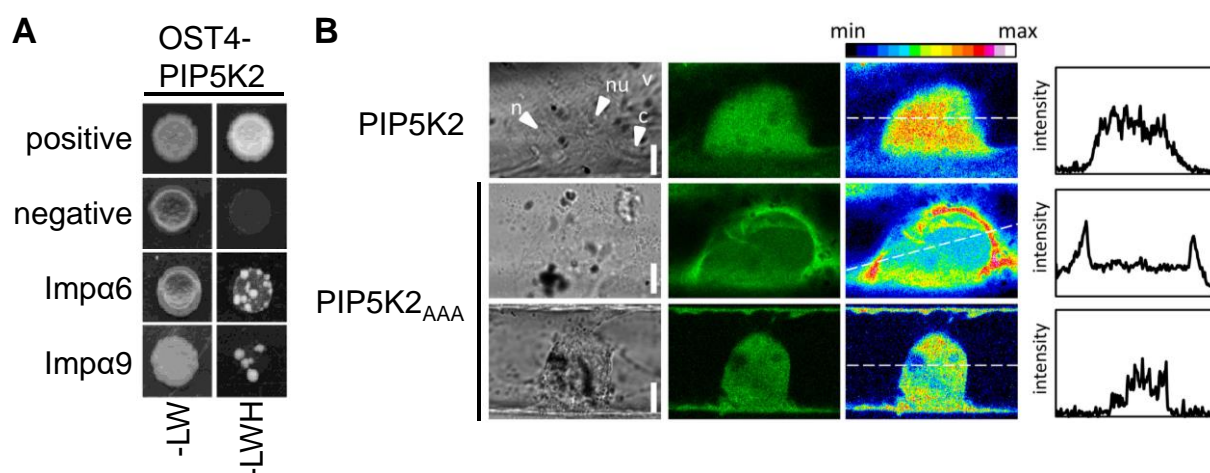


Fig. 1.3: Arabidopsis PIP5K2 interacts with the nuclear import machinery and contains a functional NLS. PIP5K2 was demonstrated to be actively transported to the plant nucleus. **A**, PIP5K2 interacts with alpha-importins Imp α 6 and Imp α 9 in an endoplasmic reticulum (ER)-localized split-ubiquitin-based yeast-two-hybrid (YTH). **B**, Replacement of the identified NLS in PIP5K2 sequence in the variant PIP5K2_{AAA} effects exclusion of the EYFP fusion protein from the nucleus in 31 % of examined onion epidermal cells. The figure was adopted and modified from (Gerth et al., 2017a).

The previously observed nuclear localization of PIP5K2 (Gerth et al., 2017a) suggests a so far unexplored regulatory effect of PIP5K2 in the plant nucleus. To test whether nuclear localization of PIP5K2 is relevant for Arabidopsis development, the PIP5K2 variant PIP5K2_{AAA} with inefficient nuclear import and reduced nuclear localization (compare Fig. 1.3, (Gerth et al., 2017a)) was expressed under control of the native *PIP5K2* promoter in the Arabidopsis *pip5k1 pip5k2* double mutant background and the resulting phenotypes were analyzed (Fig. 1.4) (Data from Dr. Katharina Gerth, AG M. Heilmann, unpublished). Plants expressing PIP5K2_{AAA}-EYFP only partially complemented the phenotypes of the *pip5k1 pip5k2* double mutant, compared to full complementation observed upon expression of wild type PIP5K2-EYFP (Fig. 1.4) (Data from Dr. Katharina Gerth, AG M. Heilmann, unpublished).

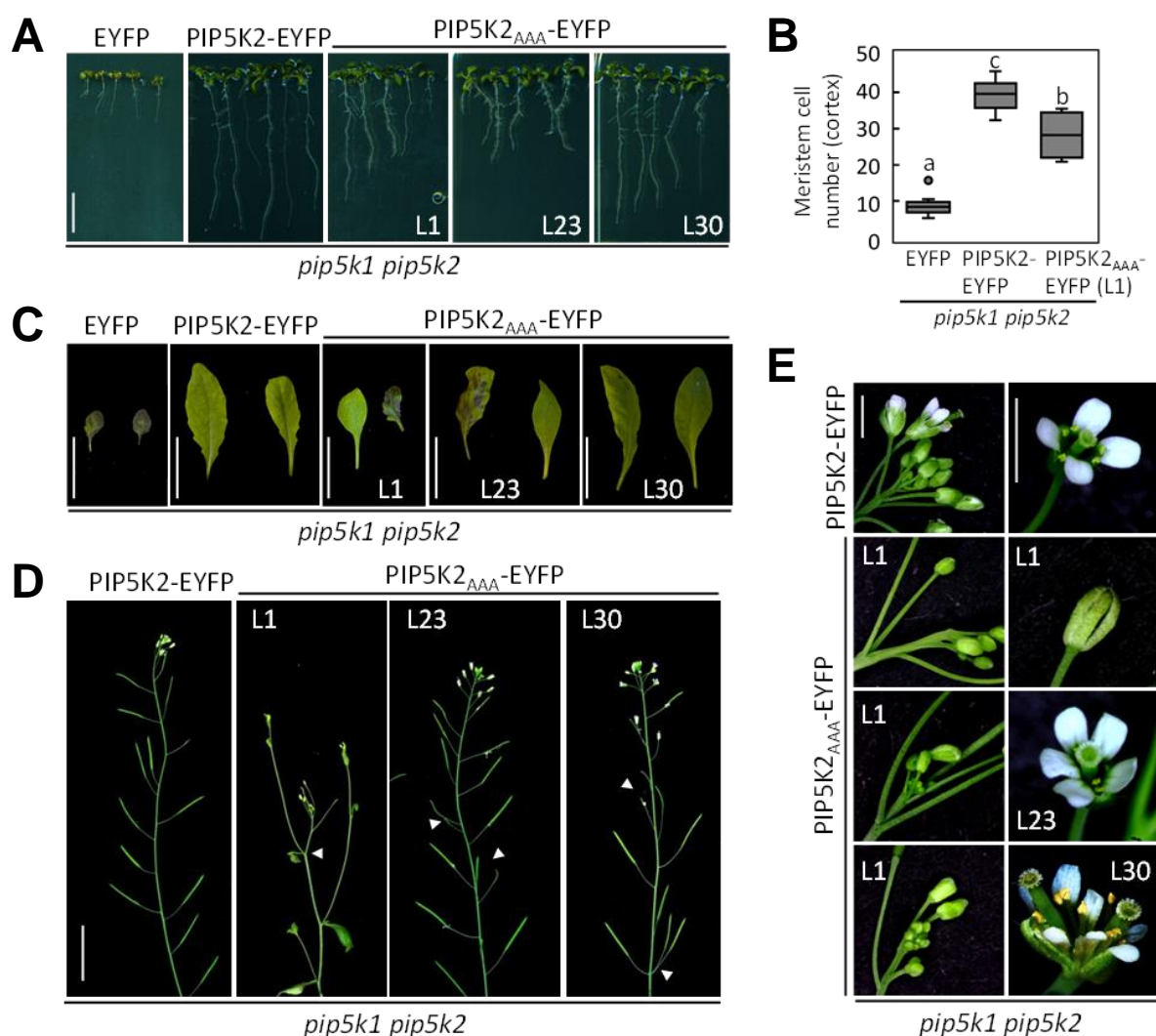


Fig. 1.4: Partial complementation of *pip5k1 pip5k2* double mutant phenotypes upon nuclear-excluded expression of PIP5K2_{AAA}-EYFP. Arabidopsis *pip5k1 pip5k2* double mutants expressing either EYFP, PIP5K2-EYFP wild type or PIP5K2_{AAA}-EYFP were grown on soil or MS medium and were analyzed for various phenotypic aspects. L1, L23 and L30 represent three independent PIP5K2_{AAA}-EYFP expressing lines. **A**, Root length of seven-day-old seedlings. Plants were grown on vertical 1/2 MS agar plates under long-day conditions (16 h light). Images are representative for 16 (EYFP control) to 65 (PIP5K2-EYFP wild type or PIP5K2_{AAA}-EYFP) analyzed seedlings. Scale bar, 1 cm. **B**, Meristem size of seven-day-old seedlings. Meristem size was determined by the number of meristematic cortex cells. The cell number of ten seedlings per line was evaluated. Statistical analysis was performed using a generalized linear model with assumed Poisson distribution and tested for differences with a two-way ANOVA. Different letters represent statistically significant differences ($P < 0.05$; Tukey's post-hoc test). **C**, Leaf morphology of six-week-old plants. Scale bar, 2 cm. **D**, Shoot phyllotaxis of six-week-old plants. Scale bar, 2 cm. **E**, Flower morphology of six-week-old plants. Scale bar, 2 mm.

While the overall habitus, like root growth (Fig. 1.4 A) and meristem size (Fig. 1.4 B), was partially rescued, remaining phenotypic aspects included deformed leaves and flowers and defects in phyllotaxis (Fig. 1.4 C, D and E) (Data from Dr. Katharina Gerth, AG M. Heilmann, unpublished). Previously, such effects were not described for the *pip5k1 pip5k2* double mutant, because these plants do usually not progress to the relevant developmental stages when

flowers or leaves are formed (Ischebeck et al., 2013; Tejos et al., 2014). Interestingly, the apparent phenotypes caused by expressing PIP5K2_{AAA}-EYFP in the double mutant background resemble, among others, defects in auxin-dependent gene expression (Hamann et al., 2002; Ha et al., 2010). While it cannot be fully excluded that polar auxin distribution is still altered in these plants, this experimental design suggests that these defects may alternatively be related to the exclusion of PIP5K2 from nuclear localization.

Overall, experimental evidence from different plants and using different experimental approaches indicates the presence of PI4P 5-kinases, of PtdIns4P and of PtdIns(4,5)P₂ in plant nuclei. However, the physiological function of nuclear PIs and their molecular mode of action are currently not well understood.

1.5. Evidence for physiological functions of nuclear PIs

As mentioned above, the PI 3-kinase VPS34, which phosphorylates PtdIns to PtdIns3P, has already been detected in the nucleus of plant cells. Catalytically active PI 3-kinase was detected in detergent-resistant isolated plant nuclei. Detection of soy PI 3-kinase in the nucleus by a monoclonal antibody indicated localization at active transcription sites, both in the nucleolus and the nucleoplasm in addition to its localization in endomembranes. A role for PI 3-kinase and therefore also for PtdIns3P in transcriptional control has been proposed (Bunney et al., 2000). Overexpression of the human PI4P 5-kinase PIP5K1 α (HsPIP5K1 α) in tobacco cell culture resulted in increased PtdIns(4,5)P₂ levels in the nucleus and reduced histone H3 lysine 9 acetylation (H3K9ac) compared with untransformed tobacco cells (Dieck et al., 2012). However, it remained unclear whether this effect was physiologically relevant and affected plant gene expression or whether it was possibly an incidental consequence of the expression of the human enzyme in a plant cell culture because the domain structures of plant type B PI4P 5-kinases differ significantly from those of human PIP5K1 isoforms.

Similarly, PI4P 5-kinases such as PIP5K2 from Arabidopsis (Lou et al., 2007; Ischebeck et al., 2011, 2013; Tejos et al., 2014), and PIs have been previously observed in plant nuclei (Bunney et al., 2000; Dieck et al., 2012; Gerth et al., 2017a). However, until now, the possible functions of PI-kinases and PIs in the plant nucleus have remained unclear. Studies with mammalian cells and other models provide evidence for a variety of possible nuclear functions of PIs and PI-kinases in different eukaryotic models. Various human PI4P 5-kinases, in addition to localizing to the plasma membrane, could also be observed in the nucleus. The isoforms HsPIP5K1 α , HsPIP5K2 α and HsPIP5K2 β could be observed in nuclear speckles in human lung fibroblasts (Boronenkov et al., 1998). Barlow and coworkers observed that HsPIP5K1 α and PtdIns(4,5)P₂ colocalize with components of the mRNA processing machinery in sub-compartments in the nucleus of lung fibroblasts (Barlow et al., 2010). Nuclear localization of HsPIP5K2 β was also observed in HeLa cells (Ciruela et al., 2000). It was shown that

PtdIns(4,5)P₂ binds to the upstream binding factor (UBF) of RNA polymerase I (Pol I) and the pre-ribosomal RNA processing factor fibrillarin (Fib) and thus induces a conformational change, affecting binding to ribosomal RNA (rRNA) genes or rRNA (Yildirim et al., 2013). In mammalian cells, PtdIns(4,5)P₂ has been shown to regulate the functionality of the Star-PAP poly(A) polymerase, thereby affecting mRNA-3' processing and mRNA expression (Mellman et al., 2008). Recently, subnuclear structures composed of PtdIns(4,5)P₂ and nuclear myosin 1 have been shown to contribute to the organization of Pol II transcriptional complexes (Sobol et al., 2018). These specialized structures were named nuclear lipid islands (NLIs) by the authors and appear to play a role in the efficient transcription of RNA Pol II (Sobol et al., 2018). The data from mammalian and other non-plant models indicate numerous potential roles for PIs in the nucleus. However, the reports from these systems cannot immediately be applied to plants, because a number of structures have no immediate counterparts in plants.

Nonetheless, studies from the plant field also provide evidence for functional roles of PI4P 5-kinases and PIs in plant nuclei. One study showed that the Arabidopsis homolog of trithorax, ATX1, a histone methyltransferase (Alvarez-Venegas et al., 2003), selectively binds to PtdIns5P through its PHD finger, leading to translocation of ATX1 from the nucleus to the cytoplasm and reduction of ATX1 transcriptional activity (Alvarez-Venegas et al., 2006; Ndamukong et al., 2010). More recently, it was shown that a PIP5K1/PIP5K2 homolog from rice (OsPIP5K1) interacts with the growth-regulating homeodomain transcription factors DWT1 and DWL2, which are homologs of the intermediate class of wuschel related homeobox (WOX) transcription factors from Arabidopsis (Fang et al., 2020). This unexpected interaction was observed in the nucleus and the results suggest that the interaction of OsPIP5K1 and WOX is essential for the regulation of coordinated growth in rice (Fang et al., 2020). So far, the molecular mechanism by which OsPIP5K1 and PtdIns(4,5)P₂ might influence DWT1 and DWL2 function are unclear. WOX11 from rice, a family member of DWT1 and DWL2, was proposed to recruit a histone acetylation module to root-specific target genes involved in diverse processes, including auxin transport, auxin responses, transcription, cell cycle regulation and plant meristem development (Zhou et al., 2017).

The data available suggest a role of nuclear PIs in the control of transcription, possibly related to the recruitment of transcription factors and/or an effect on histone modification, and possibly a link to auxin biology. As key findings of this thesis revolve around the association of PI-kinases and PIs with the machinery of histone modification, the following paragraph will provide a brief introduction to this important topic.

1.6. Histone modification and the control of gene activation

In eukaryotes, DNA is wrapped around a histone protein core and thus packaged, protected and regulated. DNA condensed in nucleosomes is called chromatin and histones represent

the protein component of chromatin. Core histones can be modified by posttranslational modifications at presented lysine (or arginine) residues at the N-terminus, called the histone tail (Millar and Grunstein, 2006; Kouzarides, 2007; Berger, 2007; Earley et al., 2007; Zhang et al., 2007). The histone tail stands out from the nucleosome, which is consisting of dimers of histones H2A, H2B, H3 and H4 each, that together form an octamer (Luger et al., 1997; Millar and Grunstein, 2006; Kouzarides, 2007; Zhang et al., 2007). Various post-translational modifications of different histones generate a complex combinatorial code that controls different nuclear functions, e.g. gene expression. The large number of posttranslational modifications at histones is introduced and removed by a variety of enzymes. Histone modifications inserted by various enzymes include phosphorylation at serine or threonine residues, ubiquitylation and SUMOylation of lysines, and of course methylation at lysine or arginine and acetylation and deacetylation of lysines. Introduced methyl- or acetyl groups at the N-termini of core histones can recruit further histone modifiers and/or have effects on chromatin structure and thus on gene expression (Kouzarides, 2007; Zhang et al., 2007; Falkenberg and Johnstone, 2014). The enzymes and proteins that mediate the introduction, removal, and reading of the histone code are therefore called writer, eraser, and reader enzymes. (Fig. 1.5) (Falkenberg and Johnstone, 2014).

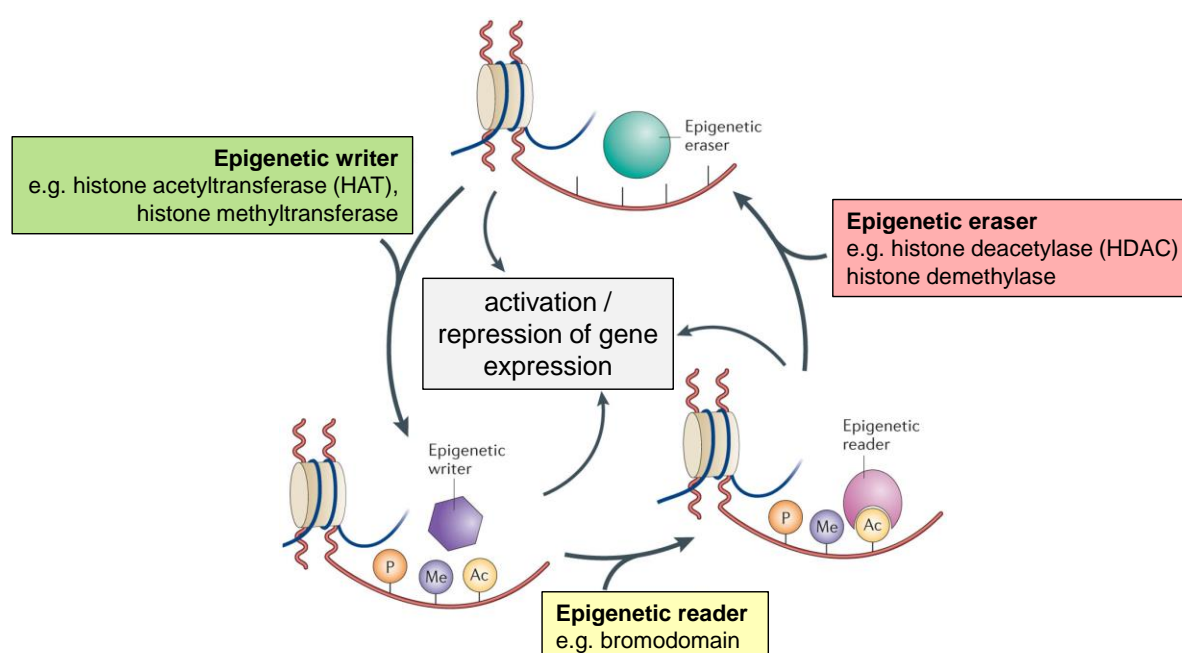


Fig. 1.5: Different enzymes are involved in epigenetic control. Epigenetic writers, readers and erasers together regulate epigenetic control dynamically. Writers introduce histone modifications, which can be recognized by readers that can mediate further modifications either by writers or erasers. By this interplay, gene activation status is controlled and gene expression can be influenced. The figure was modified from (Falkenberg and Johnstone, 2014).

Epigenetic “writers” are enzymes that insert covalent histone modifications, such as methylations or acetylations, with the nuclear consequences as already mentioned above

(Kouzarides, 2007; Servet et al., 2010; Falkenberg and Johnstone, 2014; Marmorstein and Zhou, 2014). Typical targets are lysine residues at the N-termini mainly of histones H3 and H4 (Berger, 2007; Earley et al., 2007; Zhang et al., 2007; Servet et al., 2010). Epigenetic “readers” can bind to these histone modifications and promote further modifications by recruitment of further histone-modifying enzymes, either introducing new modifications or removing existing modifications (Strahl and Allis, 2000; Pena et al., 2006; Soliman and Riabowol, 2007; Taverna et al., 2007; Pena et al., 2008; Josling et al., 2012; Patel and Wang, 2013; Falkenberg and Johnstone, 2014; Marmorstein and Zhou, 2014; Liu and Min, 2016). Epigenetic “erasers”, like histone deacetylases or histone demethylases, can remove epigenetic modifications (Berger, 2007; Kouzarides, 2007; Falkenberg and Johnstone, 2014). The interplay of these operating enzymes dynamically controls the gene activation status of specific not constitutively active gene targets (Berger, 2007; Falkenberg and Johnstone, 2014).

Histone sequences and histone codes are highly but not completely conserved between different species (Fuchs et al., 2006; Zhang et al., 2007). In general, at some specific histone residues methylation leads to a more condensed heterochromatin structure and has a repressive effect (Millar and Grunstein, 2006; Berger, 2007; Zhang et al., 2007), whereas other methylated residues lead to an opening of the chromatin structure and thus promote the formation of euchromatin areas (Millar and Grunstein, 2006; Berger, 2007; Servet et al., 2010). By covalent addition of an acetyl group to lysine residues of the histone tails, various nuclear processes can be influenced. Histone acetylation can lead to altered chromatin structure, regulation of cell cycle, DNA repair mechanisms, DNA replication, and most importantly, transcription and gene silencing (Millar and Grunstein, 2006; Berger, 2007; Kouzarides, 2007; Zhang et al., 2007). The addition of acetyl groups, especially in histones H3 and H4, is catalyzed by histone acetyltransferases (HATs), the removal of acetylation is catalyzed by histone deacetylases (HDACs). In transcriptional regulation, acetylation usually leads to opening of the condensed chromatin structure and thus to gene transcription activation (Millar and Grunstein, 2006; Berger, 2007; Kouzarides, 2007; Zhang et al., 2007; Servet et al., 2010). Methylation at lysine residues (K) of histones H3 and H4 are well-studied in plants (Cheng et al., 2020). Lysine residues K4, K9, K23 (Trejo-Arellano et al., 2017), K27, K36, and K79 of histone H3 and residue K20 of histone H4 can be mono-, di-, and/or trimethylated by histone lysine methyltransferases (Cheng et al., 2020). In most cases, these are histone lysine methyltransferases of the Su(var)3-9, Enhancer of zeste, Trithorax (SET) domain group (SDG), which carry a SET domain firstly described in *Drosophila* (Yeates, 2002; Dillon et al., 2005; Qian and Zhou, 2006). Relatively well-studied plant histone methylators that remove these methylations again include demethylase 1 homologs and Jumonji proteins (Liu et al., 2010; Xiao et al., 2016). Proteins with chromo, Tudor, MBT, WD40, PHD, and PWWP domains are considered “reader” proteins of histone methylation (Yun et al., 2011; Liu and Min, 2016).

"Reading" histone methylation usually results in transcriptional adaptation and thus changes in gene expression patterns. Di- or trimethylation of N-terminal histone H3 lysine 4 (H3K4me2/H3K4me3) is a typical target for epigenetic readers that recruit activating effector proteins (Pena et al., 2006; Berger, 2007; Pena et al., 2008; Yun et al., 2011; Liu and Min, 2016). Typical acetylation or deacetylation targets of histones in *Arabidopsis* are N-terminal lysine residues K9, K14, K18, K23 and K27 of histone H3 or lysine residues K5, K8, K12, K16 and K20 of histone H4 (Earley et al., 2007; Kouzarides, 2007; Zhang et al., 2007; Servet et al., 2010).

Histone acetylation generally activates transcription because the introduction of the negatively charged acetyl group loosens the chromatin structure (Shahbazian and Grunstein, 2007). Two groups of HATs are distinguished, those localized in the nucleus (A-type) and those localized in the cytoplasm (B-type) (Brownell and Allis, 1996; Roth et al., 2001; Boycheva et al., 2014). The HATs belonging to the nuclear-localized group are classified in the different HAT families, namely the GCN5-related N-terminal acetyltransferases (GNAT), the MOZ, Ybf2/Sas3, Sas2 and Tip60-related, briefly also called MYST, the p300/CREB-binding protein (CBP) and the TATA-binding protein-associated factor (TAF1) (Servet et al., 2010; Boycheva et al., 2014; Rymen et al., 2019). In *Arabidopsis*, three enzymes belong to the GNAT family, including general control non-repressible 5 (GCN5, or called HAG1), elongator complex protein 3 (ELP3) and HAG2. The MYST family includes two members, HAG4/HAM1 and HAG5/HAM2. The p300/CBP family includes five enzymes, HAC1, HAC2, HAC4, HAC5 and HAC12 and the TAF1 family has two members HAF1 and HAF2/TAF1 (Servet et al., 2010; Boycheva et al., 2014; Jiang et al., 2020). Proteins with bromodomains are considered "reader" proteins of histone acetylation marks (Dhalluin et al., 1999; Berger, 2007; Servet et al., 2010; Marmorstein and Zhou, 2014). The binding of proteins with bromodomain to acetylated histones can trigger a variety of responses, e.g. acetylation of further histone residues or histones, remodeling of chromatin, and recruitment of other proteins/factors such as transcriptional activators/transcription factors. Thus, reading of this histone acetylation plays a crucial role in the regulation of transcription (Josling et al., 2012).

1.7. The histone acetyltransferase GCN5

GCN5 is one of the best-studied HATs in eukaryotes and is of critical importance in transcription regulation during stress responses but also during development (Gan et al., 2021). HATs are mostly part of large multiprotein complexes, as GCN5 is part of the Spt-Ada-GCN5-acetyltransferase (SAGA)-transcriptional co-activator complex (Grant et al., 1997; Lee and Workman, 2007; Servet et al., 2010; Strahl and Briggs, 2021; Gan et al., 2021). GCN5 activity is enhanced by other factors of the SAGA complex and, in general, protein complexes can also influence the substrate specificity of HATs. The multiprotein complexes are recruited

by protein-protein interactions to target sequences in the genome (Gan et al., 2021). Thus, both HATs, such as GCN5, and HDACs can either activate or repress gene expression through their activity at histones of specific promoters (Millar and Grunstein, 2006; Berger, 2007; Li et al., 2007).

The histone-modifying enzyme complex SAGA executes a highly conserved function in yeast, mammals, and plants (Srivastava et al., 2015; Moraga and Aquea, 2015). Studies in *Tetrahymena* and yeast led to the discovery of the SAGA complex (Brownell et al., 1996; Grant et al., 1997). In yeast, the SAGA complex is involved in many processes all targeting gene expression control whereby it can act in a multifunctional role due to its modular composition (Wu et al., 2004; Moraga and Aquea, 2015). As listed by Moraga and Aquea (Moraga and Aquea, 2015), yeast SAGA complex is involved in histone acetylation (Grant et al., 1997), histone deubiquitination (Henry et al., 2003; Daniel et al., 2004), mRNA export (Rodríguez-Navarro et al., 2004), transcription elongation (Govind et al., 2007), chromatin recognition (Pray-Grant et al., 2005), and regulation of the basal transcription machinery (Stern et al., 1999).

Proteins belonging to the multiprotein complex are divided into modules with different functions and enzymatic activities (Koutelou et al., 2010; Moraga and Aquea, 2015; Vlachonasis et al., 2021). The four Arabidopsis SAGA modules are the core module consisting of TAF5, TAF6, TAF9, TAF10, TAF12, SPT3-like, SPT7, SPT20 and ADA1. The Arabidopsis SPT3-homolog within the core module interacts at active transcription sites with the TATA-binding protein (TBP) (Papai et al., 2020). The core module is connected to the TRA1 module by interaction of transcription-associated protein 1 (TRA1) with TAF12/Spt20. Interestingly, TRA1 is a member of the PI 3-kinase-like kinases (PIKK family) with three identified domains: HEAT, FAT and PI-kinase domain but seems to be catalytically inactive (Grant et al., 1998; Sharov et al., 2017). Both, the deubiquitination (DUB)-module consisting of UBP22, SGF11 and ENY2 (SGF73 is not present in Arabidopsis) and the histone acetyltransferase module (HAT module) comprising the proteins ADA2, ADA3, GCN5 and SGF29 are flexibly associated with the core module (Fig. 1.6) (Pfab et al., 2018; Nassrallah et al., 2018; Grasser et al., 2021; Vlachonasis et al., 2021; Wu et al., 2021). The histone acetylation activity of the HAT module of the SAGA complex is catalyzed by GCN5 (Grant et al., 1997; Stockinger et al., 2001; Servet et al., 2010; Srivastava et al., 2015; Moraga and Aquea, 2015; Grasser et al., 2021; Gan et al., 2021). GCN5 acetylates histone H3 at positions K9, K14, K18 and K27 (Benhamed et al., 2006; Zhang et al., 2007; Servet et al., 2010; Shen et al., 2015). ADA2A and ADA2B, components of HAT modules in Arabidopsis, are the only proteins beside histones that have been described to be acetylated by GCN5 (Mao et al., 2006).

SAGA, and in particular the functionality of ADA2B/GCN5, has been shown to play an important role in the different developmental stages of Arabidopsis. Also, in relation to abiotic

stress conditions (Srivastava et al., 2015; Moraga and Aquea, 2015), such as in the response to drought (Hark et al., 2009; Vlachonasios et al., 2011; Sakuraba et al., 2015; Li et al., 2019), salinity (Hark et al., 2009; Kaldis et al., 2011), heat (Hu et al., 2015) and cold stress (Stockinger et al., 2001; Vlachonasios et al., 2003) or nutrient deficiency (Xing et al., 2015). The subsequent adapted gene regulation is GCN5- or SAGA-dependent. In addition, GCN5 is involved in the transcriptional responses of several phytohormone pathways, such as ethylene, auxin and salicylic acid, and thus plays various roles during the plant life cycle (Weiste and Dröge-Laser, 2014; Grasser et al., 2021; Gan et al., 2021). Many of these signaling pathways that require GCN5 activity intertwine coordination of physiological processes and developmental stages (Grasser et al., 2021; Gan et al., 2021).

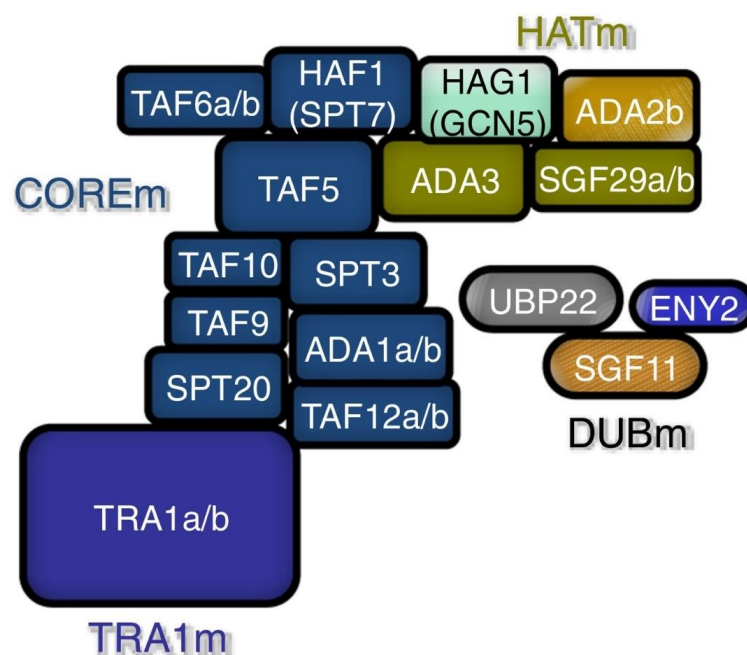


Fig. 1.6: The composition of the plant SAGA complex. The four SAGA modules, core module, TRA1 module, HAT module, and the DUB module are shown here. The arrangement and representation of the subunits is derived from the recently solved structure from yeast (Wang et al., 2020; Papai et al., 2020) and was adapted from data from Arabidopsis, which see the structure described here confirmed by co-purifications of the different proteins and modules (Pfab et al., 2018; Nassrallah et al., 2018). Figure from (Grasser et al., 2021).

In addition to the acetyltransferase domain (amino acid (aa) 222 – 371), GCN5 contains a bromodomain (aa 472 – 543) at its C-terminus (Fig. 1.7), which recruits GCN5 to already acetylated lysine residues. GCN5 is thus both writer and reader of the histone code. (Dhalluin et al., 1999; Berger, 2007; Servet et al., 2010). In chromatin immunoprecipitation experiments, GCN5 could be detected bound to 40 % of the identified promoter regions, but the bromodomain of GCN5 was required for only 11 % of the GCN5 targets (Benhamed et al., 2008).



Fig. 1.7: Domain structure of GCN5. GCN5 contains two defined protein domains. The histone acetyltransferase (HAT) domain (aa 222 – 371) and the bromodomain (BD) (aa 472 – 543).

GCN5 has previously been shown to interact with ADA2A (AT3G07740) and ADA2B (AT4G16420) (Stockinger et al., 2001; Mao et al., 2006; Servet et al., 2008). The interaction between ADA2A or ADA2B and GCN5 leads to an enhancement of the HAT activity of GCN5 (Mao et al., 2006). Different roles for ADA2A and ADA2B are discussed because expression of ADA2A under a constitutive promoter cannot complement an *ada2b* mutant (Hark et al., 2009). ADA2A and ADA2B are likely components of different HAT modules with specific target sites and could independently recruit GCN5 to the appropriate context (Hark et al., 2009; Anzola et al., 2010; Servet et al., 2010).

1.8. Physiological roles of GCN5 in phytohormone signaling and the control of growth

Previous studies have linked GCN5 HAT activity to phytohormone signaling pathways, such as ethylene signaling (Poulios and Vlachonasios, 2016; Gan et al., 2021), salicylic acid signaling (Kim et al., 2020; Gan et al., 2021) and auxin signaling (Vlachonasios et al., 2003; Kornet and Scheres, 2009; Weiste and Dröge-Laser, 2014; Gan et al., 2021).

The phenotype of *Arabidopsis gcn5-1* mutants was described as comparable to plants with reduced auxin response, displaying short hypocotyls, upcurled leaves, reduced apical dominance and dwarf phenotype (Vlachonasios et al., 2003). *ada2* mutants also showed evidence of impaired auxin response. The *Arabidopsis ada2b-1* mutant was compared with auxin-overproducing mutants and showed elongated hypocotyls, small and epinastic cotyledons, a lower leaf expansion rate, an increased number of lateral roots and overall dwarfism (Vlachonasios et al., 2003; Anzola et al., 2010). The observed dwarfism phenotype of *gcn5* and *ada2b* mutants is likely based on the fact that both GCN5 and ADA2B exert an influence on meristem maintenance (Kornet and Scheres, 2009). Overexpression of PLETHORA transcription factor 2 (PLT2) in *gcn5* mutants can restore stem cell niche defects of *gcn5* mutants, suggesting that GCN5 regulates the stem cell niche at the root tip and root growth by mediating the expression of PLT1 and PLT2 transcription (Vlachonasios et al., 2003; Kornet and Scheres, 2009; Servet et al., 2010). Thus, GCN5 together with ADA2B can increase the transcript abundance of *PLT1* and *PLT2* in the roots, regulating cell division in the meristem and cell expansion of stem cells, whereby ADA2B is not involved in stem cell maintenance. Expression regulation of PLETHORA transcription factors by GCN5 and ADA2B to maintain the root stem cell niche is a process that is also directly linked to auxin distribution (Kornet and Scheres, 2009). Also suggestive of a role of GCN5 in meristem maintenance is

the discovery that in rice ADA2B interacts with a plant homeodomain transcription factor of the WUSCHEL (WUS) family, a WOX11-like transcription factor, and possibly ADA2B subsequently recruits GCN5 to the context of WOX regulated genes (Zhou et al., 2017). In addition to evidence for root meristem regulations, there is also evidence that GCN5 is required for the maintenance of the shoot apical meristem as a negative regulator of WUS (Bertrand et al., 2003; Cohen et al., 2009; Poullos and Vlachonasios, 2016).

Transcription of PLETHORA genes depends on auxin response transcription factors (ARFs) (Aida et al., 2004) and PLETHORA expression therefore forms a gradient within the root tip that is comparable to that of auxin (Galinha et al., 2007; Grieneisen et al., 2007). In response or in combination with a phytohormone stimulus, such as auxin, transcription factors of the basic leucine zipper (bZIP) family, e.g. bZIP11, interact with ADA2B to recruit the histone acetylation machinery to specific auxin-responsive genes (Weiste and Dröge-Laser, 2014). Weiste and Dröge-Laser proposed a model which explains recruitment of GCN5 to auxin-inducible gene loci by the example of *GH3.3* (Fig. 1.8).

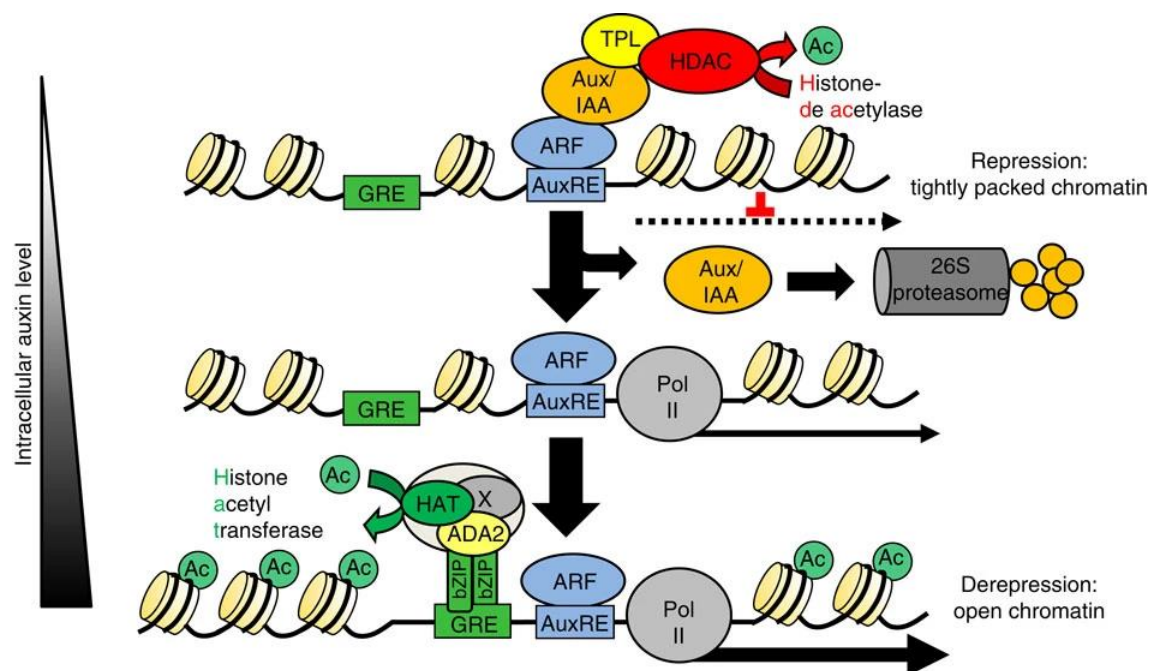


Fig. 1.8: Increasing auxin levels induce GCN5-regulated transcription. Weiste and Dröge-Laser proposed a model that explains how increasing auxin levels lead to GCN5-mediated histone acetylation, which promotes gene expression of auxin-responsive genes. AC, acetylation, ADA2B, transcriptional adaptor ADA2B; ARF, auxin response transcription factor; Aux/IAA, Aux/IAA repressor protein; AuxRE, auxin-responsive element; bZIP, bZIP transcription factor; GRE, G-box-related element; HAT, histone acetyltransferase GCN5; HDAC, histone deacetylase; Pol II, RNA polymerase; TPL, TOPLESS protein; X, unknown protein. The figure was adopted from (Weiste and Dröge-Laser, 2014).

At low auxin levels, Aux/IAA repressor proteins inhibit the expression of auxin-induced genes. In addition, the transcriptional corepressor TOPLESS (TPL) recruits histone deacetylases

which provide tightly packed inactive chromatin by deacetylating histones. As auxin levels increase, Aux/IAA repressors are polyubiquitinated by the SCF/TIR1 complex and degraded by the 26S proteasome. Auxin-responsive element (AuxRE)-binding transcription factors and ARFs mediate gene expression of auxin-dependent genes. In previous studies, in addition to auxin-responsive elements (AuxREs), G-box-related elements (GREs) have been found in promoters of auxin-inducible genes, such as *GH3.3* (Ulmasov et al., 1995; Heinekamp et al., 2004). To these GREs, bZIP transcription factors can bind. Weiste and Dröge-Laser have shown that certain bZIPs that bind to such GRE elements within auxin-inducible promoters, interact with ADA2, thereby recruiting the ADA2/GCN5-HAT module (possibly SAGA complex). GCN5/HAT module activity increases histone acetylation in the promoter region, thereby enhancing auxin-induced transcription through chromatin restructuring (Weiste and Dröge-Laser, 2014).

Histone acetylation, as a molecular tool to control dynamic gene expression in response to various stresses or phytohormone signals, depends on several factors and is adapted to the particular developmental or stress-dependent response through the interplay of different signaling pathways and components. It seems likely that not all molecular factors of these detailed regulatory mechanisms are known yet.

One indication that there are PIs among the unknown players in histone modification was that increased PtdIns(4,5)P₂ levels through overexpression of a human HsPIP5K1 α in tobacco cells had an effect on histone acetylation (Dieck et al., 2012). While this reported experiment is clearly artificial and no effects on gene expression were tested, it still suggests that PIs may have a function in epigenetic regulation of gene expression. So far, it has not been investigated in plants whether PIs and/or plant PI-kinases might contribute to histone modification and thus to transcriptional control. Also, no molecular targets for PI-dependent effects on histone modification have yet been identified in plants, and it is fully unclear what the physiological consequences of such modifications might be.

1.9. Aims of this thesis

The overall aim of this thesis was to determine whether and how nuclear PIs might contribute to the control of histone modification and gene expression in plants. The initial experimental setup was chosen to help define the subsequent direction of experimental analyses. Based on the hypothesis that PIP5K1 and/or PIP5K2 were part of a nuclear protein complex involved in histone modification, it was attempted to provide evidence for or against this hypothesis and to determine molecular details:

- The first goal was to test whether the increased or decreased expression of the intrinsic nuclear Arabidopsis PI4P 5-kinases PIP5K1 and PIP5K2 would result in a change in the histone acetylation status of Arabidopsis plants.
- To elucidate the molecular mechanism by which histone modification was influenced, a second goal was to determine relevant protein-protein and protein-lipid interactions of PIP5K1/PIP5K2 and enzymes mediating histone modification.
- A third important goal was to determine whether misexpression of PIP5K1 and/or PIP5K2 would influence auxin-regulated gene expression and to clarify the underlying molecular mechanism.
- A fourth goal was to test for potential direct effects of PIs on enzymes of histone modification by using *in vitro* activity tests with recombinant proteins.
- A last goal was to also investigate the contribution of VPS34 and PtdIns3P in the control of histone modification and gene expression.

2. Results

At the beginning of this work it was known that PIs (Bunney et al., 2000; Gerth et al., 2017a) and PI4P 5-kinases (Lou et al., 2007; Ischebeck et al., 2011, 2013; Tejos et al., 2014) are detectable in the plant nucleus in addition to the better-studied cytoplasmic and plasma membrane localization. For PIP5K2 from Arabidopsis, an NLS was identified and characterized, also indicating a targeted and active nuclear import of this enzyme (Gerth et al., 2017a). However, to date, there have been no studies on the molecular functions of PIs and the corresponding PI-forming enzymes in plant nuclei. While artificial overexpression of HsPIP5K1 α in tobacco cells previously resulted in a reduced pattern in histone H3 lysine 9 acetylation (H3K9ac) (Dieck et al., 2012), it remained unclear whether this effect was physiologically relevant and impacted on plant gene expression or whether it was an accidental consequence of expressing the human enzyme in a plant cell culture. Similarly, the Arabidopsis PI 3-kinase VPS34 had previously been detected in the nucleus of plant cells, in addition to its localization in endomembranes (Bunney et al., 2000). VPS34 localizes to sites of active transcription, and a role for PI 3-kinase and PtdIns3P in transcriptional control has been proposed that has remained undefined for two decades. While these reports suggest that PIs may influence relevant physiological processes in the nucleus of plant cells, so far there was little focused information on the molecular roles of nuclear PIs.

Therefore, this thesis further explored possible effects of Arabidopsis PI-kinases and PIs on nuclear functions, with a focus on histone modification and the epigenetic regulation of gene expression.

2.1. Histone H3 acetylation is influenced in Arabidopsis by expression level of the intrinsic PI4P 5-kinases PIP5K1 and PIP5K2

To test whether misexpression of the Arabidopsis intrinsic PI4P 5-kinases PIP5K1 or PIP5K2 resulted in changed histone acetylation patterns, the acetylation levels at histone H3 were examined in Arabidopsis *pip5k1 pip5k2* double mutants (Ischebeck et al., 2013; Tejos et al., 2014) and in *PIP5K2-EYFP* overexpression (OE) plants (Gerth et al., 2017a) (Fig. 2.1, genotyping in appendix Fig. 6.1).

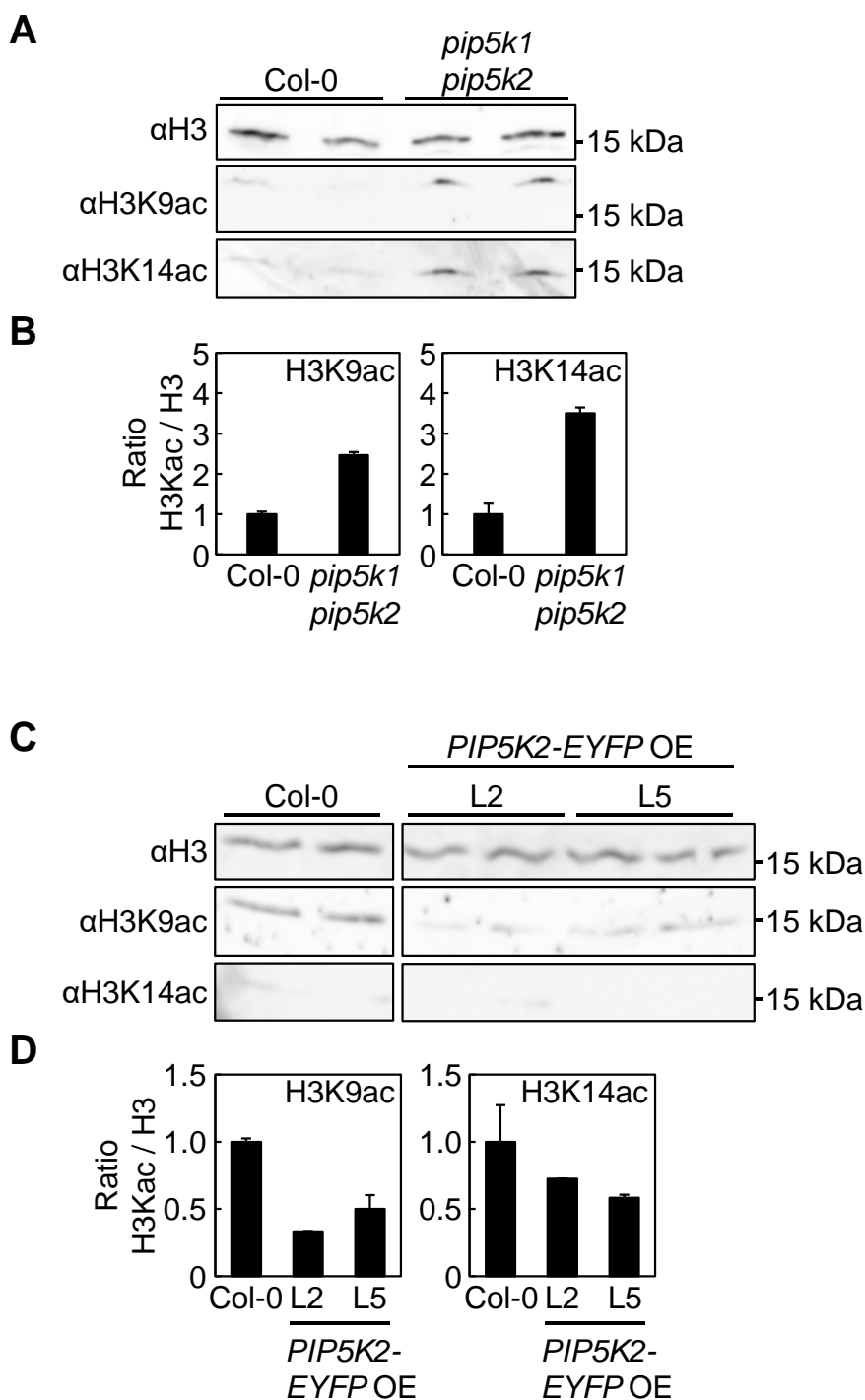


Fig. 2.1: Histone H3 acetylation levels of *pip5k1 pip5k2* double mutant and *PIP5K2-EYFP OE* lines. Histone H3 acetylation was assessed by immunodetection. Protein extracts were resolved by SDS-PAGE, blotted on a nitrocellulose membrane and analyzed with antibodies against histone H3 as control and acetylated histone H3 antibodies, α H3K9ac and α H3K14ac. Chemiluminescent signals were recorded using an ECL detection system. The expected size of histone H3 was 15.3 kDa. **A**, Immunodetection of histone H3 acetylation levels, H3K9ac and H3K14ac, of *pip5k1 pip5k2* double mutant in comparison to Col-0. **B**, Quantification of H3K9ac and H3K14ac normalized against histone H3. The intensity of the detected protein bands in A was measured with ImageJ/Fiji (Schindelin et al., 2012). Data are representative for $n = 4$ with two biological replicates for H3K9ac and $n = 2$ with two biological replicates for H3K14ac. Bars represent means, error bars represent standard deviations. **C**, Immunodetection of histone H3 acetylation levels, H3K9ac and H3K14ac, of *PIP5K2-EYFP OE* lines L2 and L5. **D**, Quantification of H3K9ac and H3K14ac normalized against histone H3. The intensity of

the detected protein bands in C was measured with ImageJ/Fiji (Schindelin et al., 2012). Analysis was performed $n = 1$ with two biological replicates of each line. Bars represent means, error bars represent standard deviations.

Nuclei were isolated from Col-0 and *pip5k1 pip5k2* Arabidopsis leaf rosettes and the levels of histone H3 acetylated at lysine residue 9 (H3K9) and at lysine residue 14 (H3K14) were investigated by immunodetection in comparison to total histone H3. The specific acetylation was tested with antisera against histone H3, against acetylated lysine residue 9 of histone H3 (H3K9ac) or against acetylated lysine residue 14 of histone H3 (H3K14ac) epitopes, respectively (Fig. 2.1 A). The specificity of the antisera was tested with histone H3 protein and various acetylated or methylated histone H3 peptides in separate assays (appendix Fig. 6.2). The degree of H3K9ac and H3K14ac was increased in the *pip5k1 pip5k2* double mutant in comparison to the Col-0 wild type control (Fig. 2.1 A and B), as indicated by the ratio of the respective detected acetylated histones vs. the total detected histone (Fig. 2.1 B). By contrast, an opposite effect on histone acetylation was observed for histones isolated from the *PIP5K2-EYFP* OE lines (L2 and L5). Overexpression of intrinsic PIP5K2-EYFP resulted in a decrease in acetylation of H3K9 and H3K14 in the lines studied, whereas histone H3 levels were comparable in all plant samples examined (Fig. 2.1 C). This observation was confirmed by determining the histone H3 to H3K9ac and histone H3 to H3K14ac ratios, respectively (Fig. 2.1 D). H3K9ac and H3K14ac levels were found to be decreased in *PIP5K2-EYFP* OE lines L2 and L5 compared with the Col-0 wild type. These observations confirm the previously described effects of overexpressed HsPIP5K1 α in tobacco cells (Dieck et al., 2012) and illustrate that in Arabidopsis, histone H3 acetylation can be positively or negatively modulated by changed production of PtdIns(4,5)P₂ by changed intrinsic expression levels of PI4P 5-kinases.

A relationship of PIP5K2 to histone H3 has been shown previously where histone H3 was found to be an interaction partner for PIP5K2 in an undirected yeast-two-hybrid (YTH) screen with a pollen tube cDNA library as prey (unpublished data, AG M. Heilmann). In the present study, it was additionally confirmed in dot-blot experiments that recombinantly expressed MBP-PIP5K1 and MBP-PIP5K2 can bind to recombinant histone H3 protein and histone H3 from calf thymus (see appendix Fig. 6.3).

2.2. PIP5K1 and PIP5K2 interact with the histone acetyltransferase GCN5

In view of the findings that altered expression of PI4P 5-kinases affected the acetylation of histone H3 and that PIP5K1 and PIP5K2 also bound to histone H3 themselves, PIP5K1 and PIP5K2 were tested *in vivo* for protein-protein interaction with various well-characterized and ubiquitously expressed histone-modifying enzymes (Fig. 2.2) (Servet et al., 2010; Espinosa-Cores et al., 2020; Jiang et al., 2020).

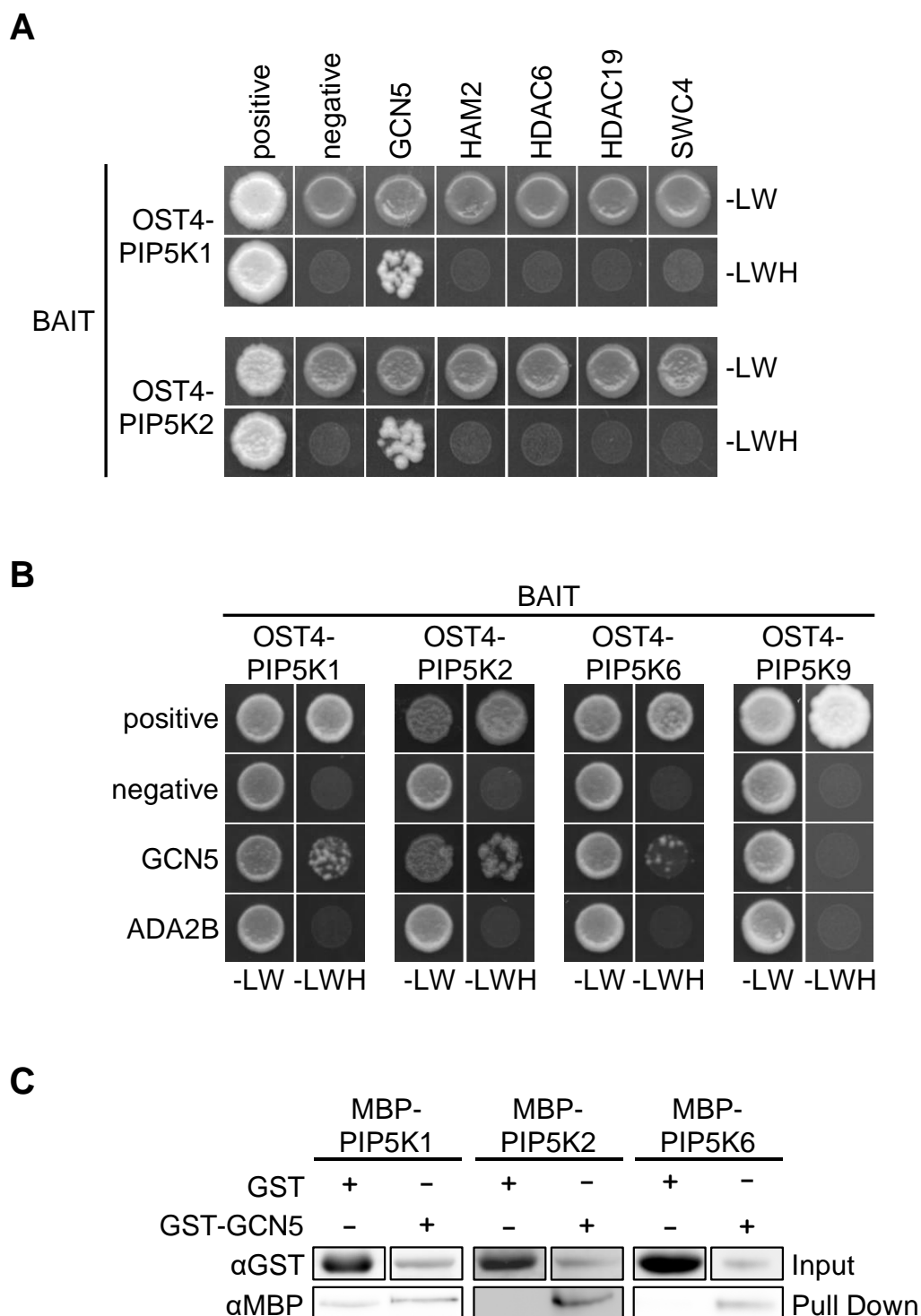


Fig. 2.2: PIP5K1 and PIP5K2 interact with the histone acetyltransferase GCN5. The interaction of PIP5K1 and PIP5K2 with various histone-modifying enzymes was tested by split-ubiquitin-based YTH analysis in *S. cerevisiae* strain NMY51 and by *in vitro* immuno pull-down analysis. **A, B**, Split-ubiquitin-based YTH analysis of OST4 fusions as bait. *pAl-Alg5* and *pDL2-Alg5* vectors were used as positive or negative controls. Uniform growth on -LW media (without leucine and tryptophane) indicates equal cell densities and the presence of the respective vectors. Interaction is indicated by growth under selective conditions on -LWH media (without leucine, tryptophane and histidine). **A**, Split-ubiquitin-based YTH of PIP5K1 and PIP5K2 (bait) with GCN5, HAM2, HDAC6, HDAC19 and SWC4 (prey). Yeast colonies were grown at 30°C for four days. A representative result of three replicates with five independent colonies of each combination is shown. **B**, Split-ubiquitin-based YTH of PIP5K1, PIP5K2, PIP5K6 and PIP5K9 (bait) with GCN5 and ADA2B (prey). Yeast colonies were grown at 30°C for three days (seven days for tests

with PIP5K9). $n = 3$ (PIP5K6, PIP5K9) or $n = 8$ (PIP5K1, PIP5K2) with five independent colonies of each combination. **C**, *In vitro* immuno pull-down of PIP5K1, PIP5K2 and PIP5K6 with GCN5. Recombinantly expressed GST, GST-GCN5 were immobilized on glutathione agarose and incubated with recombinant MBP-tagged PIP5K1, PIP5K2 and PIP5K6 (expression lysate). Bound protein was co-eluted with 50 mM reduced L-glutathione and interacting MBP-tagged proteins were analyzed by immunodetection using an α MBP antibody. Input GST-tagged protein was detected by an α GST antibody. Chemiluminescence signals were recorded with an ECL detection system. Pull-downs were performed in quadruple versions with PIP5K1, in triplicates with PIP5K2 and twice with PIP5K6. GCN5, general control non-repressible 5, a histone acetyltransferase of the GNAT family 1; GST, glutathione S-transferase; HAM2, histone acetyltransferase of the MYST family 2; HDAC6, histone deacetylase 6; HDAC19, histone deacetylase 19; MBP, maltose-binding protein; OST4, oligosaccharyltransferase 4; SWC4, SWR1-complex protein 4.

The following candidate enzymes were selected for the analysis: the HAT GCN5 (AT3G54610, general control non-repressible 5), HAM2 (AT5G09740, a histone acetyltransferase of the MYST family 2), HDAC6 (AT5G63110, a histone deacetylase of the RPD3/HDA1 family), HDAC19 (AT4G38130, or AtHD1, a histone deacetylase of the RPD3/HDA1 family) and SWC4 (AT2G47210, a DNA-binding protein recruiting the histone-modifying SWR1-complex) (Servet et al., 2010; Espinosa-Cores et al., 2020; Jiang et al., 2020). PIP5K1 and PIP5K2 (bait) were tested for interaction with the candidate proteins in split-ubiquitin-based YTH studies where the bait proteins were attached to the endoplasmic reticulum (ER) by fusion to an oligosaccharyltransferase 4 (OST4) anchor (Fig. 2.2 A). Positive protein-protein interaction was found for GCN5 with both PIP5K1 and PIP5K2 (Fig. 2.2 A). The YTH experiments shown in Fig. 2.2 B indicate interaction of GCN5 additionally with the ubiquitously expressed but functionally divergent PI4P 5-kinase PIP5K6 (Zhao et al., 2010; Stenzel et al., 2012; Hempel et al., 2017; Menzel et al., 2019; Fratini et al., 2021), but not with the nuclear-localized PI4P 5-kinase isoform PIP5K9 (Lou et al., 2007). As GCN5 is part of the HAT module of the SAGA complex and does interact with the transcriptional adaptor 2B, ADA2B (AT4G16420) (Stockinger et al., 2001; Mao et al., 2006; Servet et al., 2008), interactions of PIP5K1, PIP5K2, PIP5K6, and PIP5K9 with ADA2B were also tested (Fig. 2.2 B). The GCN5-ADA2B interaction served as a positive control (appendix Fig. 6.4); however, the four PI4P-5 kinases tested showed no interaction with ADA2B (Fig. 2.2 B).

These positive protein-protein interactions of PIP5K1, PIP5K2 and PIP5K6 with GCN5 were verified in *in vitro* immuno pull-down experiments (Fig. 2.2 C). Recombinant GST-tagged GCN5 was immobilized to a glutathione agarose matrix and incubated together with the different expression lysates including the respective MBP-tagged PI4P 5-kinases. MBP-PIP5K1, MBP-PIP5K2 and MBP-PIP5K6 were co-eluted with GST-GCN5 protein, indicating protein-protein interaction (Fig. 2.2 C) and verifying the results from the YTH analysis. Together, the data indicate interaction of PIP5K1 and PIP5K2 with the HAT GCN5.

2.2.1. Arabidopsis PIP5K1 and PIP5K2 and GCN5 interact with ING1 and ING2

To further confirm the association of PI4P 5-kinases PIP5K1 and PIP5K2 with the nuclear HAT complex, PIP5K1 and PIP5K2 were tested for interaction with known HAT complex recruiting proteins. Inhibitor of growth (ING) is an epigenetic reader recognizing trimethylated histones and recruiting HATs to mediate further acetylation of the histone substrates (Vieyra et al., 2002; Pena et al., 2006; Soliman and Riabowol, 2007). From the mammalian field of research it is known that mammalian ING proteins bind to PIs (Gozani et al., 2003) and require this interaction for their function (Bunce et al., 2006a, 2006b; Soliman and Riabowol, 2007). The two ING isoforms of Arabidopsis, ING1 (AT3G24010) and ING2 (AT1G54390), are also localized in the nucleus and, like mammalian INGs, bind to di- or trimethylated histone H3 lysine 4 (H3K4me2/H3K4me3) via their plant PHD fingers (Lee et al., 2009). Furthermore, the PHD finger of ING2 binds to PIs *in vitro* (Alvarez-Venegas et al., 2006). In split-ubiquitin-based YTH experiments both ING1 and ING2 were tested for protein-protein interaction as baits with GCN5 and PIP5K1 and PIP5K2 as prey, respectively (Fig. 2.3 A).

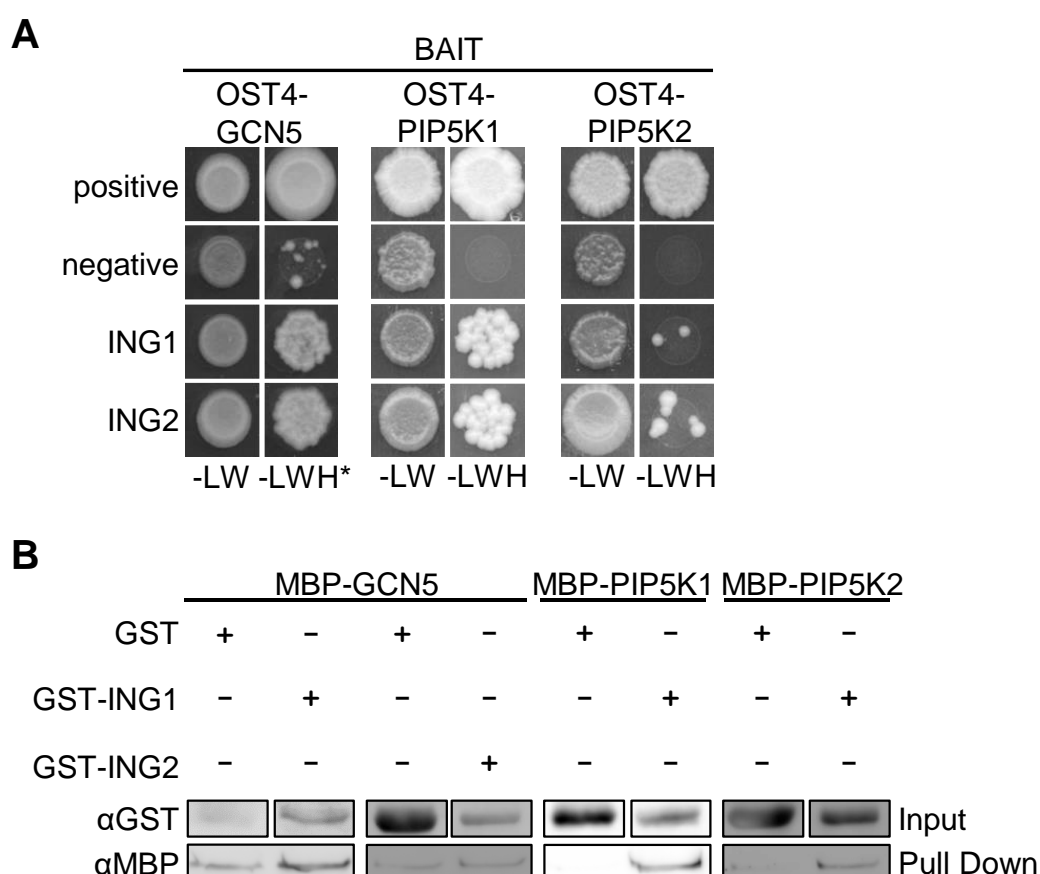


Fig. 2.3: GCN5, PIP5K1 and PIP5K2 interact with the epigenetic readers ING1 and ING2 from Arabidopsis. The interaction of GCN5, PIP5K1 and PIP5K2 with ING1 and ING2 was tested by split-ubiquitin-based YTH analysis and by *in vitro* immuno pull-down analysis. **A**, Split-ubiquitin-based YTH of GCN5, PIP5K1 and PIP5K2 (bait) with ING1 and ING2 (prey). Yeast colonies were grown at 30°C for six days. A representative result of three replicates with five independent colonies of each combination is shown. OST4 fusions localized interactions to ER membranes. *pAI-Alg5* and *pDL2-Alg5*

vectors were used as positive or negative control, respectively. Uniform growth on -LW media (without leucine and tryptophane) indicates equal cell densities and the presence of the respective vectors. Interaction is indicated by growth under selective conditions on -LWH media (without leucine, tryptophane and histidine). *, -LWH medium supplemented with 5 mM 3-amino-1,2,4-triazole (3-AT). **B**, *In vitro* immuno pull-down of GCN5, PIP5K1 and PIP5K2 with ING1 or ING2. Recombinantly expressed GST, GST-ING1 and GST-ING2 were immobilized on glutathione agarose. GST-ING1 and GST-ING2 were incubated with recombinant MBP-tagged GCN5 and GST-ING1 was co-incubated with either MBP-tagged PIP5K1 or PIP5K2 (expression lysates). Bound protein was co-eluted with 50 mM reduced L-glutathione and interacting MBP-tagged proteins were analyzed by immunodetection using an α MBP antibody. Input GST-tagged protein was detected by an α GST antibody. Chemiluminescence signals were recorded with an ECL detection system. Pull-downs were performed twice with the combination GST-ING1/MBP-GCN5; in triplicates with the combination GST-ING2/MBP-GCN5. Pull downs with GST-ING1 and MBP-PIP5K1 were performed in quadruple versions and with GST-ING1 and MBP-PIP5K2 in triplicates.

The YTH analysis indicates that both ING1 and ING2 do interact with GCN5 as well as with PIP5K1 and PIP5K2 (Fig. 2.3 A). These interactions were confirmed in *in vitro* immuno pull-down experiments (Fig. 2.3 B). GST-ING1 and GST-ING2 were immobilized to a glutathione agarose matrix and incubated with different lysates containing MBP-GCN5 or the respective MBP-tagged PI4P 5-kinases. MBP-GCN5, MBP-PIP5K1 and MBP-PIP5K2 were co-eluted with GST-ING1 or GST-ING2 protein, indicating protein-protein interaction (Fig. 2.3 B) and verifying the results from the YTH analysis. These results support the association of PI4P 5-kinases with the nuclear HAT complex. The epigenetic readers ING1 and ING2 and the HAT GCN5 do not only bind mutually but also to PI4P 5-kinases. PI4P 5-kinases or PIs as signaling lipids could be involved in epigenetic regulation and chromatin remodeling. The data indicate mutual interactions between PIP5K1 and PIP5K2 with GCN5 and with ING proteins as well as between ING proteins and GCN5. It is possible that all these components are cooperating in histone modification in the nucleus.

2.3. Overexpression of PIP5K1 or PIP5K2 attenuates GCN5-dependent activation of the *GH3.3* gene

GCN5 is known to be involved in the regulation of a variety of different genes, mainly in stress responses to abiotic stresses (Moraga and Aquea, 2015) or phytohormone signaling (Vlachonasios et al., 2003; Kornet and Scheres, 2009; Weiste and Dröge-Laser, 2014). The gene *GH3.3* (AT2G23170), an auxin-conjugase of the auxin-responsive GH3 family proteins, is regulated by both auxin and GCN5-mediated histone acetylation at *GH3.3* gene locus (Hagen and Guilfoyle, 2002; Staswick et al., 2005; Park et al., 2007; Weiste and Dröge-Laser, 2014; Chiu et al., 2018). It was previously described that in the presence of auxin, *GH3.3* transcription is induced whereas the GCN5 inhibitor butyrolactone 3 leads to a reduced transcriptional response in the presence of auxin (Weiste and Dröge-Laser, 2014). To test whether the GCN5-interactors PIP5K1 and PIP5K2 and their effects on histone acetylation

were relevant for regulating gene expression *in vivo*, we first analyzed the auxin-mediated activation of the GCN5-dependent gene *GH3.3* in the presence or absence of overexpressed PIP5K1 or PIP5K2, respectively. To test this, the experimental setup of Weiste and Dröge-Laser (Weiste and Dröge-Laser, 2014) was extended by adding the transient overexpression of the respective PI4P 5-kinases. Protoplasts as solitary cells are a suitable experimental system to study the influence of PI4P 5-kinases on the expression of genes regulated by auxin. Cells could be easily manipulated in their PI-kinase expression levels and respond individually and uniformly to exogenous auxin treatment, circumventing possible effects of altered auxin distribution between plant tissues, such as those reported for the *Arabidopsis pip5k1 pip5k2* double mutant (Ischebeck et al., 2013; Tejos et al., 2014).

First, time series experiments were performed with untransformed protoplasts to determine at what time *GH3.3* is most strongly expressed in the experimental setup used. For this purpose, protoplasts were incubated for 0.5, 1, 2, 4.25, 16, 18 or 22 h either with 0.25 μM 1-naphthaleneacetic acid (NAA) or NaOH (mock) both diluted in WI buffer (see 4.26.1) and the transcription activation of *GH3.3* was analyzed by quantitative real-time RT PCR (qPCR) (appendix Fig. 6.5). The results showed that *GH3.3* transcription increased for up to 18 h after treatment with NAA (appendix Fig. 6.5). The following experiments were performed with a NAA/mock incubation time of 14 h.

Protoplasts transiently expressing an EYFP control, PIP5K1-EYFP, PIP5K2-EYFP, the catalytically inactive PIP5K2 variant PIP5K2 K470A-EYFP (Stenzel et al., 2012), or PIP5K6-EYFP (Hempel et al., 2017) were treated with NAA or mock, and then transcriptional activation of *GH3.3* was analyzed by qPCR (Fig. 2.4). The relative transcript levels of *GH3.3* were normalized to the transcript abundance of the housekeeping gene *UBC10*.

Overexpression of PIP5K1-EYFP or PIP5K2-EYFP reduced auxin-induced *GH3.3* transcription compared with overexpression of the corresponding EYFP control (Fig. 2.4 A and B), although the transcript-reducing effect by overexpression of PIP5K2-EYFP was more pronounced and also significant (Fig. 2.4 B). By contrast, the expression of the catalytically inactive PIP5K2 K470A-EYFP variant had no effect on the auxin-activation of *GH3.3* transcription (Fig. 2.4 B). Moreover, overexpression of PIP5K6-EYFP, a functionally divergent isoenzyme, showed no effect on *GH3.3* transcription after auxin-induction (Fig. 2.4 C).

The basal *GH3.3* transcript levels of PI4P 5-kinase overexpressing mock-treated samples were also determined and were significantly increased by overexpression of PIP5K2-EYFP and slightly but significantly decreased by overexpression of PIP5K6-EYFP (appendix Fig. 6.6 A, B and C).

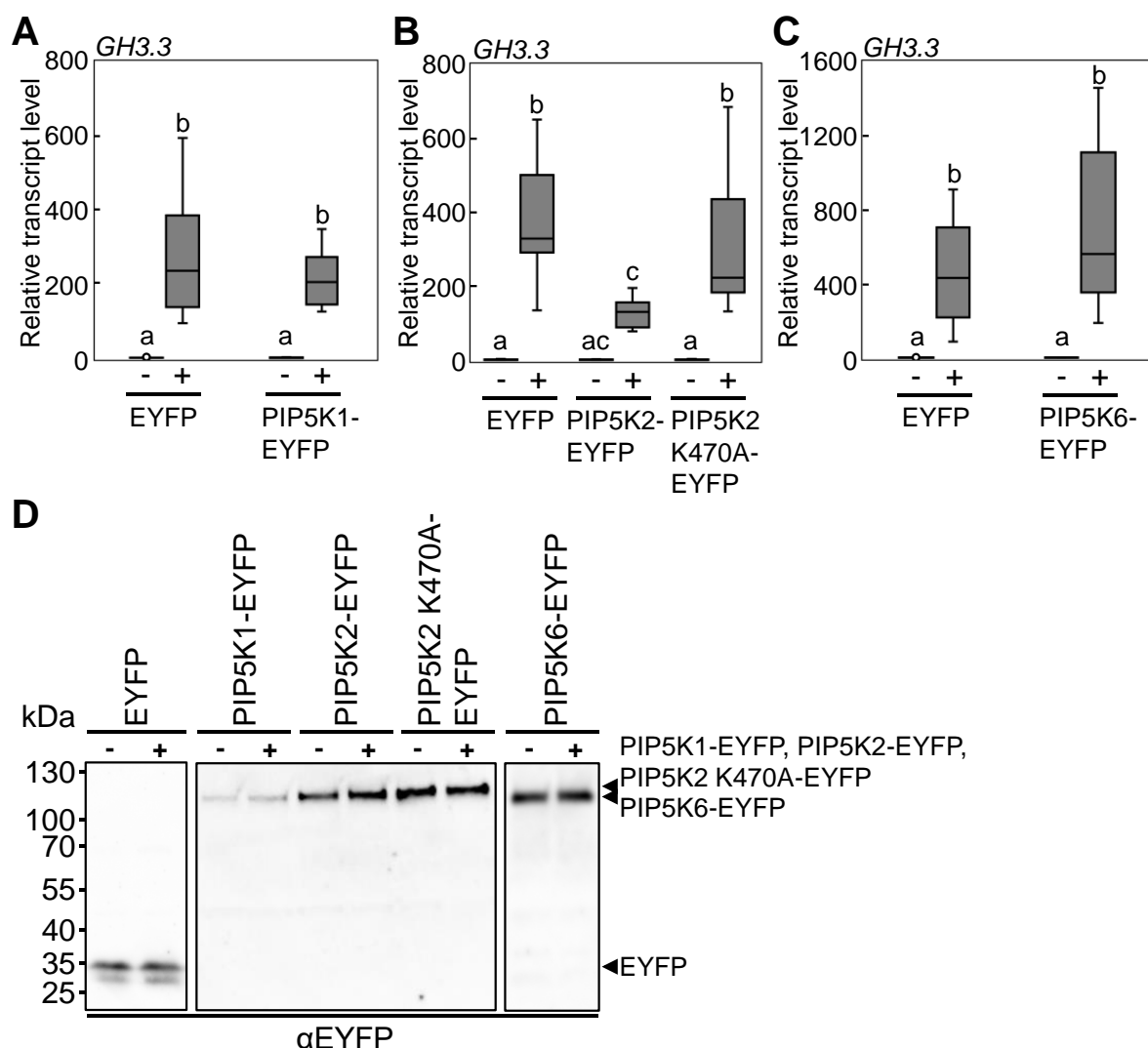


Fig. 2.4: Overexpression of PI4P 5-kinases reduces auxin-activation of *GH3.3*. Relative transcript levels of *GH3.3* in mesophyll protoplasts upon overexpressing either EYFP or the different PI4P 5-kinases and with mock (-) and with 0.25 μ M NAA (+) treatment overnight. Data represent 9 – 16 biological replicates (transformations) from three to four independent protoplast preparations. **A**, Protoplasts transformed with *pEntryA-pCaMV35S::EYFP* or *pEntryA-pCaMV35S::PIP5K1-EYFP*. **B**, Protoplasts transformed with either *pEntryA-pCaMV35S::EYFP*, *pEntryA-pCaMV35S::PIP5K2-EYFP* or *pEntryA-pCaMV35S::PIP5K2 K470A-EYFP*. **C**, Protoplasts transformed with *pEntryA-pCaMV35S::EYFP* or *pEntryD-pCaMV35S::PIP5K6-EYFP*. Transcript levels were normalized to both the reference gene *UBC10* and the transcript levels of the respective mock-treated sample (-). Relative transcript levels are shown as boxplots; dots show outliers. Significant differences were analyzed by one-way ANOVA with a subsequent Tukey's post-hoc test ($P < 0.05$) and indicated by letters a – c. **D**, Immunodetection of EYFP, PIP5K1-EYFP, PIP5K2-EYFP, PIP5K2 K470A-EYFP, and PIP5K6-EYFP overexpression in protoplasts treated as described above was performed using an α EYFP antiserum. Chemiluminescence signals were recorded with an ECL detection system. Immunodetections were performed in triplicates with overexpression of EYFP, PIP5K1-EYFP, PIP5K2-EYFP or PIP5K2 K470A-EYFP and twice with overexpression of PIP5K6-EYFP. PageRuler™ Prestained Protein Ladder was used as a molecular size marker. Expected molecular sizes of full-length proteins, EYFP, 27.0 kDa; PIP5K1-EYFP, 112.9 kDa; PIP5K2-EYFP/PIP5K2 K470A-EYFP, 113.3 kDa; PIP5K6-EYFP, 108.4 kDa.

Endogenous *GCN5* transcript levels were also tested as controls, but these did not change upon expression of the various PI4P 5-kinases and/or upon auxin application (appendix Fig. 6.7 A, B and C). The overexpression of *EYFP*, *PIP5K1-EYFP*, *PIP5K2-EYFP*, *PIP5K2 K470A-EYFP* and *PIP5K6-EYFP* was verified by qPCR (appendix Fig. 6.8 A – F). In addition, expression of the fusion proteins was confirmed by immunodetection with a specific antiserum against EYFP (Fig. 2.4 D). This experiment showed that PIP5K1-EYFP was always expressed to a lower level than the other EYFP fusion proteins, which may have been associated with the lower effect of PIP5K1-EYFP overexpression on auxin-activated *GH3.3* transcription.

The data suggest that the overexpression of PIP5K2-EYFP results in altered auxin-activation of *GH3.3* transcription. This observation is consistent with the observed effects of PIP5K2 overexpression on histone H3 acetylation in Arabidopsis plants (section 2.1, Fig. 2.1). No clear effect was obtained with PIP5K1-EYFP, possibly due to its lower expression (Fig. 2.4 D) or its lower intrinsic catalytic activity (Ischebeck et al., 2013), nor with PIP5K6-EYFP, possible also due to its lower catalytic activity (Stenzel et al., 2012) or its functional divergence from PIP5K1/PIP5K2 (Zhao et al., 2010; Stenzel et al., 2012; Hempel et al., 2017; Menzel et al., 2019; Fratini et al., 2021).

In addition to *GH3.3* gene activation, the auxin-mediated transcriptional activation of the genes *indole-3-acetic acid inducible 2 (IAA2, AT3G23030)*, *indole-3-acetic acid inducible 5 (IAA5, AT1G15580)* and *indole-3-acetic acid inducible 19 (IAA19, AT3G15540)* was also tested. Auxin treatment was adjusted to the auxin-induction maxima of *IAA2*, *IAA5*, and *IAA19* and performed for 2.5 h with 2 μ M NAA (see section 4.26.1). Data on auxin inducibility and time points were chosen according to data from the Arabidopsis eFP Browser database (Winter et al., 2007).

Overexpression of PIP5K2-EYFP had again a significant effect and attenuated auxin-mediated transcription of *IAA2* and *IAA5* as of *GH3.3* (Fig. 2.5 B and E). No effect was detected for auxin-induction of *IAA19* (appendix Fig. 6.9 E). Overexpression of PIP5K1-EYFP did not affect auxin-mediated transcription of *IAA2* and *IAA5* (Fig. 2.5 A and D), but showed that transcription of *IAA19* was reduced (appendix Fig. 6.9 D). Overexpression of PIP5K1 therefore showed a possibly differential effect on auxin-induced gene activation of *IAAs*. Overexpression of PIP5K6-EYFP had no effect on auxin-induced gene transcription of the *IAAs* studied (Fig. 2.5 C and F and appendix Fig. 6.9 F). Future experiments will have to expand in elucidating such differences, which could not be resolved in this first description of the effect. Basal transcript levels of *IAA2*, *IAA5* and *IAA19* of mock-treated samples were also determined and were not divergent upon overexpression of EYFP, PIP5K1-EYFP, PIP5K2-EYFP or PIP5K6-EYFP (appendix Fig. 6.6 D, E, F, G, H and I and appendix Fig. 6.9 A, B and C).

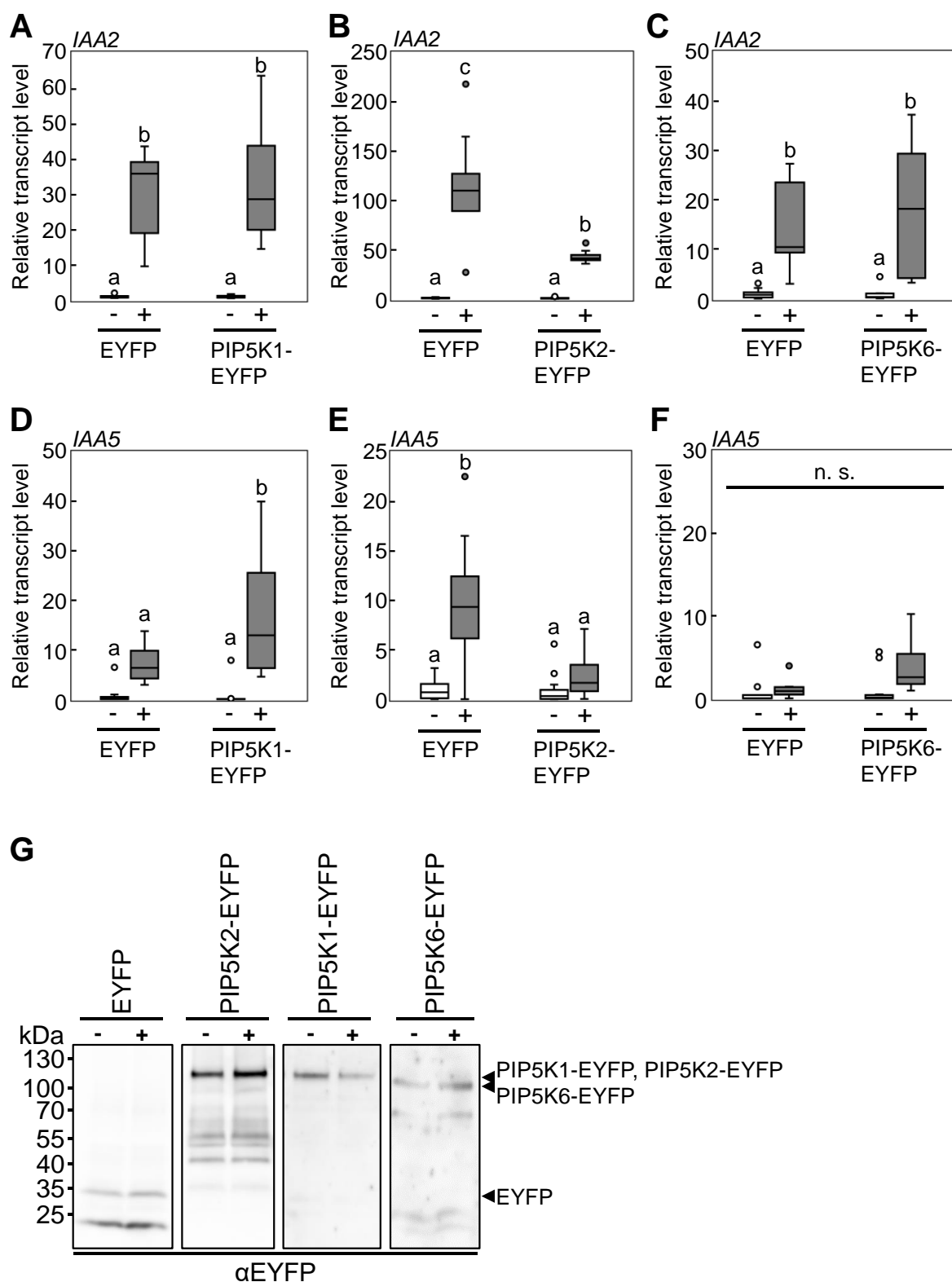


Fig. 2.5: Overexpression of PI4P 5-kinases reduces auxin-activation of *IAA2* and *IAA5*. Relative transcript levels of *IAA2* (A-C) and *IAA5* (D-F) in mesophyll protoplasts upon overexpressing either EYFP or the different PI4P 5-kinases and with mock (-) and with 2 μ M NAA (+) treatment for 2.5 h. Data represent 8 – 12 biological replicates (transformations) from three independent protoplast preparations. **A**, *IAA2* transcript levels in protoplasts transformed with *pEntryA-pCaMV35S::EYFP* or *pEntryA-pCaMV35S::PIP5K1-EYFP*. **B**, *IAA2* transcript levels in protoplasts transformed with *pEntryA-pCaMV35S::EYFP* or *pEntryA-pCaMV35S::PIP5K2-EYFP*. **C**, *IAA2* transcript levels in protoplasts transformed with *pEntryA-pCaMV35S::EYFP* or *pEntryD-pCaMV35S::PIP5K6-EYFP*.

D, *IAA5* transcript levels in protoplasts transformed with *pEntryA-pCaMV35S::EYFP* or *pEntryA-pCaMV35S::PIP5K1-EYFP*. **E**, *IAA5* transcript levels in protoplasts transformed with *pEntryA-pCaMV35S::EYFP* or *pEntryA-pCaMV35S::PIP5K2-EYFP*. **F**, *IAA5* transcript levels in protoplasts transformed with *pEntryA-pCaMV35S::EYFP* or *pEntryD-pCaMV35S::PIP5K6-EYFP*. Transcript levels were normalized to both the reference gene *UBC10* and the transcript levels of the respective mock-treated sample (-). Relative transcript levels are shown as boxplots; dots show outliers. Significant differences were analyzed by one-way ANOVA with a subsequent Tukey's post-hoc test ($P < 0.05$) and indicated by letters a – c. n.s., not significant. **G**, Immunodetection of EYFP, PIP5K1-EYFP, PIP5K2-EYFP, PIP5K2 K470A-EYFP, and PIP5K6-EYFP overexpression in protoplasts treated as described above were performed using an α EYFP antiserum. Chemiluminescence signals were recorded with an ECL detection system. Immunodetections were performed in triplicates with overexpression of EYFP, PIP5K1-EYFP or PIP5K2-EYFP and twice with overexpression of PIP5K6-EYFP. PageRuler™ Prestained Protein Ladder was used as a molecular size marker. Expected molecular sizes of full-length proteins, EYFP, 27.0 kDa; PIP5K1-EYFP, 112.9 kDa; PIP5K2-EYFP, 113.3 kDa; PIP5K6-EYFP, 108.4 kDa.

The endogenous *GCN5* transcript levels were also analyzed and can serve as a control for the overall experimental setup, as *GCN5* transcript abundance did not vary upon auxin-activation or upon transient overexpression of EYFP-tagged PI4P 5-kinases (appendix Fig. 6.7 D, E and F). The overexpression of *EYFP*, *PIP5K1-EYFP*, *PIP5K2-EYFP* and *PIP5K6-EYFP* was also verified by qPCR (appendix Fig. 6.8 G – L) and the expression of the fusion proteins was confirmed by immunodetection with a specific antiserum against EYFP (Fig. 2.5 G).

The data on the effects of overexpressed PI4P 5-kinase variants on auxin-activation of selected genes indicate that PIs contribute to transcriptional control of *GH3.3* expression and probably other auxin-inducible genes, possibly by influencing histone acetylation.

2.4. PtdIns(4,5)P₂ and other PIs inhibit histone acetyltransferase activity of recombinant GCN5 protein *in vitro*

The results so far suggested that in particular altered PIP5K2 expression may influence histone H3 acetylation and the activation of *GCN5*-regulated genes upon auxin application. These effects seemed to be dependent on PIP5K2 catalytic activity (Fig. 2.4) and, thus, on the reaction product PtdIns(4,5)P₂. Therefore, a direct effect of PtdIns(4,5)P₂ or an effect of other PIs, that can function as substrates or reaction products of PI4P 5-kinases, on *GCN5* histone acetylation activity was tested.

To test whether PIs had an effect on *GCN5*, *in vitro* histone acetylation assays were performed with recombinant *GCN5* protein in the presence or absence of different PIs. Before this experiments were started, an *in vitro* *GCN5* activity assay was established on basis of an assay by Gadhia and coworkers ((Gadhia et al., 2017), section 4.24) and was first characterized. The assay employs recombinantly expressed and affinity enriched MBP-*GCN5* protein, which is tested for catalytic activity with acetyl coenzyme A (acetyl-CoA) as acetyl donor against recombinant histone H3 as a substrate (Fig. 2.6 A).

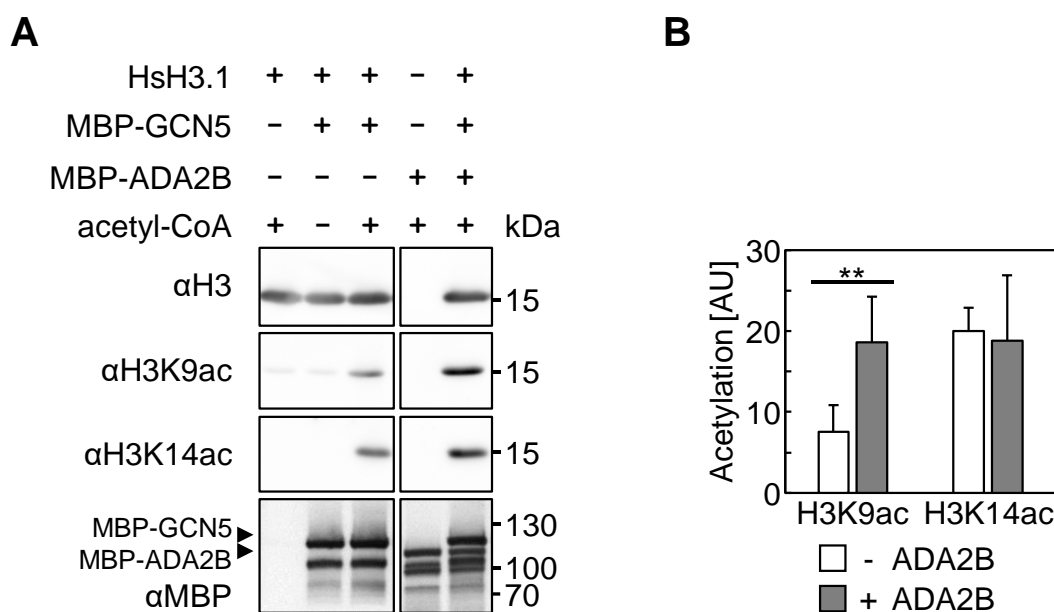


Fig. 2.6: *In vitro* GCN5 acetylation activity. Histone acetylation with enriched recombinant MBP-GCN5 protein was studied *in vitro* in the absence and presence of acetyl-CoA and ADA2B. The formation of H3K9ac and H3K14ac was detected with specific antibodies. Chemiluminescent signals were recorded using an ECL detection system. **A**, *In vitro* histone H3 acetylation activity of GCN5 in presence or absence of acetyl-CoA and with and without ADA2B. Reactions were stopped after 60 min. The data are representative for four individual experiments. PageRuler™ Prestained Protein Ladder was used as a molecular size marker. Expected molecular sizes of full-length proteins, histone H3, 15.3 kDa; MBP-GCN5, 105.6 kDa; MBP-ADA2B, 98.2 kDa. **B**, Quantification of H3K9ac and H3K14ac in presence and absence of ADA2B. The intensity of the detected H3K9ac and H3K14ac in A was analyzed with ImageJ/Fiji (Schindelin et al., 2012). The degree of acetylation is expressed in arbitrary units (AU). Data represent means, error bars show standard deviation for four independent experiments. Asterisks indicate significant differences in GCN5 activity according to a Student's T-test (** $P \leq 0.01$).

GCN5 acetylates histone H3 at positions H3K9 and H3K14 (Benhamed et al., 2006; Zhang et al., 2007; Servet et al., 2010; Shen et al., 2015). The *in vitro* formation of H3K9ac and H3K14ac was individually detected using specific antibodies, confirming the intrinsic histone acetylation activity of the recombinant MBP-GCN5 protein used (Fig. 2.6 A). Experiments with and without acetyl-CoA co-substrate showed that the specific histone H3 acetylation antibodies detect only acetylated histones when acetyl-CoA was present in the assay (Fig. 2.6 A). In addition, the activating effect of recombinant ADA2B on GCN5 (Mao et al., 2006; Servet et al., 2010; Weiste and Dröge-Laser, 2014) was tested (Fig. 3.6 A and B). The addition of recombinant ADA2B protein significantly enhanced GCN5 acetylation at H3K9 but not at H3K14, as shown in Fig. 2.6 A and B. Since GCN5 was active in the assay and the enzyme activity could be influenced by the addition of ADA2B, the HAT assay was considered functional and suitable to assess quantitative changes in histone acetylation.

MBP-GCN5-mediated histone acetylation was next tested in the presence and the absence of added PIs. PIs carry a strong anionic charge in the lipid head group and histones have strongly positively charged N-termini, resulting in electrostatic interactions. In order to minimize

saturation effects of the positive lysine residues by added PIs and thereby exclude the possibility that histone acetylation was limited only by the binding of PIs to lysines, the stoichiometric ratio of lipid to basic histone residues was estimated. There are 18 basic (i.e. putatively positively charged lysines and arginines) amino acids in the first 56 amino acids of the histone tail of histone H3. The amount of phospholipid used in the HAT reactions was 0.127 nmol per 0.055 nmol of histone H3 used (each with 18 basic residues), resulting in a lipid vs. basic residue stoichiometry of 0.127 to 1. Based on this estimate, the net charge effect between PIs and histones should thus be minimal. For effects on GCN5 activity, phosphatidylcholine (PtdCho), phosphatidic acid (PtdOH), and the PIs PtdIns3P, PtdIns4P, PtdIns(3,5)P₂, and PtdIns(4,5)P₂ were tested (Fig. 2.7 A) and immunodetection signals of H3K9ac (Fig. 2.7 B) and H3K14ac (Fig. 2.7 C) were quantified with ImageJ/Fiji (Schindelin et al., 2012).

PtdCho as a neutral lipid control did not reduce MBP-GCN5 acetylation activity and PtdOH caused a slight effect compared to a sample without lipid or the sample with PtdCho, but this effect was not significant (Fig. 2.7 A – C). By contrast, reduced MBP-GCN5 acetylation activity, in the form of reduced signal intensities for H3K9ac and H3K14ac immunodetection, was evident in the presence of the PIs (Fig. 2.7 A – C). It was noticeable that the acetylation activity toward H3K9 was not as strongly affected as that toward H3K14. The decrease in the formation of H3K14ac was significantly reduced in the presence of different PIs. The strongest and most significant inhibitory influence was exerted by PtdIns3P, PtdIns(3,5)P₂ and PtdIns(4,5)P₂ on GCN5 acetylation activity (Fig. 2.7 A – C).

Since PtdIns3P and PtdIns(4,5)P₂ showed a clear influence on the acetylation activity of GCN5, these lipids were selected to further analyze their influence on the catalytic activity of GCN5 in a temporal context as an alternative to a kinetic measurement. For this purpose, histone H3 acetylation was monitored over a period of 20 to 120 min, and samples were analyzed at 20 min-intervals (Fig. 2.8). In the presence of PtdIns3P and PtdIns(4,5)P₂, histone H3 at positions H3K9 and H3K14 was less acetylated than in the samples without PIs (Fig. 2.8). Overall, the histone H3 acetylation status of the PI treated samples never reached that of the samples without PIs (Fig. 2.8 A, B and C for PtdIns3P and Fig. 2.8 D, E and F for PtdIns(4,5)P₂). The incubation time of the previous HAT assays with or without PIs (Fig. 2.6 and Fig. 2.7) was confirmed to be optimal at 60 min. These experimental data indicate a direct effect of PIs on the GCN5-mediated acetylation of histone H3, which is expressed in decreased catalytic activity of the HAT enzyme. However, the mode of action by which PIs might affect the catalytic activity of GCN5, remains currently unclear.

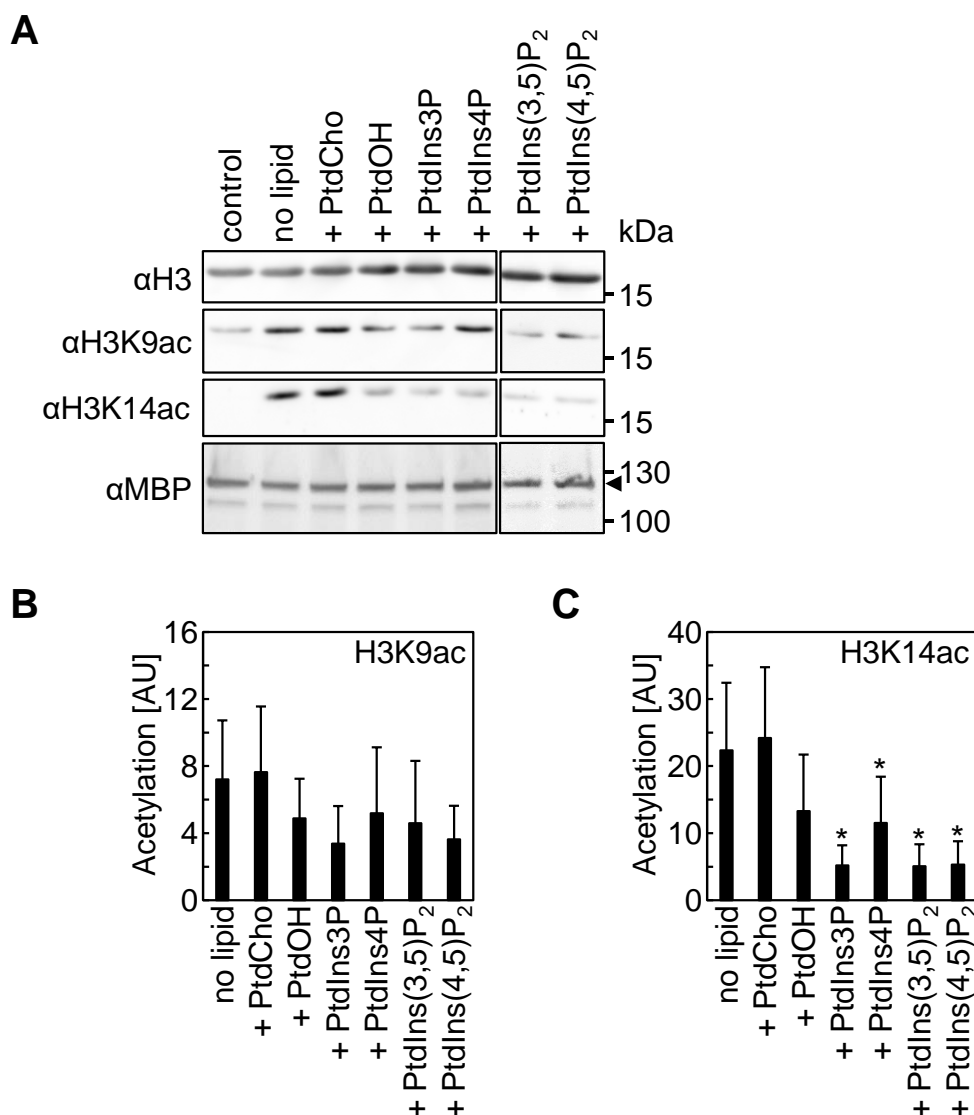


Fig. 2.7: *In vitro* GCN5 acetylation activity is compromised in presence of PIs. Histone H3 acetylation by enriched recombinant MBP-GCN5 protein was studied *in vitro* in the absence and presence of various phospholipids. The formation of H3K9ac and H3K14ac was detected with specific antibodies. PageRuler™ Prestained Protein Ladder was used as a molecular size marker. Chemiluminescent signals were recorded using an ECL detection system. The arrow indicates MBP-GCN5. **A**, Immunodetection with specific antibodies against histone H3, H3K9ac, H3K14ac and MBP. The *in vitro* histone acetylation is shown after 60 min incubation with 0.127 nmol phospholipids, as indicated. Control, reaction performed without the addition of phospholipids and without acetyl-CoA; no lipid, reaction without any phospholipids. Expected molecular sizes of full-length proteins, histone H3, H3K9ac and H3K14ac, 15.3 kDa; MBP-GCN5, 105.6 kDa. **B**, **C**, Quantification of H3K9ac and H3K14ac ECL signals in presence and absence of phospholipids with ImageJ/Fiji (Schindelin et al., 2012). Absolute acetylation was quantified and expressed in arbitrary units (AU). Data represent means, error bars show standard deviation for at least four independent experiments. Asterisks indicate significant differences in GCN5 activity between samples with PtdCho and other added phospholipids according to a Student's T-test (* $P \leq 0.05$). **B**, Quantification of H3K9ac. No significant differences were found. **C**, Quantification of H3K14ac.

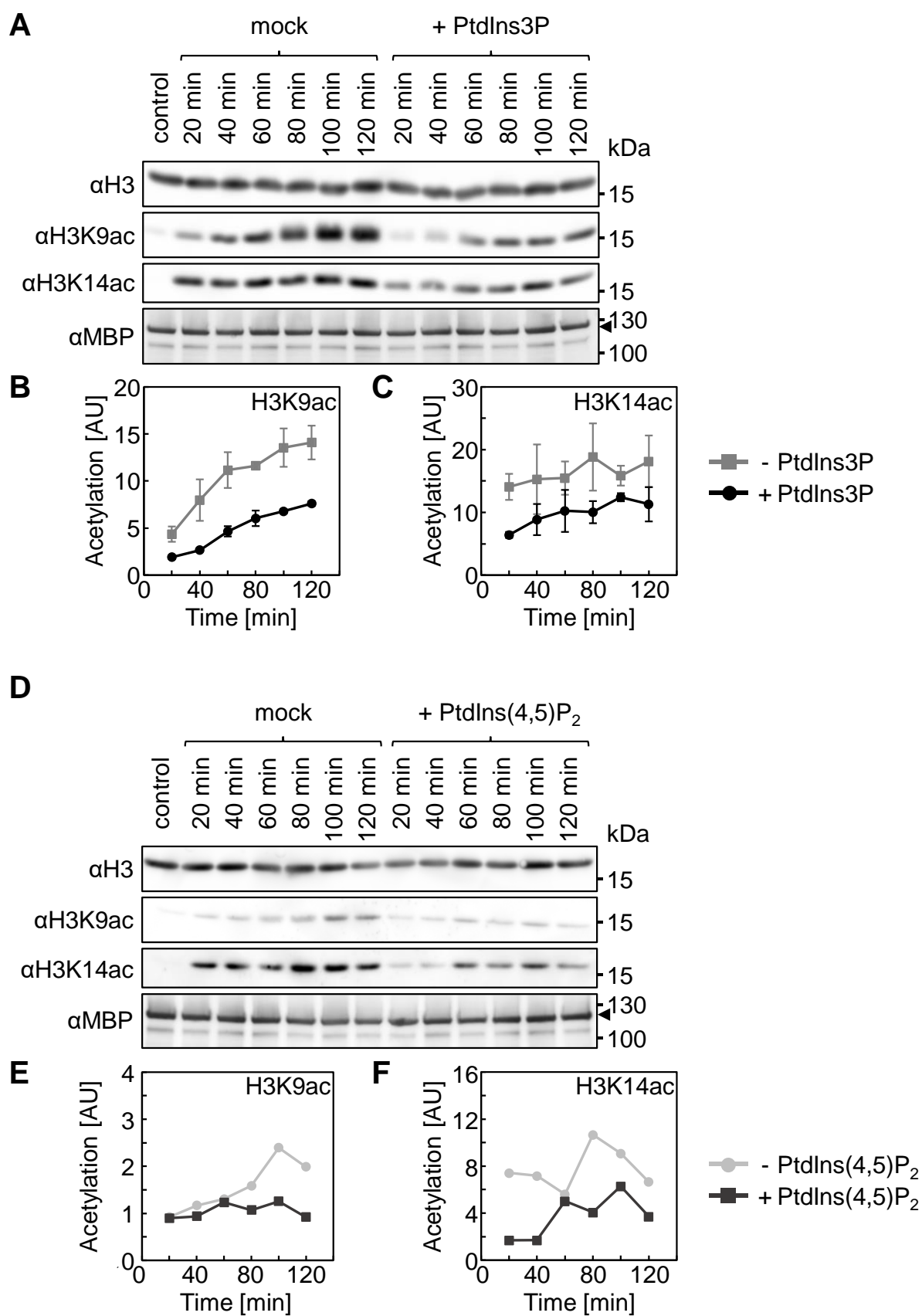


Fig. 2.8: GCN5 acetylation activity *in vitro* in presence of PIs over time. Time course experiment of histone H3 acetylation by GCN5 in the presence of 0.127 nmol PtdIns3P (**A-C**) or PtdIns(4,5)P₂. (**D-F**). The acetylation reactions were stopped after 20, 40, 60, 80, 100 and 120 min, respectively. The formation of H3K9ac and H3K14ac was detected with specific antibodies. Expected molecular sizes of

full-length proteins, histone H3, H3K9ac, H3K14ac, 15.3 kDa; MBP-GCN5, 105.6 kDa. PageRuler™ Prestained Protein Ladder was used as a molecular size marker. Chemiluminescent signals were recorded using an ECL detection system. The arrow indicates MBP-GCN5. **A**, *In vitro* acetylation of histone H3 at H3K9 and H3K14 in absence (mock) or presence of PtdIns3P. Control sample lacking acetyl-CoA was stopped after 60 min. The tests were performed in three independent experiments with similar results. **B**, **C**, Quantification of H3K9ac and H3K14ac ECL signals in presence and absence of PtdIns3P with ImageJ/Fiji (Schindelin et al., 2012). Absolute acetylation was quantified and expressed in arbitrary units (AU). Data represent means, error bars show standard deviation for three independent experiments. **B**, Quantification of H3K9ac in presence of PtdIns3P. **C**, Quantification of H3K14ac in presence of PtdIns3P. **D**, *In vitro* acetylation of histone H3 at H3K9 and H3K14 in absence (mock) or presence of PtdIns(4,5)P₂. Control sample lacking acetyl-CoA was stopped after 60 min. The tests were performed in two independent experiments with similar results. **E**, **F**, Quantification of H3K9ac and H3K14ac ECL signals in presence and absence of PtdIns(4,5)P₂ with ImageJ/Fiji (Schindelin et al., 2012). Absolute acetylation was quantified and expressed in arbitrary units (AU). The diagrams are representative for two independent experiments. **E**, Quantification of H3K9ac in the presence of PtdIns(4,5)P₂. **F**, Quantification of H3K14ac in presence of PtdIns(4,5)P₂.

2.5. Recombinant MBP-GCN5 protein binds PIs

To better understand how PIs might exert an influence on GCN5 functionality and histone acetylation, the direct binding of recombinant MBP-GCN5 to PIs was investigated *in vitro* by lipid overlay assays and by liposome sedimentation tests (Fig. 2.9). Lipid binding of recombinantly expressed and enriched MBP-GCN5 was first tested in lipid overlay assays with commercially available PIP strips containing various phospholipids, as shown in the schematic representation in Fig. 2.9 A. MBP protein was used as a negative control and did not show any lipid binding (Fig. 2.9 B, left panel). By contrast, MBP-GCN5 bound to the PtdIns-monophosphates PtdIns3P, PtdIns4P and PtdIns5P (Fig. 2.9 B, as indicated). The binding to PtdIns3P seemed to be most prominent. Arabidopsis ING proteins ING1 and ING2 were also tested for lipid binding in lipid overlay assays. The PHD domain of ING2 has already been demonstrated to bind to PIs (Alvarez-Venegas et al., 2006), and mammalian ING proteins are also known to bind to PIs (Gozani et al., 2003). Here, recombinant full-length MBP-ING1 and MBP-ING2 protein bound to PtdIns-monophosphates PtdIns3P, PtdIns4P and PtdIns5P and to PtdSer in lipid overlay assays (Fig. 2.9 B, as indicated). The enriched proteins used for lipid overlay assays are shown in appendix Fig. 6.10. The specificity of the binding assays was confirmed by using the commercial control proteins PtdIns3P Grip and PtdIns(4,5)P₂ Grip, which showed specific binding to PtdIns3P or PtdIns(4,5)P₂, respectively, as intended (appendix Fig. 6.11).

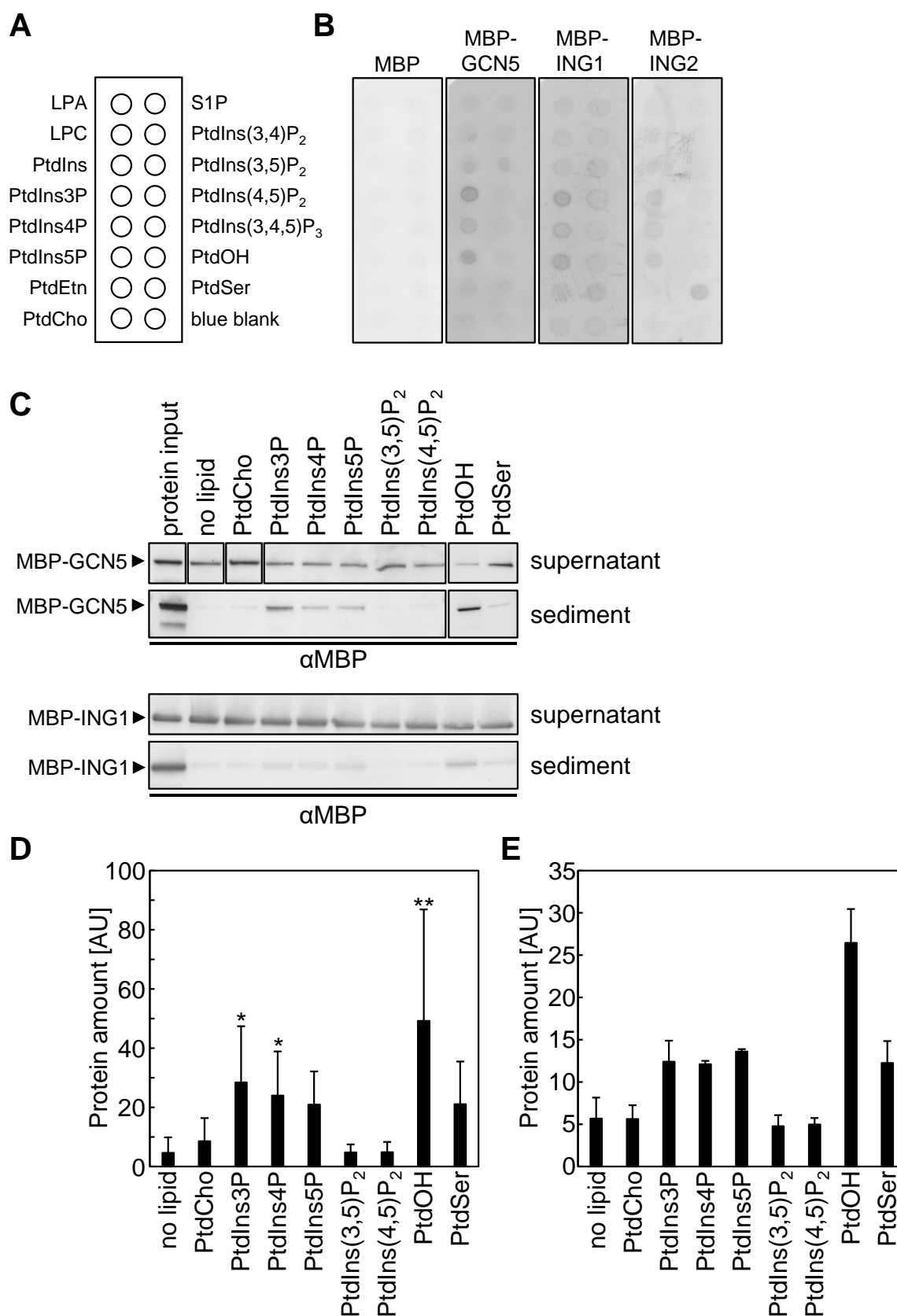


Fig. 2.9: Lipid interaction studies of GCN5 and ING proteins with PIs. The phospholipid binding of purified recombinant MBP-GCN5 and MBP-ING1/MBP-ING2 was examined by lipid overlay assays and liposome sedimentation assays. **A**, Schematic representation of the PIP strips used for lipid overlay assays. Next to the important PIs in plants (PtdIns3P, PtdIns4P, PtdIns5P, PtdIns(3,5)P₂, PtdIns(4,5)P₂) also the non-plant specific PIs, phosphatidylinositol 3,4-bisphosphate (PtdIns(3,4)P₂),

phosphatidylinositol 3,4,5-trisphosphate (PtdIns(3,4,5)P₃) and further phospholipids were spotted, lysophosphatidic acid (LPA), lysophosphatidylcholine (LPC), sphingosine 1-phosphate (S1P), phosphatidylinositol (PtdIns), phosphatidylethanolamine (PtdEtn), phosphatidylcholine (PtdCho), phosphatidic acid (PtdOH), phosphatidylserine (PtdSer). **B**, Lipid overlay assays with enriched MBP, MBP-GCN5 and MBP-ING1/MBP-ING2 protein fractions. Interactions were visualized by using a primary antiserum against MBP and a secondary antiserum with an AP conjugate. AP detection was performed. The experiment was repeated twice with similar results. **C**, Liposome sedimentation assays of MBP-GCN5 and MBP-ING1. Liposome sedimentation assays were performed with liposomes prepared with PtdCho alone (control) or with a mixture of PtdCho and either PtdIns3P, PtdIns4P, PtdIns5P, PtdIns(3,5)P₂, PtdIns(4,5)P₂, PtdOH or PtdSer. No lipid, control sample without liposomes. Supernatant, contained unbound protein. Sediment, protein that had bound to respective liposomes. Proteins were separated on an SDS-PAGE and detected by immunoblots with the use of the specific antibody against MBP and a secondary antibody conjugated to AP. AP detection was performed. PageRuler™ Prestained Protein Ladder was used as a molecular size marker. Expected molecular size of full-length proteins, MBP-GCN5, 105.6 kDa, MBP-ING1, 68.6 kDa. The samples shown in line are from the same blots; the blots were only split to show the samples in a meaningful order. Experiments were performed 3 – 11 times (MBP-GCN5) or twice (MBP-ING1) with similar results. **D**, Quantification of bound MBP-GCN5 in the liposome sedimentation assay shown in C with ImageJ/Fiji (Schindelin et al., 2012). AU, arbitrary units. Data represent means and error bars show standard deviations for at least three independent experiments. Asterisks indicate significant differences of bound MBP-GCN5 compared with the PtdCho sample according to Student's T-test (* $P \leq 0.05$; ** $P \leq 0.01$). **E**, Quantification of bound MBP-ING1 in the liposome sedimentation assay shown in C with ImageJ/Fiji (Schindelin et al., 2012). AU, arbitrary units. Data represent means and error bars show standard deviations for two independent experiments.

PI binding of MBP-GCN5 and MBP-ING1 was alternatively tested in liposome sedimentation assays, where lipids are presented in vesicles, so-called liposomes. This experimental design is considered to be more physiologically meaningful than binding studies with spotted lipids, because PIs are used in mixtures with structural lipids and are embedded into a bilayer membrane (Julkowska et al., 2013). Liposomes prepared by extrusion had a diameter of 0.2 μm and consisted of 75 % PtdCho as a backbone and 25 % of each examined PI. Protein bound to liposomes was detected in the sediment fractions, whereas the supernatant contained unbound MBP-GCN5 or MBP-ING1 protein. MBP-tagged proteins in the supernatant and sediment fractions were visualized via immunodetection with a specific antiserum against the MBP epitope. MBP-GCN5 was detected by immunodetection in the sediments of liposomes containing the PtdIns-monophosphates PtdIns3P, PtdIns4P, PtdIns5P and PtdOH (Fig. 2.9 C, as indicated), indicating binding to these lipids. A weak signal was also detected in the PtdSer-containing liposome sample (Fig. 2.9 C, as indicated). MBP-ING1 was detected in liposomes containing PtdIns3P, PtdIns4P, PtdIns5P, PtdOH and PtdSer (Fig. 2.9 C), indicating binding to these lipids. Binding tests without liposomes served as a negative control (Fig. 2.9 C, as indicated).

Immunodetection signals were quantified using ImageJ/Fiji (Schindelin et al., 2012) (Fig. 2.9 D and E). Binding of MBP-GCN5 to PtdIns-monophosphates PtdIns3P and PtdIns4P and to PtdOH was significantly higher than binding to PtdCho (Fig. 2.9 D). PI binding by MBP-ING1 was also quantified and confirmed to be higher than binding to PtdCho (Fig. 2.9 E). Again,

MBP was used as a control but showed no lipid binding in liposome sedimentation assays (appendix Fig. 6.12).

The results reveal PI binding capability for GCN5 whereas slight binding preference for PtdIns3P was observed. ING1 did not show a preference for one of the PtdIns-monophosphates in liposome sedimentation assays.

2.5.1. Identification of the putative lipid binding site in GCN5

To further elucidate PtdIns3P binding to GCN5, the GCN5 amino acid sequence was analyzed to identify amino acid residues likely to contribute to a potential lipid binding region. A computer-based analysis for hydrophobic and basic protein regions, BH-search (Brzeska et al., 2010), was used. The resulting BH-search score for each position is calculated not only based on the individual amino acid residue, but also considers the amino acid sequence surrounding each specific amino acid (Brzeska et al., 2010). Lipid/membrane binding capability is indicated by a BH-search score ≥ 0.6 . For GCN5, a small basic hydrophobic amino acid region was identified at the beginning of the acetyltransferase domain that had a score of approximately 0.6. This was the region around amino acid residue K261 with a score of 0.613. Two further positively charged residues, R260 and K263, could be identified in the immediate vicinity (Fig. 2.10 A and B). Since this cluster of basic/positively charged amino acid residues could well be part of an NLS, the amino acid sequence of GCN5 was examined using NLS prediction programs (see section 4.29.3). This analysis revealed a putative NLS at the N-terminus of GCN5 from amino acids 36 to 39. This position of a putative NLS of Arabidopsis GCN5 fits well with the information about the NLS of GCN5 from *Toxoplasma gondii*, which is found at a similar position (Bhatti and Sullivan, 2005; Dixon et al., 2011).

To examine whether this predicted basic-hydrophobic amino acid stretch is responsible for PI binding capability of GCN5, the relevant basic amino acid residues R260, K261 and K263 within the candidate region were substituted with either non-polar or acidic amino acids. The GCN5 sequence variants generated contained the amino acid substitutions GCN5_{R260I,K261L,K263L} and GCN5_{R260E,K261D,K263D} and were consequently named GCN5_{ILL} and GCN5_{EDD} (Fig. 2.10 A). BH-analyses of these substitution variants revealed that the basic hydrophobic amino acid region previously predicted in GCN5 was now undetectable in both substitution variants and none of the amino acids exceeded a value of 0.6 (appendix Fig. 6.13 A and B). For MBP-ING1, MBP-ING2 and MBP, a BH-search was performed as a control. While MBP-ING1 and MBP-ING2 contain amino acids which exceed a BH-score of 0.6, indicating lipid binding motifs (appendix Fig. 6.13 C and D), none of the residues in the MBP sequence exceeded a BH-score of 0.6 (appendix Fig. 6.13 E). This result is consistent with the lipid binding capability of the proteins as shown in Fig. 2.9.

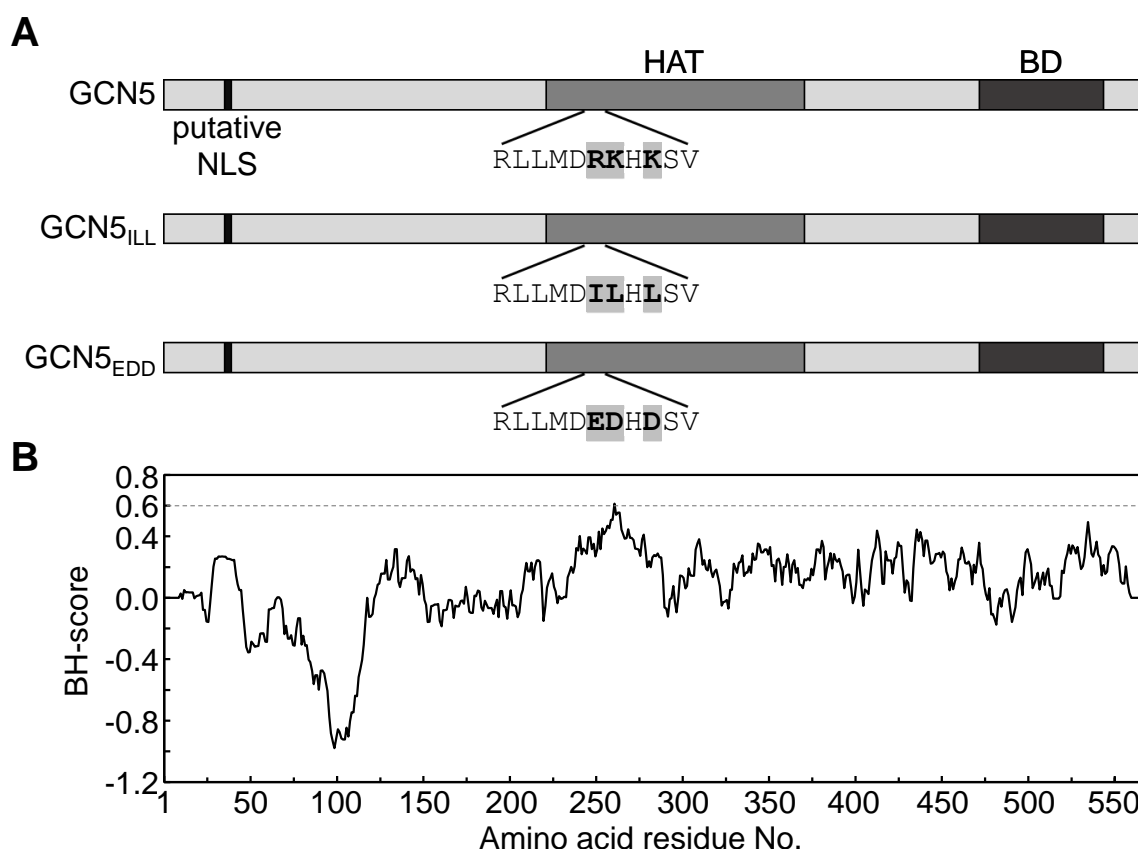


Fig. 2.10: GCN5 amino acid sequence contains a putative phospholipid binding site. The amino acid sequence of GCN5 was analyzed for lipid binding sites. **A**, Schematic view of GCN5, GCN5_{ILL} and GCN5_{EDD}. GCN5 variants consist of 568 aa. GCN5 contains a putative NLS sequence at the N-terminus (aa 36 – 39), a HAT domain (aa 222 – 371) and a bromodomain (aa 472 – 543). The HAT domain contains a basic hydrophobic region within the sequence aa 255 – 265. Abbreviations are BD, bromodomain; HAT, histone acetyltransferase, NLS, nuclear localization sequence. **B**, BH-search of GCN5. BH-search was conducted with the online tool according to Brzeska and coworkers (Brzeska et al., 2010). Per amino acid a value is calculated that includes the amino acid surrounding of the single amino acid. Values higher than the threshold 0.6 indicate a basic-hydrophobic (BH) amino acid stretch, a putative phospholipid binding site. K261 within the GCN5 sequence reaches score 0.613. In GCN5_{ILL} the three amino acid substitutions R260I, K261L and K263L were introduced. In GCN5_{EDD} the three amino acid substitutions R260E, K261D and K263D were introduced. BH-searches of GCN5_{ILL} and GCN5_{EDD} are shown in appendix Fig. 6.13.

The recombinantly expressed and enriched MBP-GCN5_{ILL} and MBP-GCN5_{EDD} proteins were analyzed in liposome sedimentation assays, and both showed attenuated to undetectable PI binding (Fig. 2.11). However, both GCN5_{ILL} and GCN5_{EDD} still bound to PtdOH, but to a somewhat lesser degree than wild type GCN5 (compare Fig. 2.9 C and Fig. 2.11 A and B). The signal intensities detected for the MBP-GCN5_{ILL} and MBP-GCN5_{EDD} variants in the liposome sediments were quantified using ImageJ/Fiji (Schindelin et al., 2012) and were all comparable to those of the PtdCho-controls (PtdCho liposomes, Fig. 2.11 C and D). Thus, the amino acid residues R260, K261 and K263 might be involved in PI binding of GCN5 and the substitutions in the basic/hydrophobic motif in the beginning of the HAT domain of GCN5 lead to a loss of PI binding capability.

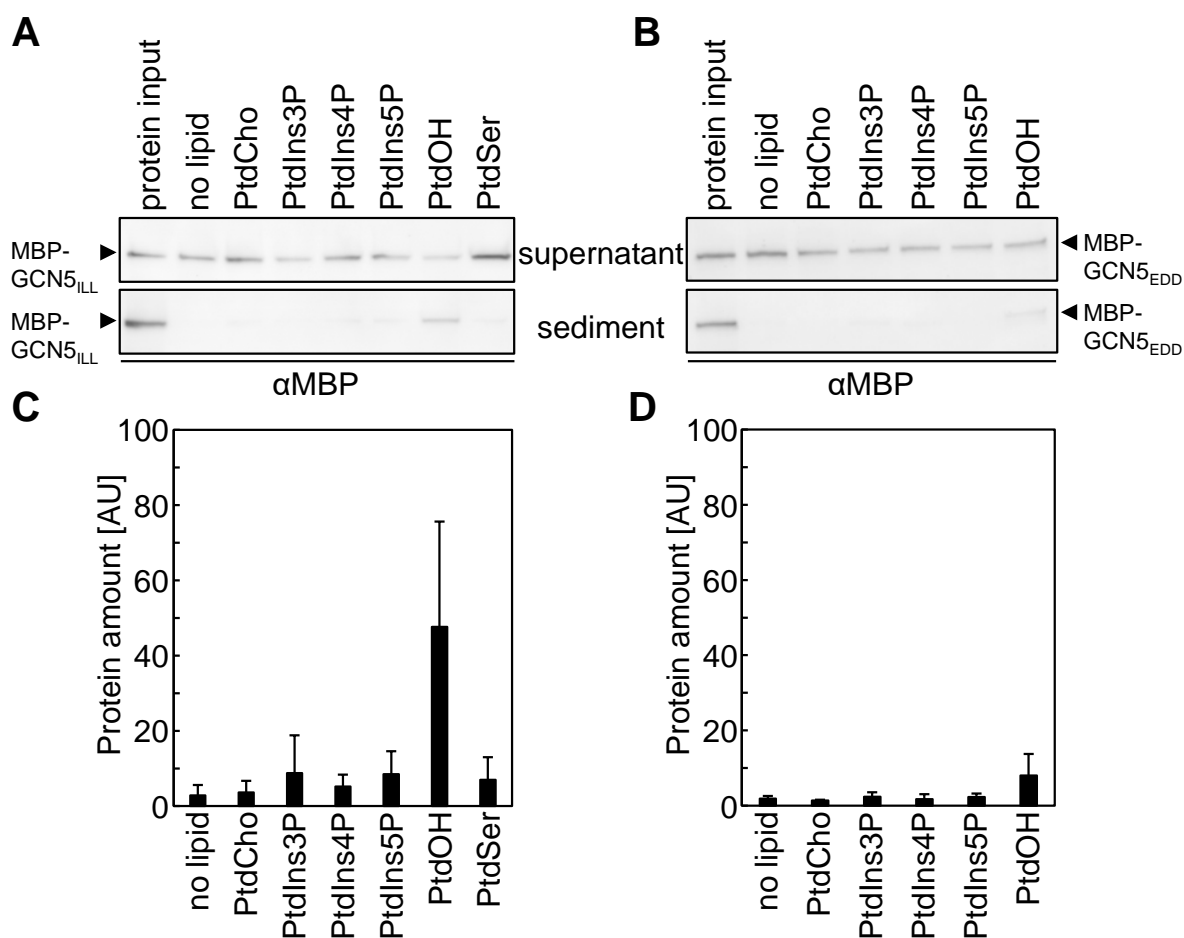


Fig. 2.11: Lipid interaction studies of GCN5^{ILL} and GCN5^{EDD}. The phospholipid binding of purified recombinant MBP-GCN5^{ILL} and MBP-GCN5^{EDD} was examined by liposome sedimentation assays. **A, B**, Liposome sedimentation assays were performed with liposomes prepared with PtdCho alone (control) or with a mixture of PtdCho and either PtdIns3P, PtdIns4P, PtdIns5P, PtdOH (or PtdSer). No lipid, control sample without liposomes. Supernatant, contained unbound protein. Sediment, protein that had bound to respective liposomes. Proteins were separated on an SDS-PAGE and detected by immunoblots with the use of the specific antibody against MBP and a secondary antibody conjugated to AP. AP detection was performed. PageRuler™ Prestained Protein Ladder was used as a molecular size marker. Expected molecular size of full-length proteins, MBP-GCN5^{ILL}/MBP-GCN5^{EDD}, 105.6 kDa. Experiments were performed in triplicates with similar results. **A**, Liposome sedimentation assay of MBP-GCN5^{ILL}. **B**, Liposome sedimentation assay of MBP-GCN5^{EDD}. **C, D**, Quantification of bound MBP-GCN5^{ILL} or MBP-GCN5^{EDD} in the liposome sedimentation assays shown in A or B, respectively with ImageJ/Fiji (Schindelin et al., 2012). AU, arbitrary units. Data represent means and error bars show standard deviations for three independent experiments. No significant differences of bound MBP-GCN5^{ILL}/MBP-GCN5^{EDD} compared to the PtdCho samples were found according to Student's T-test. **C**, Quantification of bound MBP-GCN5^{ILL} in A. **D**, Quantification of bound MBP-GCN5^{EDD} in B.

To address the possibility that the loss of PI binding is the result of a severe secondary structure defect (misfolding) of the GCN5 variants, circular dichroism (CD) spectra of purified recombinant MBP-GCN5, MBP-GCN5^{ILL}, GCN5^{EDD} and MBP as a control were prepared (appendix Fig. 6.14). Far-UV CD spectra were recorded from at least 200 to 250 nm to investigate the secondary structure of the backbone of the amino acid sequence and ellipticity was calculated. MBP showed a CD spectrum that was strongly influenced by α -helical

structures. Also, α -helical structures can be derived from the CD spectra of MBP-GCN5 and the variants, but these CD spectra for α -helical structures were less pronounced than in MBP. The CD-spectra of GCN5, GCN5_{ILL} and GCN5_{EDD} were indistinguishable. Therefore, it was concluded that the overall secondary structures of GCN5_{ILL} and GCN5_{EDD} were not diminished or altered.

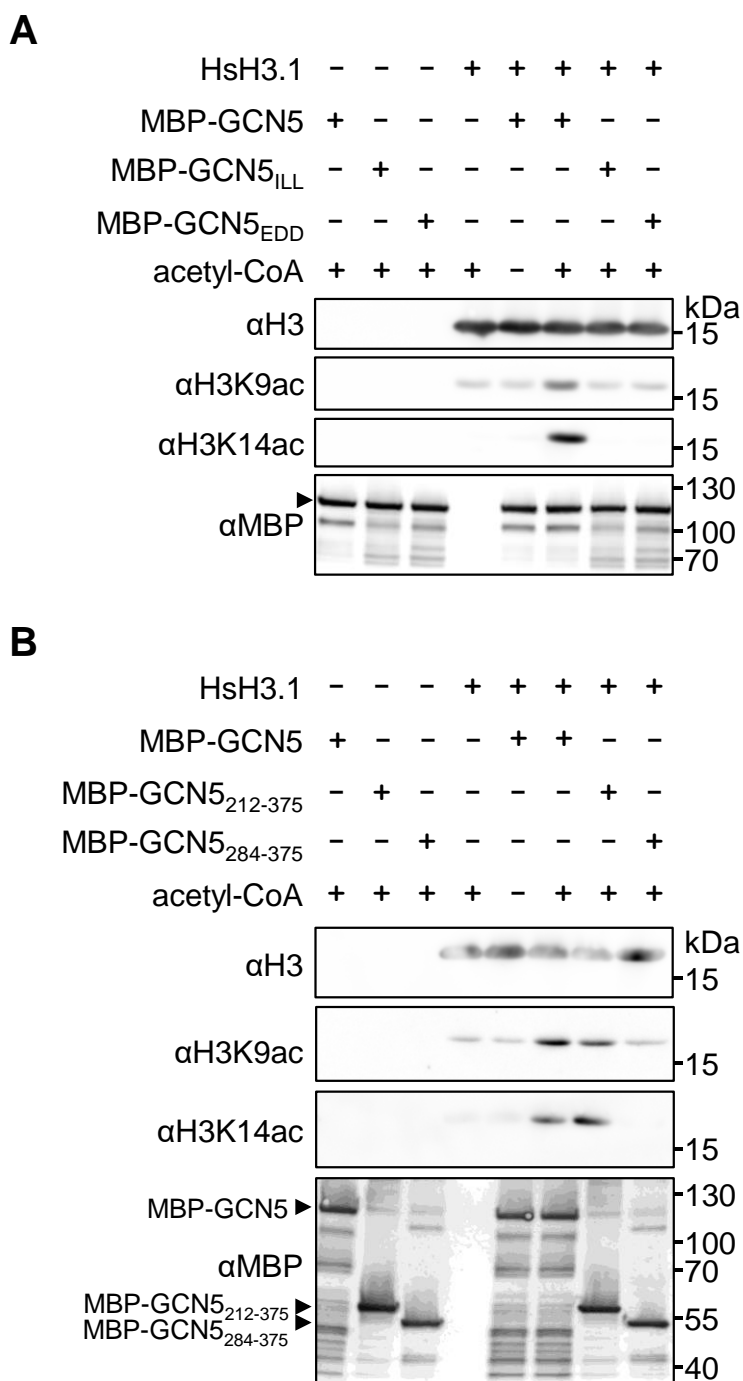


Fig. 2.12: *In vitro* acetylation activity of GCN5 and variants. Histone acetylation by enriched recombinant MBP-GCN5, MBP-GCN5_{ILL}, MBP-GCN5_{EDD}, MBP-GCN5₂₁₂₋₃₇₅ and MBP-GCN5₂₈₄₋₃₇₅ proteins was studied *in vitro*. The formation of H3K9ac and H3K14ac was detected with specific antibodies. Chemiluminescent signals were recorded using an ECL detection system. **A**, *In vitro* histone H3 acetylation activity of GCN5, GCN5_{ILL} and GCN5_{EDD}. GCN5 in absence of acetyl-CoA

functioned as control. Enriched proteins were tested alone as control. Reactions were stopped after 60 min. The data are representative for four individual experiments. PageRuler™ Prestained Protein Ladder was used as a molecular size marker. The arrow indicates MBP-GCN5/MBP-GCN5_{ILL}/MBP-GCN5_{EDD}. Expected molecular sizes of full-length proteins, histone H3, 15.3 kDa; MBP-GCN5/MBP-GCN5_{ILL}/MBP-GCN5_{EDD}, 105.6 kDa. **B**, *In vitro* histone H3 acetylation activity of GCN5, GCN5₂₁₂₋₃₇₅ and GCN5₂₈₄₋₃₇₅. GCN5 in absence of acetyl-CoA functioned as control. Enriched proteins were tested alone as control. Reactions were stopped after 60 min. The data are representative for four individual experiments. PageRuler™ Prestained Protein Ladder was used as a molecular size marker. Expected molecular sizes of full-length proteins, histone H3, 15.3 kDa; MBP-GCN5, 105.6 kDa; MBP-GCN5₂₁₂₋₃₇₅, 61.5 kDa, MBP-GCN5₂₈₄₋₃₇₅, 53.1 kDa.

Alternatively, the biochemical functionality of the modified proteins was tested in *in vitro* activity assays. Despite their proper folding according to CD spectroscopy, the *in vitro* histone H3 acetylation assays showed that both amino acid substitution variants, GCN5_{ILL} and GCN5_{EDD}, were catalytically inactive (Fig. 2.12 A and appendix Fig. 6.15).

For the GCN5 homolog from *S. cerevisiae* (ScGCN5) it was shown that ScGCN5 is still catalytically active even with an N-terminally truncated HAT domain (Candau et al., 1997). Therefore, a HAT domain variant, GCN5₂₈₄₋₃₇₅, truncated by the area of the lipid binding site, was created, recombinantly expressed in *E. coli* as an MBP fusion and the purified protein was used in *in vitro* histone H3 acetylation tests (Fig. 2.12 B). As a control, the complete GCN5 HAT domain, MBP-GCN5₂₁₂₋₃₇₅, was also tested (Fig. 2.12 B). For the full HAT domain MBP-GCN5₂₁₂₋₃₇₅, *in vitro* histone H3 acetylation activity was observed which was comparable to that of full-length MBP-GCN5. The truncated MBP-GCN5₂₈₄₋₃₇₅ variant, however, was catalytically inactive. The results from yeast could, thus, not be reproduced with GCN5 from Arabidopsis. Despite the reduced/abolished catalytic activity of the GCN5 variants with reduced lipid binding capability, the GCN5_{ILL} and GCN5_{EDD} variants represented tools to further investigate the contribution of lipid binding to GCN5 functionality.

2.6. PI 3-kinase VPS34 has no impact on the GCN5-dependent activation of GH3.3

The catalytic activity of MBP-GCN5 was impaired *in vitro* by both, PtdIns3P and PtdIns(4,5)P₂, and GCN5 itself bound preferentially to PtdIns3P (Fig. 2.9). Therefore, next the effects of PtdIns3P on GCN5 function were examined *in vivo*. PtdIns3P is formed by the PI 3-kinase, VPS34, which is encoded by a single gene in Arabidopsis (Mueller-Roeber and Pical, 2002; Lee et al., 2010). The VPS34 protein contains several functional/regulatory domains, such as an N-terminal calcium-dependent lipid-binding (C2) domain (Welters et al., 1994; Meijer and Munnik, 2003) and a helical domain, in addition to its C-terminal catalytic domain (Mueller-Roeber and Pical, 2002) (Fig. 2.13 A). Importantly, VPS34 has previously been detected at active transcription sites in cell nuclei of soybean root cells by immunocytochemistry (Bunney et al., 2000).

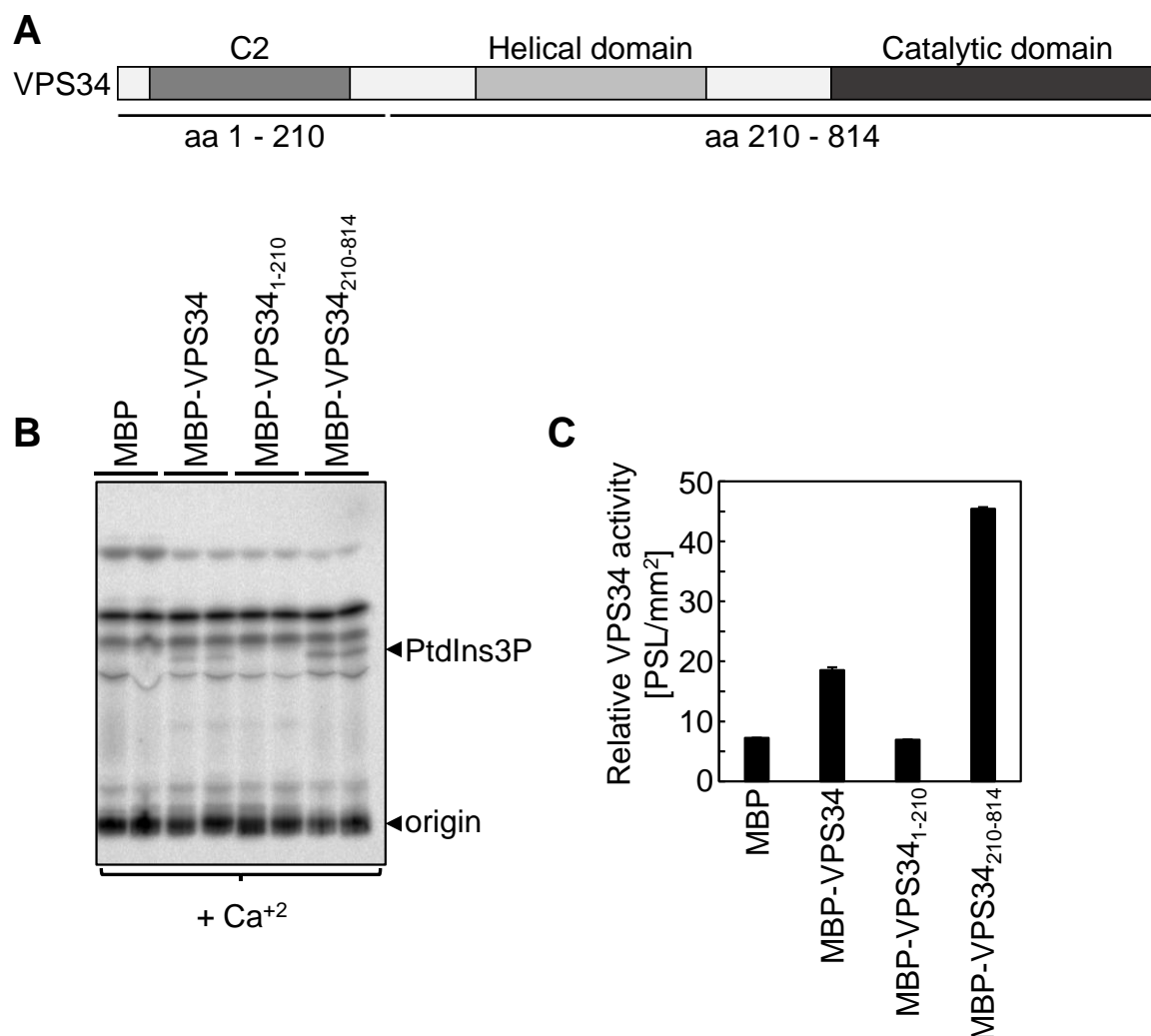


Fig. 2.13: The VPS34 gene product is active as a PI 3-kinase. *In vitro* activity of VPS34 and truncated variants was tested. **A**, Schematic view of VPS34. VPS34 consists of 814 aa. VPS34 contains a C2 domain (aa 25 – 177), a helical domain conserved in PI 3-kinases, formerly named PIK domain (aa 274 – 459) and a catalytic PI-kinase domain (aa 465 – 813). aa, amino acids; C2, calcium-dependent lipid binding domain. **B**, Protein extracts were incubated with PtdIns substrate in the presence of γ -[³²P]-ATP and Ca²⁺, anionic lipids were extracted under acidic conditions, separated by thin layer chromatography (TLC), and radiolabeled lipids were visualized by phosphorimaging. Full-length MBP-VPS34 protein and MBP-VPS34₂₁₀₋₈₁₄ displayed catalytic activity against PtdIns substrate *in vitro*. A representative autoradiograph is shown. The experiment was performed twice with similar results. **C**, Quantification of phosphorimager signals from B using TINA 2.0 Software (Raytest, Straubenhardt, Germany). Data represent means and error bars show standard deviations for two independent experiments.

While Arabidopsis VPS34 has been described previously as a PI 3-kinase (Welters et al., 1994; Dove et al., 1994; Heilmann and Heilmann, 2015), catalytic activity of the recombinant protein has not previously been reported. Here, recombinant MBP-VPS34 protein displayed catalytic activity *in vitro* (Fig. 2.13 B and C). Catalytic activity was also demonstrated for a truncated variant lacking the N-terminal C2 domain, VPS34₂₁₀₋₈₁₄, but the C2 domain itself, VPS34₁₋₂₁₀, showed no PtdIns3P formation (Fig. 2.13 B and C). Therefore, PI 3-kinase activity of Arabidopsis VPS34 was confirmed *in vitro*.

Transient overexpression of VPS34-mCherry in *Arabidopsis* mesophyll protoplasts showed VPS34-mCherry in both cytoplasm and nucleus (Fig. 2.14), consistent with a putative role of VPS34 in the control of nuclear processes (Bunney et al., 2000). The mCherry control also showed cytosolic and nuclear localization, as expected, and therefore expression of full-length VPS34-mCherry was tested and confirmed by immunodetection (appendix Fig. 6.16).

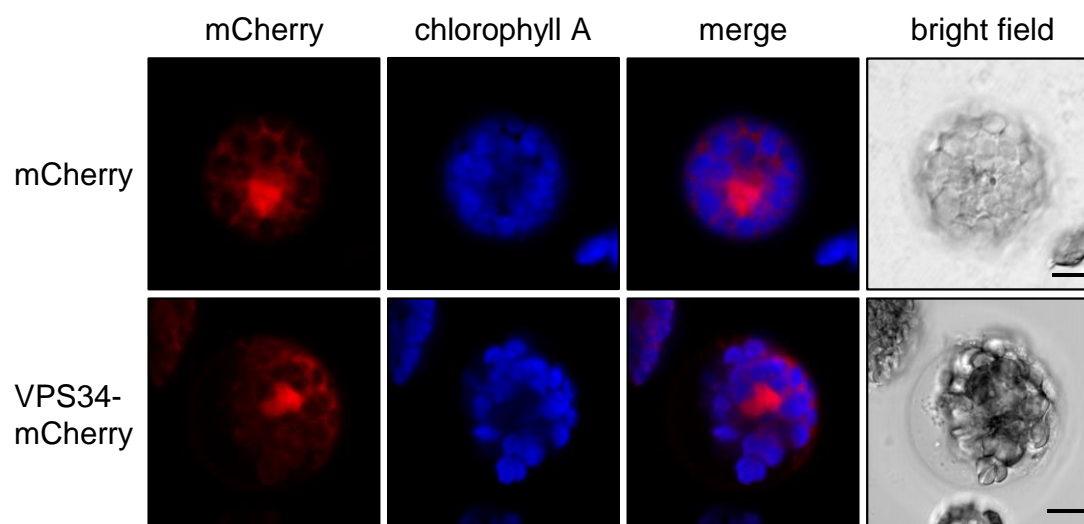


Fig. 2.14: Subcellular localization of VPS34-mCherry in *Arabidopsis* mesophyll protoplasts. *Arabidopsis* mesophyll protoplasts were transiently transformed with *pEntryD-pCaMV35S::mCherry* or *pEntryA-pCaMV35S::VPS34-mCherry*. Subcellular localization of fluorescence-tagged proteins was observed by confocal microscopy with an LSM 880 (Carl Zeiss, Jena, Germany). Cells were recorded in single levels dissecting the nucleus. Blue, autofluorescence of chlorophyll A; red, mCherry. The excitation wavelengths for mCherry and chlorophyll A were 561 nm and 633 nm, respectively, and emission was detected between 565 – 620 nm (mCherry) and 680 – 720 nm (chlorophyll A). The experiment was performed twice for mCherry, recording 22 cells, and eight times for VPS34-mCherry, recording 77 cells. Scale bar, 10 μ m.

Based on the available information and the additional experiments performed for this thesis, VPS34 was selected for further analysis of its relation to GCN5. In split-ubiquitin-based YTH, VPS34 and the two truncated variants were tested for interaction with GCN5 (Fig. 2.15 A). Both, the full-length protein VPS34, and the C2 domain, VPS34₁₋₂₁₀, interacted with GCN5. The variant lacking the C2 domain, VPS34₂₁₀₋₈₁₄, did not interact with GCN5, indicating that the C2 domain appears to be important for the interaction with GCN5 (Fig. 2.15 A). None of the three variants of VPS34 interacted with ADA2B. The positive protein-protein interactions of VPS34 and VPS34₁₋₂₁₀ with GCN5 were verified in immuno pull-down experiments (Fig. 2.15 B). GST and GST-tagged GCN5 were bound to a glutathione agarose matrix and were then co-incubated with recombinant protein extracts of MBP-tagged VPS34, VPS34₁₋₂₁₀ or VPS34₂₁₀₋₈₁₄. Interacting proteins were co-eluted with 50 mM reduced L-glutathione. For all MBP-VPS34 variants only low unspecific binding to GST was observed (Fig. 2.15 B). Interaction of the MBP-VPS34 full-length protein with GCN5 was only weakly detected;

however, a truncated MBP-VPS34 fragment of approximately 50 kDa was always enriched by binding to GST-GCN5 (Fig. 2.15 B). MBP-VPS34₁₋₂₁₀ bound to GST-GCN5, whereas MBP-VPS34₂₁₀₋₈₁₄ was unable to bind more clearly to GST-GCN5 than to GST (Fig. 2.15 B). These results confirmed the findings of YTH studies that the C2 domain of VPS34 could mediate binding to GCN5.

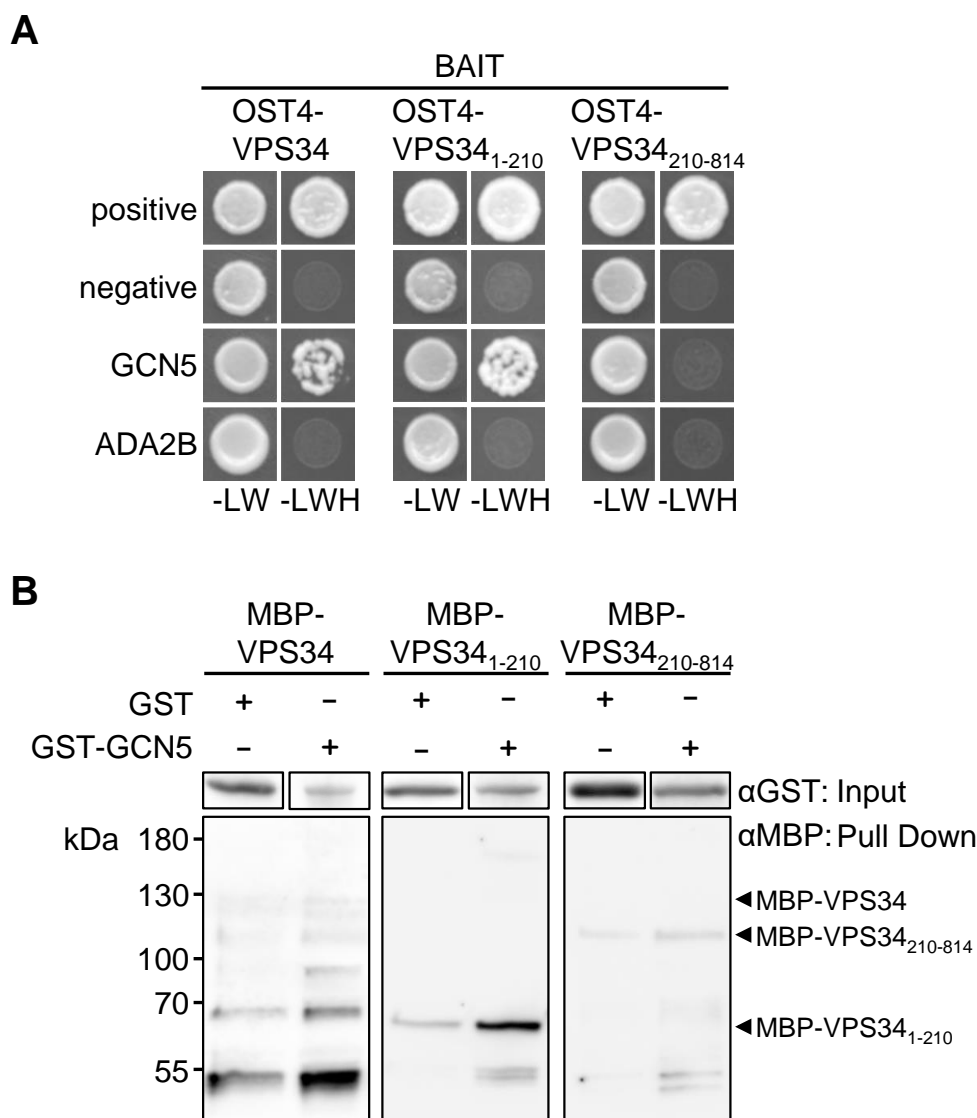


Fig. 2.15: The PI 3-Kinase VPS34 interacts with GCN5. The interaction of VPS34 and truncated variants VPS34₁₋₂₁₀ and VPS34₂₁₀₋₈₁₄ with GCN5 and ADA2B was tested by split-ubiquitin-based YTH analysis in *S. cerevisiae* strain NMY51 and by *in vitro* immuno pull-down analysis (GCN5). **A**, Split-ubiquitin-based YTH of VPS34, VPS34₁₋₂₁₀ and VPS34₂₁₀₋₈₁₄ (bait) with GCN5 and ADA2B (prey). OST4 fusions localized interactions to ER membranes. *pAl-Alg5* and *pDL2-Alg5* vectors were used as positive or negative control. Uniform growth on -LW media (without leucine and tryptophane) indicates equal cell densities and the presence of the respective vectors. Interaction is indicated by growth under selective conditions on -LWH media (without leucine, tryptophane and histidine). Yeast colonies were grown at 30°C for four days. A representative result of three (VPS34, VPS34₁₋₂₁₀) or two (VPS34₂₁₀₋₈₁₄) replicates with five independent colonies of each combination is shown. **B**, *In vitro* immuno pull-down of VPS34, VPS34₁₋₂₁₀ and VPS34₂₁₀₋₈₁₄ with GCN5. Recombinantly expressed GST, GST-GCN5 were immobilized on glutathione agarose and incubated with recombinant MBP-tagged

VPS34, VPS34₁₋₂₁₀ and VPS34₂₁₀₋₈₁₄ (expression lysate). Bound protein was co-eluted with 50 mM reduced L-glutathione and interacting MBP-tagged proteins were analyzed by immunodetection using an α MBP antibody. Input GST-tagged protein was detected by an α GST antibody. Chemiluminescence signals were recorded with an ECL detection system. Expected molecular sizes of full-length proteins, GST, 26 kDa; GST-GCN5, 89.1 kDa; MBP-VPS34, 135.8 kDa; MBP-VPS34₁₋₂₁₀, 66.2 kDa; MBP-VPS34₂₁₀₋₈₁₄, 112.3 kDa. Pull-downs were performed twice.

The interaction of VPS34 and GCN5 suggested that these proteins might be associating to control transcription. Therefore, the effect of VPS34 on the GCN5-dependent auxin-mediated transcription of *GH3.3* was tested in a setup identical to the experiments described for PI4P 5-kinases (section 2.3). Protoplasts overexpressing either mCherry or VPS34-mCherry were treated with NAA or mock, and again the transcription activation of *GH3.3* was analyzed by qPCR (Fig. 2.16 A). In contrast to the results for PIP5K2, protoplasts expressing VPS34-mCherry did not show a significantly different response in *GH3.3* transcription upon VPS34-mCherry expression. As controls, *mCherry* and *VPS34-mCherry* expression in the protoplasts was verified by qPCR (appendix Fig. 6.8 M and N) and the expression of fusion proteins was confirmed via immunodetection with suitable antisera (Fig. 2.16 B). The basal levels of *GH3.3* transcript and *GCN5* transcript were also tested by qPCR and were not affected neither by auxin treatment nor by VPS34-mCherry expression (appendix Fig. 6.17 A and B).

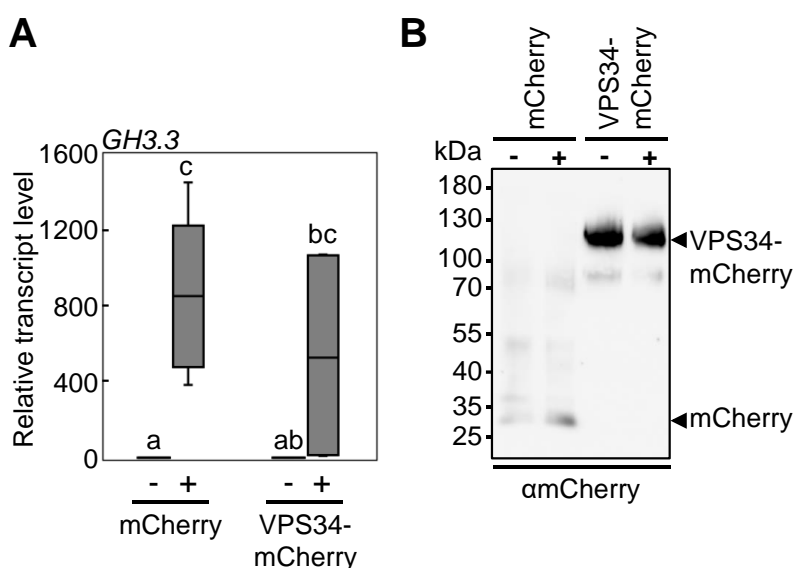


Fig. 2.16: Overexpression of VPS34 does not impact auxin-activation of *GH3.3*. Relative transcript levels for *GH3.3* in mesophyll protoplasts upon overexpressing either mCherry or VPS34-mCherry and with mock (-) and with 0.25 μ M NAA (+) treatment overnight. Data represent 6 – 8 biological replicates (transformations) from two independent protoplast preparations. **A**, Protoplasts transformed with *pEntryD-pCaMV35S::mCherry* or *pEntryA-pCaMV35S::VPS34-mCherry*. Transcript levels were normalized to both the reference gene *UBC10* and the transcript levels of the respective mock-treated sample (-). Relative transcript levels are shown as boxplots; dots show outliers. Significant differences were analyzed by one-way ANOVA with a subsequent Tukey's post-hoc test ($P < 0.05$) and indicated

by letters a – c. **B**, Immunodetection of mCherry and VPS34-mCherry overexpression in protoplasts treated as described above was performed using an α mCherry antiserum. Chemiluminescence signals were recorded with an ECL detection system. Immunodetections were performed twice. PageRuler™ Prestained Protein Ladder was used as a molecular size marker. Expected molecular sizes of full-length proteins, mCherry, 26.7 kDa; VPS34-mCherry, 120.0 kDa.

Taken together, these data suggest that auxin-induced GCN5-mediated histone acetylation is not directly attenuated by VPS34 (and thus PtdIns3P) *in vivo*. While an effect of VPS34 or PtdIns3P on GCN5 activity *in vivo* cannot be ruled out, it has previously been suggested that PtdIns3P may act as a positional signal to recruit GCN5 to the nucleus and to sites of active transcription (Bunney et al., 2000). A similar effect was shown for ING proteins in mammalian cells (Bunce et al., 2006a, 2006b; Soliman and Riabowol, 2007). Therefore, it was next tested whether the capability to bind PtdIns3P influenced the localization of GCN5 in the nucleus.

2.7. PI binding contributes to nuclear localization of GCN5

As PIs are generally described positional signals for the correct recruitment of proteins (Heilmann, 2016a; Gerth et al., 2017b; Jaillais and Ott, 2020) and previous data for GCN5 had suggested that GCN5 may be recruited by binding to PIs, the role of lipid binding of GCN5 in its subcellular localization was investigated. To analyze the contribution of lipid binding of GCN5 to its subcellular distribution, GCN5 and its lipid binding-impaired variants GCN5_{ILL} and GCN5_{EDD}, were transiently expressed as EYFP fusion proteins in Arabidopsis mesophyll protoplasts and examined for their nuclear localization (Fig. 2.17 A). EYFP served as control (Fig. 2.17 A). Subcellular localization analyses were performed with a laser scanning microscope LSM 880 (Carl Zeiss, Jena, Germany). As a positive control, an *NLS-DsRed* construct was used, which contained a strong NLS from the simian virus SV40 and served as a *bona fide* nuclear marker (Gerth et al., 2017a). Images in Fig. 2.17 A show representative localization patterns in confocal z-projections covering both cytoplasm and nucleus.

The fluorescence of EYFP-GCN5 showed a distinct, almost exclusive nuclear distribution pattern (Fig. 2.17 A) similar to that of the nuclear marker, and only in very few cells, a weak cytoplasmic fluorescence was detectable (Fig. 2.17 A), as displayed in the respective corresponding intensity profiles. By contrast, EYFP-GCN5_{ILL} and EYFP-GCN5_{EDD} localized in a more relaxed pattern to the nucleus and to the cytosol in a pattern resembling that of the EYFP negative control (Fig. 2.17 A).

For the respective EYFP fluorescence observed and DsRed fluorescence, Pearson correlation coefficients were calculated using the JACoP plugin (Bolte and Cordelières, 2006) for ImageJ/Fiji (Schindelin et al., 2012) (Fig. 2.17 B). A Pearson correlation coefficient of 0 means no co-localization, whereas a Pearson correlation coefficient of 1 reflects perfect co-localization. As EYFP localized to nucleus and cytosol, the fluorescence signals of EYFP and NLS-DsRed did only partly overlap which resulted in a low Pearson correlation coefficient

of 0.45. For EYFP-GCN5 and NLS-DsRed a coefficient of 0.84 was determined which reflects a strong co-localization. Pearson correlation coefficients of EYFP-GCN5_{ILL} (0.66) or EYFP-GCN5_{EDD} (0.74) with NLS-DsRed were significantly lower than that of EYFP-GCN5/NLS-DsRed, confirming the observed more relaxed nuclear localization pattern of EYFP-GCN5_{ILL} and EYFP-GCN5_{EDD} (Fig. 2.17 A).

The distribution patterns of EYFP, EYFP-GCN5, EYFP-GCN5_{ILL} and EYFP-GCN5_{EDD} in transformed protoplasts were scored according to their exclusive nuclear localization, cytosolic and nuclear localization, or exclusive cytosolic localization (Fig. 2.17 C). All cells overexpressing EYFP showed fluorescence in nucleus and cytosol. Cells overexpressing EYFP-GCN5 showed to a percentage of 37.4 % exclusive nuclear localization and to 58.9 % a nuclear and cytosolic localization pattern. In some cells the nucleus was not visible (cytosolic fluorescence). None of the cells overexpressing EYFP-GCN5_{ILL} or EYFP-GCN5_{EDD} showed an exclusive nuclear fluorescence, but 97.5 % (EYFP-GCN5_{ILL}) or 94.7 % (EYFP-GCN5_{EDD}) of the transformed cells showed nuclear and cytosolic fluorescence. Also here, in some cells the nucleus was not visible, and cells were classified as cytoplasmic localized.

The overexpression of the EYFP-tagged proteins was confirmed via immunodetection of the transformed protoplasts (appendix Fig. 6.18 A). These controls showed that EYFP-GCN5 was overexpressed to a substantially stronger degree than the EYFP-GCN5_{ILL} and EYFP-GCN5_{EDD} variants in all experiments. Therefore, differences in localization, particularly the increased cytosolic localization of the two amino acid substitution variants of GCN5, were likely not due to excessive overexpression of EYFP-GCN5 variants. To test whether the lower expression of GCN5_{ILL} and GCN5_{EDD} was caused by proteolytic degradation via the 26S proteasome, protoplasts overexpressing GCN5 variants were treated with the proteasome inhibitor MG-132. Inhibition of the 26S proteasome resulted in a slight increase in protein levels of EYFP-GCN5, EYFP-GCN5_{ILL}, and EYFP-GCN5_{EDD} in all cases (appendix Fig. 6.18 B), suggesting that the introduced amino acid substitutions in EYFP-GCN5_{ILL} and EYFP-GCN5_{EDD} causing the loss of PI binding ability did likely not result in differentially increased proteasomal degradation of the substitution variants.

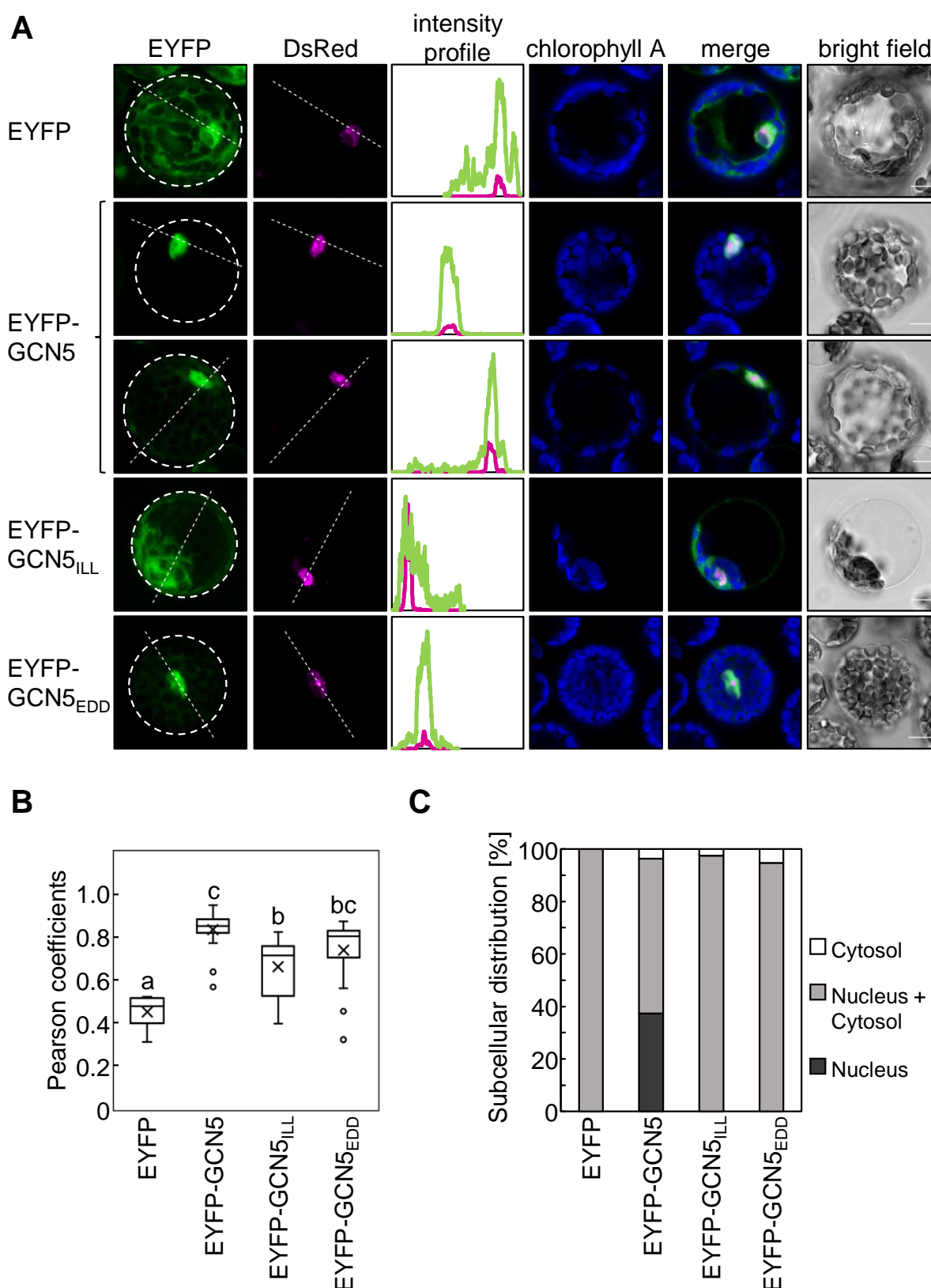


Fig. 2.17: Subcellular localization of GCN5 amino acid substitution variants in *Arabidopsis mesophyll* protoplasts. *Arabidopsis mesophyll* protoplasts were transiently transformed with *pEntryA-pCaMV35S::EYFP*, *pEntryA-pCaMV35S::EYFP-GCN5*, *pEntryA-pCaMV35S::EYFP-GCN5_{ILL}* or *pEntryA-pCaMV35S::EYFP-GCN5_{EDD}*. Subcellular distribution of fluorescence-tagged proteins was observed by confocal microscopy with an LSM 880 (Carl Zeiss, Jena, Germany). Cells were imaged either in single layers or in z-stacks with a maximum spacing of 0.85 μm between sections, and

z-projections of EYFP (green) and DsRed (magenta) fluorescence were obtained. Intensity profiles along the dashed lines shown in the EYFP and DsRed images are given, as indicated, and are generated with ImageJ/Fiji (Schindelin et al., 2012). The intrinsic chlorophyll A fluorescence (blue) and bright field images are also shown, as indicated. The excitation wavelengths for EYFP, DsRed and chlorophyll A were 514 nm, 561 nm, and 633 nm, respectively, and emission was detected between 520 – 555 nm (EYFP), 565 – 620 nm (DsRed) and 680 – 720 nm (chlorophyll A). **A**, EYFP localized in the cytoplasm and in the nucleus in three independent experiments, recording 13 cells. EYFP-GCN5 localized in the nucleus (upper panel), if cytosolic localization of EYFP-GCN5 was observed, it was very weak (lower panel); three independent experiments, recording 19 cells. EYFP-GCN5_{ILL} and EYFP-GCN5_{EDD} localized in the nucleus and the cytosol in each of three independent experiments, recording 16 and 18 cells, respectively. Scale bar, 10 μ m. **B**, Pearson correlation of EYFP and DsRed fluorescence of cells shown in A. Pearson correlation coefficients of NLS-DsRed and EYFP/EYFP-GCN5/EYFP-GCN5_{ILL}/EYFP-GCN5_{EDD} were calculated in ImageJ (Schindelin et al., 2012) with the JACoP plugin (Bolte and Cordelières, 2006). Pearson correlation coefficients are shown in a boxplot depicting the two inner quartiles and with whiskers indicating maximum and minimum. The cross marks the mean, the line marks the median. Circles represent outliers. One-way ANOVA was performed with a Tukey's post-hoc test ($P < 0.05$). **C**, Subcellular distribution patterns of EYFP, EYFP-GCN5, EYFP-GCN5_{ILL} and EYFP-GCN5_{EDD}. Cells were counted and categorized into three groups, either showing fluorescence in the nucleus, in nucleus and cytosol or in the cytosol. Data are normalized to the results of EYFP expressing cells. Experiments were performed five times, with 25 (EYFP), 107 (EYFP-GCN5), 79 (EYFP-GCN5_{ILL}) and 76 (EYFP-GCN5_{EDD}) analyzed cells.

Taken together, the different localization patterns observed for EYFP-GCN5 and EYFP-GCN5_{ILL}/EYFP-GCN5_{EDD} indicate that PI binding capability influences the nuclear localization of the GCN5 protein. This finding is consistent with the notion that PIs, such as PtdIns3P, may act as positional signals to recruit GCN5 to its site of action to control histone modification and transcription in the plant nucleus.

3. Discussion

In this thesis, the little-explored roles of plant nuclear PIs are addressed to broaden our view of how PIs influence plant physiology and development. Studies on the functions of PIs in plants have mostly been performed using *Arabidopsis* mutants or other transgenic models with defects in PI biosynthetic enzymes, and in some instances these plants showed strong pleiotropic phenotypes (Mei et al., 2012; Ischebeck et al., 2013; Tejos et al., 2014). The complexity of intertwined cellular processes that influence each other over the course of plant development complicates the interpretation which particular metabolic or signaling defects are primarily responsible for the manifestation of any given phenotype. For instance, it has been shown that PIs influence auxin biology (Mei et al., 2012; Ischebeck et al., 2013; Tejos et al., 2014). However, the interpretation of defects in auxin biology is difficult because auxin distribution, e.g. auxin gradients within different tissues, as well as auxin perception and auxin-regulated gene expression may all be affected. While the drastic and pleiotropic phenotype of the *Arabidopsis pip5k1 pip5k2* double mutant has previously been rationalized based on clear defects in the trafficking and polar distribution of PIN proteins (Mei et al., 2012; Ischebeck et al., 2013; Tejos et al., 2014), these trafficking processes might not account for all aspects of the pleiotropic phenotype of these plants. In preparation of this thesis, *pip5k1 pip5k2* double mutants expressing the PIP5K2 variant PIP5K2_{AAA} were generated, which displays inefficient nuclear import and reduced nuclear localization (Dr. Katharina Gerth). These plants displayed a partial complementation of the *pip5k1 pip5k2* phenotypes, but phenotypes such as deformed leaves and flowers and defects in phyllotaxis emerged that were not previously observed (Fig. 1.4). While it cannot be excluded that the polar auxin distribution in these plants is still altered, the remaining defects could as well result from the fact that PIP5K2_{AAA} expressed in the *pip5k1 pip5k2* double mutant is no longer transported into the nucleus and the remaining phenotypes result from PIP5K2 missing from the nucleus. This interpretation is supported by the fact that PI biosynthesis mutants show defects in PIN distribution (Mei et al., 2012; Ischebeck et al., 2013; Tejos et al., 2014), but their phenotypes differ markedly from those of *Arabidopsis pin* mutants (Okada et al., 1991; Müller et al., 1998; Benková et al., 2003) in which the phenotypes are evidently due to altered auxin distribution and an impaired auxin gradient. As the phenotype of the *pip5k1 pip5k2* double mutant can furthermore not be rescued by the application of exogenous auxin (Ischebeck et al., 2013), it was hypothesized about additional functional contributions of PIs in the nucleus, beyond their effects on auxin distribution. The phenotype of *pip5k1 pip5k2* double mutants complemented with PIP5K2_{AAA} may be thus related to the exclusion of PIP5K2 from the nucleus and represent defects in nuclear signaling or function. As previous studies indicated regulatory functions of PIs in the regulation of transcription and specifically in histone modification (Bunney et al., 2000; Dieck et al., 2012),

it was the aim of this work to determine to what extent the observed nuclear localization of Arabidopsis PI4P 5-kinase is biologically relevant and by what mechanism PIP5K1 and PIP5K2 might influence auxin-regulated gene expression.

3.1. PI4P 5-kinases interact with GCN5 and putative components of the histone acetylation machinery

In accordance with the previous observations by Dieck and coworkers for overexpression of human HsPIP5K1 α in tobacco cell cultures (Dieck et al., 2012), overexpression of the intrinsic Arabidopsis PIP5K2 led to reduced acetylation levels at H3K9 and H3K14 in both examined transgenic lines, compared to a Col-0 wild type control (Fig. 2.1 C and D). The opposite effect was observed for the *pip5k1 pip5k2* double mutant that displayed enhanced acetylation levels (Fig. 2.1 A and B), confirming that the intrinsic biosynthetic machinery for PIs influences histone acetylation in Arabidopsis.

Changed histone acetylation levels imply an influence of PIs or PI4P 5-kinases on histone-modifying enzymes, which can introduce histone modifications, like acetyl residues, to histones or remove them (Patel and Wang, 2013; Ueda and Seki, 2020). This finding was supported by the specific interaction of the ubiquitously expressed PI4P 5-kinases PIP5K1, PIP5K2 and PIP5K6 with the HAT GCN5 in YTH assays and in immuno pull-down experiments. The interaction of PI4P 5-kinases with GCN5 seemed to be specific, because not every tested ubiquitously expressed PI4P 5-kinase showed an interaction (Fig. 2.2).

GCN5 is described as a HAT component of the SAGA complex (Grant et al., 1997; Servet et al., 2010; Srivastava et al., 2015; Moraga and Aquea, 2015). In the HAT module, GCN5 binds, among others, to ADA2B (Stockinger et al., 2001; Mao et al., 2006; Servet et al., 2008). ADA2B recruits GCN5 to specific promoter regions and influences GCN5 activity by increasing the binding affinity of GCN5 to acetyl-CoA (Hark et al., 2009; Anzola et al., 2010; Servet et al., 2010; Weiste and Dröge-Laser, 2014; Sun et al., 2018). While GCN5 and ADA2B interacted directly in YTH experiments (appendix Fig. 6.4), consistent with earlier findings (Stockinger et al., 2001; Mao et al., 2006; Servet et al., 2008), a direct interaction of any of the PI4P 5-kinases tested with ADA2B was not detected. However, both PIP5K1 and PIP5K2 interacted with ING proteins (Fig. 2.3), providing additional evidence for the presence of a nuclear protein complex containing elements of the HAT module and PI4P 5-kinases. ING proteins are reader proteins recognizing H3K4me₂/H3K4me₃ and recruit other enzyme complexes, such as HATs, to the corresponding promoter regions (Pena et al., 2006; Soliman and Riabowol, 2007; Lee et al., 2009; Kim et al., 2016). Studies with mammalian ING proteins showed that these proteins get recruited to their histone target sites by binding to PtdIns-monophosphates that act as recruiting signaling molecules (Bunce et al., 2006a, 2006b; Soliman and Riabowol, 2007). Binding of the Arabidopsis isoforms ING1 and ING2 to GCN5 and PI4P 5-kinases PIP5K1 and

PIP5K2 (Fig. 2.2 and Fig. 2.3) suggests an involvement of PI4P 5-kinases or PIs in the formation of a HAT complex, which might be recruited by ING proteins. The details of how PIP5K1 and PIP5K2 interact with GCN5 have so far not been analyzed and the specific amino acid residues or domains mediating the interaction have not yet been identified. In the future, it will be interesting to elucidate actual subcellular or suborganellar localization of the interaction between PI4P 5-kinases and GCN5 in detail, possibly with advanced high-resolution microscopy. It is also possible that PI4P 5-kinases themselves are acetylation targets of GCN5. However, initial mass spectrometry studies did not detect acetylated PIP5K1 or PIP5K2 fragments (preliminary data, not shown). Furthermore, it cannot be excluded that the interaction between PI4P 5-kinases and GCN5 does not take place in the nucleus at all. Several HATs in yeast and mammals have been shown to shuttle between the nucleus and cytosol and might acetylate non-histone proteins in the cytosol (Tran et al., 2012; Scott et al., 2012; Parthun, 2012; Shen et al., 2015). To further dissect this issue, the nuclear-excluded PIP5K2_{AAA} could be a tool to investigate the interaction of PI4P 5-kinases and GCN5 in the future.

While it remains unclear whether PIP5K1 or PIP5K2 interact also with other components of the HAT module or the SAGA complex, there is evidence indirectly linking the SAGA complex to PI signaling. For instance, the large SAGA subunit TRA1 (about 400 kDa) belongs to the phosphatidylinositol 3-kinase-related kinase (PIKK) family, a group of highly conserved protein kinases that includes the important proteins TOR, ATM, ATR, DNA-PKcs and SMG-1. TRA1 is the only PIKK family member which seems to be a catalytically inactive kinase and shows no catalytic activity, neither against lipids nor proteins (Templeton and Moorhead, 2005; Lovejoy and Cortez, 2009; Sharov et al., 2017). In Arabidopsis two TRA1 isoforms are present, TRA1a and TRA1b, and as in yeast and mammals, both isoforms could be found in the SAGA complex and in nucleosome acetyltransferase of H4 (NuA4), another essential HAT complex in eukaryotes (Grant et al., 1998; Cheung and Diaz-Santin, 2019; Espinosa-Cores et al., 2020). The precise function of TRA1 proteins is currently not clear. Studies in yeast and mammals show that TRA1 proteins mediate the recruitment of large activator complexes like SAGA and thereby influence enzymatic activities such as histone acetylation or histone exchange mechanisms to influence chromatin status (Grant et al., 1998; Altaf et al., 2010; Espinosa-Cores et al., 2020). The presence of a major protein component of these large activator complexes SAGA and NuA4 with homology to PI-kinases provides further evidence and supports the data of this work that PIs and/or PI-kinases can affect histone acetylation.

3.2. PIP5K2 activity markedly affects auxin-induced *GH3.3* transcription

The interaction of the nuclear-localized PI4P 5-kinases PIP5K1 and PIP5K2 with GCN5, a HAT, matched well with the results of histone acetylation levels of H3K9ac and H3K14ac in

the PIP5K2 overexpression lines and the *pip5k1 pip5k2* double mutant, respectively. Based on these data, the effect of altered histone acetylation seems to be due to a direct influence of PI4P 5-kinase on histone-modifying enzymes. Since GCN5-mediated histone acetylation at the *GH3.3* gene locus has been described (Weiste and Dröge-Laser, 2014) for the auxin-regulated gene *GH3.3* (Hagen and Guilfoyle, 2002; Staswick et al., 2005), transcript levels of the *GH3.3* gene were tested in the presence or absence of overexpressed PI4P 5-kinases (Fig. 2.4). Experiments were performed in *Arabidopsis* mesophyll protoplasts and the assay setup was adapted with modifications from experiments of Weiste and Dröge-Laser (Weiste and Dröge-Laser, 2014). Weiste and Dröge-Laser used this experimental design to investigate in which manner *GH3.3* transcription is activated upon auxin application and requires GCN5-mediated histone acetylation at the *GH3.3* gene locus. Additional important reasons to use protoplasts were that, on the one hand, the uptake of auxin in protoplast suspensions should occur equally well in all cells, and on the other hand, prevents vectorial auxin transport from being affected by manipulation of PI levels as has been described previously, e.g. for the *pip5k1 pip5k2* double mutant (Ischebeck et al., 2013; Tejos et al., 2014), thus complicating interpretation. In addition, manipulation of the different PI4P 5-kinase expression levels is straightforward because cells can be easily transformed with different constructs and allow comparative studies of the influences of the different PI4P 5-kinases. Stable overexpressor lines for PI4P 5-kinases have proven to be difficult to establish and maintain, in our laboratory and in others (Ischebeck et al., 2013; Tejos et al., 2014). For this thesis, the further use of the stable *PIP5K2-EYFP* OE lines was omitted, although they had shown altered histone acetylation (Fig. 2.1 C and D), because these lines are only weak overexpressors with a patchy fluorescence pattern and thus patchy expression pattern of PIP5K2-EYFP and do not show detectable changes in PtdIns(4,5)P₂ levels (Gerth et al., 2017a).

In addition, no stable *PIP5K6-EYFP* OE line was available as a control, but PIP5K6 overexpression should be used as a control since the ubiquitously expressed PIP5K6 showed interaction with GCN5 (Fig. 2.2 B and C), but acts in different cellular processes than PIP5K1 or PIP5K2 (Zhao et al., 2010; Stenzel et al., 2012; Heilmann, 2016a; Hempel et al., 2017; Menzel et al., 2019; Fratini et al., 2021). Thus, for numerous reasons the use of protoplasts appeared to be most suitable for experiments on auxin-induced gene expression in this thesis. The results showed that overexpression of PIP5K2-EYFP significantly attenuated auxin-activation of *GH3.3* and impairs several other genes, *IAA2*, *IAA5* and *IAA19*, compared with observations when EYFP control was expressed (Fig. 2.4, Fig. 2.5 and appendix Fig. 6.9). Comparable effects were observed with overexpression of PIP5K1-EYFP, but these results were not significant (Fig. 2.4, Fig. 2.5 and appendix Fig. 6.9). Interestingly, expression of the catalytically inactive PIP5K2 K470A-EYFP had no effect on auxin-activation of *GH3.3* transcription (Fig. 2.4 B). Likewise, expression of the functionally divergent isoenzyme

PIP5K6-EYFP (Zhao et al., 2010; Stenzel et al., 2012; Heilmann, 2016a; Hempel et al., 2017; Menzel et al., 2019; Fratini et al., 2021) was tested, which had no impact on auxin-activation of *GH3.3* transcription or on the other auxin-inducible genes (Fig. 2.4, Fig. 2.5 and appendix Fig. 6.9). The observation that the catalytically inactive PIP5K2 K470A had no influence on *GH3.3* transcriptional activation in this experimental setup confirmed that PIP5K2 kinase activity is important for the inhibition of auxin-induced *GH3.3* transcription. This means that the formation of the lipid product PtdIns(4,5)P₂ or the consumption of the substrate lipid PtdIns4P of PIP5K2 and probably similarly of PIP5K1 is at the base of the effect. To test in the future whether an influence of PI4P 5-kinase/PI on gene regulation is restricted to individual genes or whether it is a general mechanism, RNAseq experiments would be informative. Additional analysis via chromatin immunoprecipitation (ChIP) assays to detect the effects of PI4P 5-kinases on GCN5-mediated histone modification would also provide information about the nature of the target genes and their promoters.

The overexpression of PIP5K1 had, in the experiments performed here, less pronounced effects on the transcript regulation of the *GH3.3* gene or on *IAA2*, *IAA5*, and *IAA19* than was observed by the expression of PIP5K2. This might be related to the fact that PIP5K1 was always less well expressed than PIP5K2 in protoplasts (Fig. 2.4 D and Fig. 2.5 G) and that the protein itself displays lower catalytic activity than PIP5K2 in *in vitro* assays (Ischebeck et al., 2013). However, even though PIP5K1 and PIP5K2 have been described as functionally redundant (Ischebeck et al., 2013), it cannot be ruled out that there are functional differences in PIP5K2 and PIP5K1.

3.3. Inhibition of GCN5 and lipid binding

The data so far suggested an effect of PIP5K2 on histone acetylation and an influence on the activation of GCN5-dependent auxin-regulated genes. PI4P 5-kinase activity was required for the *in vivo* effect on gene expression (Fig. 2.4 B), suggesting that the conversion of a substrate of this enzyme (PtdIns4P or PtdIns3P) to a product (PtdIns(4,5)P₂ or PtdIns(3,5)P₂, respectively) influenced the effect of the PIs on histone H3 acetylation, which contributes to controlling the transcriptional activity of *GH3.3* and probably other auxin-inducible genes. When the influence of different PIs on GCN5 activity was tested *in vitro*, all PIs including PtdIns(4,5)P₂ and PtdIns3P showed inhibitory effects on histone acetylation (Fig. 2.7).

When the histone acetylation was monitored in time course experiments over a reaction time of 120 min, substantial reduction in GCN5-mediated H3K9 and H3K14 acetylation was observed in the presence of either PtdIns3P or PtdIns(4,5)P₂, compared with the corresponding controls without lipid addition (Fig. 2.8). It is important to note that phospholipids were added in very small amounts to a molar excess of histone substrate to minimize the influence of electrostatic interactions between the basic lysine residues of histones and the

anionic lipids. The data suggest that PIs can affect the catalytic activity of GCN5, but it remains unclear how precisely PIs can affect GCN5.

To better understand the influence of PIs on GCN5 functionality and histone acetylation, the binding of purified recombinant MBP-GCN5 protein to various lipids was examined by lipid overlay tests (Fig. 2.9 B) and by liposome sedimentation assays (Fig. 2.9 C and D). GCN5 was found to bind PtdIns3P and weakly also PtdIns4P and PtdIns5P (Fig. 2.9 B, C and D), but showed no binding to PtdIns(4,5)P₂. The notion that nuclear PIs influence histone modification and that GCN5 binds to PtdIns3P is consistent with reports from the mammalian field where an interaction of ING protein homologs with PtdIns-monomphosphates has been shown (Gozani et al., 2003). As a reader protein binding to trimethylated histone H3K4 (Lee et al., 2009), it has been proposed that PI binding of ING is required for the subsequent recruitment of human HATs into a functional HAT complex (Bunce et al., 2006a, 2006b; Soliman and Riabowol, 2007). Most importantly, the ING isoforms of Arabidopsis, ING1 and ING2, also bound to PtdIns3P (Fig. 2.9 B, C and E), suggesting that a similar regulatory mechanism exists for the Arabidopsis HAT element GCN5 and ING, which both bind PtdIns3P (Fig. 2.9 B and C). A capability for the binding of anionic lipids has also been reported for yeast ADA2, which was demonstrated to bind PtdSer (Hoke et al., 2008). Preliminary findings of our group indicate possible PI binding of Arabidopsis ADA2B (unpublished data, AG M. Heilmann). Although, ADA2B did not interact in YTH studies with PI4P 5-kinases (Fig. 2.2 B), these observations support the hypothesis that PIs exert a regulatory influence on the SAGA complex.

3.4. Possible modes of GCN5 inhibition by PIs

At the molecular level, PIs might inhibit histone acetylation in several ways. For instance, PIs could affect the MBP-GCN5 protein or the histone substrates or possibly even both. PtdIns(4,5)P₂ inhibited GCN5 activity *in vitro* (Fig. 2.7) but did not bind to the MBP-GCN5 protein in lipid binding experiments (Fig. 2.9). The *in vitro* lipid binding assays may not reflect all aspects of possible interactions between lipids and GCN5. Alternatively, the anionic PtdIns(4,5)P₂ could interact with the basic surface of histone substrates, thereby affecting the formation of the GCN5/histone enzyme/substrate complex that is required for histone modification. The latter mode of action cannot currently be supported or ruled out by experimental evidence. However, PtdIns(4,5)P₂ has already been shown in other contexts to exert regulatory functions by interfering with certain protein-protein interactions, such as the interaction between Rho of plants (ROP) and guanidine nucleotide dissociation inhibitor (GDI) (Fauré et al., 1999; Kost, 2008). An electrostatic effect seems nonspecific at first, but it must be considered that PIs are lipids of low abundance and would not randomly distribute in the nucleoplasm. Instead, the effects of PIs on histone modification and possibly on chromatin transitions likely occur at sites of contact of chromatin with the inner surface of the nuclear

envelope. Several studies have already been conducted for such chromatin-nuclear envelope contact sites in both animals and plants (Kinney et al., 2018; Bishop et al., 2021). This subnuclear distribution of PtdIns(4,5)P₂ and other PIs as well as nuclear PI4P 5-kinases will be the target of future analyses using advanced high-resolution microscopy.

Basic hydrophobicity analyses (Fig. 2.10 B and appendix Fig. 6.13 A and B) (Brzeska et al., 2010) and the resulting amino acid substitution variants, GCN5_{ILL} and GCN5_{EDD}, showed that only a small region at the beginning of the catalytic HAT domain of GCN5 seems to be responsible for PtdIns3P binding. In any case, the variants GCN5_{ILL} and GCN5_{EDD} no longer bound to PtdIns3P in liposome sedimentation assays (Fig. 2.11). While the substitutions in the proposed lipid binding region of GCN5 did not result in a clear misfolding of the GCN5 variants, as shown by the CD spectra of the purified recombinant proteins (appendix Fig. 6.14), both substitution variants were catalytically inactive *in vitro* (Fig. 2.12 A).

To our knowledge, there is currently no crystal structure of Arabidopsis GCN5. A recent model of the Arabidopsis GCN5 protein predicted on the AlphaFold Protein Structure Database (Jumper et al., 2021) predicts surface exposition of the putative PtdIns3P-binding amino acids R260, K261, and K263 with high confidence. Furthermore, according to comparative analysis of GCN5 sequences from yeast and animals, the residues R260, K261, and K263 are unlikely to be responsible for acetyl-CoA binding and thus for the catalytic activity of GCN5 (Rojas et al., 1999; Schuetz et al., 2007; Sun et al., 2018). It appears possible that the amino acid substitutions in GCN5_{ILL} and GCN5_{EDD} lead to slight changes in tertiary structure, that might result in a slight conformational change in the substrate binding pocket, and thus a changed binding ability to histone H3 or acetyl-CoA. To further elucidate the effect of lipid binding on catalytic activity of GCN5, in the future single amino acid substitutions, e.g. only at position K261 with the highest BH-score, should be analyzed, which might still prohibit PtdIns3P binding while still enabling an active enzyme. A GCN5 variant with limited lipid binding but still catalytic activities would also be a helpful tool for future mutant complementation assays to further analyze the proposed GCN5/SAGA regulation by PIs.

3.5. PI binding contributes to nuclear localization of GCN5

Both lipid overlays and liposome sedimentation assays indicated that MBP-GCN5 bound most prominently to PtdIns3P (Fig. 2.9 B, C and D). This observation appears relevant, because PtdIns3P is the product of the PI 3-kinase VPS34, which has previously been reported to associate with sites of active transcription in plant cells (Bunney et al., 2000). Please note that the catalytic activity of recombinant Arabidopsis VPS34 as a PI 3-kinase was confirmed here for the first time (Fig. 2.13 B and C). A role of VPS34 in a GCN5-related process is supported by its interaction with GCN5 in YTH tests (Fig. 2.15 A). While the analysis of the subcellular distribution of VPS34-mCherry in Arabidopsis mesophyll protoplasts also confirmed the

localization to nuclei in addition to cytoplasmic localization (Fig. 2.14), the expression of VPS34-mCherry did not affect the auxin-activation of *GH3.3* (Fig. 2.16 A) in a manner comparable to the effects of overexpressed PIP5K1-EYFP or PIP5K2-EYFP (Fig. 2.4). The data suggest that overexpressed VPS34 did not influence GCN5-mediated histone acetylation *in vivo*, even though PtdIns3P had shown an inhibitory effect on histone acetylation by GCN5 *in vitro* (Fig. 2.7). Together with the previous reports, the data obtained here on GCN5 binding to PtdIns3P and on Arabidopsis VPS34 suggest a role for PtdIns3P in the recruitment of GCN5 to the sites of transcription, but do not indicate that PtdIns3P contributes to the control of GCN5 activity.

The substantially relaxed subcellular distribution of the EYFP-GCN5_{ILL} and EYFP-GCN5_{EDD} variants with reduced lipid binding capability compared to the clear nuclear localization of EYFP-GCN5 (Fig. 2.17) indicate a malfunction in the subcellular localization of GCN5 that is consistent with a role for PtdIns3P as a factor recruiting GCN5 to the nucleus. While data on the more precise subnuclear localization of EYFP-GCN5 or its variants are currently missing, based on the previous observations by Bunney and coworkers (Bunney et al., 2000) it is tempting to speculate that VPS34 and PtdIns3P mark the sites of active transcription to enable the recruitment of ING proteins and a HAT module containing GCN5. On the other hand, it cannot be ruled out that alternatively an essential part of an NLS in GCN5 was accidentally destroyed. However, an NLS prediction tool (SeqNLS; (Lin et al., 2012)) identified a putative NLS from amino acid K36 to L39 in the amino acid sequence of Arabidopsis GCN5 that matches the position of the NLS at the N-terminus of GCN5 from *Toxoplasma gondii* (Bhatti and Sullivan, 2005; Dixon et al., 2011), suggesting that substitutions in positions R260, K261, and K263 might leave the NLS of GCN5 unaffected.

Overall, the data show that PIs affect the acetylation of histones in the nucleus. It is conceivable that PIs establish contact sites between protein complexes and chromatin and the inner nuclear envelope. Such contacts might be relevant for chromatin transitions and the transcriptional activation of specific genes.

Based on the experimental results obtained in this study, a model for a hypothetical molecular mechanism can be proposed to explain the contribution of PIs in GCN5-mediated auxin-inducible transcription in the Arabidopsis nucleus (Fig. 3.1).

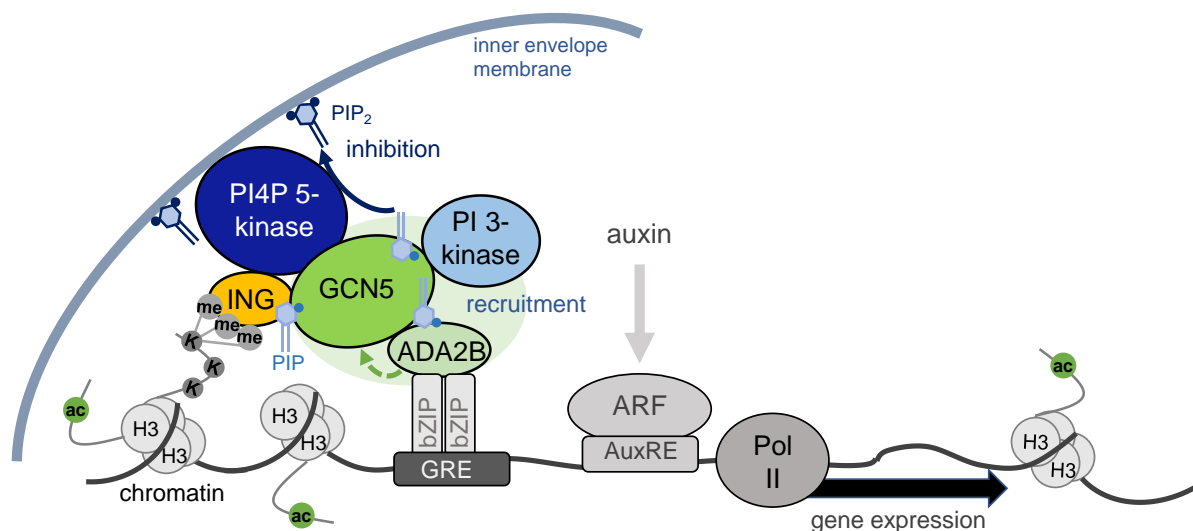


Fig. 3.1: Proposed model of PIs involved in epigenetic control. ING and GCN5, the HAT of the SAGA complex, are recruited to active transcription sites in the nucleus by PtdIns-monophosphate (PIP) binding. ING, the epigenetic reader, binds to H3K4me3 in the promoter region of auxin-inducible genes, like *GH3.3*, and recruits GCN5. Bound to histone H3, GCN5 mediates acetylation at lysine residues of the N-terminus of histone H3. PI4P 5-kinases convert the PtdIns-monophosphates to PtdIns-bisphosphates (PIP₂) and thereby induce inhibition of GCN5. PtdIns-bisphosphates attach the active transcription site to the inner envelope membrane of the nucleus. PI 3-kinase VPS34 interacts with GCN5 and synthesizes PtdIns3P to retain GCN5 at the gene locus. The model was designed on basis of a model of Weiste and Dröge-Laser (compare Fig. 1.8, (Weiste and Dröge-Laser, 2014)).

In this model, the epigenetic reader ING and the HAT GCN5, as a part of the SAGA complex, are recruited to an active transcription site of an auxin-inducible gene by PtdIns-monophosphates acting as recruiting signals. PI4P 5-kinases can bind to histone H3 at the active transcription site and could facilitate positioning of GCN5 and ING by stabilizing the complex at the interface with the inner nuclear envelope membrane. ING binds to H3K4me3 and recruits GCN5. GCN5 positions at the N-terminus of histone H3, probably with additional support of its bromodomain. H3K9, H3K14 or H3K27 are acetylated by GCN5, which was activated and regulated by ADA2B, the transcriptional adaptor within the SAGA complex that recruits the complex to bZIP transcription factors/GREs. PI4P 5-kinases, particularly PIP5K2 or PIP5K1, localize in the nucleus and convert the PtdIns-monophosphates to PtdIns-bisphosphates, which inhibit GCN5 after acetylation has occurred. PtdIns-bisphosphates attach the active transcription sites to the inner envelope membrane. PI 3-kinase VPS34 binds to GCN5 and generates PtdIns3P to retain GCN5 at the gene locus. Evidently, this model is still highly speculative and will require to be modified based on future research. However, I hope that this model summarized the finding of this thesis and can serve as a basis to expand the knowledge on the exciting and new field of nuclear PIs in plants.

4. Material and Methods

4.1. Equipment and devices

Equipment and technical devices used for experiments described in this thesis are listed in appendix Tab. 6.1 and are also mentioned in the description of each method.

4.2. Chemicals

Chemicals used are listed in appendix Tab. 6.2. All other chemicals used but not specifically mentioned were purchased from the companies Sigma-Aldrich/Merck (Munich/Darmstadt, Germany), Carl Roth GmbH (Karlsruhe, Germany) or AppliChem (Darmstadt, Germany).

4.2.1. Antibiotics used for the selection of bacteria

Antibiotic	Stock solution	Final concentration	Supplier
Carbenicillin disodium	100 mg/ml	100 µg/ml	Duchefa, Haarlem, Netherlands
Kanamycin monosulfate	50 mg/ml	50 µg/ml	Duchefa, Haarlem, Netherlands

4.2.2. Phospholipids

All phospholipids were ordered from Avanti Polar Lipids Inc. (Merck, Darmstadt, Germany) and are listed in appendix Tab. 6.3.

4.3. Consumables and Kits

Used kits and single-use material are listed in appendix Tab. 6.4.

4.4. Enzymes, proteins, peptides and molecular size markers

Restriction enzymes *Ascl*, *BamHI*, *NdeI*, *NheI*, *NotI*, *Sall*, *SfiI*, *XbaI* and *XhoI* were purchased from New England Biolabs Inc. (Frankfurt, Germany). Other used enzymes, proteins, peptides and molecular size markers and their suppliers are listed in appendix Tab. 6.5.

4.5. Microorganisms

Escherichia coli (*E. coli*) strain NEB5α (New England Biolabs Inc., Frankfurt, Germany) was used for cloning and vector/plasmid amplification.

Genotype: *fhuA2* Δ(*argF-lacZ*)*U169 phoA glnV44* Φ80 Δ(*lacZ*)*M15 gyrA96 recA1 relA1 endA1 thi-1 hsdR17*

E. coli strain Rosetta2(DE3) (Merck (Novagen), Darmstadt, Germany) was used for recombinant protein expression.

Genotype: F⁻ *ompT hsdS_B(r_B⁻ m_B⁻) gal dcm* (DE3) pRARE2 (Cam^R)

Saccharomyces cerevisiae (*S. cerevisiae*) strain NMY51 (Dualsystems Biotech, Zurich, Switzerland) was used for split-ubiquitin-based yeast-two-hybrid analyses.

Genotype: *MATa, his3Δ200, trp1-901, leu2-3,112, ade2, LYS2::(lexAop)4-HIS3, ura3::(lexAop)8-lacZ (lexAop)8-ADE2 GAL4*

4.6. Plants

The plant material used in this study was of *Arabidopsis thaliana* Columbia (Col-0) background.

wild type *Arabidopsis* Col-0: originally obtained from Lehle seeds
(<http://www.arabidopsis.com>)

pip5k1 pip5k2: crossing of single mutants with T-DNA insertions in *PIP5K1* (SALK_146728) and *PIP5K2* (SALK_012487), stock is heterozygous for *PIP5K1* (Ischebeck et al., 2013).

pCaMV35S::PIP5K2-EYFP: expresses *PIP5K2-EYFP* under control of the *pCaMV35S* promotor (*pMDC123* vector), individual lines L2 (T3 generation) and L5 (T2 generation) (Gerth et al., 2017a).

4.7. Culture media

Before using, media were autoclaved for 20 min at 121°C. Media containing saccharides were autoclaved for 15 min.

4.7.1. Media for *E. coli*

Media for cultivation of *E. coli* are listed in Tab. 4.1. For solid medium, 1.5 % (w/v) micro-agar was added before autoclaving. For applied antibiotics see section 4.2.1.

Tab. 4.1: Media for *E. coli*.

Component	LB medium	2YT medium
Yeast extract	0.5 % (w/v)	1 % (w/v)
Tryptone	1 % (w/v)	1.6 % (w/v)
NaCl	0.5 % (w/v)	0.5 % (w/v)
Glucose	-	0.2 % (w/v)

4.7.2. Media for yeast

Media for cultivation of *S. cerevisiae* NMY51 are listed in Tab. 4.2. For solid medium, 2 % (w/v) micro-agar was added before autoclaving. Glucose and amino acid supplements were autoclaved for 15 min at 121°C and added freshly to SD medium before use.

Tab. 4.2: Media for yeast.

Component	YPAD medium	SD medium
Yeast extract	1 % (w/v)	-
Peptone	2 % (w/v)	-
Adenine hemisulfate	0.004 % (w/v)	-
Yeast nitrogen base w/o amino acids and ammonium sulfate	-	0.17 % (w/v)
(NH ₄) ₂ SO ₄	-	0.5 % (w/v)
Micro-agar	2 % (w/v)	2 % (w/v)
Glucose	2 % (w/v)	2 % (w/v)
Amino acid supplement	-	1x -LW or 1x -LWH

Amino acid stock solution for supplementation of SD medium

-LW (10x)	200 mg/l L-adenine hemisulfate, 200 mg/l L-arginine HCl, 200 mg/l L-histidine HCl monohydrate, 300 mg/l L-isoleucine, 300 mg/l L-lysine HCl, 200 mg/l L-methionine, 500 mg/l L-phenylalanine, 2000 mg/l L-threonine, 300 mg/l L-tyrosine, 200 mg/l L-uracil, 1500 mg/l L-valine und 200 mg/l L-serine.
-LWH (10x)	same as -LW (10x) but without L-histidine HCl monohydrate

4.7.3. Plant medium

Medium for cultivation of Arabidopsis seedlings is listed in Tab. 4.3. For solid medium, 0.8 % (w/v) micro-agar was added before autoclaving.

Tab. 4.3: Plant medium.

Component	1/2 Murashige & Skoog (MS) medium
Murashige & Skoog-Medium, incl. modified vitamins	0.22 % (w/v)
Sucrose	1 % (w/v)
pH was adjusted with 1 M KOH to pH 5.6.	

4.8. Growth conditions

4.8.1. Growth conditions for Arabidopsis plants

Plants were grown at the conditions described below in either Adaptis A1000 plant chambers (Convion, Winnipeg, MB, Canada) or PERCIVAL AR-66/L3 plant chambers (Percival Scientific, Perry, IA, USA). For sterile growth on 1/2 MS medium, Arabidopsis seeds were sterilized in 1 ml sodium hypochlorite solution (6 % (w/v) NaOCl, 0.1 % (v/v) Triton X-100) for 15 min while shaking and washed six times with 1 ml ddH₂O afterwards. Sterilized seeds were directly sown on 1/2 MS medium. Seeds sown on 1/2 MS medium were first stratified for three days at 4°C in the dark and then cultivated under long-day conditions (16 h light, 8 h darkness) at ambient humidity and 21°C.

Protoplast experiments and nuclei isolation were performed using approximately six-week-old leaf material from Arabidopsis grown on soil at ambient humidity at 21°C in short-day conditions (8 h light, 16 h darkness). Apart from the *pip5k1 pip5k2* double mutant, plants were sown directly on soil. *pip5k1 pip5k2* was grown on 1/2 MS medium for ten days for preselection, and only plants with the appropriate mutant phenotype were transplanted to soil. The soil used was a mixture of nine parts substrate 1 (Klasmann-Deilmann GmbH, Geeste, Germany) and one part vermiculite and was sterilized by steaming at 80°C for 8 h.

4.8.2. Maintenance of yeast strain NMY51

To obtain the *S. cerevisiae* NMY51 strain, colonies were freshly plated out on YPAD medium every two to three weeks, grown at 28°C for two to three days, and then stored at 4°C.

4.9. Vectors used in this study

4.9.1. Vectors for recombinant protein expression in *E. coli*

Vector	Description	Source
<i>pGEX-6P-1</i>	<i>Amp^R</i> , contains under control of the <i>ptac</i> promotor the copy DNA (cDNA) coding for GST and a multiple cloning site (mcs) for expressing proteins with N-terminal GST tag.	GE Healthcare GmbH, Solingen, Germany

<i>pMAL-c5G</i>	<i>Amp^R</i> , contains under control of the <i>ptac</i> promoter the <i>malE</i> gene and a mcs for expressing fusion proteins with N-terminal MBP tag. MBP sequence was optimized for enrichment via amylose. MBP can be cleaved from protein of interest with the specific protease Genenase I.	New England Biolabs Inc., Frankfurt, Germany
-----------------	--	--

4.9.2. Vectors for yeast-two-hybrid studies

Vector	Description	Source
<i>pBT3-C-OST4</i>	<i>Kan^R</i> , <i>LEU2</i> auxotrophic marker for selection in yeast, bait vector, based on <i>pBT3-C</i> , contains under control of <i>pCYC1</i> promoter a mcs and 3' the cDNAs coding for the C-terminal part of ubiquitin (Cub, aa 34 – 76), LexA DNA binding domain and VP16 transactivation domain, <i>CYC1</i> terminator. Dr. Mareike Heilmann introduced <i>OST4</i> (coding for oligosaccharyltransferase 4) via <i>XbaI</i> restriction sites.	Dualsystems Biotech, Zurich, Switzerland; modified by Dr. Mareike Heilmann, MLU Halle Wittenberg
<i>pPR3-N</i>	<i>Amp^R</i> , <i>TRP1</i> auxotrophic marker for selection in yeast, prey vector, contains under control of <i>pCYC1</i> promoter the cDNA coding for the N-terminal part of ubiquitin (NubG, aa 1 – 38, I13 mutated to G) 5' of HA epitope tag and mcs, <i>CYC1</i> terminator.	Dualsystems Biotech, Zurich, Switzerland
<i>pAI-Alg5</i>	<i>Amp^R</i> , <i>TRP1</i> auxotrophic marker for selection in yeast, prey vector, contains the cDNA of unmodified Nub fused to <i>dolichyl-phosphate beta-glucosyltransferase</i> (<i>Alg5</i>).	Dualsystems Biotech, Zurich, Switzerland
<i>pDL2-Alg5</i>	<i>Amp^R</i> , <i>TRP1</i> auxotrophic marker for selection in yeast, prey vector, contains the cDNA of NubG fused to <i>Alg5</i> .	Dualsystems Biotech, Zurich, Switzerland

4.9.3. Vectors for transient protein expression in Arabidopsis protoplasts

Vector	Description	Source
<i>pEntryA</i>	<i>Amp^R</i> , based on <i>pUC18</i> , mcs under control of a <i>pCaMV35S</i> promoter, that has been introduced via <i>SfiI</i> restriction sites, poly(A) terminator of the octopine synthase (OCS) from tumor-inducing (Ti) plasmid of <i>Agrobacterium tumefaciens</i> (<i>A. tumefaciens</i>) (MacDonald et al., 1991), flanked by recombination sites attL1 (5' of mcs) and attL4 (3' of mcs).	Dr. Mareike Heilmann, MLU Halle-Wittenberg

<i>pEntryD</i>	<i>Amp^R</i> , based on <i>pUC18</i> , mcs under control of a <i>pCaMV35S</i> promoter, that has been introduced via <i>SfiI</i> restriction sites, poly(A) terminator of the OCS from Ti plasmid of <i>A. tumefaciens</i> (MacDonald et al., 1991), flanked by recombination sites attR4 (5' of mcs) and attL2 (3' of mcs).	Dr. Mareike Heilmann, MLU Halle-Wittenberg
----------------	--	--

4.10. Molecular biology methods

4.10.1. DNA isolation

Genomic DNA was extracted from rosette leaves using the cetyltrimethylammonium bromide (CTAB) method (Murray and Thompson, 1980). For this purpose, plant material frozen in liquid N₂ was pulverized in a 1.5 ml centrifuge tube and immersed in 250 µl of CTAB extraction solution (2 % (w/v) CTAB, 100 mM Tris-HCl pH 8.0, 1.4 M NaCl, 20 mM ethylenediaminetetraacetic acid (EDTA) pH 8.0, 2 % (v/v) 2-mercaptoethanol), and incubated for 30 min at 65°C. The extracts were then mixed with 250 µl chloroform:isoamyl alcohol (24:1 (v/v)) and centrifuged at 7,500 x *g* and room temperature (RT) for 3 min for phase separation. The upper phase was transferred to a new tube and mixed with 20 µl CTAB/NaCl solution (10 % (w/v) CTAB, 0.7 % (w/v) NaCl, preheated to 65°C). Samples were incubated for 2 min at RT. 220 µl 2-propanol were added and tubes were inverted several times. Samples were again incubated for 2 min at RT and centrifuged at 18,400 x *g* and RT for 10 min. The supernatant was carefully removed, and the DNA was washed with 100 µl 75 % (v/v) ethanol. The samples were centrifuged at 9,400 x *g* and RT for 5 min and the supernatant was carefully removed. The DNA was dried and finally dissolved in 30 µl ddH₂O.

4.10.2. RNA isolation

For RNA preparation from protoplasts, 400 µl transformed protoplasts (see section 4.26) were dissolved in 1 ml Trizol solution (38 % (v/v) Phenol (saturated with 0.1 M citrate buffer, pH 4.3 (#P4682, Sigma-Aldrich, Munich, Germany), 0.8 M guanidinium thiocyanate, 0.4 M ammonium thiocyanate, 0.1 M sodium acetate pH 5.0, 5 % (v/v) glycerol). Afterwards, all samples were incubated for 10 min at RT and centrifuged at 15,870 x *g* and 4°C for 10 min. Supernatant was transferred to a new tube and mixed vigorously for 15 s with 200 µl chloroform. Samples were incubated for 3 min at RT and were centrifuged at 15,870 x *g* and 4°C for 10 min. The upper phase was transferred to a new tube and combined with 1/2 volume of 2-propanol and 1/2 volume of high salt precipitation buffer (0.8 M sodium citrate, 1.2 M NaCl). Samples were inverted several times and incubated for 10 to 20 min at RT. RNA was precipitated by centrifuging at 15,870 x *g* and 4°C for 15 min. Supernatant was removed and precipitate was washed two times with 900 µl 75 % (v/v) ethanol. Samples were centrifuged at 15,870 x *g* and 4°C for 5 min and RNA was dried at RT. Dried RNA was resolved in 20 µl ddH₂O. RNA

concentration was measured at 260 nm with an Ultrospec 2100 pro UV/Vis spectrometer (Biochrom, Cambridge, United Kingdom) or Ultrospec 3000 UV/Vis spectrometer (Pharmacia Biotech AG, Dübendorf, Germany). RNA quality was determined by the ratio of absorbances $A_{260/280}$ and electrophoresis (see section 4.11).

4.10.3. cDNA synthesis

For cDNA synthesis, approximately 1 to 5 mg of total RNA from Arabidopsis seedlings and 1 μ l of total RNA from protoplasts were used. The cDNA synthesis was performed using the RevertAid H Minus First Strand cDNA Synthesis Kit (#K1632, Thermo Fisher Scientific, Schwerte, Germany) according to the manufacturer's instructions. If RNA was frozen prior to cDNA synthesis, it was incubated for 5 min at 65°C after thawing to achieve complete denaturation.

4.11. Separation of DNA and RNA in agarose gels

DNA and RNA molecules were separated according to their size in 1 % or 2 % (w/v) agarose gels in 1x Tris-Acetate-EDTA buffer (TAE buffer) (40 mM Tris, 20 mM glacial acetic acid, 1 mM EDTA). For this, samples were mixed with 5x sample buffer (60 % (v/v) glycerol, 0.4 % (w/v) Orange G, 0.03 % (w/v) bromophenol blue, 0.03 % (w/v) xylene cyanol PP) and loaded into the gels. The GeneRuler™ 100 bp DNA Ladder or GeneRuler™ 1 kb DNA Ladder (both Thermo Fisher Scientific, Schwerte, Germany) were used as molecular size markers. Electrophoresis was performed with MINI and MIDI chambers (cti, Idstein, Germany) with a voltage of 120 V to 150 V (DNA) or 70 V (RNA) per gel. For detection, gels were incubated in ethidium bromide (10 μ g/ml in ddH₂O) for 10 to 15 min and nucleic acids were visualized under UV light in a Gel Detection System Gel iX Imager (INTAS, Göttingen Germany) or a Gel Detection System Quantum ST4 (Vilber Lourmat Deutschland GmbH, Eberhardzell, Germany).

4.11.1. Extraction of DNA from gels

To isolate DNA vectors or fragments from agarose gels, the GeneJET™ Gel Extraction Kit (#K0692, Thermo Fisher Scientific, Schwerte, Germany) was used. Cut gel pieces were dissolved in manufacturer's binding buffer in a 1:1 ratio (v/v) for approximately 10 min at 50 to 60°C. The DNA was then loaded onto the purification column, washed with washing buffer, and the DNA was eluted with 20 to 30 μ l ddH₂O.

4.12. PCR strategies

4.12.1. Genotyping of Arabidopsis plants

To investigate Arabidopsis genotypes, wild type alleles, T-DNA insertions and the presence of transgenic expression cassettes, specific oligonucleotide pairs were used. Oligonucleotides are given in appendix Tab. 6.6. The polymerase chain reaction (PCR) was performed in a total volume of 25 µl with 2 µl isolated DNA (section 4.10.1) and with the TAQ-DNA-Polymerase (peqlab, VWR International GmbH, Darmstadt, Germany) as described in the manufacturer's instructions. The used standard PCR program started with an initial heating of the samples to 94°C for 5 min followed by 40 cycles, alternating the steps of denaturation at 94°C for 30 s, oligonucleotide annealing at 60°C for 30 s, and elongation at 72°C for 30 s/kilo bases (kb). PCR samples were separated using gel electrophoresis (section 4.11).

4.12.2. Quantitative real-time RT PCR (qPCR)

Transcript levels of various target genes were analyzed by quantitative real-time RT PCR (qPCR) on cDNA from section 4.10.3. For this purpose, 2 µl of respective cDNA sample and the Luna® Universal qPCR Master Mix (New England Biolabs Inc., Frankfurt, Germany) (for mesophyll protoplasts) were used as described in the manuals. Specific oligonucleotides for amplification of the corresponding transcripts were designed using the online tool Primer-BLAST (National Center for Biotechnology Information, U.S. National Library of Medicine, Bethesda, MD, USA (Ye et al., 2012)). Oligonucleotide pairs were designed to specifically amplify a cDNA fragment of no more than 200 base pairs (bp). Used oligonucleotides are listed in appendix Tab. 6.7. Data were normalized to the transcript level of the housekeeping gene *ubiquitin-conjugating enzyme 10 (UBC10)*. qPCRs were performed in a Rotor Gene Q 2-Plex (Qiagen, Hilden, Germany) using the program Rotor-Gene Q Series Software (Qiagen, Hilden, Germany). The used standard PCR program started with an initial heating of the samples to 95°C for 10 min followed by 40 to 50 cycles, alternating the steps of denaturation at 95°C for 10 s, oligonucleotide annealing at 60°C for 20 s, and elongation at 72°C for 30 s. The respective transcript data were analyzed using the Rotor-Gene Q Series software (Qiagen, Hilden, Germany) and the program LinRegPCR (J. M. Ruijter, Academic Medical Center, Amsterdam, Netherlands, based on (Ruijter et al., 2009; Tuomi et al., 2010; Ruijter et al., 2014)).

4.12.3. Amplification of DNA fragments by PCR

To clone the gene or cDNA of interest into a vector, the coding sequence regions had to be amplified by PCR. To avoid errors in the sequences as far as possible, Phusion® High Fidelity DNA-Polymerase with a proofreading ability (New England Biolabs Inc., Frankfurt, Germany) was used for this purpose according to the manufacturer's instructions. Templates were either

cDNAs already cloned as plasmids (1:20 dilution) or prepared cDNA (2 µl) (see section 4.10.3). Used oligonucleotides are listed in appendix Tab. 6.8. The used standard PCR program started with an initial heating of the samples to 98°C for 1 min followed by 40 cycles, alternating the steps of denaturation at 98°C for 30 s, oligonucleotide annealing at 65°C for 30 s, and elongation at 72°C for 30 s/kb, followed by a final oligonucleotide annealing at 60°C for 30 s and a final elongation at 72°C for 5 min. PCR products were separated on agarose gels (section 4.11) and purified as described in section 4.11.1.

4.12.4. Introduction of amino acid substitutions: fusion PCR

Amino acid substitutions were introduced by fusion PCR and appropriately modified oligonucleotide pairs. Forward and reverse oligonucleotides (fusion mutation oligonucleotides) were designed to anneal to the position where the desired substitutions were to be introduced. These fusion mutation oligonucleotides overlapped by at least 20 bp. In two separate PCR reactions, the forward mutagenesis oligonucleotide was used with the 3'-end oligonucleotide and the reverse mutagenesis primer was used together with the 5'-binding forward oligonucleotide. This resulted in two PCR fragments which were separated on an agarose gel (section 4.11), gel extracted (section 4.11.1) and fused in another PCR with the corresponding 5'-binding forward oligonucleotide and the 3'-end oligonucleotide. Initial templates were 1:100 dilutions of the plasmids carrying the cDNAs to be modified. The polymerase used for this purpose was the Phusion® High Fidelity DNA-Polymerase with a proofreading ability (New England Biolabs Inc., Frankfurt, Germany) as described in section 4.12.3. The used standard PCR program started with an initial heating of the samples to 98°C for 1 min followed by 40 cycles, alternating the steps of denaturation at 98°C for 30 s, oligonucleotide annealing at 65°C for 30 s, and elongation at 72°C for 30 s/kb, followed by a final elongation step at 72°C for 10 min. Finally, it was proceeded as described in section 4.12.3.

4.13. Restriction

Restriction enzymes (Ascl, BamHI, NdeI, NheI, NotI, Sall, SfiI, XbaI and XhoI) were used as described in the manuals from New England Biolabs Inc. (Frankfurt, Germany).

PCR products and vector backbones were digested overnight at the corresponding temperature. The restriction reactions were stopped by incubating the samples for 30 min at 80°C. The digested vectors were then purified via an agarose gel (section 4.11) and the GeneJET™ Gel Extraction Kit (#K0692, Thermo Fisher Scientific, Schwerte, Germany) (section 4.11.1).

4.14. Ligation

For ligation of digested DNA fragments in vectors, T4-DNA-Ligase (New England Biolabs Inc., Frankfurt, Germany) was used according to the manufacturer's instructions. Briefly, the reaction mixtures had a total volume of 20 μ l and each consisted of 3 μ l of digested PCR/cDNA insert, 1 μ l of the digested vector, 2 μ l of 10x T4-DNA-Ligase buffer, and 1 μ l of T4-DNA-Ligase and was incubated for 30 min at RT. Subsequently, the complete reactions were transformed into chemo-competent *E. coli* NEB5 α (section 4.15).

4.15. Amplification of plasmid- and vector DNA in *E. coli*

4.15.1. Preparation of chemo-competent *E. coli*

Chemo-competent *E. coli* NEB5 α cells were prepared after the protocol of Inoue and coworkers (Inoue et al., 1990). A pre-culture of 50 ml LB medium was inoculated with 500 μ l of *E. coli* NEB5 α (New England Biolabs Inc., Frankfurt, Germany) and incubated overnight at 180 rpm and 30°C. The pre-culture was used to inoculate a larger culture with an OD₆₀₀ of 0.05 which was incubated at 180 rpm and 37°C. At an OD₆₀₀ between 0.4 and 0.6, cell suspensions were aliquoted to 50 ml reaction tubes and were incubated on ice for 10 min. Cells were centrifuged at 3,320 x *g* and 4°C for 10 min and the supernatant was discarded. Sediments were resuspended in 20 ml pre-cooled TFB buffer (10 mM PIPES pH 6.7, 15 mM CaCl₂ x 2 H₂O, 250 mM KCl, 55 mM MnCl₂) and incubated for 10 min at 4°C. Cell suspensions were centrifuged at 3,320 x *g* and 4°C for 10 min, and the supernatant was discarded. Cells were resuspended in 4 ml TFB buffer, dimethyl sulfoxide (DMSO) was added to a final concentration of 7 % (v/v) and the cell suspension was incubated on ice for 10 min. Cells were then divided into 500 μ l aliquots each, frozen in liquid N₂, and stored at -80°C.

4.15.2. Transformation of chemo-competent *E. coli*

For the transformation of ligation approaches, 100 μ l of chemically competent *E. coli* NEB5 α cells each were used. For the transformation of already existing plasmids (retransformation/propagation), 50 μ l of chemically competent cells each were used. Cells were mixed with ligation mixtures/plasmid DNA and incubated on ice for 30 min. Then, a heat shock at 42°C was performed for 45 s, and the reactions were incubated again on ice for 5 min. 900 μ l LB medium were added and cells were incubated at 37°C for 1 h. For transformed ligations, the entire transformation mixture and for retransformations, only 50 μ l of the transformation mixture were plated out on LB medium with the appropriate antibiotics and cultured overnight at 37°C.

For retransformation, 50 μ l of chemo-competent *E. coli* cells were combined with 1 μ l of plasmid DNA. *E. coli* Rosetta2 cells were also transformed in volumes of 50 μ l with 1 μ l of plasmid DNA.

4.15.3. Plasmid isolation from *E. coli*

Plasmid DNA was isolated from *E. coli* using either the GeneJET™ Plasmid Miniprep Kit (Thermo Fisher Scientific, Schwerte, Germany) for small-scale plasmid isolation or the CompactPrep Plasmid Midi Kit (Qiagen, Hilden, Germany) for larger scale plasmid isolation. For small-scale plasmid isolation, 2 to 5 ml of LB medium and for larger scale (midi-) plasmid isolations 50 to 100 ml LB medium containing the appropriate antibiotics were inoculated with a single *E. coli* NEB5 α colony each and grown overnight while shaking at 150 to 180 rpm and 37°C. Plasmid DNA concentration was measured at 260 nm with an Ultrospec 2100 pro UV/Vis Spectrometer (Biochrom, Cambridge, United Kingdom) or a Ultrospec 3000 UV/Vis Spectrometer (Pharmacia Biotech AG, Dübendorf, Germany). DNA quality was determined by the ratio of absorbances $A_{260/280}$ and electrophoresis (section 4.11).

4.16. Sequencing

Clonings were verified by sequencing. For this purpose, 1 μ g of plasmid DNA was mixed with 5 μ l of a 5 μ M solution of a sequence- or vector-specific oligonucleotide in a total volume of 10 μ l. The oligonucleotides used are listed in appendix Tab. 6.9. The samples were sequenced using GATC Biotech AG (Eurofins Genomics Germany GmbH, Ebersberg, Germany) and the sequence data were analyzed using Chromas software (version 2.6.6, Technelysium Pty Ltd, South Brisbane, Australia) and the online tools Multalin (Corpet, 1988), Clustal Omega (Madeira et al., 2019) and BoxShade (version 3.21, K. Hofmann, M. Baron, ExPASy Bioinformatics Resource Portal, SIB Swiss Institute of Bioinformatics, Lausanne, Switzerland). Reference sequences were obtained from the NCBI gene database (National Center for Biotechnology Information, U.S. National Library of Medicine, Rockville Pike, Bethesda, MD, USA).

4.17. Cloning strategies

4.17.1. Constructs for recombinant protein expression

For recombinant protein expression in *E. coli*, the respective cDNAs of *GCN5*, *GCN5_{ILL}*, *GCN5_{EDD}*, *GCN5₂₁₂₋₃₇₅*, *GCN5₂₈₄₋₃₇₅*, *ADA2B*, *ING1*, *ING2*, *VPS34*, *VPS34₁₋₂₁₀* and *VPS34₂₁₀₋₈₁₄* were moved into *pGEX-6P-1* or *pMAL-c5G* (section 4.9.1) to get either glutathione S-transferase (GST)- or maltose-binding protein (MBP)-fusion constructs. cDNAs coding for the proteins of interest were introduced to *pGEX-6P-1* or *pMAL-c5G* vectors using NotI and Sall restriction sites. Oligonucleotide information is given in appendix Tab. 6.8. Cloning techniques were performed according to sections 4.12 to 4.15.

Constructs, that were designed during this study or previously, are listed in Tab. 4.4.

Tab. 4.4: Constructs for recombinant protein expression.

Abbreviations: **FH**: created by Franziska Heinrich, **FM**: created by Dr. Franziska Meyer, **JL**: created by Dr. Jennifer Lerche, **MA**: created in master thesis (FD), **MH**: created by Dr. Mareike Heilmann, **PHD**: created in this study.

Vector	cDNA	Created by
<i>pGEX-6P-1</i>	<i>GCN5, ING1, ING2</i>	MA
<i>pMAL-c5G</i>	<i>GCN5</i>	MA
	<i>GCN5₂₁₂₋₃₇₅, GCN5₂₈₄₋₃₇₅, GCN5_{ILL}, GCN5_{EDD}, ADA2B, VPS34, VPS34₁₋₂₁₀, VPS34₂₁₀₋₈₁₄</i>	PHD
	<i>ING1, ING2</i>	FH
	<i>PIP5K1</i>	MH
	<i>PIP5K2</i>	JL
	<i>PIP5K6</i>	FM

4.17.2. Constructs for split-ubiquitin-based yeast-two-hybrid

The vector *pBT3-C-OST4* (section 4.9.2) was used to clone bait constructs and the vector *pPR3-N* (section 4.9.2) was used to clone prey constructs. cDNAs coding for the proteins of interest were introduced to *pBT3-C-OST4* and *pPR3-N* vectors using SfiIA and SfiIB restriction sites, respectively. In *pBT3-C-OST4*, cDNAs were introduced in reading frame with 5' *OST4* and 3' *Cub*, *LexA* and *VP16*. In *pPR3-N*, cDNAs were introduced in reading frame with 5' *NubG*. The respective specific oligonucleotides for cloning are listed in appendix Tab. 6.8. Cloning techniques were performed according to sections 4.12 to 4.15.

Constructs, that were designed during this study or previously, are listed in Tab. 4.5.

Tab. 4.5: Constructs for split-ubiquitin-based yeast-two-hybrid assays.

Abbreviations: **FM**: created by Dr. Franziska Meyer, **MA**: created in master thesis (FD), **MH**: created by Dr. Mareike Heilmann, **PHD**: created in this study.

Vector	cDNA	Created by
<i>pBT3-C-OST4</i> (bait)	<i>PIP5K1, PIP5K2</i>	MH
	<i>GCN5, PIP5K9</i>	MA
	<i>VPS34, VPS34₁₋₂₁₀, VPS34₂₁₀₋₈₁₄</i>	PHD
	<i>PIP5K6</i>	FM/PHD
<i>pPR3-N</i> (prey)	<i>GCN5, ING1, ING2, HAM2, HDAC6, HDAC19, SWC4 (MYB1-like)</i>	MH
	<i>ADA2B</i>	PHD

4.17.3. Constructs for transformation of Arabidopsis protoplasts

For transient expression under the *pCaMV35S* promoter in protoplasts, *pEntryA-pCaMV35S* or *pEntryD-pCaMV35S* vectors were used (section 4.9.3). In control experiments, *pEntryA-pCaMV35S::EYFP* and *pEntryD-pCaMV35S::mCherry* were used, both were provided by Larissa Launhardt. In brief, *EYFP* and *mCherry* were amplified with 5'-Sall and 3'-Ascl restriction sites and moved into the respective *pEntry-pCaMV35S* vector. The coding sequences for *EYFP-GCN5*, *EYFP-GCN5_{ILL}* and *EYFP-GCN5_{EDD}* were amplified by PCR introducing 5'-Ascl and 3'-NotI restriction sites and moved into the above described *pCaMV35S::EYFP*, resulting in *pEntryA-pCaMV35S::EYFP-GCN5*, *pEntryA-pCaMV35S::EYFP-GCN5_{ILL}* and *pEntryA-pCaMV35S::EYFP-GCN5_{EDD}*. The respective specific oligonucleotides for cloning are listed in appendix Tab. 6.8.

PIP5K1, *PIP5K2*, *PIP5K2 K470A* and *PIP5K6* were cloned as C-terminal *EYFP* fusions (provided by Dr. Mareike Heilmann and Dr. Franziska Meyer) into *pEntryA-pCaMV35S::EYFP* or *pEntryD-pCaMV35S::EYFP* (*PIP5K6*) by using Ascl and XhoI restriction sites. The cDNA of *VPS34* was introduced via Ascl and NheI into a *pEntryA-pCaMV35S::mCherry*.

The *NLS_{SV40}DsRed* (*NLS-DsRed*) marker was produced by PCR fusion of the *NLS_{SV40}* sequence (*NLS_{SV40}*, strong NLS PKKKRKV of the large T-antigen of simian virus 40 (Kalderon et al., 1984)) 5'-prime to the *DsRed* sequence using the oligonucleotides *NLSRedStar-Asclfor/RedStar-Xholrev* and cloned into *pEntryA-pCaMV35S* (provided by Dr. Mareike Heilmann).

Cloning techniques were performed according to sections 4.12 to 4.15.

Constructs, that were designed during this study or previously, are listed in Tab. 4.6.

Tab. 4.6: Transformation vectors for Arabidopsis leaf protoplasts.

Abbreviations: **FM**: created by Dr. Franziska Meyer, **LL**: created by Larissa Launhardt, **MH**: created by Dr. Mareike Heilmann, **PHD**: created in this study.

Vector	cDNA	Restriction sites (gene)	Restriction sites (tag)	Created by
<i>pEntryA</i>	<i>EYFP</i>	-	Sall/Ascl	LL
	<i>PIP5K1-EYFP</i>	Ascl/XhoI	XhoI/NotI	MH
	<i>PIP5K2-EYFP</i>	Ascl/XhoI	XhoI/NotI	MH
	<i>PIP5K2 K470A-EYFP</i>	Ascl/XhoI	XhoI/NotI	MH
	<i>EYFP-GCN5</i>	Ascl/NotI	Sall/Ascl	PHD
	<i>EYFP-GCN5_{ILL}</i>	Ascl/NotI	Sall/Ascl	PHD
	<i>EYFP-GCN5_{EDD}</i>	Ascl/NotI	Sall/Ascl	PHD
	<i>VPS34-mCherry</i>	Ascl/NheI	NheI/BamHI	MH
	<i>NLS-DsRed</i>	Ascl/XhoI	-	MH
<i>pEntryD</i>	<i>PIP5K6-EYFP</i>	Ascl/XhoI		FM

Vector	cDNA	Restriction sites (gene)	Restriction sites (tag)	Created by
<i>pEntryD</i>	<i>mCherry</i>	-	Sall/Ascl	LL

4.18. Recombinant expression and enrichment of fusion proteins

4.18.1. Recombinant expression of fusion proteins in *E. coli*

Proteins were recombinantly expressed in *E. coli* Rosetta2 cells. Competent cells (section 4.15.1) were transformed with respective expression plasmids (sections 4.15.2 and 4.17.1). Starter cultures were incubated overnight at 180 rpm and 30°C in 2YT medium (section 4.7.1) with appropriate antibiotics and were used to inoculate main expression cultures with an OD₆₀₀ of 0.05. For MBP-tagged protein expression, the 2YT medium was supplemented with 0.2 % (w/v) glucose. Main cultures were shaken with 300 ml 2YT medium either in normal flasks and at 180 rpm or in baffled flasks and at 90 rpm and 37°C until an OD₆₀₀ of 0.6 to 0.8 was achieved. MBP-PIP5K1, MBP-PIP5K2 and MBP-VPS34 and variants were expressed at 28°C in baffled flasks and expression was induced with 1 mM isopropyl β-D-1-thiogalactopyranoside (IPTG) for 4 h. MBP-PIP5K6 was expressed at 22°C in baffled flasks and expression was induced with 0.1 mM IPTG for 4 h. GST/MBP-GCN5, MBP-GCN5 substitution variants and truncated MBP-GCN5 variants, GST/MBP-ING1, GST/MBP-ING2 and MBP-ADA2B were expressed at 18°C and expression was induced with 0.1 mM IPTG for 20 h. As controls GST and MBP were expressed. Expression was at 37°C and expression was induced with 0.1 mM IPTG for 2 h. After expression, cells were harvested in aliquots of 50 ml at 3,220 x g and 4°C for 15 min, frozen in liquid N₂ and stored until use at -20°C.

4.18.2. Lysis of cells expressing recombinant fusion proteins

Cell pellets with expressed GST-tagged proteins were solubilized in 2.5 ml GST buffer (50 mM Tris-HCl pH 8.0, 150 mM NaCl, 1x Protease-Inhibitor (SIGMAFAST™ Protease Inhibitor Cocktail, EDTA-Free, Sigma-Aldrich, Munich, Germany)) and cell pellets with expressed MBP-tagged proteins were solubilized in 2.5 ml MBP buffer (20 mM Tris-HCl pH 7.4, 200 mM NaCl, 1 mM EDTA pH 8.0, 1x Protease-Inhibitor (SIGMAFAST™ Protease Inhibitor Cocktail, EDTA-Free)). Cell disruption was initiated with 1 mg/ml lysozyme and incubation on ice for 30 min followed by sonication with 1,600 to 2,000 J in pulses of 2 s (Vibra-Cell™ 72442, Bioblock Scientific, Sonics & Materials Inc., Newton CT, USA). The lysates were centrifuged at 20,800 x g and 4°C for 15 min, and the soluble protein fraction was retained.

For protein enrichment, cell pellets with expressed MBP-PIP5K1 and MBP-PIP5K2 were solubilized by Lennart Schwalgun according to Dejonghe and coworkers (Dejonghe et al., 2016).

Exemplary cell lysates of all expressed proteins are displayed in appendix Fig. 6.19.

4.18.3. Enrichment of recombinant fusion proteins

For protein enrichment, the soluble protein fractions from section 4.18.2 were used. For enrichment of GST- or MBP-tagged proteins, Pierce™ centrifuge columns with 500 µl Pierce™ glutathione agarose (both Thermo Fisher Scientific, Schwerte, Germany) or 500 to 700 µl amylose resin (New England Biolabs Inc., Frankfurt, Germany) were used. The resins were washed three times with either 3 ml GST equilibration buffer (50 mM Tris-HCl pH 8.0, 150 mM NaCl) or MBP equilibration buffer (20 mM Tris-HCl pH 7.4, 200 mM NaCl, 1 mM EDTA pH 8.0). Then, cell lysates were incubated with the resins in the columns for 1 h while shaking at RT followed by 1 h while shaking at 4°C. The flow-through was discarded, and the matrices were washed three times with 3 ml equilibration buffer each. For enhancing the yield, the steps were repeated with a second cell lysate, that was incubated with the resins for 1 h while shaking at RT followed by overnight incubation at 4°C. The flow-through was discarded, and the matrices were washed three times with 3 ml equilibration buffer each. Proteins were eluted from the resins with 300 µl of elution buffer each in five replicates. GST-tagged proteins were eluted with 50 mM reduced glutathione in GST equilibration buffer, MBP-tagged proteins were eluted with 10 mM maltose in MBP equilibration buffer. Enriched protein fractions were checked via sodium dodecyl sulfate polyacrylamide gel electrophoresis (SDS-PAGE) (see section 4.19). Protein concentrations were determined via Bradford assay (see section 4.18.4).

Soluble protein fractions containing MBP-PIP5K1 and MBP-PIP5K2 were enriched by Lennart Schwalgun according to Dejonghe and coworkers (Dejonghe et al., 2016).

Exemplary fractions of all enriched proteins are displayed in appendix Fig. 6.19.

4.18.4. Determination of protein concentrations via Bradford assay

Protein concentrations were determined using a Bradford assay (Bradford, 1976). 10 µl of the enriched protein fraction were mixed with 990 µl 1x Bradford reagent (5x Bradford reagent, SERVA Electrophoresis GmbH, Heidelberg, Germany) and incubated for 5 min at RT. Absorption was measured at 595 nm using an Ultrospec 2100 pro UV/Vis spectrometer (Biochrom, Cambridge, United Kingdom) or an Ultrospec 3000 UV/Vis spectrometer (Pharmacia Biotech AG, Dübendorf, Germany). The relative protein content was calculated using a bovine serum albumin (BSA) standard curve.

4.19. Sodium dodecyl sulfate polyacrylamide gel electrophoresis (SDS-PAGE)

Cell lysates and protein enrichments were separated according to their molecular weight in an electric field on an SDS-PAGE using a method according to Laemmli (Laemmli, 1970). For this purpose, samples were mixed with 4x Laemmli sample buffer (240 mM Tris-HCl pH 6.8,

8 % (w/v) sodium dodecyl sulfate (SDS), 0.08 % (w/v) bromophenol blue, 40 % (v/v) glycerol, 20 % (v/v) 2-mercaptoethanol (Julkowska et al., 2013) or 250 mM Tris-HCl pH 6.8, 8 % (w/v) SDS, 0.04 % (w/v) bromophenol blue, 40 % (v/v) glycerol, 400 mM dithiothreitol (DTT)) and separated using either pre-casted 4 – 20 % SDS gradient gels (SERVAGE^{ITM} TG PRIMETM, SERVA Electrophoresis GmbH, Heidelberg, Germany) or self-casted SDS gels with a 5 % stacking gel and a 10 % separation gel (w/v of polyacrylamide). Self-casted gels were prepared in a Multiple Gel Caster (SE 200 series) (Hoefer Scientific Instruments, Holliston, MA, USA). The gel composition is listed in appendix Tab. 6.10.

Gel electrophoreses were performed in SDS running buffer (0.3 % (w/v) Tris, 1.44 % (w/v) glycine, 0.1 % (w/v) SDS) in a SE250 Electrophoresis Chamber (Hoefer Pharmacia Biotech Inc., San Francisco, CA, USA) at constant 35 mA/gel (pre-casted gels) or at constant 25 mA/gel (self-casted gels) until the dye bromophenol blue of the Laemmli sample buffer reached the bottom of the gels. Either PageRulerTM Prestained Protein Ladder (10 to 180 kDa) or PageRulerTM Unstained Protein Ladder (10 to 200 kDa) (both Thermo Fisher Scientific, Schwerte, Germany) were used as molecular size markers. After separation, gels were either stained with Quick Coomassie[®] Stain (SERVA Electrophoresis GmbH, Heidelberg, Germany) or used for immunodetection (see section 4.20).

4.20. Immunodetection of proteins (Western blotting)

For immunodetection, proteins separated by size via SDS-PAGE (section 4.19) were transferred to nitrocellulose membranes (Amersham Protran 0,45 NC, GE Healthcare GmbH, Solingen, Germany) according to the method of Towbin and coworkers (Towbin et al., 1979). Protein transfer was performed in a Mini-PROTEAN[®] Tetra System Blotting Chamber (BioRad Laboratories GmbH, Munich, Germany) in transfer buffer (0.582 % (w/v) Tris, 0.293 % (w/v) glycine, 0.375 % (w/v) SDS, 20 % (v/v) methanol) for 60 to 75 min at constant 60 V and 400 mA. Subsequently, the membranes were blocked for 30 min at RT in 3 % (w/v) milk powder in 1x TBS buffer (50 mM Tris-HCl pH 7.5, 150 mM NaCl) while shaking. The blocked membranes were subsequently incubated with the primary antibody, diluted as recommended in manufacturer's instructions in 3 % (w/v) milk powder in 1x TBS buffer for 90 min at RT or overnight at 4°C while shaking. Membranes were washed three times for 10 min with 1x TBS and then incubated with the respective secondary antibody diluted in 3 % (w/v) milk powder in 1x TBS buffer for 45 to 60 min at RT. Secondary antibodies used were either conjugated to horse radish peroxidase (HRP) or to alkaline phosphatase (AP). Therefore, the membranes were washed either three times each for 10 min with 1x TBS buffer for HRP detection or twice in 1x TBS buffer and once in AP buffer (100 mM Tris-HCl pH 9.5, 100 mM NaCl, 5 mM MgCl₂) for AP detection. Primary and secondary antibodies used are listed in appendix Tab. 6.11.

HRP detection was performed with SuperSignal™ West Femto Maximum Sensitivity Substrate (Thermo Fisher Scientific, Schwerte, Germany) in a Fusion Solo S (Vilber Lourmat Deutschland GmbH, Eberhardzell, Germany) using the FusionCapt Advance Solo 7 (version 17.01) software. AP detection was performed with 0.175 mg/ml 5-bromo-4-chloro-3-indolyl phosphate disodium salt (BCIP, 50 mg/ml stock solution in ddH₂O) and 0.338 mg/ml p-nitrotetrazolium blue chloride (NBT, 75 mg/ml stock solution in 70 % (v/v) dimethylformamide) in AP buffer.

4.20.1. Characterization of antibody specificity

Antibodies against histone H3 and its posttranslational acetylation events at lysines 9 and 14 (see Tab. 6.11) were tested for their specificity by using different histone peptides (see appendix Tab. 6.5) in a dot-blot analysis.

1.5 µg and 0.3 µg of histone H3 from calf thymus (#11034758001, Roche Diagnostics GmbH, Mannheim, Germany), recombinant human histone H3 protein (active, HsH3.1, #ab198757, Abcam, Cambridge, United Kingdom), acetyl-histone H3 (Lys9) peptide (#12-358, Sigma-Aldrich, Munich, Germany), acetyl-histone H3 (Lys14) peptide (#12-359, Sigma-Aldrich, Munich, Germany), acetyl-histone H3 (Lys9/14) peptide (#12-360, Sigma-Aldrich, Munich, Germany), human histone H3 (di methyl K4) peptide (#ab7768, Abcam, Cambridge, United Kingdom) and human histone H3 (tri methyl K4) peptide (#ab1342, Abcam, Cambridge, United Kingdom) were spotted on nitrocellulose membranes (Amersham Protran 0,45 NC, GE Healthcare GmbH, Solingen, Germany). The blocked membranes were incubated with primary antibodies (anti-H3, anti-H3K9ac and anti-H3K14ac, see appendix Tab. 6.11) overnight at 4°C and then with the corresponding secondary antibody (see appendix Tab. 6.11). Finally, HRP detection was performed as described in section 4.20.

4.21. Examining protein secondary structure using circular dichroism (CD) spectroscopy

Protein secondary structures of recombinantly expressed MBP, MBP-GCN5, MBP-GCN5_{ILL} and MBP-GCN5_{EDD} were analyzed by using far-UV circular dichroism (CD) spectroscopy (Kelly et al., 2005). As control, CD spectra of MBP-GCN5 denatured with 4.5 M guanidinium chloride for 6.5 h were recorded. Enriched protein fractions with a concentration of 0.3 to 0.6 µg/µl were measured in a precision cell with a light path length of 0.2 mm (Hellma GmbH, & Co. KG, Müllheim, Germany) in a J-810 spectropolarimeter (JASCO Deutschland GmbH, Pfungstadt, Germany). The associated Peltier element PTC-423S (JASCO Deutschland GmbH, Pfungstadt, Germany) was adjusted to 20°C. Ellipticity Θ was measured as an average of 64 repetitions with a scan speed of 50 nm/min and intervals of 1 nm between data points. Data were taken from 195 (or up to 199) to 250 nm. Measurements were corrected with MBP elution

buffer (for denatured protein control combined with 4.5 M guanidinium chloride) and mean residue weight ellipticity $[\Theta]_{MRW}$ was calculated by using the following formula:

$$[\Theta]_{MRW} = \frac{\Theta * M}{10 * d * c * N} \text{ in } [\text{deg} * \text{cm}^2 * \text{dmol}^{-1}]$$

with Θ : ellipticity [mdeg], M : molecular weight [g/mol] (calculated using ProtParam, ExPASy Bioinformatics Resource Portal, SIB Swiss Institute of Bioinformatics, Lausanne, Switzerland, (Gasteiger et al., 2005)), d : light path length [cm], c : concentration [mg/ml], N : number of amino acids.

4.22. Studies of protein-protein interactions

4.22.1. Split-ubiquitin-based yeast-two-hybrid (YTH)

For the study of protein-protein interactions, the DUALmembrane Kit 3 (Dualsystems Biotech AG, Zurich, Switzerland) was used, which is based on a method published by Johnsson and Varshavsky (Johnsson and Varshavsky, 1994). As described in a study by Möckli and coworkers (Möckli et al., 2007), a cytosolic-localized split-ubiquitin-based yeast-two-hybrid (YTH) screen was developed by fusing the bait proteins to the yeast OST4 protein localized in the ER membrane.

This YTH utilizes the eukaryotic conserved mechanism that reconstituted ubiquitin fusion proteins are subsequently cleaved by ubiquitin-specific proteases at the last amino acid position of ubiquitin. Split-ubiquitin-based YTH exploits the fact that the N-terminal half of ubiquitin fused as prey (Nub, residues 1 – 38) and the C-terminal half of ubiquitin fused as bait (Cub, 34 – 76), which is fused to the transcription factor LexA-VP16, reconstitute upon protein-protein interaction of bait and prey, and only then the ubiquitin-specific protease cleaves the transcription factors. The YTH vectors are described in section 4.9.2 and the constructs used in YTH are described in section 4.17.2. The transcription factors then activate the reporter genes *HIS3*, *ADE2* and *lacZ*, and the yeast is able to grow on medium lacking these components. The control prey vector *pAI-Alg5* ensures spontaneous non-protein-protein interaction-dependent reconstitution of the ubiquitin halves and is used as a positive control. *pDL2-Alg5* contains a ubiquitin half not capable of spontaneous reconstitution, so this is used as a negative control along with the bait.

4.22.1.1. Preparation of chemo-competent *S. cerevisiae* cells

Chemo-competent *S. cerevisiae* NMY51 cells (Dualsystems Biotech AG, Zurich, Switzerland) were prepared and transformed by the lithium acetate method (Ito et al., 1983). 50 ml of YPAD medium were inoculated with a yeast colony and grown overnight at 180 rpm and 30°C. The next day, for seven transformation reactions, 50 ml each of YPAD medium was inoculated with

the pre-culture to an OD₆₀₀ between 0.15 and 0.2 and grown at 180 rpm and 30°C to an OD₆₀₀ of 0.6. The yeast cells were sedimented as 50 ml aliquots by centrifugation at 2,500 x g and RT for 5 min and were washed in 20 ml TE buffer (10 mM Tris-HCl pH 7.5, 1 mM EDTA pH 8.0). After sedimentation at 2,500 x g for 5 min, the cells were washed in 1 ml lithium acetate/TE buffer (110 mM lithium acetate, 11 mM Tris-HCl pH 7.5, 1.1 mM EDTA pH 8.0) and sedimented at 2,500 x g for 3 min and subsequently resuspended in 700 µl lithium acetate/TE buffer.

4.22.1.2. Transformation of chemo-competent *S. cerevisiae* NMY51 cells

For each transformation reaction, 1 to 1.5 µg bait construct and 1 to 1.5 µg prey construct (see Tab. 4.5) were mixed with 100 µl chemo-competent cell suspension and 700 µl PEG/lithium acetate mix (40 % (w/v) polyethylene glycol (PEG), 100 mM lithium acetate, 10 mM Tris-HCl pH 7.5, 1 mM EDTA pH 8.0) and incubated at 180 rpm and 30°C for 30 min. Then, 80 µl DMSO were added, cell suspensions were mixed, and heat shocked for 15 to 20 min at 42°C. Cells were sedimented at 700 x g for 5 min, supernatant was discarded, and cells were washed with 500 µl 0.9 % (w/v) NaCl solution and sedimented for 30 s at 700 x g. Finally, cells were resuspended in 150 µl 0.9 % (w/v) NaCl solution and plated on SD selection medium lacking leucine and tryptophane (-LW). Plates were incubated for three to seven days at 30°C.

4.22.1.3. Analysis of protein-protein interactions by yeast-two-hybrid tests

Positive selected colonies on SD-LW selection medium were used for drop tests on selection medium lacking leucine, tryptophane and histidine (SD-LWH). Therefore, cells were resuspended in TE buffer to an OD₆₀₀ of 0.5. Then, 3 µl of each cell suspension were dropped on SD-LW and SD-LWH (see section 4.7.2). For more stringent selection conditions, 5 or 10 mM 3-amino-1,2,4-triazole (3-AT) were added as an inhibitor of histidine biosynthesis. Cell growth was monitored at 30°C incubation over a period of eight days.

4.22.2. Analysis of protein-protein interactions by *in vitro* immuno pull-down assays

For pull-down experiments, 100 µl each of Pierce™ glutathione agarose (Thermo Fisher Scientific, Schwerte, Germany) were loaded in microcentrifuge spin columns (Pierce™ centrifuge columns, 0.8 ml volume, Thermo Fisher Scientific, Schwerte, Germany), washed three times with 600 µl GST equilibration buffer (25 mM Tris-HCl pH 7.2, 75 mM NaCl) and centrifuged in between each time at 100 x g for 1 min. Recombinant GST-tagged protein lysates were loaded onto the resin and GST-tagged proteins were immobilized on glutathione agarose by incubating the mixture for 1 h at 4°C with agitation. Unbound protein was eluted by

washing the resins three times with 600 μ l of GST equilibration buffer each time, and the bound GST-labeled protein was incubated with the corresponding recombinant MBP-labeled protein lysates overnight at 4°C under swirling. Upon washing of the resin (see above), GST-bound proteins were eluted with 50 mM glutathione in GST equilibration buffer. Elution was repeated twice. Interacting MBP fusion proteins were detected using a monoclonal anti-MBP antibody. Protein input was detected using a polyclonal anti-GST antibody (see sections 4.19 and 4.20). Tab. 4.7 shows used amounts of protein lysates. Volumes were filled up with GST equilibration buffer to 600 μ l. MBP-tagged proteins were incubated with resin before adding to a resin with bound GST-tagged protein.

Tab. 4.7: Used amounts of protein crude extracts in *in vitro* immuno pull-down assays.

Protein	Volume [μ l]
GST	50
GST-GCN5	400
GST-ING1, GST-ING2	600
MBP-GCN5, MBP-PIP5K1, MBP-PIP5K2, MBP-VPS34, MBP-VPS34 ₁₋₂₁₀ , MBP-VPS34 ₂₁₀₋₈₁₄	600
MBP-PIP5K6	300

4.22.3. Analysis of protein-protein interactions by dot-blot analyses

Binding of PIP5K1 and PIP5K2 to histone H3 was tested with the recombinant histone H3 protein and the histone H3 from calf thymus that are described in appendix Tab. 6.5 and that were used in antibody specificity tests (see section 4.20.1).

Histone H3 and histone H3 from calf thymus were spotted on nitrocellulose membranes in dots of 2 μ g, 1 μ g, 200 ng, 100 ng, 50 ng, 10 ng, 5 ng, 1 ng and 0.5 ng. 2 μ l of used enriched protein fractions were spotted three times on the membranes as control. Membranes were blocked for 45 min with 3 % (w/v) milk powder in 1x TBS buffer. 50 to 100 μ g of enriched MBP, MBP-PIP5K1 or MBP-PIP5K2 were added to 3 % (w/v) milk powder in 1x TBS buffer and were incubated with the membranes overnight at 4°C while shaking. The next day, membranes were treated with suitable antibodies as described in section 4.20. Protein binding was visualized via AP detection.

4.23. Analysis of protein-lipid interactions

Proteins were tested concerning their ability to bind PIs. Lipid overlay assays and liposome sedimentation assays were performed as described.

4.23.1. Lipid overlay assay

For lipid overlay assays, PIP Strips (#P-6001, Echelon Biosciences Inc., MoBiTec, Göttingen, Germany) were used. The membranes were blocked for 30 min in 3 % milk powder (w/v) in 1x TBS buffer and were then incubated with the respective enriched recombinant proteins (50 to 100 µg) solved in 3 % milk powder (w/v) in 1x TBS overnight at 4°C while shaking. Membranes were washed three times each for 10 min with 1x TBS buffer and incubated with anti-MBP antibody diluted in 3 % milk powder (w/v) in 1x TBS buffer (appendix Tab. 6.11) for 1.5 h at RT. Membranes were washed three times for 10 min with 1x TBS buffer and were incubated with secondary antibody (anti-mouse conjugated with AP diluted in 3 % milk powder (w/v) in 1x TBS buffer (appendix Tab. 6.11)) for 1 h at RT. After two times washing with 1x TBS buffer, the membranes were washed once with AP buffer for equilibration and detection was performed using BCIP/NBT as substrates for AP (section 4.20). As lipid blot functionality test, the commercial PIP grips PtdIns3P Grip (#G-0302) and PtdIns(4,5)P₂ Grip (#G-4501) (Echelon Biosciences Inc., MoBiTec, Göttingen, Germany) were tested with the PIP Strips. The test was performed according to the manufacturer's instructions.

4.23.2. Liposome sedimentation assay

Liposome sedimentation assays were performed according to Julkowska and coworkers (Julkowska et al., 2013). For each reaction, 300 nmol PtdCho were mixed with 100 nmol phosphoglycerolipid of choice (see appendix Tab. 6.3) in a 2 ml Protein LoBind Tube (Eppendorf AG, Hamburg, Germany). Lipids were dried under air stream and solved in 500 µl extrusion buffer (250 mM raffinose pentahydrate, 25 mM Tris-HCl pH 7.5, 1 mM DTT). Then, lipids were hydrated for 90 min at RT with occasionally mixing and afterwards treated for 30 s in an ultrasonic water bath. Multilamellar lipid vesicle mixtures were extruded 13 times through a polycarbonate membrane (pore size 0.2 µm, Whatman, Maidstone, United Kingdom) with filter supports (Avanti Polar Lipids Inc., Merck, Darmstadt, Germany) with an extruder. For washing, lipid vesicles were diluted in three volumes of 1x binding buffer (125 mM KCl, 25 mM Tris-HCl pH 7.5, 1 mM DTT, 0.5 mM EDTA) and sedimented at 20,800 x g and 22°C for 15 min. Supernatant was discarded and liposome pellets were solved in 25 µl 1x binding buffer. Per sample 750 ng (MBP, MBP-GCN5, MBP-GCN5_{ILL}, MBP-GCN5_{EDD}) or 1.5 µg (MBP-ING1) of purified protein (section 4.18) were made up to 25 µl with 4.2 µl of 6x binding buffer (750 mM KCl, 150 mM Tris-HCl pH 7.5, 6 mM DTT, 3 mM EDTA) and corresponding volume of ddH₂O, combined with the liposome suspension and incubated for 30 to 45 min at RT. Liposomes were sedimented at 16,000 x g and 22°C for 30 min, supernatant was transferred into a new tube and 16.7 µl 4x Laemmli sample buffer (section 4.19) were added. Liposome pellets were resuspended in 300 µl 1x binding buffer, transferred into a new tube and sedimented again at 16,000 x g and 22°C for 30 min. Supernatant was discarded and

pellets were resuspended in 33 μ l 1x Laemmli sample buffer. Samples were heated for 90 min at 95°C and 20 μ l of supernatant and 20 μ l or 30 μ l of liposome fraction were analyzed via immunodetection using the primary anti-MBP antibody followed by the AP-tagged secondary antibody (sections 4.19 and 4.20).

4.24. Histone acetyltransferase assay

For *in vitro* histone acetylation studies, recombinant enriched histone acetyltransferase (section 4.18) was mixed with human histone H3 protein (#ab198757, Abcam, Cambridge, United Kingdom) and 7.5 μ M acetyl-CoA (Sigma-Aldrich, Munich, Germany; dissolved in 50 mM sodium acetate pH 5.0) in 1x acetylation assay buffer (50 mM Tris-HCl pH 8.0, 50 mM NaCl, 0.1 mM EDTA, 0.01 % (w/v) Triton X-100, 50 μ g/ml BSA, 1 mM DTT) at 20°C for 1 h. In some assays, enriched ADA2B protein was added to the assay. The total volume of the reactions was 15 μ l, and the maximum amount of histone acetyltransferase used did not exceed 10 % of the total volume. To ensure comparability, the same volume of histone acetyltransferase elution buffer was added to each sample. The protein amounts and buffer conditions used are listed in Tab. 4.8.

Tab. 4.8: *In vitro* acetylation assay of GCN5.

Component	Stock solution	Final
Acetylation assay buffer	5x	3 μ l
Acetyl-CoA	50 μ M	7.5 μ M
Human histone H3	0.84 μ g/ μ l	0.84 μ g
MBP-GCN5 and variants		0.75 μ g
MBP-ADA2B		0.75 μ g
Total volume		filled up with ddH ₂ O to 15 μ l

To test the effect of PIs on GCN5 activity, either PtdCho, PtdOH, PtdIns3P, PtdIns4P, PtdIns(3,5)P₂, or PtdIns(4,5)P₂ was added to the reaction. For specification and origin of lipids see appendix Tab. 6.3. Lipids were dried under streaming air, resolved in 5x acetylation buffer, sonicated for 10 min in an ultrasonic bath and added to the acetylation mix. Molar amount/dilution of the corresponding phospholipids per reaction was 0.127 nmol, so about 12.7 % of the positively charged amino acid residues of histone tails can interact with negatively charged PIs. Time course experiments from 20 to 120 min, with intervals of 20 min, were performed as described above.

Assays were stopped with 5 μ l 4x Laemmli sample buffer (section 4.19) and histone acetylation was visualized by immunoblotting with primary antibodies against H3K9ac and H3K14ac and against histone H3 and MBP as a control (see sections 4.19 and 4.20).

4.25. *In vitro* lipid kinase activity assay with VPS34

The activity of VPS34 was determined as described previously for lipid kinases (Im et al., 2013). 20 μ l MBP-VPS34 or MBP-VPS34 variant enzyme soluble protein lysates were mixed with 6.2 μ g PtdIns substrate in 2 % Triton X-100 (v/v) and 10 μ l buffer mix. Final buffer concentrations were 30 mM Tris-HCl pH 7.2, 8.7 mM MgCl₂, 7.6 mM MnCl₂, 7.6 mM CaCl₂, 0.77 mM Na₂MoO₄, 1.5 mM ATP and 10 μ Ci γ -[³²P]-ATP (Hartmann Analytic, Braunschweig, Germany). For this purpose, PtdIns was dried under streaming air and resolved in 5 μ l 2 % (v/v) Triton X-100 and sonicated for 10 min in an ultrasonic bath. Reactions were filled up with 30 mM Tris-HCl pH 7.2 to 65 μ l and incubated for 1 h at RT. Phospholipids were extracted with 1.5 ml chloroform:methanol (1:2 v/v), 500 μ l 2.4 M HCl, 250 μ l 0.5 M EDTA pH 8.0 and 500 μ l chloroform. Chloroform phases were transferred to vials and samples were reextracted with 500 μ l chloroform. Chloroform phases from the reextraction were combined with the first extracts, 750 μ l 0.5 M HCl in methanol:ddH₂O (1:1 (v/v)) was added and mixed. The upper phase was transferred to a new glass vial and evaporated under streaming air. Samples were solved in 40 μ l chloroform and analyzed by thin layer chromatography (TLC) (TLC Silica gel 60, 20 x 20 cm, Merck, Darmstadt, Germany) with chloroform:methanol:ammonium hydroxide:ddH₂O (45:45:4:11 (v/v/v/v)) as developing solvent. Radioactive PtdIns3P was visualized/quantified by exposing a phosphorimager screen (BAS-MP 2040s, Fujifilm, Düsseldorf, Germany) and the extent of ³²P-incorporation was analyzed by phosphorimaging using a BAS-1500 system (Fujifilm, Düsseldorf, Germany). Signals were quantified with the TINA Software (Raytest, Straubenhardt, Germany).

4.26. Isolation and transformation of Arabidopsis leaf protoplasts

Leaf mesophyll protoplasts were prepared from six- to eight-week-old Col-0 wild type plants according to Yoo and coworkers (Yoo et al., 2007). Buffers required for protoplast preparation and transformation were freshly prepared and are listed in Tab. 4.9. For protoplast isolation, Arabidopsis rosette leaves were first sliced into fine strips using a razor blade and immersed in the enzyme solution. The enzyme solution listed in Tab. 4.9 was filtered through a Filtropur S 0.45 (Sarstedt, Nürnberg, Germany) before use. Then, the enzyme solution was infiltrated into the tissue of the leaf strips by vacuum infiltration in the dark for 30 min. Cell wall disruption was first performed for 2.5 h at RT at rest and then for 30 min under gentle shaking in the dark. The released protoplasts were then separated from the undigested tissue by filtration through a sterile 100 μ m nylon membrane using an EASYstrainer™ (Greiner Bio-One GmbH,

Frickenhausen, Germany) and sedimented at 200 x *g* and 11°C for 2 min. To wash the protoplasts, they were gently resuspended twice in 2 ml of W5 buffer and sedimented on ice for 40 min in the dark. Protoplasts were then resuspended in MMG buffer and diluted to the desired concentration for transformation.

For transformation, 10 µg plasmid DNA (sections 4.9.3 and 4.17.3) per 100 µl protoplast solution were combined in Cellstar® Cell Culture Tubes (12 ml, round bottom) (Greiner Bio-One GmbH, Frickenhausen, Germany) or in 50 ml tubes with conical bottom. 1.1x volume of PEG solution was carefully mixed with protoplast suspension. The transformation mixtures were incubated for 15 min at RT and diluted with 4.4x volume of W5 buffer. Protoplasts were sedimented at 200 x *g* and 11°C for 2 min, the supernatant was discarded, protoplasts were resuspended in WI buffer (initial volume of protoplast solution used) and incubated overnight in the dark. If RNA was to be isolated from the transformed protoplasts, 2 to 3.2 ml of protoplast solution were used. If the protoplasts were prepared for histone isolation, 5 ml of protoplast solution were used.

400 µl of protoplast transformations were made for samples used exclusively for microscopic examination. Protoplasts were checked for transient protein expression by immunodetection. For this purpose, either 400 µl or 1 ml of protoplast solution were sedimented and resuspended in 10 µl of 5x loading buffer (225 mM Tris-HCl pH 6.8, 5 % (w/v) glycerol, 5 % (w/v) SDS, 0.05 % (w/v) Coomassie Brilliant Blue G250) or 4x Laemmli buffer (section 4.19) and analyzed by SDS-PAGE (section 4.19) followed by Western blot (section 4.20) and immunodetection with the corresponding antibodies (section 4.20).

Tab. 4.9: Buffers for protoplast preparation.

Component	Stock solution	Enzyme solution	W5	MMG	PEG	WI
Mannitol	0.8 M	0.4 M	-	0.4 M	0.2 M	0.5 M
KCl	0.1 M	20 mM	5 mM	-	-	20 mM
MES pH 5.7	0.2 M	20 mM	2 mM	4 mM	-	4 mM
Cellulase R-10	-	1.5 % (w/v)	-	-	-	-
Maceroenzyme R-10	-	0.4 % (w/v)	-	-	-	-
CaCl ₂	1 M	10 mM	125 mM	-	0.1 M	-
BSA	-	1 mg/ml	-	-	-	-
NaCl	5 M	-	154 mM	-	-	-
MgCl ₂	0.15 M	-	-	15 mM	-	-
PEG 4000	-	-	-	-	40 % (w/v)	-

4.26.1. Auxin treatment of Arabidopsis leaf protoplasts

Arabidopsis protoplasts were treated with auxin after a modified protocol from Weiste and Dröge-Laser (Weiste and Dröge-Laser, 2014). 400 µl of Col-0 protoplasts were treated with 0.25 µM 1-naphthaleneacetic acid (NAA, Sigma-Aldrich, Munich, Germany) either for 14 h overnight or with 2 µM NAA for 2.5 h the day after transformation. For this, NAA was initially dissolved in 1 N NaOH and diluted with WI buffer. After NAA treatment, protoplasts were sedimented at 200 x g and 11°C for 2 min and supernatant was removed. Protoplasts were frozen in liquid N₂. RNA isolation and transcript level analysis were performed as described in sections 4.10.2 and 4.12.2.

4.26.2. Treatment of Arabidopsis leaf protoplasts with a proteasome inhibitor

400 µl of Arabidopsis protoplasts were transformed transiently with either *pEntryA-pCaMV35S::EYFP-GCN5*, *pEntryA-pCaMV35S::EYFP-GCN5_{ILL}*, or *pEntryA-pCaMV35S::EYFP-GCN5_{EDD}* (see section 4.26). The next day, protoplasts were treated for 6 h with 50 µM proteasome inhibitor MG-132 (dissolved in DMSO, stock concentration: 10 mM, SERVA Electrophoresis GmbH, Heidelberg, Germany) or DMSO as a mock. The treatment was performed according to Grimmer and coworkers (Grimmer et al., 2020). The effects of MG-132 treatment were analyzed via SDS-PAGE and subsequent Western blotting with immunodetection (see sections 4.19 and 4.20).

4.27. Microscopy

Microscopic images were taken with an inverted confocal laser scanning microscope LSM 880 (Carl Zeiss, Jena, Germany) using 10x, 20x or 40x objectives without immersion. The excitation wavelengths for EYFP, mCherry/DsRed and chlorophyll A were 514 nm, 561 nm and 633 nm, respectively, and emission was detected between 520 – 555 nm (EYFP), 565 – 620 nm (mCherry/DsRed) and 680 – 720 nm (chlorophyll A). Cells were documented either in single layers or in z-stacks with a maximum interval of 0.85 µm. Combinations of different fluorophores were recorded in different tracks to obtain the best signal and avoid crosstalk between channels. Z-stacks were used to create z-projections with ImageJ 1.51s (Fiji) (Schindelin et al., 2012). Line plots were performed on the z-projections to generate intensity profiles and analyze fluorescence intensity in different subcellular compartments, especially to see differences between nucleus and cytoplasm. Pearson coefficients R were generated with the JACoP plugin (Bolte and Cordelières, 2006) for ImageJ. After evaluation and for representation in figures, pictures were contrast-enhanced with a maximum of 0.1 % saturated pixels.

4.28. Isolation of nuclei and histones

4.28.1. Isolation of nuclei for histone analysis

Plant nuclei for detection of histones were isolated according to Folta and Kaufman (Folta and Kaufman, 2006). All steps were performed on ice. For this, six- to eight-week-old Arabidopsis Col-0 or *pip5k1 pip5k2* tissues (one rosette of Col-0 or ten to twelve rosettes of *pip5k1 pip5k2*) were sliced into approximately 1 mm thin strips, mixed in a total volume of 30 ml or 20 ml, respectively, with ice-cold extraction puffer (2 M hexylene glycol, 20 mM PIPES-KOH pH 7.0, 10 mM MgCl₂, 5 mM 2-mercaptoethanol) and disrupted with an Ultra-Turrax® T 25 basic (IKA®-Werke GmbH, Staufen, Germany) at 24,000 rpm for 10 min. The homogenate was filtered through three layers of cheesecloth (soaked with extraction buffer). The volume of the homogenate was filled up with extraction buffer to 30 ml (Col-0) or 20 ml (*pip5k1 pip5k2*) and 25% (v/v) Triton X-100 solution was added dropwise with constant stirring until a final concentration of 1% (v/v) was reached.

Percoll suspensions containing 30 % or 80 % Percoll and 1x gradient buffer were prepared by mixing appropriate volumes of 100 % Percoll (GE Healthcare GmbH, Solingen, Germany) with 5x gradient buffer (2.5 M hexylene glycol, 25 mM PIPES-KOH pH 7.0, 50 mM MgCl₂, 25 mM 2-mercaptoethanol, 5 % (v/v) Triton X-100) and ddH₂O. Density gradients were prepared by first adding 6 ml of the 30 % Percoll solution to a 50 ml centrifuge tube, then carefully underlaying 6 ml of the 80 % Percoll solution by carefully adding the solution to the bottom of the tube. In this way, the two Percoll layers were not mixed and had a sharp interface between the layers. The plant extract was gently loaded on top of the Percoll gradient and was centrifuged at 2,000 x g and 4°C for 30 min. The top layer and the 30 % Percoll solution were carefully removed and nuclei were collected from the 30 % - 80 % interface. The nuclei fraction was transferred to a new tube and filled up to a volume of 10 ml with 1x gradient buffer (0.5 M hexylene glycol, 5 mM PIPES-KOH pH 7.0, 10 mM MgCl₂, 5 mM 2-mercaptoethanol, 1 % (v/v) Triton X-100). This nuclei suspension was underlaid with 6 ml of 30 % Percoll solution and centrifuged at 2,000 x g and 4°C for 10 min. The supernatant was removed and the nuclei were washed with 1 ml 1x gradient buffer. After sedimentation at 1,000 x g and 4°C for 10 min the nuclei pellet was resuspended in 150 to 200 µl nuclei storage buffer (50 mM Tris-HCl pH 7.8, 20 % (v/v) glycerol, 5 mM MgCl₂, 0.44 M sucrose, 10 mM 2-mercaptoethanol). Histones were analyzed by gradient SDS-PAGE (4-20%) followed by immunodetection with specific histone antibodies (sections 4.19 and 4.20).

4.28.2. Isolation of histones using a histone extraction kit

Histones were isolated from Arabidopsis leaf protoplasts by using the Histone Extraction Kit (#ab113476, Abcam, Cambridge, United Kingdom). Col-0 wild type protoplasts or *PIP5K2-EYFP* OE protoplasts were sedimented at 200 x g and 11°C for 2 min, resuspended

in 400 μ l of 1x pre-lysis buffer and homogenized with the help of a tube plunger. Samples were incubated for 15 min on ice and then centrifuged at 9,400 x *g* and 4°C for 1 min. Supernatant was removed and the sediment was resuspended in 50 μ l of lysis buffer and incubated on ice for 30 min. Samples were centrifuged at 13,500 x *g* and 4°C for 5 min, the supernatant was harvested and combined with 0.3 volumes of balance-DTT buffer. 30 μ l of the suspensions were analyzed by SDS-PAGE and immunodetection (sections 4.19 and 4.20) with antibodies against histone H3 and modifications at lysine residues 9 and 14.

4.29. Computer-based analyses: software and online tools

Used software and online tools and their applications are listed in appendix Tab. 6.12 and are mentioned in the description of the methods.

4.29.1. Prediction of protein domains

The NCBI protein database (National Center for Biotechnology Information, U.S. National Library of Medicine, Rockville Pike, Bethesda, MD, USA), the online tool PROSITE (Expasy Bioinformatics Resource Portal, SIB Swiss Institute of Bioinformatics, Lausanne, Switzerland, (Sigrist et al., 2002, 2013)) and the online tool InterPro (European Bioinformatics Institute, Cambridge, United Kingdom, (Blum et al., 2021)) were used for identification and prediction of protein domains.

4.29.2. Identification of basic hydrophobic stretches in protein sequences

A bioinformatic program for identification of potential membrane binding sites was published by Brzeska and coworkers (Brzeska et al., 2010). The program which is available as online tool (<https://hpcwebapps.cit.nih.gov/bhsearch/>) was used in this study. The BH-search indicates a calculated hydrophobicity value for every amino acid of a sequence. A value higher than 0.6 indicates a basic hydrophobic amino acid that putatively binds to negatively charged phospholipids, like PIs.

4.29.3. Identification of putative NLS sequences

Putative NLS sequences were identified by using the online tools cNLS Mapper (Kosugi et al., 2008, 2009a, 2009b) and SeqNLS (Department of Computer Science and Engineering, University of South Carolina, SC, USA, (Lin et al., 2012)).

4.30. Statistics and data management

Data were analyzed unbiased and tested for statistical relevance by two-sided Student's T-tests or one-way ANOVA with a subsequent Tukey's post-hoc test ($P < 0.05$). T-tests and graphs were performed with Microsoft Excel (Microsoft Corporation, Redmond, WA, USA). R and R Studio were used for ANOVA (R Studio, PBC, Boston, MA, USA (Hothorn et al., 2008) for multcomp package).

5. Literature

- Aida, M., Beis, D., Heidstra, R., Willemsen, V., Blilou, I., Galinha, C., Nussaume, L., Noh, Y.S., Amasino, R., and Scheres, B.** (2004). The PLETHORA genes mediate patterning of the Arabidopsis root stem cell niche. *Cell* **119**: 109–120.
- Altaf, M., Auger, A., Monnet-Saksouk, J., Brodeur, J., Piquet, S., Cramet, M., Bouchard, N., Lacoste, N., Utleay, R.T., Gaudreau, L., and Cote, J.** (2010). NuA4-dependent acetylation of nucleosomal histones H4 and H2A directly stimulates incorporation of H2A.Z by the SWR1 complex. *J Biol Chem* **285**: 15966–15977.
- Alvarez-Venegas, R., Pien, S., Sadler, M., Witmer, X., Grossniklaus, U., and Avramova, Z.** (2003). ATX-1, an Arabidopsis Homolog of Trithorax, Activates Flower Homeotic Genes. *Current Biology* **13**: 627–637.
- Alvarez-Venegas, R., Sadler, M., Hlavacka, A., Baluska, F., Xia, Y., Lu, G., Firsov, A., Sarath, G., Moriyama, H., Dubrovsky, J.G., and Avramova, Z.** (2006). The Arabidopsis homolog of trithorax, ATX1, binds phosphatidylinositol 5-phosphate, and the two regulate a common set of target genes. *Proc Natl Acad Sci USA* **103**: 6049–6054.
- Anzola, J.M., Sieberer, T., Ortbauer, M., Butt, H., Korbei, B., Weinhofer, I., Mullner, A.E., and Luschnig, C.** (2010). Putative Arabidopsis transcriptional adaptor protein (PROPORZ1) is required to modulate histone acetylation in response to auxin. *Proc Natl Acad Sci U S A* **107**: 10308–10313.
- Barlow, C.A., Laishram, R.S., and Anderson, R.A.** (2010). Nuclear phosphoinositides: a signaling enigma wrapped in a compartmental conundrum. *Trends Cell Biol* **20**: 25–35.
- Benhamed, M. et al.** (2008). Genome-scale Arabidopsis promoter array identifies targets of the histone acetyltransferase GCN5. *Plant J* **56**: 493–504.
- Benhamed, M., Bertrand, C., Servet, C., and Zhou, D.X.** (2006). Arabidopsis GCN5, HD1, and TAF1/HAF2 interact to regulate histone acetylation required for light-responsive gene expression. *Plant Cell* **18**: 2893–2903.
- Benková, E., Michniewicz, M., Sauer, M., Teichmann, T., Seifertová, D., Jürgens, G., and Friml, J.** (2003). Local, Efflux-Dependent Auxin Gradients as a Common Module for Plant Organ Formation. *Cell* **115**: 591–602.
- Berger, S.L.** (2007). The complex language of chromatin regulation during transcription. *Nature* **447**: 407–412.
- Bertrand, C., Bergounioux, C., Domenichini, S., Delarue, M., and Zhou, D.X.** (2003). Arabidopsis histone acetyltransferase AtGCN5 regulates the floral meristem activity through the WUSCHEL/AGAMOUS pathway. *J Biol Chem* **278**: 28246–28251.
- Bhatti, M.M. and Sullivan, W.J.** (2005). Histone acetylase GCN5 enters the nucleus via importin- α in protozoan parasite *Toxoplasma gondii*. *J Biol Chem* **280**: 5902–5908.
- Bishop, J., Swan, H., Valente, F., and Nutzmans, H.W.** (2021). The Plant Nuclear Envelope and Its Role in Gene Transcription. *Front Plant Sci* **12**: 674209.
- Blum, M. et al.** (2021). The InterPro protein families and domains database: 20 years on. *Nucleic Acids Res* **49**: D344–D354.

- Bolte, S. and Cordelières, F.P.** (2006). A guided tour into subcellular colocalization analysis in light microscopy. *J Microsc* **224**: 213–232.
- Boronenkov, I.V., Loijens, J.C., Umeda, M., and Anderson, R.A.** (1998). Phosphoinositide signaling pathways in nuclei are associated with nuclear speckles containing pre-mRNA processing factors. *Mol Biol Cell* **9**: 3547–3560.
- Boss, W.F. and Im, Y.J.** (2012). Phosphoinositide signaling. *Annu Rev Plant Biol* **63**: 409–429.
- Boycheva, I., Vassileva, V., and Iantcheva, A.** (2014). Histone acetyltransferases in plant development and plasticity. *Curr Genomics* **15**: 28–37.
- Bradford, M.M.** (1976). A Rapid and Sensitive Method for the Quantitation of Microgram Quantities of Protein Utilizing the Principle of Protein-Dye Binding. *Anal Biochem* **72**: 248–254.
- Brownell, J.E. and Allis, C.D.** (1996). Special HATs for special occasions: linking histone acetylation to chromatin assembly and gene activation. *Curr Opin Genet Dev* **6**: 176–184.
- Brownell, J.E., Zhou, J., Ranalli, T., Kobayashi, R., Edmondson, D.G., Roth, S.Y., and Allis, C.D.** (1996). Tetrahymena histone acetyltransferase A: a homolog to yeast Gcn5p linking histone acetylation to gene activation. *Cell* **84**: 843–851.
- Brzeska, H., Guag, J., Remmert, K., Chacko, S., and Korn, E.D.** (2010). An experimentally based computer search identifies unstructured membrane-binding sites in proteins: application to class I myosins, PAKS, and CARMIL. *J Biol Chem* **285**: 5738–5747.
- Bunce, M.W., Bergendahl, K., and Anderson, R.A.** (2006a). Nuclear PI(4,5)P(2): a new place for an old signal. *Biochim Biophys Acta* **1761**: 560–569.
- Bunce, M.W., Gonzales, M.L., and Anderson, R.A.** (2006b). Stress-ING out: phosphoinositides mediate the cellular stress response. *Sci STKE* **2006**: pe46.
- Bunney, T.D., Watkins, P.A., Beven, A.F., Shaw, P.J., Hernandez, L.E., Lomonossoff, G.P., Shanks, M., Peart, J., and Drobak, B.K.** (2000). Association of phosphatidylinositol 3-kinase with nuclear transcription sites in higher plants. *Plant Cell* **12**: 1679–1688.
- Burd, C.G. and Emr, S.D.** (1998). Phosphatidylinositol(3)-phosphate signaling mediated by specific binding to RING FYVE domains. *Mol Cell* **2**: 157–162.
- Camacho, L., Smertenko, A.P., Perez-Gomez, J., Hussey, P.J., and Moore, I.** (2009). Arabidopsis Rab-E GTPases exhibit a novel interaction with a plasma-membrane phosphatidylinositol-4-phosphate 5-kinase. *J Cell Sci* **122**: 4383–4392.
- Candau, R., Zhou, J.X., Allis, C.D., and Berger, S.L.** (1997). Histone acetyltransferase activity and interaction with ADA2 are critical for GCN5 function in vivo. *EMBO J* **16**: 555–565.
- Cheng, K., Xu, Y., Yang, C., Ouellette, L., Niu, L., Zhou, X., Chu, L., Zhuang, F., Liu, J., Wu, H., Charron, J.B., and Luo, M.** (2020). Histone tales: lysine methylation, a protagonist in Arabidopsis development. *J Exp Bot* **71**: 793–807.
- Cheung, A.C.M. and Diaz-Santin, L.M.** (2019). Share and share alike: the role of Tra1 from the SAGA and NuA4 coactivator complexes. *Transcription* **10**: 37–43.

- Chiu, L.-W., Heckert, M.J., You, Y., Albanese, N., Fenwick, T., Siehl, D.L., Castle, L.A., and Tao, Y.** (2018). Members of the GH3 Family of Proteins Conjugate 2,4-D and Dicamba with Aspartate and Glutamate. *Plant and Cell Physiol* **59**: 2366–2380.
- Ciruela, A., Hinchliffe, K.A., Divecha, N., and Irvine, R.F.** (2000). Nuclear targeting of the beta isoform of type II phosphatidylinositol phosphate kinase (phosphatidylinositol 5-phosphate 4-kinase) by its alpha-helix 7. *Biochem J* **346 Pt 3**: 587–591.
- Cohen, R., Schocken, J., Kaldis, A., Vlachonasios, K.E., Hark, A.T., and McCain, E.R.** (2009). The histone acetyltransferase GCN5 affects the inflorescence meristem and stamen development in Arabidopsis. *Planta* **230**: 1207–1221.
- Colin, L.A. and Jaillais, Y.** (2020). Phospholipids across scales: lipid patterns and plant development. *Curr Opin Plant Biol* **53**: 1–9.
- Corpet, F.** (1988). Multiple sequence alignment with hierarchical clustering. *Nucleic Acids Res* **16**: 10881–10890.
- Daniel, J.A., Torok, M.S., Sun, Z.W., Schieltz, D., Allis, C.D., Yates, J.R., and Grant, P.A.** (2004). Deubiquitination of histone H2B by a yeast acetyltransferase complex regulates transcription. *J Biol Chem* **279**: 1867–1871.
- Dasso, M.** (2002). The Ran GTPase: theme and variants. *Curr Biol* **12**: R502-508.
- Dejonghe, W. et al.** (2016). Mitochondrial uncouplers inhibit clathrin-mediated endocytosis largely through cytoplasmic acidification. *Nat Commun* **7**: 11710.
- Dhalluin, C., Carlson, J.E., Zeng, L., He, C., Aggarwal, A.K., and Zhou, M.M.** (1999). Structure and ligand of a histone acetyltransferase bromodomain. *Nature* **399**: 491–496.
- Dieck, C.B., Wood, A., Brglez, I., Rojas-Pierce, M., and Boss, W.F.** (2012). Increasing phosphatidylinositol (4,5) bisphosphate biosynthesis affects plant nuclear lipids and nuclear functions. *Plant Physiol Biochem* **57**: 32–44.
- Dillon, S.C., Zhang, X., Trievel, R.C., and Cheng, X.** (2005). The SET-domain protein superfamily: protein lysine methyltransferases. *Genome Biol* **6**: 227.
- Dixon, S.E., Bhatti, M.M., Uversky, V.N., Dunker, A.K., and Sullivan, W.J.** (2011). Regions of intrinsic disorder help identify a novel nuclear localization signal in *Toxoplasma gondii* histone acetyltransferase TgGCN5-B. *Mol Biochem Parasitol* **175**: 192–195.
- Dove, S.K., Lloyd, C.W., and Drobak, B.K.** (1994). Identification of phosphatidylinositol 3-hydroxy kinase in plant cells: association with the cytoskeleton. *Biochem J* **303**: 347–350.
- Earley, K.W., Shook, M.S., Brower-Toland, B., Hicks, L., and Pikaard, C.S.** (2007). In vitro specificities of Arabidopsis co-activator histone acetyltransferases: implications for histone hyperacetylation in gene activation. *Plant J* **52**: 615–626.
- Elge, S., Brearley, C., Xia, H.-J., Kehr, J., Xue, H.-W., and Mueller-Roeber, B.** (2001). An Arabidopsis inositol phospholipid kinase strongly expressed in procambial cells: Synthesis of PtdIns(4,5)P₂ and PtdIns(3,4,5)P₃ in insect cells by 5-phosphorylation of precursors: Arabidopsis inositol phospholipid 5-kinase produces PIP₃. *The Plant Journal* **26**: 561–571.

- Emans, N., Zimmermann, S., and Fischer, R.** (2002). Uptake of a fluorescent marker in plant cells is sensitive to brefeldin A and wortmannin. *Plant Cell* **14**: 71–86.
- Espinosa-Cores, L., Bouza-Morcillo, L., Barrero-Gil, J., Jimenez-Suarez, V., Lazaro, A., Piqueras, R., Jarillo, J.A., and Pineiro, M.** (2020). Insights Into the Function of the NuA4 Complex in Plants. *Front Plant Sci* **11**: 125.
- Falkenberg, K.J. and Johnstone, R.W.** (2014). Histone deacetylases and their inhibitors in cancer, neurological diseases and immune disorders. *Nat Rev Drug Discov* **13**: 673–691.
- Fang, F., Ye, S., Tang, J., Bennett, M.J., and Liang, W.** (2020). DWT1/DWL2 act together with OsPIP5K1 to regulate plant uniform growth in rice. *New Phytol* **225**: 1234–1246.
- Fauré, J., Vignais, P.V., and Dagher, M.C.** (1999). Phosphoinositide-dependent activation of Rho A involves partial opening of the RhoA/Rho-GDI complex. *Eur J Biochem* **262**: 879–889.
- Folta, K.M. and Kaufman, L.S.** (2006). Isolation of Arabidopsis nuclei and measurement of gene transcription rates using nuclear run-on assays. *Nat Protoc* **1**: 3094–3100.
- Fratini, M., Krishnamoorthy, P., Stenzel, I., Riechmann, M., Matzner, M., Bacia, K., Heilmann, M., and Heilmann, I.** (2021). Plasma membrane nano-organization specifies phosphoinositide effects on Rho-GTPases and actin dynamics in tobacco pollen tubes. *Plant Cell* **33**: 642–670.
- Fuchs, J., Demidov, D., Houben, A., and Schubert, I.** (2006). Chromosomal histone modification patterns--from conservation to diversity. *Trends Plant Sci* **11**: 199–208.
- Gadhia, S., Shrimp, J.H., Meier, J.L., McGee, J.E., and Dahlin, J.L.** (2017). Histone Acetyltransferase Assays in Drug and Chemical Probe Discovery. In *Assay Guidance Manual*, G.S. Sittampalam, A. Grossman, K. Brimacombe, and et al, eds (Eli Lilly & Company and the National Center for Advancing Translational Sciences, Bethesda (MD)), pp. 235–274.
- Galinha, C., Hofhuis, H., Luijten, M., Willemsen, V., Blilou, I., Heidstra, R., and Scheres, B.** (2007). PLETHORA proteins as dose-dependent master regulators of Arabidopsis root development. *Nature* **449**: 1053–1057.
- Gan, L., Wei, Z., Yang, Z., Li, F., and Wang, Z.** (2021). Updated Mechanisms of GCN5-The Monkey King of the Plant Kingdom in Plant Development and Resistance to Abiotic Stresses. *Cells* **10**: 979.
- Gasteiger, E., Hoogland, C., Gattiker, A., Duvaud, S., Wilkins, M.R., Appel, R.D., and Bairoch, A.** (2005). Protein Identification and Analysis Tools on the ExPASy Server. In *The Proteomics Protocols Handbook*, J.M. Walker, ed (Humana Press: Totowa, NJ), pp. 571–607.
- Gerth, K., Lin, F., Daamen, F., Menzel, W., Heinrich, F., and Heilmann, M.** (2017a). Arabidopsis phosphatidylinositol 4-phosphate 5-kinase 2 contains a functional nuclear localization sequence and interacts with alpha-importins. *Plant J* **92**: 862–878.
- Gerth, K., Lin, F., Menzel, W., Krishnamoorthy, P., Stenzel, I., Heilmann, M., and Heilmann, I.** (2017b). Guilt by Association: A Phenotype-Based View of the Plant Phosphoinositide Network. *Annu Rev Plant Biol* **68**: 349–374.

- Gillooly, D.J., Morrow, I.C., Lindsay, M., Gould, R., Bryant, N.J., Gaullier, J.M., Parton, R.G., and Stenmark, H.** (2000). Localization of phosphatidylinositol 3-phosphate in yeast and mammalian cells. *EMBO J* **19**: 4577–4588.
- Govind, C.K., Zhang, F., Qiu, H., Hofmeyer, K., and Hinnebusch, A.G.** (2007). Gcn5 promotes acetylation, eviction, and methylation of nucleosomes in transcribed coding regions. *Mol Cell* **25**: 31–42.
- Gozani, O. et al.** (2003). The PHD Finger of the Chromatin-Associated Protein ING2 Functions as a Nuclear Phosphoinositide Receptor. *Cell* **114**: 99–111.
- Grant, P.A., Duggan, L., Côté, J., Roberts, S.M., Brownell, J.E., Candau, R., Ohba, R., Owen-Hughes, T., Allis, C.D., Winston, F., Berger, S.L., and Workman, J.L.** (1997). Yeast Gcn5 functions in two multisubunit complexes to acetylate nucleosomal histones: characterization of an Ada complex and the SAGA (Spt/Ada) complex. *Genes Dev* **11**: 1640–1650.
- Grant, P.A., Schieltz, D., Pray-Grant, M.G., Yates 3rd, J.R., and Workman, J.L.** (1998). The ATM-related cofactor Tra1 is a component of the purified SAGA complex. *Mol Cell* **2**: 863–867.
- Grasser, K.D., Rubio, V., and Barneche, F.** (2021). Multifaceted activities of the plant SAGA complex. *Biochim Biophys Acta Gene Regul Mech* **1864**: 194613.
- Grieneisen, V.A., Xu, J., Maree, A.F., Hogeweg, P., and Scheres, B.** (2007). Auxin transport is sufficient to generate a maximum and gradient guiding root growth. *Nature* **449**: 1008–1013.
- Grimmer, J., Helm, S., Dobritzsch, D., Hause, G., Shema, G., Zahedi, R.P., and Baginsky, S.** (2020). Mild proteasomal stress improves photosynthetic performance in Arabidopsis chloroplasts. *Nat Commun* **11**: 1662.
- Ha, C.M., Jun, J.H., and Fletcher, J.C.** (2010). Control of Arabidopsis leaf morphogenesis through regulation of the YABBY and KNOX families of transcription factors. *Genetics* **186**: 197–206.
- Hagen, G. and Guilfoyle, T.** (2002). Auxin-responsive gene expression: genes, promoters and regulatory factors. *Plant Mol Biol* **49**: 373–385.
- Hamann, T., Benkova, E., Baurle, I., Kientz, M., and Jurgens, G.** (2002). The Arabidopsis BODENLOS gene encodes an auxin response protein inhibiting MONOPTEROS-mediated embryo patterning. *Genes Dev* **16**: 1610–1615.
- Hark, A.T., Vlachonasios, K.E., Pavangadkar, K.A., Rao, S., Gordon, H., Adamakis, I.D., Kaldis, A., Thomashow, M.F., and Triezenberg, S.J.** (2009). Two Arabidopsis orthologs of the transcriptional coactivator ADA2 have distinct biological functions. *Biochim Biophys Acta* **1789**: 117–124.
- Heilmann, I.** (2016a). Phosphoinositide signaling in plant development. *Development* **143**: 2044–2055.
- Heilmann, I.** (2016b). Plant phosphoinositide signaling - dynamics on demand. *Biochim Biophys Acta* **1861**: 1345–1351.
- Heilmann, I.** (2009). Using genetic tools to understand plant phosphoinositide signalling. *Trends in Plant Science* **14**: 171–179.

- Heilmann, M. and Heilmann, I.** (2015). Plant phosphoinositides-complex networks controlling growth and adaptation. *Biochim Biophys Acta* **1851**: 759–769.
- Heinekamp, T., Strathmann, A., Kuhlmann, M., Froissard, M., Muller, A., Perrot-Rechenmann, C., and Droge-Laser, W.** (2004). The tobacco bZIP transcription factor BZI-1 binds the GH3 promoter in vivo and modulates auxin-induced transcription. *Plant J* **38**: 298–309.
- Hempel, F., Stenzel, I., Heilmann, M., Krishnamoorthy, P., Menzel, W., Golbik, R., Helm, S., Dobritzsch, D., Baginsky, S., Lee, J., Hoehenwarter, W., and Heilmann, I.** (2017). MAPKs Influence Pollen Tube Growth by Controlling the Formation of Phosphatidylinositol 4,5-Bisphosphate in an Apical Plasma Membrane Domain. *Plant Cell* **29**: 3030–3050.
- Henry, K.W., Wyce, A., Lo, W.S., Duggan, L.J., Emre, N.C., Kao, C.F., Pillus, L., Shilatifard, A., Osley, M.A., and Berger, S.L.** (2003). Transcriptional activation via sequential histone H2B ubiquitylation and deubiquitylation, mediated by SAGA-associated Ubp8. *Genes Dev* **17**: 2648–2663.
- Hoke, S.M., Genereaux, J., Liang, G., and Brandl, C.J.** (2008). A conserved central region of yeast Ada2 regulates the histone acetyltransferase activity of Gcn5 and interacts with phospholipids. *J Mol Biol* **384**: 743–755.
- Hothorn, T., Bretz, F., and Westfall, P.** (2008). Simultaneous inference in general parametric models. *Biom J* **50**: 346–363.
- Hu, Z. et al.** (2015). Histone acetyltransferase GCN5 is essential for heat stress-responsive gene activation and thermotolerance in Arabidopsis. *Plant J* **84**: 1178–1191.
- Im, Y.J., Brglez, I., Dieck, C., Perera, I.Y., and Boss, W.F.** (2013). Phosphatidylinositol 4-kinase and phosphatidylinositol 4-phosphate 5-kinase assays. *Methods Mol Biol* **1009**: 163–174.
- Inoue, H., Nojima, H., and Okayama, H.** (1990). High efficiency transformation of Escherichia coli with plasmids. *Gene* **96**: 23–28.
- Irvine, R.F.** (2003). Nuclear lipid signalling. *Nat Rev Mol Cell Biol* **4**: 349–360.
- Ischebeck, T. et al.** (2013). Phosphatidylinositol 4,5-bisphosphate influences PIN polarization by controlling clathrin-mediated membrane trafficking in Arabidopsis. *Plant Cell* **25**: 4894–4911.
- Ischebeck, T., Stenzel, I., and Heilmann, I.** (2008). Type B phosphatidylinositol-4-phosphate 5-kinases mediate Arabidopsis and Nicotiana tabacum pollen tube growth by regulating apical pectin secretion. *Plant Cell* **20**: 3312–3330.
- Ischebeck, T., Stenzel, I., Hempel, F., Jin, X., Mosblech, A., and Heilmann, I.** (2011). Phosphatidylinositol-4,5-bisphosphate influences Nt-Rac5-mediated cell expansion in pollen tubes of Nicotiana tabacum. *Plant J* **65**: 453–468.
- Ito, H., Fukuda, Y., Murata, K., and Kimura A** (1983). Transformation of Intact Yeast Cells Treated with Alkali Cations. *J Bacteriol* **153**: 163–168.
- Jaillais, Y., Fobis-Loisy, I., Miege, C., Rollin, C., and Gaude, T.** (2006). AtSNX1 defines an endosome for auxin-carrier trafficking in Arabidopsis. *Nature* **443**: 106–109.

- Jaillais, Y. and Ott, T.** (2020). The Nanoscale Organization of the Plasma Membrane and Its Importance in Signaling: A Proteolipid Perspective. *Plant Physiol.* **182**: 1682–1696.
- Jiang, J., Ding, A.B., Liu, F., and Zhong, X.** (2020). Linking signaling pathways to histone acetylation dynamics in plants. *J Exp Bot* **71**: 5179–5190.
- Johnsson, N. and Varshavsky, A.** (1994). Split ubiquitin as a sensor of protein interactions in vivo. *Proc Natl Acad Sci USA* **91**: 10340–10344.
- Josling, G.A., Selvarajah, S.A., Petter, M., and Duffy, M.F.** (2012). The role of bromodomain proteins in regulating gene expression. *Genes (Basel)* **3**: 320–343.
- Julkowska, M.M., Rankenberg, J.M., and Testerink, C.** (2013). Liposome-binding assays to assess specificity and affinity of phospholipid-protein interactions. *Methods Mol Biol* **1009**: 261–271.
- Jumper, J. et al.** (2021). Highly accurate protein structure prediction with AlphaFold. *Nature*: 1–7.
- Kalderon, D., Roberts, B.L., Richardson, W.D., and Smith, A.E.** (1984). A short amino acid sequence able to specify nuclear location. *Cell* **39**: 499–509.
- Kaldis, A., Tsementzi, D., Tanriverdi, O., and Vlachonasios, K.E.** (2011). Arabidopsis thaliana transcriptional co-activators ADA2b and SGF29a are implicated in salt stress responses. *Planta* **233**: 749–762.
- Kelly, S.M., Jess, T.J., and Price, N.C.** (2005). How to study proteins by circular dichroism. *Biochimica et Biophysica Acta (BBA) - Proteins and Proteomics* **1751**: 119–139.
- Kim, S. et al.** (2020). GCN5 modulates salicylic acid homeostasis by regulating H3K14ac levels at the 5' and 3' ends of its target genes. *Nucleic Acids Res* **48**: 5953–5966.
- Kim, S., Natesan, S., Cornilescu, G., Carlson, S., Tonelli, M., McClurg, U.L., Binda, O., Robson, C.N., Markley, J.L., Balaz, S., and Glass, K.C.** (2016). Mechanism of Histone H3K4me3 Recognition by the Plant Homeodomain of Inhibitor of Growth 3. *J Biol Chem* **291**: 18326–18341.
- Kinney, N.A., Sharakhov, I.V., and Onufriev, A.V.** (2018). Chromosome-nuclear envelope attachments affect interphase chromosome territories and entanglement. *Epigenetics Chromatin* **11**: 3.
- König, S., Ischebeck, T., Lerche, J., Stenzel, I., and Heilmann, I.** (2008). Salt-stress-induced association of phosphatidylinositol 4,5-bisphosphate with clathrin-coated vesicles in plants. *Biochemical Journal* **415**: 387–399.
- Kornet, N. and Scheres, B.** (2009). Members of the GCN5 histone acetyltransferase complex regulate PLETHORA-mediated root stem cell niche maintenance and transit amplifying cell proliferation in Arabidopsis. *Plant Cell* **21**: 1070–1079.
- Kost, B.** (2008). Spatial control of Rho (Rac-Rop) signaling in tip-growing plant cells. *Trends Cell Biol* **18**: 119–127.
- Kost, B., Lemichez, E., Spielhofer, P., Hong, Y., Tolia, K., Carpenter, C., and Chua, N.H.** (1999). Rac homologues and compartmentalized phosphatidylinositol 4,5-bisphosphate act in a common pathway to regulate polar pollen tube growth. *J Cell Biol* **145**: 317–330.

- Kosugi, S., Hasebe, M., Entani, T., Takayama, S., Tomita, M., and Yanagawa, H.** (2008). Design of peptide inhibitors for the importin alpha/beta nuclear import pathway by activity-based profiling. *Chem Biol* **15**: 940–949.
- Kosugi, S., Hasebe, M., Matsumura, N., Takashima, H., Miyamoto-Sato, E., Tomita, M., and Yanagawa, H.** (2009a). Six classes of nuclear localization signals specific to different binding grooves of importin alpha. *J Biol Chem* **284**: 478–485.
- Kosugi, S., Hasebe, M., Tomita, M., and Yanagawa, H.** (2009b). Systematic identification of cell cycle-dependent yeast nucleocytoplasmic shuttling proteins by prediction of composite motifs. *Proc Natl Acad Sci USA* **106**: 10171–10176.
- Koutelou, E., Hirsch, C.L., and Dent, S.Y.** (2010). Multiple faces of the SAGA complex. *Curr Opin Cell Biol* **22**: 374–382.
- Kouzarides, T.** (2007). Chromatin modifications and their function. *Cell* **128**: 693–705.
- Kuroda, R., Kato, M., Tsuge, T., and Aoyama, T.** (2021). Arabidopsis phosphatidylinositol 4-phosphate 5-kinase genes PIP5K7, PIP5K8, and PIP5K9 are redundantly involved in root growth adaptation to osmotic stress. *Plant J* **106**: 913–927.
- Kusano, H., Testerink, C., Vermeer, J.E.M., Tsuge, T., Shimada, H., Oka, A., Munnik, T., and Aoyama, T.** (2008). The Arabidopsis Phosphatidylinositol Phosphate 5-Kinase PIP5K3 Is a Key Regulator of Root Hair Tip Growth. *The Plant Cell* **20**: 367–380.
- Laemmli, U.K.** (1970). Cleavage of Structural Proteins during the Assembly of the Head of Bacteriophage T4. *Nature* **227**: 680–685.
- Lee, K.K. and Workman, J.L.** (2007). Histone acetyltransferase complexes: one size doesn't fit all. *Nat Rev Mol Cell Biol* **8**: 284–295.
- Lee, W.Y., Lee, D., Chung, W.I., and Kwon, C.S.** (2009). Arabidopsis ING and Alfin1-like protein families localize to the nucleus and bind to H3K4me3/2 via plant homeodomain fingers. *Plant J* **58**: 511–524.
- Lee, Y., Kim, E.S., Choi, Y., Hwang, I., Staiger, C.J., Chung, Y.Y., and Lee, Y.** (2008). The Arabidopsis phosphatidylinositol 3-kinase is important for pollen development. *Plant Physiol* **147**: 1886–1897.
- Lee, Y., Munnik, T., and Lee, Y.** (2010). Plant Phosphatidylinositol 3-Kinase. In *Lipid Signaling in Plants*, Plant Cell Monographs., pp. 95–106.
- van Leeuwen, W., Okresz, L., Bogre, L., and Munnik, T.** (2004). Learning the lipid language of plant signalling. *Trends Plant Sci* **9**: 378–384.
- Leshem, Y., Seri, L., and Levine, A.** (2007). Induction of phosphatidylinositol 3-kinase-mediated endocytosis by salt stress leads to intracellular production of reactive oxygen species and salt tolerance. *Plant J* **51**: 185–197.
- Li, B., Carey, M., and Workman, J.L.** (2007). The role of chromatin during transcription. *Cell* **128**: 707–719.
- Li, S. et al.** (2019). The AREB1 Transcription Factor Influences Histone Acetylation to Regulate Drought Responses and Tolerance in *Populus trichocarpa*. *Plant Cell* **31**: 663–686.

- Lin, J.-R., Mondal, A.M., Liu, R., and Hu, J.** (2012). Minimalist ensemble algorithms for genome-wide protein localization prediction. *BMC Bioinformatics* **13**: 157.
- Liu, C., Lu, F., Cui, X., and Cao, X.** (2010). Histone methylation in higher plants. *Annu Rev Plant Biol* **61**: 395–420.
- Liu, Y. and Min, J.** (2016). Structure and function of histone methylation-binding proteins in plants. *Biochem J* **473**: 1663–1680.
- Lou, Y., Gou, J.Y., and Xue, H.W.** (2007). PIP5K9, an Arabidopsis phosphatidylinositol monophosphate kinase, interacts with a cytosolic invertase to negatively regulate sugar-mediated root growth. *Plant Cell* **19**: 163–181.
- Lovejoy, C.A. and Cortez, D.** (2009). Common mechanisms of PIKK regulation. *DNA Repair* **8**: 1004–1008.
- Luger, K., Mäder, A.W., Richmond, R.K., Sargent, D.F., and Richmond, T.J.** (1997). Crystal structure of the nucleosome core particle at 2.8 Å resolution. *Nature* **389**: 251–260.
- Ma, X., Shor, O., Diminshtein, S., Yu, L., Im, Y.J., Perera, I., Lomax, A., Boss, W.F., and Moran, N.** (2009). Phosphatidylinositol (4,5)bisphosphate inhibits K⁺-efflux channel activity in NT1 tobacco cultured cells. *Plant Physiol* **149**: 1127–1140.
- MacDonald, M.H., Mogen, B.D., and Hunt, A.G.** (1991). Characterization of the polyadenylation signal from the T-DNA-encoded octopine synthase gene. *Nucleic Acids Res* **19**: 5575–5581.
- Madeira, F., Park, Y.M., Lee, J., Buso, N., Gur, T., Madhusoodanan, N., Basutkar, P., Tivey, A.R.N., Potter, S.C., Finn, R.D., and Lopez, R.** (2019). The EMBL-EBI search and sequence analysis tools APIs in 2019. *Nucleic Acids Res* **47**: W636–W641.
- Mao, Y., Pavangadkar, K.A., Thomashow, M.F., and Triezenberg, S.J.** (2006). Physical and functional interactions of Arabidopsis ADA2 transcriptional coactivator proteins with the acetyltransferase GCN5 and with the cold-induced transcription factor CBF1. *Biochim Biophys Acta* **1759**: 69–79.
- Marmorstein, R. and Zhou, M.M.** (2014). Writers and readers of histone acetylation: structure, mechanism, and inhibition. *Cold Spring Harb Perspect Biol* **6**: a018762.
- Mei, Y., Jia, W.J., Chu, Y.J., and Xue, H.W.** (2012). Arabidopsis phosphatidylinositol monophosphate 5-kinase 2 is involved in root gravitropism through regulation of polar auxin transport by affecting the cycling of PIN proteins. *Cell Res* **22**: 581–597.
- Meijer, H.J., Berrie, C.P., Iurisci, C., Divecha, N., Musgrave, A., and Munnik, T.** (2001). Identification of a new polyphosphoinositide in plants, phosphatidylinositol 5-monophosphate (PtdIns5P), and its accumulation upon osmotic stress. *Biochem J* **360**: 491–498.
- Meijer, H.J. and Munnik, T.** (2003). Phospholipid-based signaling in plants. *Annu Rev Plant Biol* **54**: 265–306.
- Mellman, D.L., Gonzales, M.L., Song, C., Barlow, C.A., Wang, P., Kendzioriski, C., and Anderson, R.A.** (2008). A PtdIns4,5P₂-regulated nuclear poly(A) polymerase controls expression of select mRNAs. *Nature* **451**: 1013–1017.
- Menzel, W., Stenzel, I., Helbig, L.M., Krishnamoorthy, P., Neumann, S., Eschen-Lippold, L., Heilmann, M., Lee, J., and Heilmann, I.** (2019). A PAMP-triggered MAPK cascade

- inhibits phosphatidylinositol 4,5-bisphosphate production by PIP5K6 in *Arabidopsis thaliana*. *New Phytol* **224**: 833–847.
- Millar, C.B. and Grunstein, M.** (2006). Genome-wide patterns of histone modifications in yeast. *Nat Rev Mol Cell Biol* **7**: 657–666.
- Mishkind, M., Vermeer, J.E., Darwish, E., and Munnik, T.** (2009). Heat stress activates phospholipase D and triggers PIP accumulation at the plasma membrane and nucleus. *Plant J* **60**: 10–21.
- Misra, S. and Hurley, J.H.** (1999). Crystal structure of a phosphatidylinositol 3-phosphate-specific membrane-targeting motif, the FYVE domain of Vps27p. *Cell* **97**: 657–666.
- Möckli, N., Deplazes, A., Hassa, P.O., Zhang, Z., Peter, M., Hottiger, M.O., Stagljar, I., and Auerbach, D.** (2007). Yeast split-ubiquitin-based cytosolic screening system to detect interactions between transcriptionally active proteins. *Biotechniques* **42**: 725–730.
- Moraga, F. and Aquea, F.** (2015). Composition of the SAGA complex in plants and its role in controlling gene expression in response to abiotic stresses. *Front Plant Sci* **6**: 865.
- Mueller-Roeber, B. and Pical, C.** (2002). Inositol phospholipid metabolism in *Arabidopsis*. Characterized and putative isoforms of inositol phospholipid kinase and phosphoinositide-specific phospholipase C. *Plant Physiol* **130**: 22–46.
- Müller, A., Guan, C., Gälweiler, L., Tänzler, P., Huijser, P., Marchant, A., Parry, G., Bennett, M., Wisman, E., and Palme, K.** (1998). AtPIN2 defines a locus of *Arabidopsis* for root gravitropism control. *EMBO J* **17**: 6903–6911.
- Murray, M.G. and Thompson, W.F.** (1980). Rapid isolation of high molecular weight plant DNA. *Nucleic Acids Res* **8**: 4321–4325.
- Nassrallah, A. et al.** (2018). DET1-mediated degradation of a SAGA-like deubiquitination module controls H2Bub homeostasis. *Elife* **7**: e37892.
- Ndamukong, I., Jones, D.R., Lapko, H., Divecha, N., and Avramova, Z.** (2010). Phosphatidylinositol 5-phosphate links dehydration stress to the activity of ARABIDOPSIS TRITHORAX-LIKE factor ATX1. *PLoS One* **5**: e13396.
- Okada, K., Ueda, J., Komaki, M.K., Bell, C.J., and Shimura, Y.** (1991). Requirement of the Auxin Polar Transport System in Early Stages of *Arabidopsis* Floral Bud Formation. *Plant Cell* **3**: 677–684.
- Osborne, S.L., Thomas, C.L., Gschmeissner, S., and Schiavo, G.** (2001). Nuclear PtdIns(4,5)P₂ assembles in a mitotically regulated particle involved in pre-mRNA splicing. *J Cell Sci* **114**: 2501–2511.
- Papai, G., Frechard, A., Kolesnikova, O., Crucifix, C., Schultz, P., and Ben-Shem, A.** (2020). Structure of SAGA and mechanism of TBP deposition on gene promoters. *Nature* **577**: 711–716.
- Park, J.E., Park, J.Y., Kim, Y.S., Staswick, P.E., Jeon, J., Yun, J., Kim, S.Y., Kim, J., Lee, Y.H., and Park, C.M.** (2007). GH3-mediated auxin homeostasis links growth regulation with stress adaptation response in *Arabidopsis*. *J Biol Chem* **282**: 10036–10046.
- Parthun, M.R.** (2012). Histone acetyltransferase 1: more than just an enzyme? *Biochim Biophys Acta* **1819**: 256–263.

- Patel, D.J. and Wang, Z.** (2013). Readout of Epigenetic Modifications. *Annu. Rev. Biochem.* **82**: 81–118.
- Pena, P.V. et al.** (2008). Histone H3K4me3 binding is required for the DNA repair and apoptotic activities of ING1 tumor suppressor. *J Mol Biol* **380**: 303–312.
- Pena, P.V., Davrazou, F., Shi, X., Walter, K.L., Verkhusha, V.V., Gozani, O., Zhao, R., and Kutateladze, T.G.** (2006). Molecular mechanism of histone H3K4me3 recognition by plant homeodomain of ING2. *Nature* **442**: 100–103.
- Pfab, A., Bruckmann, A., Nazet, J., Merkl, R., and Grasser, K.D.** (2018). The Adaptor Protein ENY2 Is a Component of the Deubiquitination Module of the Arabidopsis SAGA Transcriptional Co-activator Complex but not of the TREX-2 Complex. *Journal of Molecular Biology* **430**: 1479–1494.
- Poulios, S. and Vlachonasios, K.E.** (2016). Synergistic action of histone acetyltransferase GCN5 and receptor CLAVATA1 negatively affects ethylene responses in *Arabidopsis thaliana*. *J Exp Bot* **67**: 905–918.
- Pray-Grant, M.G., Daniel, J.A., Schieltz, D., Yates 3rd, J.R., and Grant, P.A.** (2005). Chd1 chromodomain links histone H3 methylation with SAGA- and SLIK-dependent acetylation. *Nature* **433**: 434–438.
- Qian, C. and Zhou, M.-M.** (2006). SET domain protein lysine methyltransferases: Structure, specificity and catalysis. *Cell. Mol. Life Sci.* **63**: 2755–2763.
- Rodríguez-Navarro, S., Fischer, T., Luo, M.-J., Antúez, O., Brettschneider, S., Lechner, J., Pérez-Ortín, J.E., Reed, R., and Hurt, E.** (2004). Sus1, a functional component of the SAGA histone acetylase complex and the nuclear pore-associated mRNA export machinery. *Cell* **116**: 75–86.
- Rojas, J.R., Trievel, R.C., Zhou, J., Mo, Y., Li, X., Berger, S.L., Allis, C.D., and Marmorstein, R.** (1999). Structure of Tetrahymena GCN5 bound to coenzyme A and a histone H3 peptide. *Nature* **401**: 93–98.
- Roth, S.Y., Denu, J.M., and Allis, C.D.** (2001). Histone acetyltransferases. *Annu Rev Biochem* **70**: 81–120.
- Ruijter, J.M., Lorenz, P., Tuomi, J.M., Hecker, M., and van den Hoff, M.J.** (2014). Fluorescent-increase kinetics of different fluorescent reporters used for qPCR depend on monitoring chemistry, targeted sequence, type of DNA input and PCR efficiency. *Mikrochim Acta* **181**: 1689–1696.
- Ruijter, J.M., Ramakers, C., Hoogaars, W.M., Karlen, Y., Bakker, O., van den Hoff, M.J., and Moorman, A.F.** (2009). Amplification efficiency: linking baseline and bias in the analysis of quantitative PCR data. *Nucleic Acids Res* **37**: e45.
- Rymen, B. et al.** (2019). Histone acetylation orchestrates wound-induced transcriptional activation and cellular reprogramming in *Arabidopsis*. *Commun Biol* **2**: 404.
- Sakuraba, Y., Kim, Y.S., Han, S.H., Lee, B.D., and Paek, N.C.** (2015). The Arabidopsis Transcription Factor NAC016 Promotes Drought Stress Responses by Repressing AREB1 Transcription through a Trifurcate Feed-Forward Regulatory Loop Involving NAP. *Plant Cell* **27**: 1771–1787.
- Schindelin, J. et al.** (2012). Fiji: an open-source platform for biological-image analysis. *Nat Methods* **9**: 676–682.

- Schu, P.V., Takegawa, K., Fry, M.J., Stack, J.H., Waterfield, M.D., and Emr, S.D.** (1993). Phosphatidylinositol 3-kinase encoded by yeast VPS34 gene essential for protein sorting. *Science* **260**: 88–91.
- Schuetz, A., Bernstein, G., Dong, A., Antoshenko, T., Wu, H., Loppnau, P., Bochkarev, A., and Plotnikov, A.N.** (2007). Crystal structure of a binary complex between human GCN5 histone acetyltransferase domain and acetyl coenzyme A. *Proteins* **68**: 403–407.
- Scott, I., Webster, B.R., Li, J.H., and Sack, M.N.** (2012). Identification of a molecular component of the mitochondrial acetyltransferase programme: a novel role for GCN5L1. *Biochem J* **443**: 655–661.
- Servet, C., Benhamed, M., Latrasse, D., Kim, W., Delarue, M., and Zhou, D.X.** (2008). Characterization of a phosphatase 2C protein as an interacting partner of the histone acetyltransferase GCN5 in Arabidopsis. *Biochim Biophys Acta* **1779**: 376–382.
- Servet, C., Conde e Silva, N., and Zhou, D.X.** (2010). Histone acetyltransferase AtGCN5/HAG1 is a versatile regulator of developmental and inducible gene expression in Arabidopsis. *Mol Plant* **3**: 670–677.
- Shahbazian, M.D. and Grunstein, M.** (2007). Functions of site-specific histone acetylation and deacetylation. *Annu Rev Biochem* **76**: 75–100.
- Sharov, G., Voltz, K., Durand, A., Kolesnikova, O., Papai, G., Myasnikov, A.G., Dejaegere, A., Ben Shem, A., and Schultz, P.** (2017). Structure of the transcription activator target Tra1 within the chromatin modifying complex SAGA. *Nat Commun* **8**: 1556.
- Shen, Y., Wei, W., and Zhou, D.X.** (2015). Histone Acetylation Enzymes Coordinate Metabolism and Gene Expression. *Trends Plant Sci* **20**: 614–621.
- Sigrist, C.J., de Castro, E., Cerutti, L., Cuche, B.A., Hulo, N., Bridge, A., Bougueleret, L., and Xenarios, I.** (2013). New and continuing developments at PROSITE. *Nucleic Acids Res* **41**: D344-347.
- Sigrist, C.J., Cerutti, L., Hulo, N., Gattiker, A., Falquet, L., Pagni, M., Bairoch, A., and Bucher, P.** (2002). PROSITE: A documented database using patterns and profiles as motif descriptors. *Brief Bioinform* **3**: 265–274.
- Simon, M.L., Platre, M.P., Assil, S., van Wijk, R., Chen, W.Y., Chory, J., Dreux, M., Munnik, T., and Jaillais, Y.** (2014). A multi-colour/multi-affinity marker set to visualize phosphoinositide dynamics in Arabidopsis. *Plant J* **77**: 322–337.
- Sobol, M. et al.** (2018). Nuclear phosphatidylinositol 4,5-bisphosphate islets contribute to efficient RNA polymerase II-dependent transcription. *J Cell Sci* **131**: jcs211094.
- Soliman, M.A. and Riabowol, K.** (2007). After a decade of study-ING, a PHD for a versatile family of proteins. *Trends Biochem Sci* **32**: 509–519.
- Sousa, E., Kost, B., and Malho, R.** (2008). Arabidopsis phosphatidylinositol-4-monophosphate 5-kinase 4 regulates pollen tube growth and polarity by modulating membrane recycling. *Plant Cell* **20**: 3050–3064.
- Srivastava, R., Rai, K.M., Pandey, B., Singh, S.P., and Sawant, S.V.** (2015). Spt-Ada-Gcn5-Acetyltransferase (SAGA) Complex in Plants: Genome Wide Identification, Evolutionary Conservation and Functional Determination. *PLoS One* **10**: e0134709.

- Staswick, P.E., Serban, B., Rowe, M., Tiryaki, I., Maldonado, M.T., Maldonado, M.C., and Suza, W.** (2005). Characterization of an Arabidopsis enzyme family that conjugates amino acids to indole-3-acetic acid. *Plant Cell* **17**: 616–627.
- Stenzel, I., Ischebeck, T., Konig, S., Holubowska, A., Sporysz, M., Hause, B., and Heilmann, I.** (2008). The type B phosphatidylinositol-4-phosphate 5-kinase 3 is essential for root hair formation in Arabidopsis thaliana. *Plant Cell* **20**: 124–141.
- Stenzel, I., Ischebeck, T., Quint, M., and Heilmann, I.** (2012). Variable Regions of PI4P 5-Kinases Direct PtdIns(4,5)P(2) Toward Alternative Regulatory Functions in Tobacco Pollen Tubes. *Front Plant Sci* **2**: 114.
- Sterner, D.E., Grant, P.A., Roberts, S.M., Duggan, L.J., Belotserkovskaya, R., Pacella, L.A., Winston, F., Workman, J.L., and Berger, S.L.** (1999). Functional organization of the yeast SAGA complex: distinct components involved in structural integrity, nucleosome acetylation, and TATA-binding protein interaction. *Mol Cell Biol* **19**: 86–98.
- Stockinger, E.J., Mao, Y., Regier, M.K., Triezenberg, S.J., and Thomashow, M.F.** (2001). Transcriptional adaptor and histone acetyltransferase proteins in Arabidopsis and their interactions with CBF1, a transcriptional activator involved in cold-regulated gene expression. *Nucleic Acids Res* **29**: 1524–1533.
- Strahl, B.D. and Allis, C.D.** (2000). The language of covalent histone modifications. *Nature* **403**: 41–45.
- Strahl, B.D. and Briggs, S.D.** (2021). The SAGA continues: The rise of cis- and trans-histone crosstalk pathways. *Biochim Biophys Acta Gene Regul Mech* **1864**: 194600.
- Sun, J., Paduch, M., Kim, S.A., Kramer, R.M., Barrios, A.F., Lu, V., Luke, J., Usatyuk, S., Kossiakoff, A.A., and Tan, S.** (2018). Structural basis for activation of SAGA histone acetyltransferase Gcn5 by partner subunit Ada2. *Proc Natl Acad Sci U S A* **115**: 10010–10015.
- Taverna, S.D., Li, H., Ruthenburg, A.J., Allis, C.D., and Patel, D.J.** (2007). How chromatin-binding modules interpret histone modifications: lessons from professional pocket pickers. *Nat Struct Mol Biol* **14**: 1025–1040.
- Tejos, R., Sauer, M., Vanneste, S., Palacios-Gomez, M., Li, H., Heilmann, M., van Wijk, R., Vermeer, J.E., Heilmann, I., Munnik, T., and Friml, J.** (2014). Bipolar Plasma Membrane Distribution of Phosphoinositides and Their Requirement for Auxin-Mediated Cell Polarity and Patterning in Arabidopsis. *Plant Cell* **26**: 2114–2128.
- Templeton, G.W. and Moorhead, G.B.G.** (2005). The phosphoinositide-3-OH-kinase-related kinases of *Arabidopsis thaliana*. *EMBO Rep* **6**: 723–728.
- Towbin, H., Staehelin, T., and Gordon, J.** (1979). Electrophoretic transfer of proteins from polyacrylamide gels to nitrocellulose sheets: Procedure and some applications. *Proc Natl Acad Sci USA* **76**: 4350–4354.
- Tran, H.T., Nimick, M., Uhrig, R.G., Templeton, G., Morrice, N., Gourlay, R., DeLong, A., and Moorhead, G.B.** (2012). Arabidopsis thaliana histone deacetylase 14 (HDA14) is an alpha-tubulin deacetylase that associates with PP2A and enriches in the microtubule fraction with the putative histone acetyltransferase ELP3. *Plant J* **71**: 263–272.

- Trejo-Arellano, M.S., Mahrez, W., Nakamura, M., Moreno-Romero, J., Nanni, P., Kohler, C., and Hennig, L.** (2017). H3K23me1 is an evolutionarily conserved histone modification associated with CG DNA methylation in *Arabidopsis*. *Plant J* **90**: 293–303.
- Tuomi, J.M., Voorbraak, F., Jones, D.L., and Ruijter, J.M.** (2010). Bias in the C_q value observed with hydrolysis probe based quantitative PCR can be corrected with the estimated PCR efficiency value. *Methods* **50**: 313–322.
- Ueda, M. and Seki, M.** (2020). Histone Modifications Form Epigenetic Regulatory Networks to Regulate Abiotic Stress Response. *Plant Physiol* **182**: 15–26.
- Ulmasov, T., Liu, Z.B., Hagen, G., and Guilfoyle, T.J.** (1995). Composite structure of auxin response elements. *Plant Cell* **7**: 1611–1623.
- Vanhaesebroeck, B., Leever, S.J., Ahmadi, K., Timms, J., Katso, R., Driscoll, P.C., Woscholski, R., Parker, P.J., and Waterfield, M.D.** (2001). Synthesis and function of 3-phosphorylated inositol lipids. *Annu Rev Biochem* **70**: 535–602.
- Viaud, J., Mansour, R., Antkowiak, A., Mujalli, A., Valet, C., Chicanne, G., Xuereb, J.M., Terrisse, A.D., Severin, S., Gratacap, M.P., Gaits-lacovoni, F., and Payrastré, B.** (2016). Phosphoinositides: Important lipids in the coordination of cell dynamics. *Biochimie* **125**: 250–258.
- Vieyra, D. et al.** (2002). Human ING1 proteins differentially regulate histone acetylation. *J Biol Chem* **277**: 29832–29839.
- Vincent, P., Chua, M., Nogue, F., Fairbrother, A., Mekeel, H., Xu, Y., Allen, N., Bibikova, T.N., Gilroy, S., and Bankaitis, V.A.** (2005). A Sec14p-nodulin domain phosphatidylinositol transfer protein polarizes membrane growth of *Arabidopsis thaliana* root hairs. *J Cell Biol* **168**: 801–812.
- Vlachonasios, K., Poullos, S., and Mougiou, N.** (2021). The Histone Acetyltransferase GCN5 and the Associated Coactivators ADA2: From Evolution of the SAGA Complex to the Biological Roles in Plants. *Plants (Basel)* **10**: 308.
- Vlachonasios, K.E., Kaldis, A., Nikoloudi, A., and Tsementzi, D.** (2011). The role of transcriptional coactivator ADA2b in *Arabidopsis* abiotic stress responses. *Plant Signal Behav* **6**: 1475–1478.
- Vlachonasios, K.E., Thomashow, M.F., and Triezenberg, S.J.** (2003). Disruption Mutations of ADA2b and GCN5 Transcriptional Adaptor Genes Dramatically Affect *Arabidopsis* Growth, Development, and Gene Expression[W]. *The Plant Cell* **15**: 626–638.
- Wang, H., Dienemann, C., Stutzer, A., Urlaub, H., Cheung, A.C.M., and Cramer, P.** (2020). Structure of the transcription coactivator SAGA. *Nature* **577**: 717–720.
- Weiste, C. and Dröge-Laser, W.** (2014). The *Arabidopsis* transcription factor bZIP11 activates auxin-mediated transcription by recruiting the histone acetylation machinery. *Nat Commun* **5**: 3883.
- Welters, P., Takegawa, K., Emr, S.D., and Chrispeels, M.J.** (1994). AtVPS34, a phosphatidylinositol 3-kinase of *Arabidopsis thaliana*, is an essential protein with homology to a calcium-dependent lipid binding domain. *Proc Natl Acad Sci USA* **91**: 11398–11402.

- Winter, D., Vinegar, B., Nahal, H., Ammar, R., Wilson, G.V., and Provart, N.J.** (2007). An “Electronic Fluorescent Pictograph” browser for exploring and analyzing large-scale biological data sets. *PLoS One* **2**: e718.
- Wu, C.J., Liu, Z.Z., Wei, L., Zhou, J.X., Cai, X.W., Su, Y.N., Li, L., Chen, S., and He, X.J.** (2021). Three functionally redundant plant-specific paralogs are core subunits of the SAGA histone acetyltransferase complex in Arabidopsis. *Mol Plant* **14**: 1071–1087.
- Wu, P.Y., Ruhlmann, C., Winston, F., and Schultz, P.** (2004). Molecular architecture of the *S. cerevisiae* SAGA complex. *Mol Cell* **15**: 199–208.
- Xiao, J., Lee, U.S., and Wagner, D.** (2016). Tug of war: adding and removing histone lysine methylation in Arabidopsis. *Curr Opin Plant Biol* **34**: 41–53.
- Xing, J., Wang, T., Liu, Z., Xu, J., Yao, Y., Hu, Z., Peng, H., Xin, M., Yu, F., Zhou, D., and Ni, Z.** (2015). GENERAL CONTROL NONREPPRESSED PROTEIN5-Mediated Histone Acetylation of FERRIC REDUCTASE DEFECTIVE3 Contributes to Iron Homeostasis in Arabidopsis. *Plant Physiol* **168**: 1309–1320.
- Ye, J., Coulouris, G., Zaretskaya, I., Cutcutache, I., Rozen, S., and Madden, T.L.** (2012). Primer-BLAST: A tool to design target-specific primers for polymerase chain reaction. *BMC Bioinformatics* **13**: 134.
- Yeates, T.O.** (2002). Structures of SET domain proteins: protein lysine methyltransferases make their mark. *Cell* **111**: 5–7.
- Yildirim, S., Castano, E., Sobol, M., Philimonenko, V.V., Dzajak, R., Venit, T., and Hozak, P.** (2013). Involvement of phosphatidylinositol 4,5-bisphosphate in RNA polymerase I transcription. *J Cell Sci* **126**: 2730–2739.
- Yoo, S.D., Cho, Y.H., and Sheen, J.** (2007). Arabidopsis mesophyll protoplasts: a versatile cell system for transient gene expression analysis. *Nat Protoc* **2**: 1565–1572.
- Yu, H., Fukami, K., Watanabe, Y., Ozaki, C., and Takenawa, T.** (1998). Phosphatidylinositol 4,5-bisphosphate reverses the inhibition of RNA transcription caused by histone H1. *Eur J Biochem* **251**: 281–287.
- Yun, M., Wu, J., Workman, J.L., and Li, B.** (2011). Readers of histone modifications. *Cell Res* **21**: 564–578.
- Zhang, K., Sridhar, V.V., Zhu, J., Kapoor, A., and Zhu, J.K.** (2007). Distinctive core histone post-translational modification patterns in Arabidopsis thaliana. *PLoS One* **2**: e1210.
- Zhao, K., Wang, W., Rando, O.J., Xue, Y., Swiderek, K., Kuo, A., and Crabtree, G.R.** (1998). Rapid and phosphoinositol-dependent binding of the SWI/SNF-like BAF complex to chromatin after T lymphocyte receptor signaling. *Cell* **95**: 625–636.
- Zhao, Y., Yan, A., Feijo, J.A., Furutani, M., Takenawa, T., Hwang, I., Fu, Y., and Yang, Z.** (2010). Phosphoinositides regulate clathrin-dependent endocytosis at the tip of pollen tubes in Arabidopsis and tobacco. *Plant Cell* **22**: 4031–4044.
- Zhou, S., Jiang, W., Long, F., Cheng, S., Yang, W., Zhao, Y., and Zhou, D.X.** (2017). Rice Homeodomain Protein WOX11 Recruits a Histone Acetyltransferase Complex to Establish Programs of Cell Proliferation of Crown Root Meristem. *Plant Cell* **29**: 1088–1104.

6. Appendix

6.1. Additional information to the obtained results

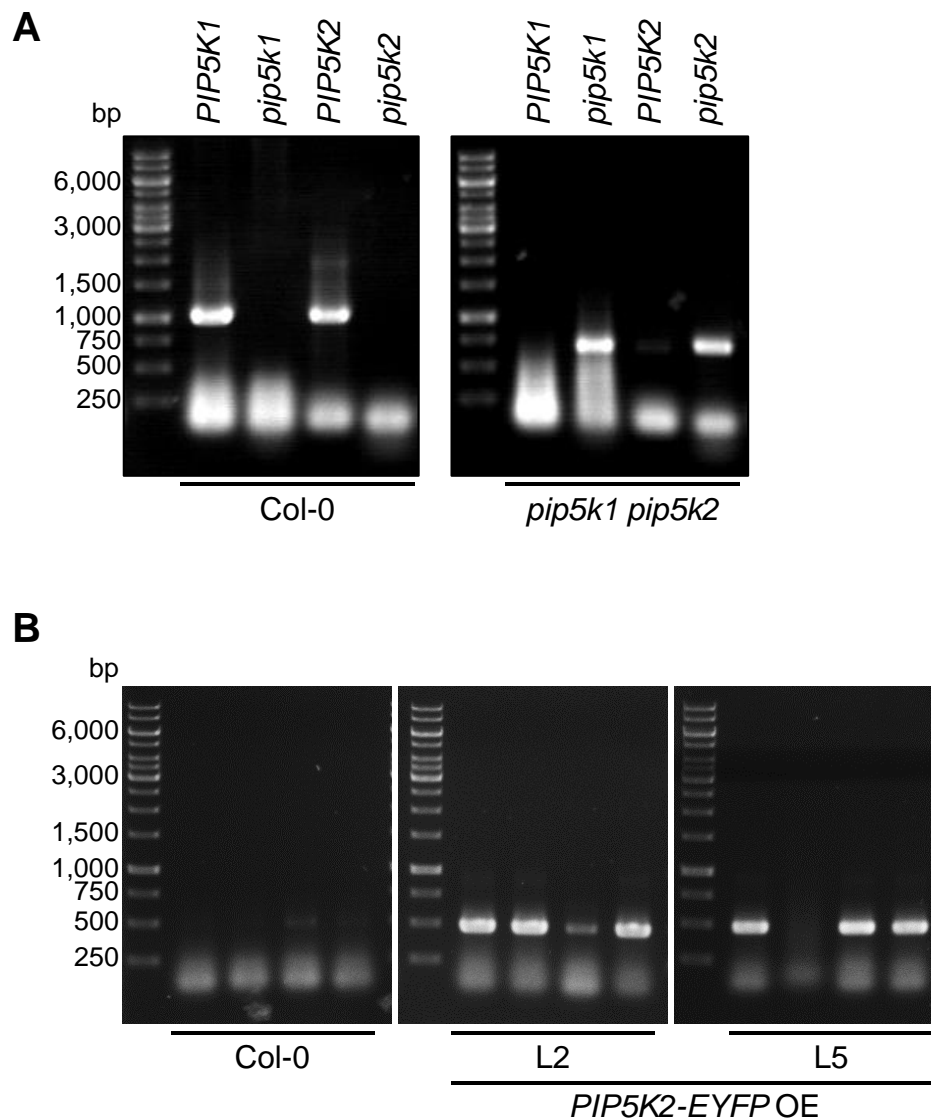


Fig. 6.1: Genotypic characterization of *pip5k1 pip5k2* double mutant and *pCaMV35S::PIP5K2-EYFP* OE lines with specific oligonucleotides. Col-0 was used as control. The applied marker is GeneRuler™ 1 kb DNA Ladder (Thermo Fisher Scientific, Schwerte Germany). **A**, Genotypic characterization of one representative Col-0 plant and one representative *pip5k1 pip5k2* plant. DNA fragments were amplified with specific oligonucleotides. *PIP5K1*, SALK-146728-*PIP5K1*-for, SALK-146728-*PIP5K1*-rev; *pip5k1*, LBa1-SALK-for, SALK-146728-*PIP5K1*-rev; *PIP5K2*, SALK_012487-*PIP5K2*-for, SALK-012487-*PIP5K2*-rev; *pip5k2*, LBa1-SALK-for, SALK-012487-*PIP5K2*-rev. Expected fragment sizes are *PIP5K1*, 1037 bp; *pip5k1*, 750 bp; *PIP5K2*, 1001 bp; *pip5k2*, 750 bp. **B**, Genotypic characterization of *pCaMV35S::PIP5K2-EYFP* OE lines L2 and L5. A fragment of *PIP5K2-EYFP* (477 bp length) was amplified with the specific oligonucleotides *gPIP5K2*-for and *gVYFP*-rev. Four plants each of Col-0 and *pCaMV35S::PIP5K2-EYFP* OE lines L2 and L5 were genotyped.

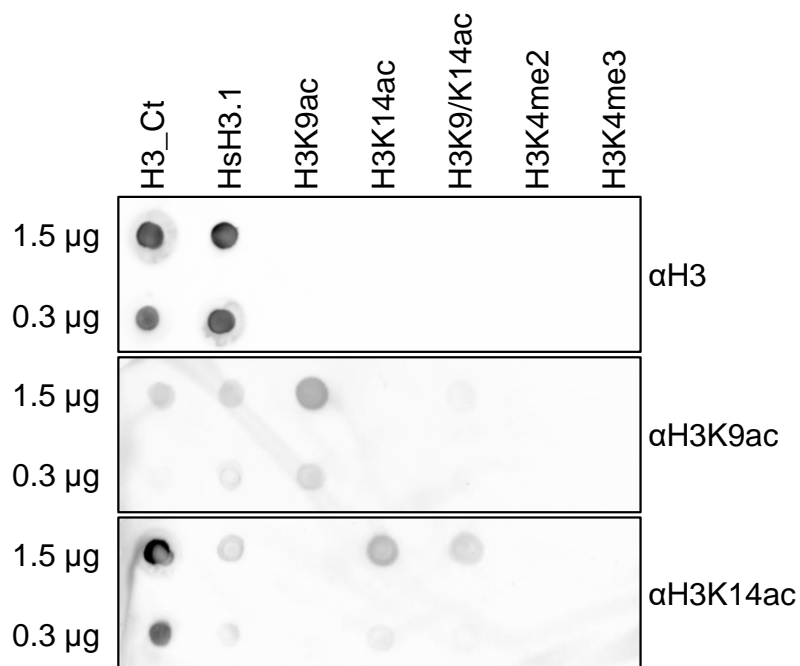


Fig. 6.2: Test for epitope specificity of antisera against different histone H3 acetylation events. Primary antisera against histone H3, H3K9ac and H3K14ac were tested for their epitope specificity by using histone H3 and differently modified histone H3 peptides. Used peptides are listed in appendix Tab. 6.5 and were spotted on a nitrocellulose membrane in dots of 1.5 μg and 0.3 μg . Immunodetection was performed as described in section 4.20. Primary antisera were applied overnight as recommended in 3 % milk powder (w/v) in 1x TBS buffer. The next day, a secondary antiserum against rabbit with a HRP conjugate was applied. HRP detection was performed. Tested and used antisera are listed in appendix Tab. 6.11. $n = 4$ (except the use of H3K9ac peptide, $n = 2$).

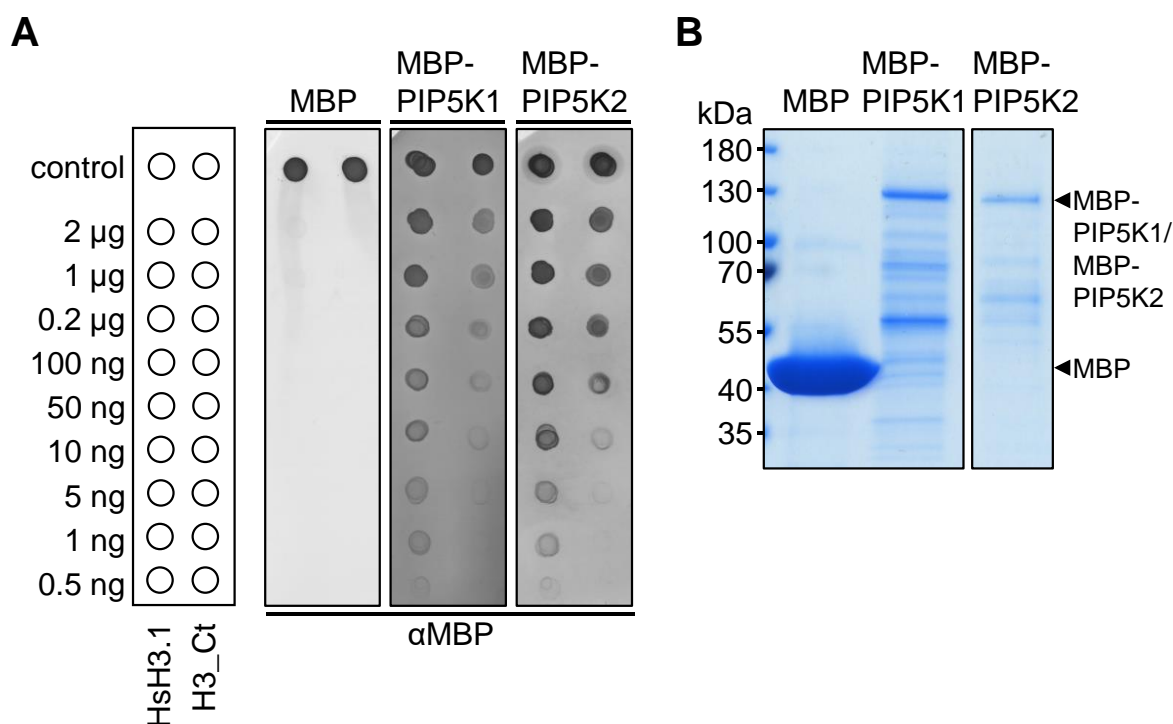


Fig. 6.3: Interaction test of PI4P 5-kinases PIP5K1 and PIP5K2 with histone H3. **A**, Dot-blot analysis of histone H3 binding of PIP5K1 and PIP5K2. Recombinant human histone H3 (HsH3.1) and histone H3 from calf thymus (H3_Ct) were spotted on a nitrocellulose membrane in amounts of 2 μg, 1 μg, 0.2 μg, 100 ng, 50 ng, 10 ng, 5 ng, 1 ng and 0.5 ng per dot. As a control, two times 2 μl of a 1:1 dilution of recombinantly expressed and enriched MBP, MBP-PIP5K1 and MBP-PIP5K2 protein fractions were spotted. Applied protein fractions are shown in B. 20 μl of MBP, 150 μl of MBP-PIP5K1 and 300 μl of MBP-PIP5K2 fractions (50 to 100 μg protein) were incubated with the blocked membranes overnight. The next day, immunodetections were performed with suitable antibodies. AP detection was conducted for 2 h. n = 4, for this setup combination n = 1. **B**, Applied protein fractions of enriched recombinant MBP, MBP-PIP5K1 and MBP-PIP5K2 proteins for A. 10 μl of protein fractions were separated on an SDS-PAGE and were stained with Coomassie afterwards. PageRuler™ Prestained Protein Ladder was used as a molecular size marker. MBP was affinity purified and obtained from Larissa Launhardt. MBP-PIP5K1 and MBP-PIP5K2 proteins were enriched by Lennart Schwalgun according to Dejonghe and coworkers (Dejonghe et al., 2016). Expected molecular sizes of full-length proteins MBP, 42.5 kDa; MBP-PIP5K1, 128.4 kDa; MBP-PIP5K2, 128.8 kDa. n = 3.

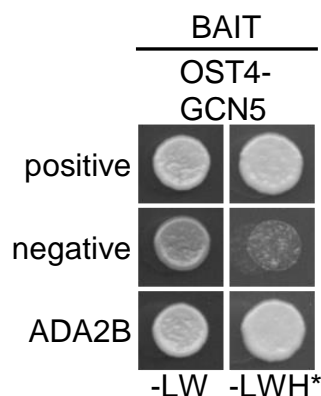


Fig. 6.4: GCN5 and ADA2B interact in YTH. The interaction of GCN5 (bait) and ADA2B (prey) was tested by split-ubiquitin-based YTH analysis in *S. cerevisiae* strain NMY51. OST4 fusions localized interactions to ER membranes. *pAl-Alg5* and *pDL2-Alg5* vectors were used as positive or negative control. Uniform growth on -LW media (without leucine and tryptophane) indicates equal cell densities and the presence of the respective vectors. Interaction is indicated by growth under selective conditions on -LWH media (without leucine, tryptophane and histidine). *, -LWH medium supplemented with 10 mM 3-AT. Yeast colonies were grown at 30°C for two days. A representative result of three replicates with five independent colonies of each combination is shown. ADA2B, transcriptional adaptor 2B; GCN5, general control non-repressible 5; OST4, oligosaccharyltransferase 4.

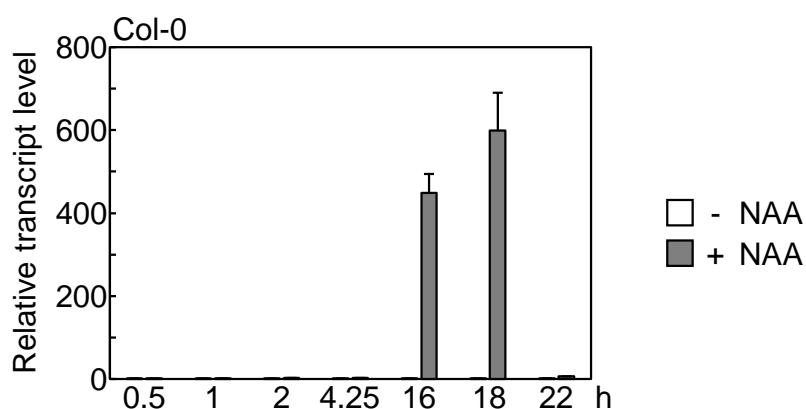


Fig. 6.5: Relative transcript levels of *GH3.3* in mesophyll protoplasts over time. Arabidopsis mesophyll protoplasts were prepared from Col-0 wild type and were treated for 0.5, 1, 2, 4.25, 16, 18 or 22 h with 0.25 μ M NAA. Relative transcript levels of *GH3.3* were measured in a qPCR. Transcript levels were normalized to both the reference gene *UBC10* and the transcript levels of the respective mock-treated samples. Bars show the mean. Error bars indicate standard deviation. The experiment was conducted once with four biological replicates (three replicates for 18 h time point).

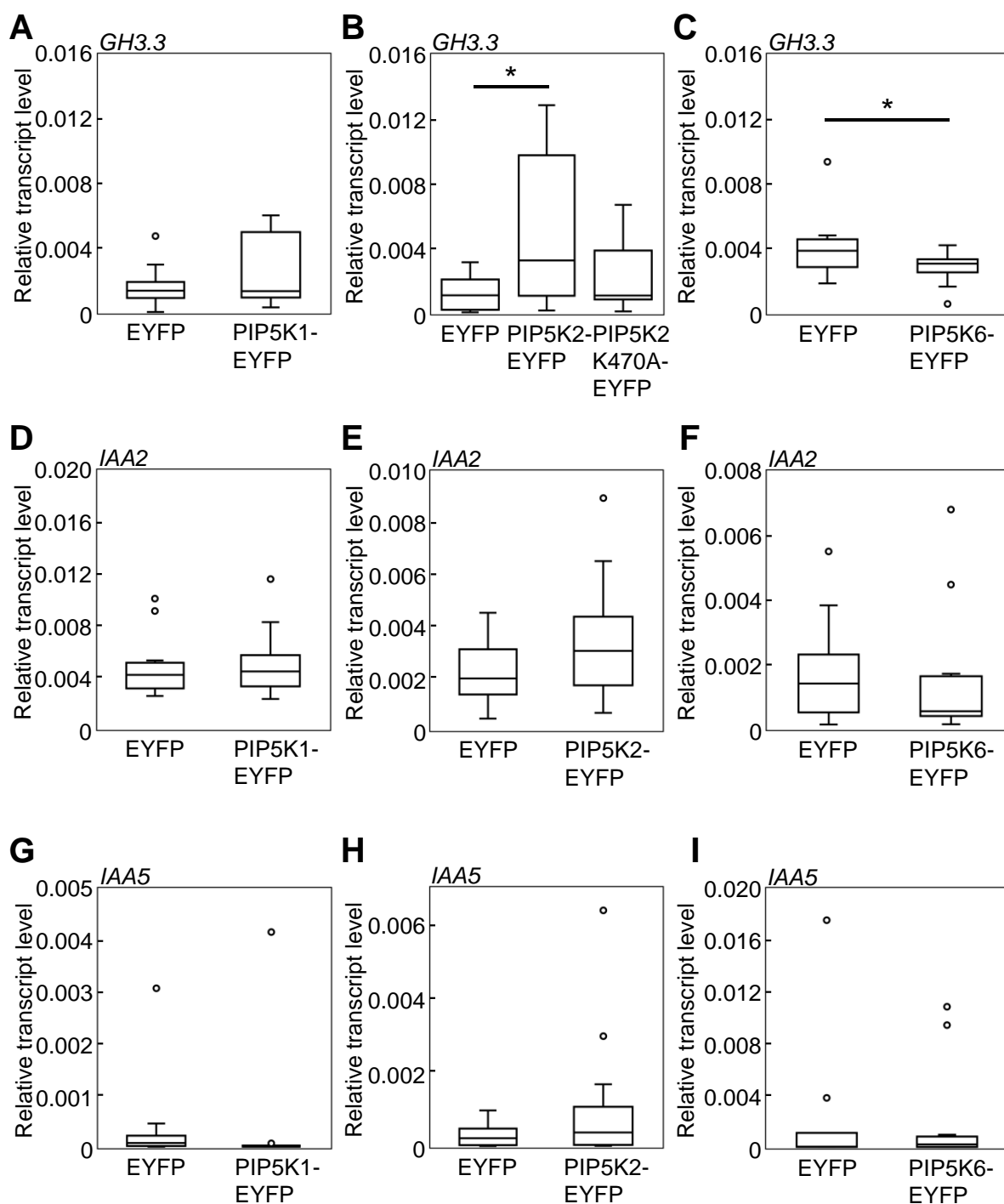


Fig. 6.6: Basal transcript levels of *GH3.3*, *IAA2* and *IAA5* upon overexpression of PI4P 5-kinases. Relative basal transcript levels of *GH3.3*, *IAA2* and *IAA5* in mesophyll protoplasts upon overexpressing either EYFP or the different PI4P 5-kinases. Data represent 8–16 biological replicates (transformations) from three to four independent protoplast preparations. **A**, *GH3.3* transcript levels in protoplasts transformed with *pEntryA-pCaMV35S::EYFP* or *pEntryA-pCaMV35S::PIP5K1-EYFP*. **B**, *GH3.3* transcript levels in protoplasts transformed with either *pEntryA-pCaMV35S::EYFP*, *pEntryA-pCaMV35S::PIP5K2-EYFP* or *pEntryA-pCaMV35S::PIP5K2 K470A-EYFP*. **C**, *GH3.3* transcript levels in protoplasts transformed with *pEntryA-pCaMV35S::EYFP* or *pEntryD-pCaMV35S::PIP5K6-EYFP*. **D**, *IAA2* transcript levels in protoplasts transformed with *pEntryA-pCaMV35S::EYFP* or *pEntryA-pCaMV35S::PIP5K1-EYFP*. **E**, *IAA2* transcript levels in protoplasts transformed with *pEntryA-pCaMV35S::EYFP* or *pEntryA-pCaMV35S::PIP5K2-EYFP*. **F**, *IAA2* transcript levels in protoplasts transformed with *pEntryA-pCaMV35S::EYFP* or

pEntryD-pCaMV35S::PIP5K6-EYFP. **G**, *IAA5* transcript levels in protoplasts transformed with *pEntryA-pCaMV35S::EYFP* or *pEntryA-pCaMV35S::PIP5K1-EYFP*. **H**, *IAA5* transcript levels in protoplasts transformed with *pEntryA-pCaMV35S::EYFP* or *pEntryA-pCaMV35S::PIP5K2-EYFP*. **I**, *IAA5* transcript levels in protoplasts transformed with *pEntryA-pCaMV35S::EYFP* or *pEntryD-pCaMV35S::PIP5K6-EYFP*. Transcript levels were normalized to the reference gene *UBC10*. Relative transcript levels are shown as boxplots; dots show outliers. Asterisks indicate significant differences compared to EYFP control according to a Student's T-test (* $P \leq 0.05$).

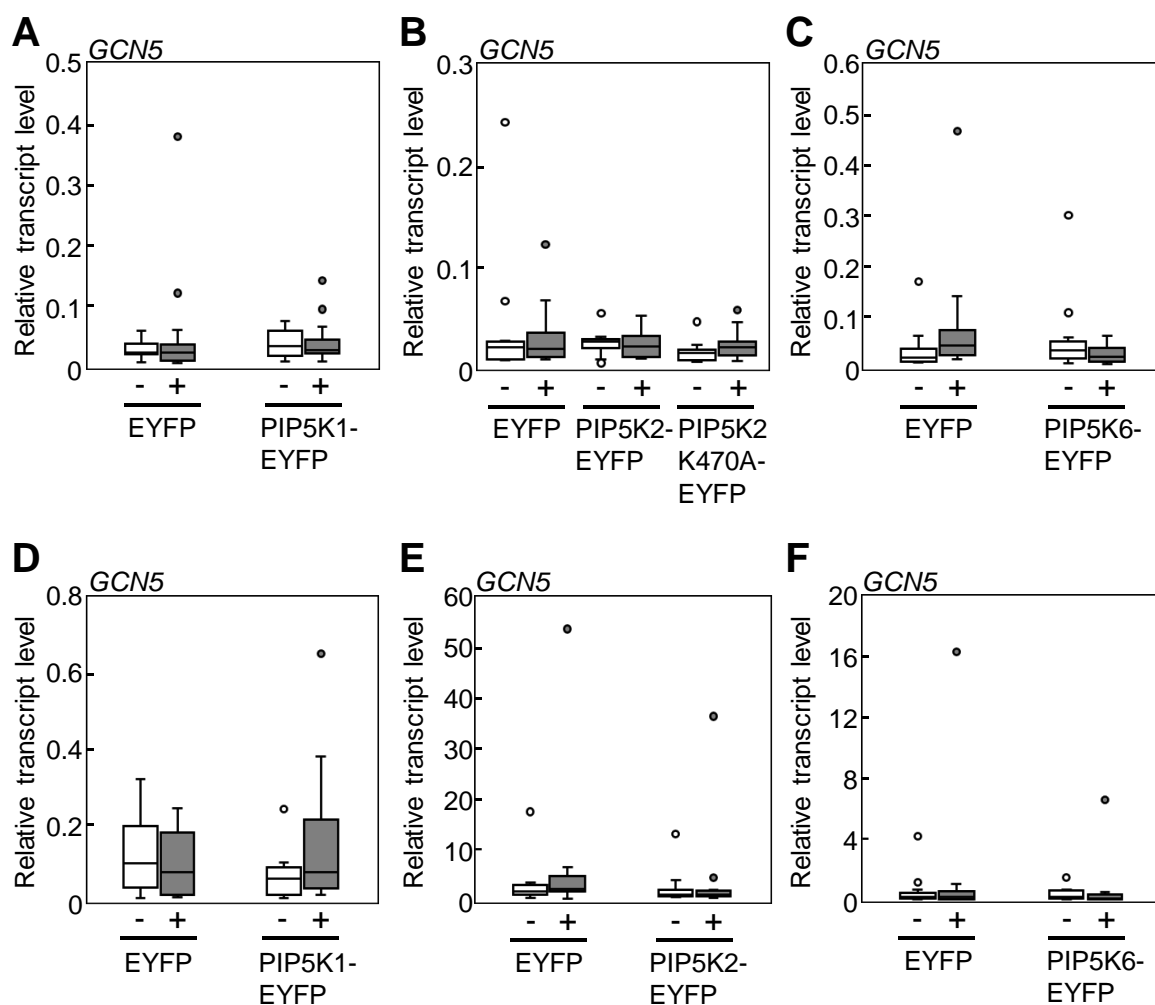
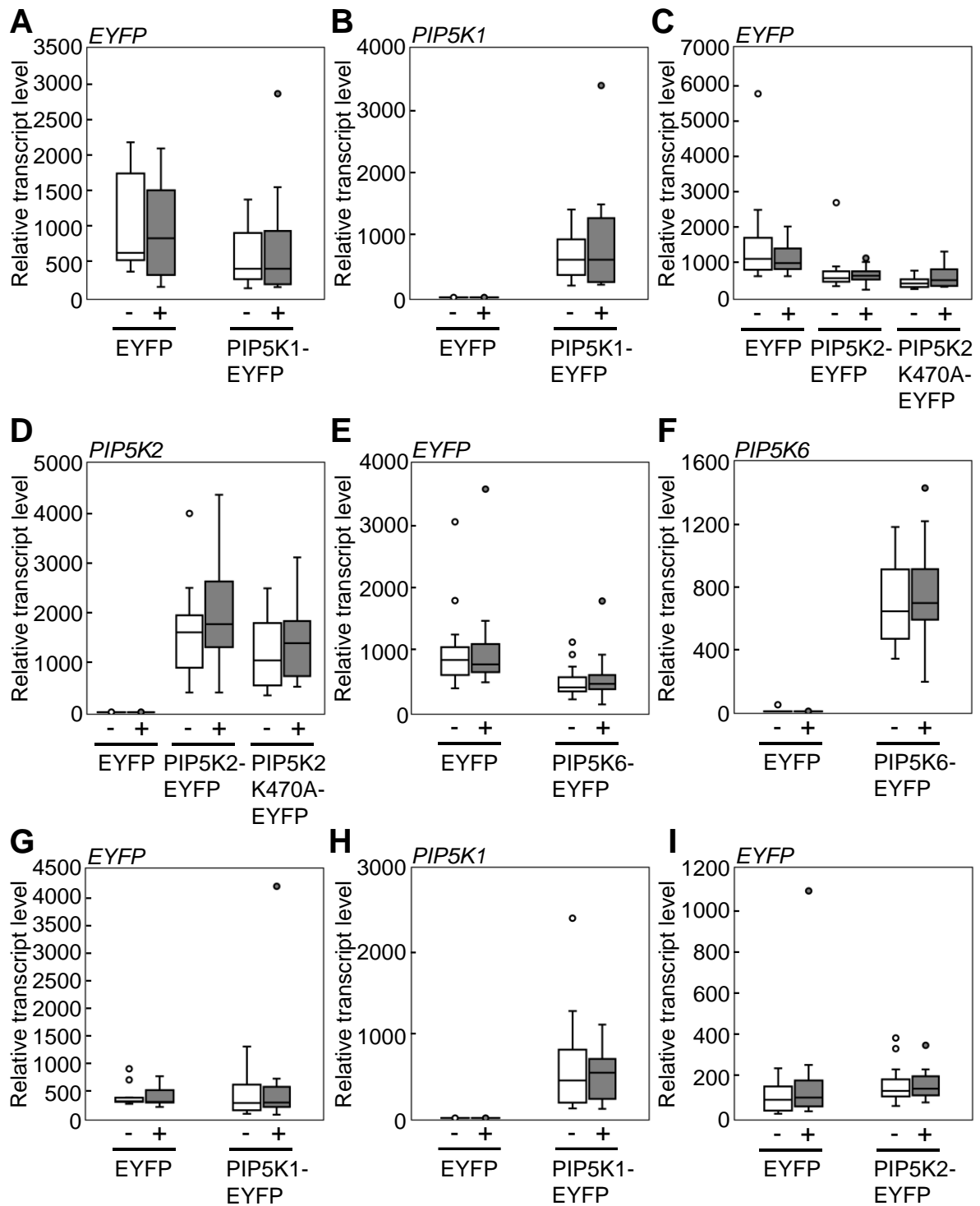


Fig. 6.7: Endogenous transcript levels of *GCN5* upon transient expression of different PI4P 5-kinases. Relative transcript levels of *GCN5* in mesophyll protoplasts upon overexpressing either EYFP or the different PI4P 5-kinases and with mock (-) and with 0.25 μ M NAA (+) treatment overnight (**A-C**) or 2 μ M NAA (+) for 2.5 h (**D-F**). Data represent 11 – 16 biological replicates (transformations) from three to four independent protoplast preparations. **A**, Protoplasts transformed with *pEntryA-pCaMV35S::EYFP* or *pEntryA-pCaMV35S::PIP5K1-EYFP* and treated with 0.25 μ M NAA. **B**, Protoplasts transformed with either *pEntryA-pCaMV35S::EYFP*, *pEntryA-pCaMV35S::PIP5K2-EYFP* or *pEntryA-pCaMV35S::PIP5K2 K470A-EYFP* and treated with 0.25 μ M NAA. **C**, Protoplasts transformed with *pEntryA-pCaMV35S::EYFP* or *pEntryD-pCaMV35S::PIP5K6-EYFP* and treated with 0.25 μ M NAA. **D**, Protoplasts transformed with *pEntryA-pCaMV35S::EYFP* or *pEntryA-pCaMV35S::PIP5K1-EYFP* and treated with 2 μ M NAA. **E**, Protoplasts transformed with *pEntryA-pCaMV35S::EYFP* or *pEntryA-pCaMV35S::PIP5K2-EYFP* and treated with 2 μ M NAA. **F**, Protoplasts transformed with *pEntryA-pCaMV35S::EYFP* or *pEntryD-pCaMV35S::PIP5K6-EYFP* and treated with 2 μ M NAA. Transcript levels were normalized to the reference gene *UBC10*. Relative transcript levels are shown as boxplots; dots show outliers. Significant differences were analyzed by one-way ANOVA with a subsequent Tukey's post-hoc test ($P < 0.05$).



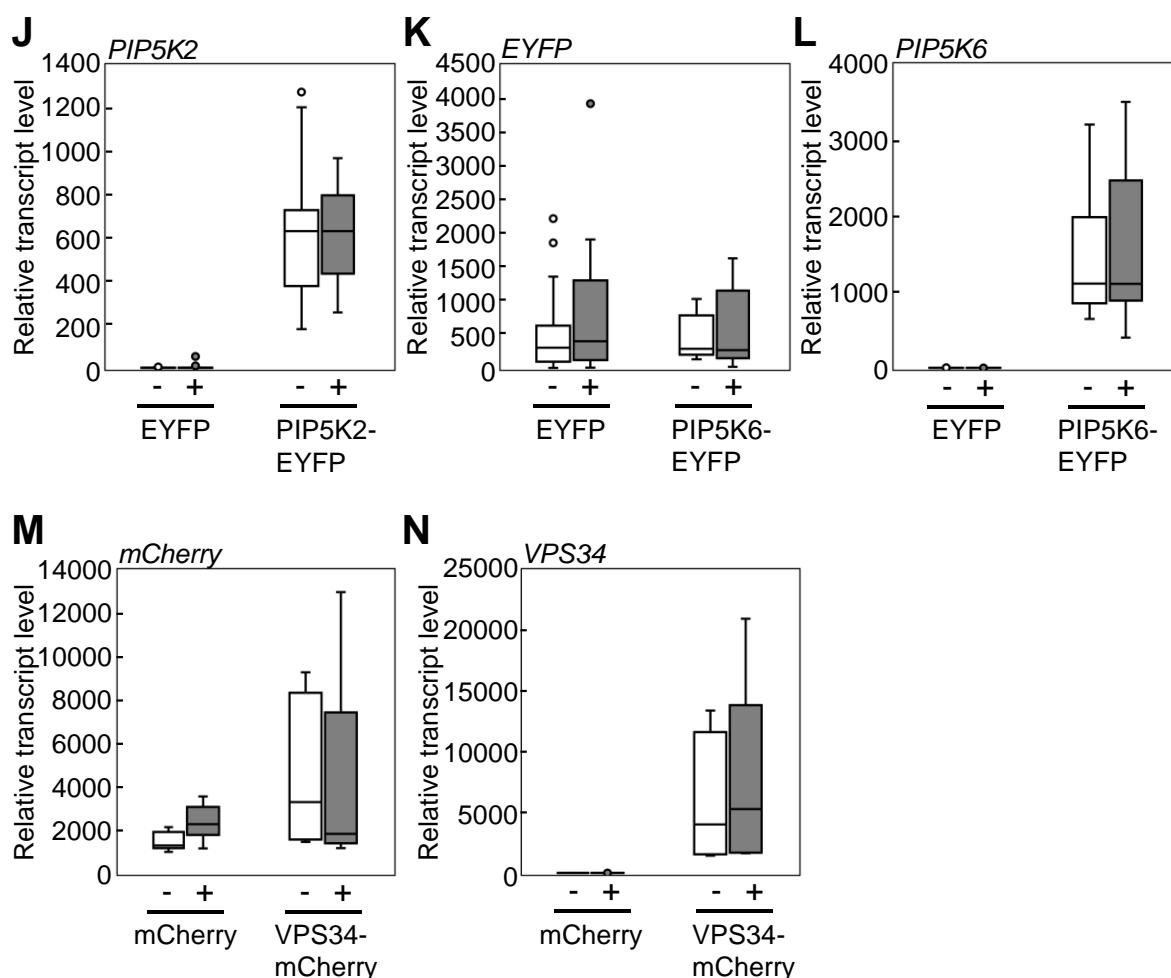


Fig. 6.8: Transcript levels of overexpressed PI-kinases and respective controls in protoplasts.

Relative transcript levels of *EYFP/mCherry* or *PIP5K1/PIP5K2/PIP5K2 K470A/PIP5K6/VPS34* in mesophyll protoplasts upon overexpressing either *EYFP/mCherry* or the different PI4P 5-kinases/*VPS34* and with mock (-) and with 0.25 μM NAA (+) treatment overnight or 2 μM NAA for 2.5 h, as indicated. Data represent 11 – 16 biological replicates (transformations) from three to four independent protoplast preparations (*EYFP/PIP5K1-EYFP/PIP5K2-EYFP/PIP5K2 K470A-EYFP/PIP5K6-EYFP*) or 7 – 8 biological replicates (transformations) from two independent protoplast preparations (*mCherry/VPS34-mCherry*). **A – F**, Protoplasts treated with 0.25 μM NAA overnight. **A**, *EYFP* transcript levels in protoplasts transformed with *pEntryA-pCaMV35S::EYFP* or *pEntryA-pCaMV35S::PIP5K1-EYFP*. **B**, *PIP5K1* transcript levels in protoplasts transformed with *pEntryA-pCaMV35S::EYFP* or *pEntryA-pCaMV35S::PIP5K1-EYFP*. **C**, *EYFP* transcript levels in protoplasts transformed with either *pEntryA-pCaMV35S::EYFP*, *pEntryA-pCaMV35S::PIP5K2-EYFP* or *pEntryA-pCaMV35S::PIP5K2 K470A-EYFP*. **D**, *PIP5K2* transcript levels in protoplasts transformed with either *pEntryA-pCaMV35S::EYFP*, *pEntryA-pCaMV35S::PIP5K2-EYFP* or *pEntryA-pCaMV35S::PIP5K2 K470A-EYFP*. **E**, *EYFP* transcript levels in protoplasts transformed with *pEntryA-pCaMV35S::EYFP* or *pEntryD-pCaMV35S::PIP5K6-EYFP*. **F**, *PIP5K6* transcript levels in protoplasts transformed with *pEntryA-pCaMV35S::EYFP* or *pEntryD-pCaMV35S::PIP5K6-EYFP*. **G – L**, Protoplasts treated with 2 μM NAA for 2.5 h. **G**, *EYFP* transcript levels in protoplasts transformed with *pEntryA-pCaMV35S::EYFP* or *pEntryA-pCaMV35S::PIP5K1-EYFP*. **H**, *PIP5K1* transcript levels in protoplasts transformed with *pEntryA-pCaMV35S::EYFP* or *pEntryA-pCaMV35S::PIP5K1-EYFP*. **I**, *EYFP* transcript levels in protoplasts transformed with *pEntryA-pCaMV35S::EYFP* or *pEntryA-pCaMV35S::PIP5K2-EYFP*. **J**, *PIP5K2* transcript levels in protoplasts transformed with *pEntryA-pCaMV35S::EYFP* or *pEntryA-pCaMV35S::PIP5K2-EYFP*. **K**, *EYFP* transcript levels in protoplasts transformed with *pEntryA-pCaMV35S::EYFP* or *pEntryD-pCaMV35S::PIP5K6-EYFP*. **L**, *PIP5K6* transcript levels in protoplasts transformed with *pEntryA-pCaMV35S::EYFP* or

pEntryD-pCaMV35S::PIP5K6-EYFP. **M, N**, Protoplasts treated with 0.25 μ M NAA overnight. **M**, *mCherry* transcript levels in protoplasts transformed with *pEntryD-pCaMV35S::mCherry* or *pEntryA-pCaMV35S::VPS34-mCherry*. **N**, *VPS34* transcript levels in protoplasts transformed with *pEntryD-pCaMV35S::mCherry* or *pEntryA-pCaMV35S::VPS34-mCherry*. Transcript levels were normalized to the reference gene *UBC10*. Relative transcript levels are shown as boxplots; dots show outliers. Significant differences were analyzed by one-way ANOVA with a subsequent Tukey's post-hoc test ($P < 0.05$) and indicated by letters a – c.

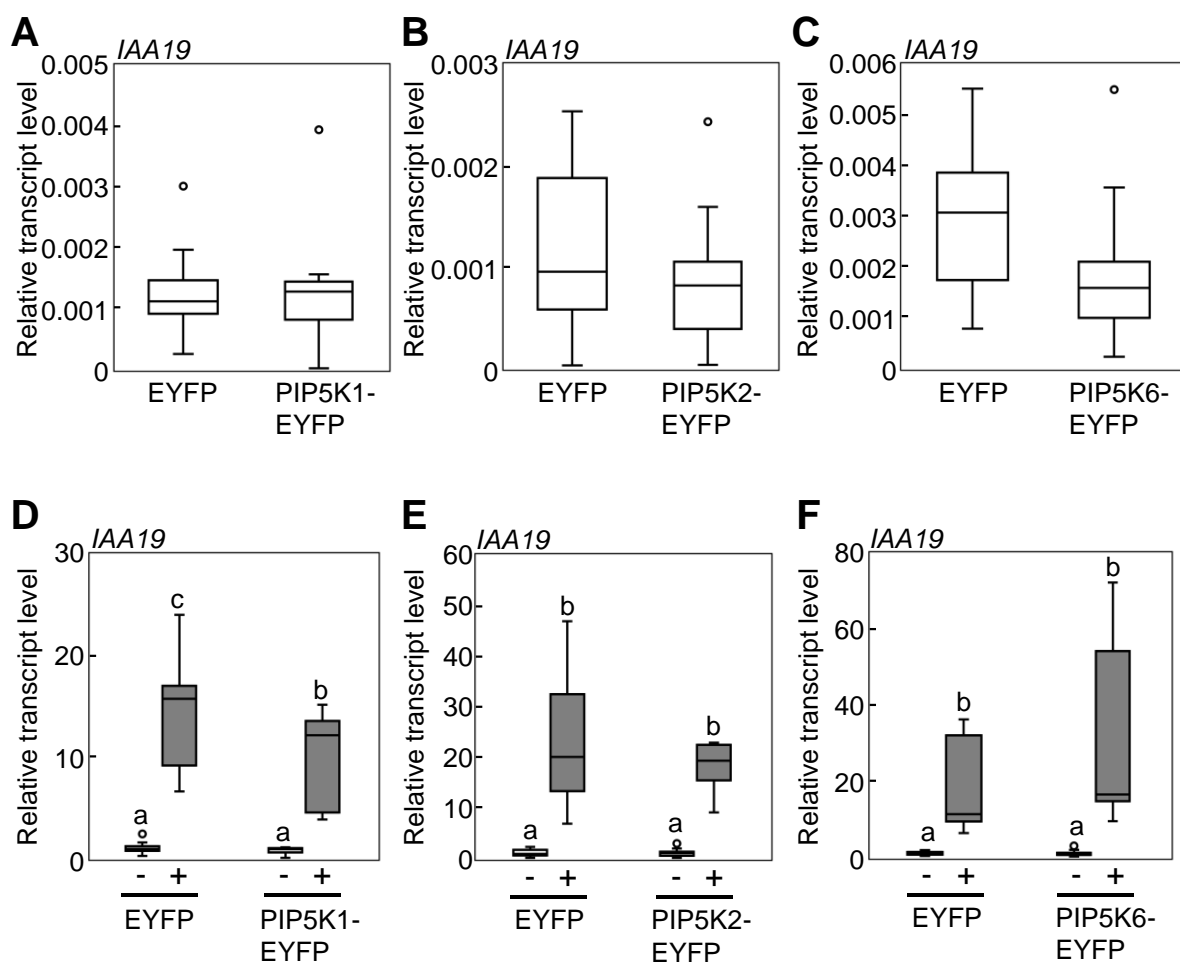


Fig. 6.9: Overexpression of PI4P 5-kinases reduces auxin-activation of *IAA19*. Relative transcript levels of *IAA19* in mesophyll protoplasts upon overexpressing either EYFP or the different PI4P 5-kinases and with mock (-) and with 2 μ M NAA (+) treatment for 2.5 h. **A, B, C**, Basal transcript levels of *IAA19*. Data represent 8 – 12 biological replicates (transformations) from three independent protoplast preparations. **A**, *IAA19* transcript levels in protoplasts transformed with *pEntryA-pCaMV35S::EYFP* or *pEntryA-pCaMV35S::PIP5K1-EYFP*. **B**, *IAA19* transcript levels in protoplasts transformed with *pEntryA-pCaMV35S::EYFP* or *pEntryA-pCaMV35S::PIP5K2-EYFP*. **C**, *IAA19* transcript levels in protoplasts transformed with *pEntryA-pCaMV35S::EYFP* or *pEntryD-pCaMV35S::PIP5K6-EYFP*. Significant differences were analyzed by Student's T-test. No significances were observed. **D, E, F**, Relative transcript levels of *IAA19* in mesophyll protoplasts upon overexpressing either EYFP or the different PI4P 5-kinases and with mock (-) and with 2 μ M NAA (+) treatment for 2.5 h. Data represent 8 – 12 biological replicates (transformations) from three independent protoplast preparations. **D**, Protoplasts transformed with *pEntryA-pCaMV35S::EYFP* or *pEntryA-pCaMV35S::PIP5K1-EYFP*. **E**, Protoplasts transformed with *pEntryA-pCaMV35S::EYFP* or *pEntryA-pCaMV35S::PIP5K2-EYFP*. **F**, Protoplasts transformed with *pEntryA-pCaMV35S::EYFP* or *pEntryD-pCaMV35S::PIP5K6-EYFP*. Transcript levels were normalized to both the reference gene *UBC10* and the transcript levels of the respective mock-treated sample (-). Mock data are based on data in A – C. Relative transcript levels are shown as boxplots; dots show outliers. Significant differences were analyzed by one-way ANOVA with a subsequent Tukey's post-hoc test ($P < 0.05$) and indicated by letters a – c.

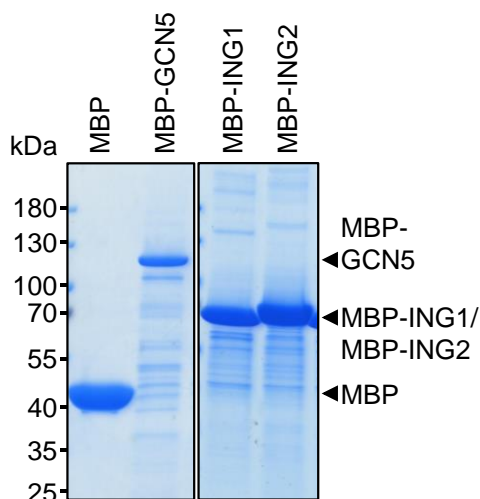


Fig. 6.10: Enriched proteins used for lipid overlay assays. Coomassie-stained SDS-PAGE of enriched MBP, MBP-GCN5 and MBP-ING1/MBP-ING2 protein fractions used in lipid overlay assays. Enriched protein fractions were proven for protein content on an SDS-PAGE to equalize used protein amounts. 50 to 100 μg of enriched proteins (20 μl of MBP, 120 μl of MBP-GCN5, 100 μl of MBP-ING1 or 150 μl MBP-ING2) were utilized for lipid overlay assays shown in Fig. 2.9 B. PageRuler™ Prestained Protein Ladder was used as a molecular size marker. Expected molecular size of full-length proteins, MBP, 42.5 kDa; MBP-GCN5, 105.6 kDa; MBP-ING1, 68.6 kDa; MBP-ING2, 72.6 kDa.

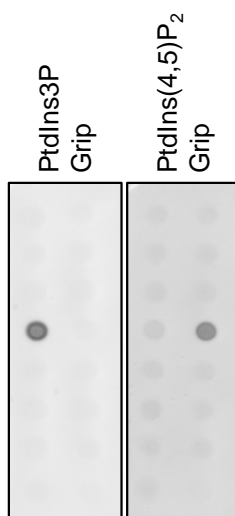


Fig. 6.11: Lipid binding studies of PIP grips. Lipid overlay assays were controlled for functionality of experimental setup with purchased PIP grips with known lipid binding capability. Lipid overlay assays with 2.5 μg PtdIns3P Grip (#G-0302) and PtdIns(4,5)P₂ Grip (#G-4501) (both Echelon Biosciences Inc., MoBiTec, Göttingen, Germany) and PIP strips shown in Fig. 2.9 A. Interactions were visualized by using a primary antiserum against GST and a secondary antiserum with an AP conjugate. AP detection was performed. The experiment was conducted once.

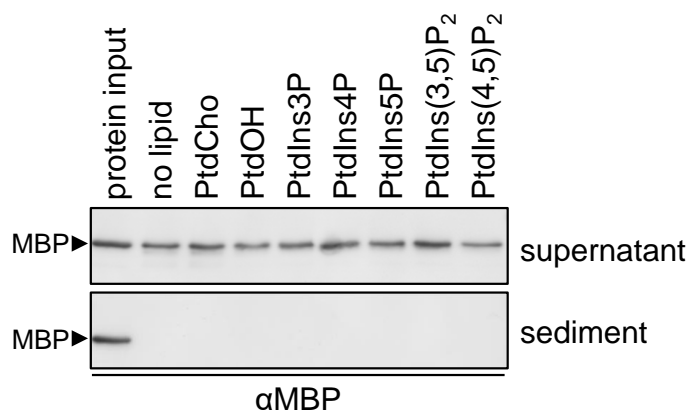


Fig. 6.12: Liposome sedimentation assay of MBP. Liposome sedimentation assay was performed with liposomes prepared with PtdCho alone (control) or with a mixture of PtdCho and either PtdIns3P, PtdIns4P, PtdIns5P, PtdIns(3,5)P₂, PtdIns(4,5)P₂ or PtdOH. No lipid, control sample without liposomes. Supernatant, contained unbound protein. Sediment, protein that had bound to respective liposomes. Proteins were separated on an SDS-PAGE and detected by immunoblots with the use of the specific antibody against MBP and a secondary antibody conjugated to AP. AP detection was performed. PageRuler™ Prestained Protein Ladder was used as a molecular size marker. Expected molecular size of full-length protein, MBP, 42.5 kDa. Experiments were performed twice with similar results.

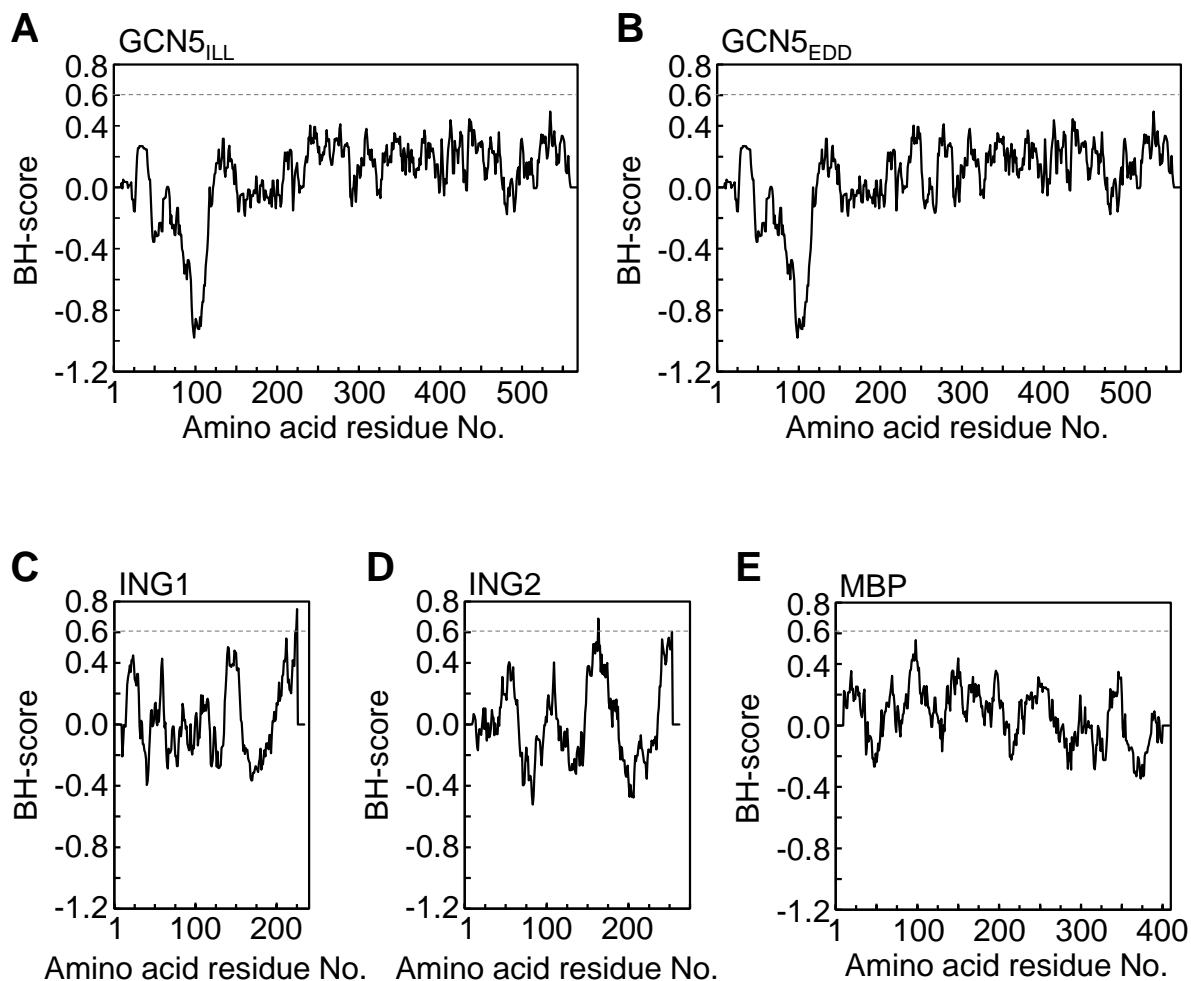


Fig. 6.13: BH-search analyses of GCN5_{ILL} and GCN5_{EDD}, ING1, ING2 and MBP. BH-searches of **A**, GCN5_{ILL}. **B**, GCN5_{EDD}. **C**, ING1. **D**, ING2. **E**, MBP. BH-searches were conducted with the online tool according to Brzeska and coworkers (Brzeska et al., 2010). Per amino acid a value is calculated that includes the amino acid surrounding of the single amino acid. Values higher than the threshold 0.6 indicate a basic hydrophobic (BH) stretch which putatively binds phospholipids.

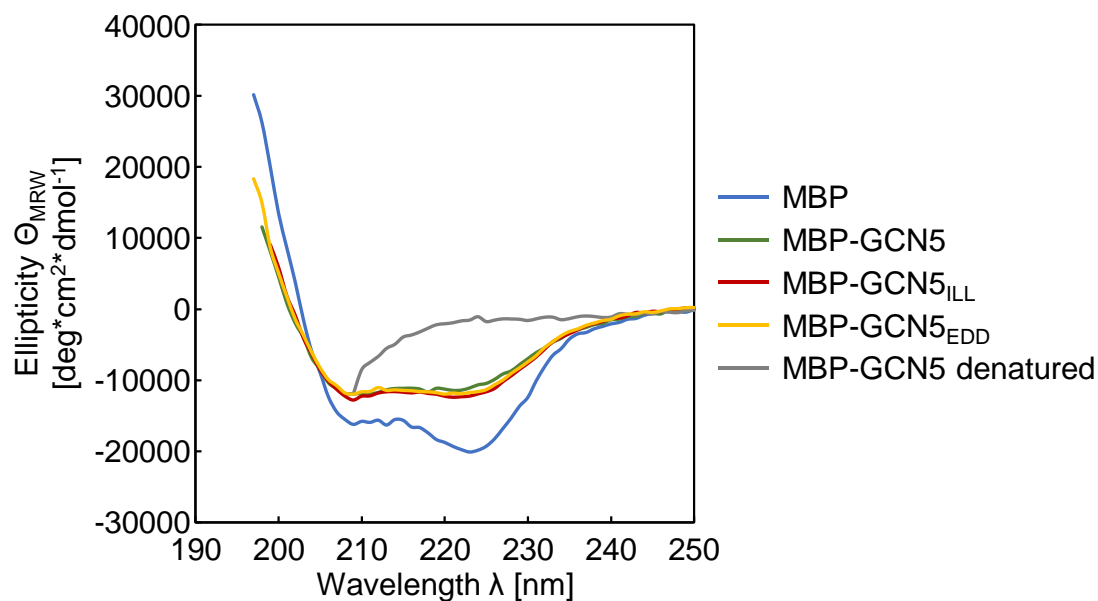


Fig. 6.14: CD spectroscopy of MBP-GCN5, MBP-GCN5_{ILL}, MBP-GCN5_{EDD} and MBP. CD spectra were recorded at 20°C. Each sample was measured 64 times with 50 nm/min in an interval of 1 nm. Ellipticity Θ_{MRW} was calculated for the wavelength range from around 200 to 250 nm. As control, MBP-GCN5 was denatured for 6.5 h in 4.5 M guanidinium chloride. Blue, MBP; green, MBP-GCN5; red, MBP-GCN5_{ILL}; yellow, MBP-GCN5_{EDD}; grey, MBP-GCN5 denatured. CD spectra are representative for $n = 4$ (MBP, MBP-GCN5_{ILL}, MBP-GCN5_{EDD}), $n = 7$ (MBP-GCN5), $n = 2$ (MBP-GCN5 denatured).

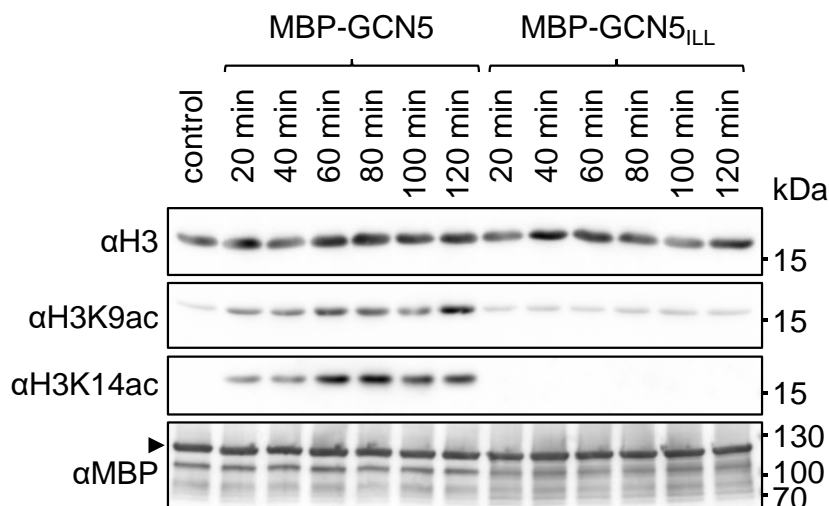


Fig. 6.15: GCN5 and GCN5_{ILL} acetylation activity *in vitro* over time. *In vitro* acetylation of histone H3 at H3K9 and H3K14 by GCN5 and GCN5_{ILL} over time. The acetylation reactions were stopped after 20, 40, 60, 80, 100 and 120 min, respectively. Control sample with GCN5 lacking acetyl-CoA was stopped after 60 min. The formation of H3K9ac and H3K14ac was detected with specific antibodies. Expected molecular sizes of full-length proteins, histone H3, H3K9ac, H3K14ac, 15.3 kDa; MBP-GCN5, 105.6 kDa. PageRuler™ Prestained Protein Ladder was used as a molecular size marker. Chemiluminescent signals were recorded using an ECL detection system. The arrow indicates MBP-GCN5/MBP-GCN5_{ILL}. The test was performed once.

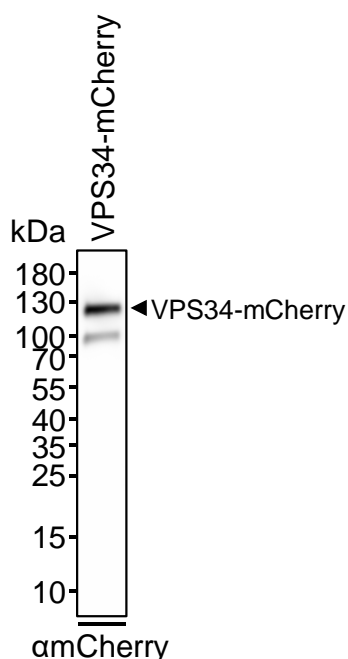


Fig. 6.16: Immunodetection of mesophyll protoplasts overexpressing mCherry-tagged VPS34. Arabidopsis mesophyll protoplasts used for examination of subcellular localization of mCherry-tagged VPS34 were tested for transient protein expression. Transiently transformed protoplasts were applied to an SDS-PAGE and were blotted on a nitrocellulose membrane. The mCherry-tagged proteins were detected with specific antibodies. Chemiluminescent signals were recorded using an ECL detection system. PageRuler™ Prestained Protein Ladder was used as a molecular size marker. Expected molecular size of full-length protein, VPS34-mCherry, 120.0 kDa. The experiment was conducted seven times with similar results.

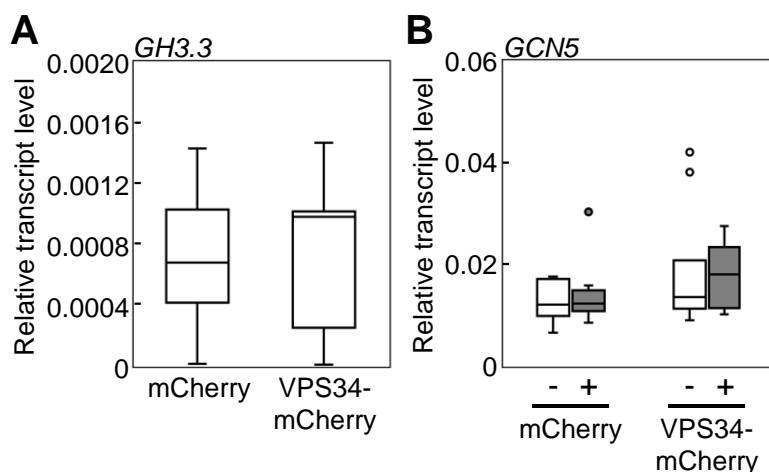


Fig. 6.17: Basal *GH3.3* transcript levels and endogenous *GCN5* transcript levels in protoplasts upon overexpression of *VPS34*. Relative basal transcript levels of *GH3.3* and relative transcript levels of *GCN5* in mesophyll protoplasts upon overexpressing either mCherry or VPS34-mCherry and with mock (-) and with 0.25 μ M NAA (+) treatment overnight. Data represent 6 – 8 biological replicates (transformations) from two protoplast preparations. **A**, Basal *GH3.3* transcript levels in protoplasts transformed with *pEntryD-pCaMV35S::mCherry* or *pEntryA-pCaMV35S::VPS34-mCherry*. **B**, Endogenous *GCN5* transcript levels in protoplasts transformed with *pEntryD-pCaMV35S::mCherry* or *pEntryA-pCaMV35S::VPS34-mCherry*. Transcript levels were normalized to the reference gene *UBC10*. Relative transcript levels are shown as boxplots; dots show outliers. Significant differences were analyzed by Student's T-test (A) or by one-way ANOVA with a subsequent Tukey's post-hoc test ($P < 0.05$) (B).

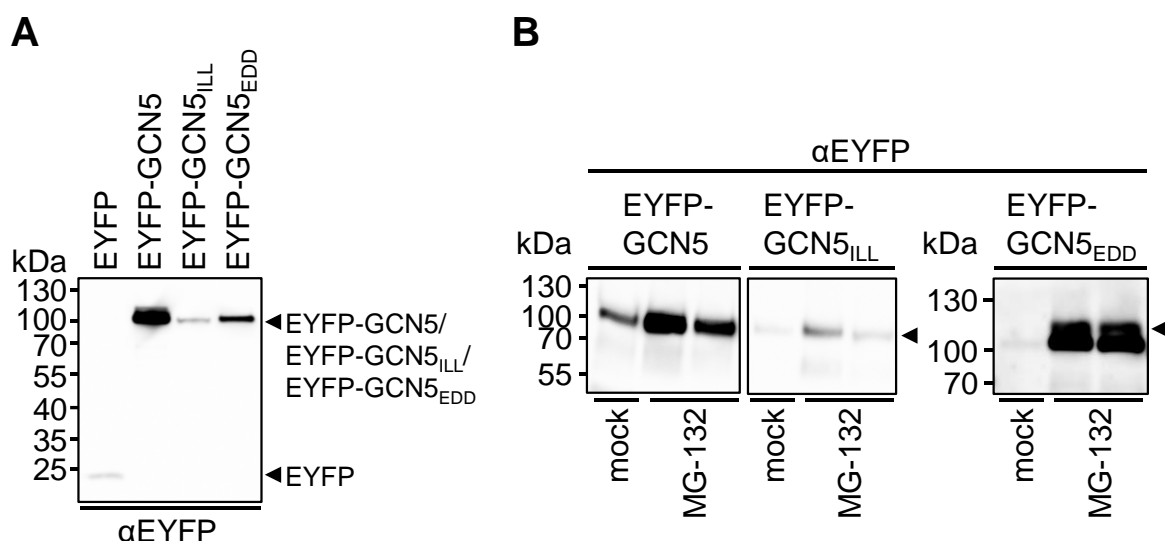


Fig. 6.18: Immunodetection of mesophyll protoplasts overexpressing EYFP-tagged GCN5 amino acid substitution variants. Arabidopsis mesophyll protoplasts used for examination of subcellular localization of EYFP-tagged GCN5 variants were tested for transient protein expression. Transiently transformed protoplasts were applied to an SDS-PAGE and were blotted on a nitrocellulose membrane. The EYFP-tagged proteins were detected with specific antibodies. Chemiluminescent signals were recorded using an ECL detection system. PageRuler™ Prestained Protein Ladder was used as a molecular size marker. Expected molecular sizes of full-length proteins, EYFP, 27.0 kDa; EYFP-GCN5/EYFP-GCN5_{ILL}/EYFP-GCN5_{EDD}, 90.1 kDa. **A**, Protoplasts overexpressing EYFP, EYFP-GCN5, EYFP-GCN5_{ILL} or EYFP-GCN5_{EDD}. The experiment was conducted five times with similar results. **B**, Protoplasts overexpressing EYFP-GCN5, EYFP-GCN5_{ILL} or EYFP-GCN5_{EDD} were treated for 6 h with 50 μ M proteasome inhibitor MG-132 according to Grimmer and coworkers (Grimmer et al., 2020). Mock, DMSO solvent as control; MG-132, proteasome inhibitor solved in DMSO. The experiment was conducted twice with similar results. The arrow indicates EYFP-GCN5/EYFP-GCN5_{ILL}/EYFP-GCN5_{EDD}.

6.2. Additional information to Material and Methods

6.2.1. Specification of equipment and devices

Tab. 6.1: Equipment and devices.

Equipment/device	Supplier
Plant Chamber Adaptis A1000	Conviron, Winnipeg, MB, Canada
Plant Chamber PERCIVAL AR-66/L3	Percival Scientific, Perry, IA, USA
Eppendorf centrifuges 5424, 5417 R, 5424 R and 5810 R	Eppendorf AG, Hamburg, Germany
Agarose gel chambers, MINI and MIDI with gel slides	cti, Idstein, Germany
Gel Detection System Gel iX Imager	INTAS, Göttingen Germany
Gel Detection System Quantum ST4	Vilber Lourmat Deutschland GmbH, Eberhardzell, Germany
TADVANCED or TProfessional Thermocycler	Biometra, Göttingen, Germany
Rotor Gene Q 2-Plex	Qiagen, Hilden, Germany
Ultrospec 2100 pro UV/Vis Spectrometer	Biochrom, Cambridge, United Kingdom
Ultrospec 3000 UV/Vis Spectrometer	Pharmacia Biotech AG, Dübendorf, Germany
Multiple Gel Caster (SE 200 series)	Hoefer Scientific Instruments, Holliston, MA, USA
SE250 Electrophoresis Chamber	Hoefer Pharmacia Biotech Inc., San Francisco, CA, USA
Mini-PROTEAN® Tetra System Blotting Chamber	BioRad Laboratories GmbH, Munich, Germany
Fusion Solo S	Vilber Lourmat Deutschland GmbH, Eberhardzell, Germany
Ultra-Turrax® T 25 basic	IKA®-Werke GmbH, Staufen, Germany
Branson B12 Ultrasonics Sonifier	Branson, Emerson Electric, Dietzenbach-Steinberg, Germany
Vibra-Cell™ 72442	Bioblock Scientific, Sonics & Materials Inc., Newtown, CT, USA
J-810 Spectropolarimeter	JASCO Deutschland GmbH, Pfungstadt, Germany
Peltier Element PTC-423S	JASCO Deutschland GmbH, Pfungstadt, Germany
Water Recirculator Thermo Haake® WKL 26	JASCO Deutschland GmbH, Pfungstadt, Germany

Equipment/device	Supplier
Precision Cell (made of Quartz SUPRASIL [®] , Type No. 105.201-QS, Light Path 10 mm)	Hellma GmbH, & Co. KG, Müllheim, Germany
Precision Cell (made of Quartz SUPRASIL [®] , Type No. 106-QS, Light Path 0.2 mm, transmission matched)	Hellma GmbH, & Co. KG, Müllheim, Germany
Laser Scanning Microscope LSM 880 with HXP 120V metal halide fluorescence light source	Carl Zeiss, Jena, Germany
Phosphorimager Screen BAS-MP 2040s	Fujifilm, Düsseldorf, Germany
Phosphorimager BAS-1500	Fujifilm, Düsseldorf, Germany

6.2.2. Specification of chemicals

Tab. 6.2: Chemicals used in this study.

Chemical	Supplier
Acetyl coenzyme A sodium salt (Acetyl-CoA) (#A2056)	Sigma-Aldrich, Munich, Germany
Albumin Fraction V (BSA)	Carl Roth, Karlsruhe, Germany
3-Amino-1,2,4-triazole (3-AT)	Sigma-Aldrich, Munich, Germany
Amylose Resin	New England Biolabs Inc., Frankfurt, Germany
Biozym LE Agarose	Biozym Scientific GmbH, Hessisch Oldendorf, Germany
Blotting-Grade Blocker Nonfat dry milk	BioRad Laboratories GmbH, Munich, Germany
Bradford reagent, 5x	SERVA Electrophoresis GmbH, Heidelberg, Germany
5-Bromo-4-chloro-3-indolyl phosphate disodium salt (X-phosphate)	Carl Roth, Karlsruhe, Germany
1,4-Dithiothreitol (DTT)	Carl Roth, Karlsruhe, Germany
Pierce [™] Glutathione Agarose	Thermo Fisher Scientific, Schwerte, Germany
L-Glutathione reduced	Sigma-Aldrich, Munich, Germany
Hexylene glycol	Sigma-Aldrich, Munich, Germany
Isopropyl β -D-1-thiogalactopyranoside (IPTG), dioxane free	Thermo Fisher Scientific, Schwerte, Germany

Chemical	Supplier
2-Mercaptoethanol	Carl Roth, Karlsruhe, Germany
Micro-Agar	Duchefa, Haarlem, Netherlands
Murashige & Skoog-Medium, incl. modified vitamins	Duchefa, Haarlem, Netherlands
1-Naphthaleneacetic acid (NAA) (#N0640)	Sigma-Aldrich, Munich, Germany
p-Nitrotetrazolium blue chloride (NBT)	Carl Roth, Karlsruhe, Germany
Percoll™	GE Healthcare GmbH, Solingen, Germany
Phenol solution, saturated with 0.1 M citrate buffer, pH 4.3, (#P4682)	Sigma-Aldrich, Munich, Germany
Poly(ethylene glycol), average Mn 4,000 platelets (PEG)	Sigma-Aldrich, Munich, Germany
Proteasome Inhibitor MG-132 (#33766)	SERVA Electrophoresis GmbH, Heidelberg, Germany
Quick Coomassie® Stain	SERVA Electrophoresis GmbH, Heidelberg, Germany
Rotiphorese® Gel 30 (37,5:1)	Carl Roth, Karlsruhe, Germany
SIGMAFAST™ Protease Inhibitor Cocktail, EDTA-Free	Sigma-Aldrich, Munich, Germany
Skim milk powder for blotting	SERVA Electrophoresis GmbH, Heidelberg, Germany
N,N,N',N'-Tetramethyl-ethylenediamine (TEMED)	Sigma-Aldrich, Munich, Germany
yeast nitrogen base w/o amino acids and ammonium sulfate	Difco, Detroit, MI, USA

Tab. 6.3: Used Phospholipids.

All phospholipids were purchased from Avanti Polar Lipids Inc. (Merck, Darmstadt, Germany) and were dissolved in chloroform.

Phospholipid	Stock solution	Product No.
18:1 PtdIns3P	1 mg/ml	850150P
18:1 PtdIns4P	1 mg/ml	850151P
18:1 PtdIns5P	1 mg/ml	850152P
18:1 PtdIns(3,5)P ₂	1 mg/ml	850154P
18:1 PtdIns(4,5)P ₂	1 mg/ml	850155P
18:1 PtdOH	10 mg/ml	840875P
18:1 PtdCho	10 mg/ml	850375P / 850375C
18:1 PtdEtn	10 mg/ml	850725P
18:1 PtdSer	10 mg/ml	840035P

6.2.3. Used consumables and kits**Tab. 6.4: Consumables and kits.**

Consumable	Supplier
Amersham Protran 0,45 NC (nitrocellulose membrane)	GE Healthcare GmbH, Solingen, Germany
Biosphere [®] Filter Tip (10, 100, 1000 µl)	Sarstedt, Nürnbrecht, Germany
Cellstar [®] Cell Culture Tube (12 ml, round bottom)	Greiner Bio-One GmbH, Frickenhausen, Germany
Cellview [™] Cell Culture Dish (35/10 mm, glass bottom)	Greiner Bio-One GmbH, Frickenhausen, Germany
EASYstrainer [™] (100 µm, sterile)	Greiner Bio-One GmbH, Frickenhausen, Germany
Filter paper	Whatman (GE Healthcare), Maidstone, United Kingdom
Filter Supports (10 mm)	Avanti Polar Lipids Inc., Merck, Darmstadt, Germany
Filtropur S 0.45 (filter for syringes)	Sarstedt, Nürnbrecht, Germany
Micro Bio-Spin [™] Columns (0.8 ml)	BioRad Laboratories GmbH, Munich, Germany
Nucleopore Track-Etch Membrane (polycarbonate membrane, pore size 0.2 µm)	Whatman (GE Healthcare), Maidstone, United Kingdom

Consumable	Supplier
PCR 0.1 ml 4-Tube & 4-Cap Strips (for Qiagen/Corbett Rotor-Gene (TM))	Biozym Scientific GmbH, Hessisch Oldendorf, Germany
Pierce™ Centrifuge Columns, 0.8 ml, 2 ml, 5 ml	Thermo Fisher Scientific, Schwerte, Germany
PIP Strips (#P-6001)	Echelon Biosciences Inc., MoBiTec, Göttingen, Germany
Protein LoBind Tube 2.0 mL	Eppendorf AG, Hamburg, Germany
SERVAge™ TG PRIME™ 4 – 20 % (precast gels with 10, 12 or 15 sample wells)	SERVA Electrophoresis GmbH, Heidelberg, Germany
Whatman paper (550 g/m ²)	A. Hartenstein GmbH, Würzburg, Germany
Kit	Supplier
CompactPrep Plasmid Midi Kit	Qiagen, Hilden, Germany
DUALmembrane Kit 3	Dualsystems Biotech AG, Zurich, Switzerland
GeneJET™ Plasmid Miniprep Kit	Thermo Fisher Scientific, Schwerte, Germany
GeneJET™ Gel Extraction Kit	Thermo Fisher Scientific, Schwerte, Germany
Histone Extraction Kit (#ab113476)	Abcam, Cambridge, United Kingdom
Luna® Universal qPCR Master Mix (#M3003)	New England Biolabs Inc., Frankfurt, Germany
RevertAid H Minus First Strand cDNA Synthesis Kit (#K1632)	Thermo Fisher Scientific, Schwerte, Germany
SuperSignal™ West Femto Maximum Sensitivity Substrate (#34095)	Thermo Fisher Scientific, Schwerte, Germany

6.2.4. Used enzymes, proteins, peptides and molecular size markers

Tab. 6.5: Enzymes, proteins, peptides and molecular size markers.

Enzyme	Supplier
Cellulase "Onozuka R-10" from <i>Trichoderma viride</i> ca. 1 U/mg	SERVA Electrophoresis GmbH, Heidelberg, Germany
Lysozyme from chicken egg white, min. 100 000 units/mg, cryst.	SERVA Electrophoresis GmbH, Heidelberg, Germany
Maceroenzyme R-10 from <i>Rhizopus sp.</i> lyophile.	SERVA Electrophoresis GmbH, Heidelberg, Germany
Phusion® High Fidelity DNA-Polymerase	New England Biolabs Inc., Frankfurt, Germany
TAQ-DNA-Polymerase	peqlab, VWR International GmbH, Darmstadt, Germany
T4-DNA-Ligase, 5 Weiss Units/µl	New England Biolabs Inc., Frankfurt, Germany
Protein/peptide	Supplier
Recombinant human Histone H3 protein HsH3.1 (Active) (#ab198757)	Abcam, Cambridge, United Kingdom
Histone H3 from calf thymus (#11034758001)	Roche Diagnostics GmbH, Mannheim, Germany
Acetyl-Histone H3 (Lys9) Peptide (#12-358)	Sigma-Aldrich, Munich, Germany
Acetyl-Histone H3 (Lys14) Peptide (#12-359)	Sigma-Aldrich, Munich, Germany
Acetyl-Histone H3 (Lys9/14) Peptide (#12-360)	Sigma-Aldrich, Munich, Germany
Human Histone H3 (di methyl K4) peptide (#ab7768)	Abcam, Cambridge, United Kingdom
Human Histone H3 (tri methyl K4) peptide (#ab1342)	Abcam, Cambridge, United Kingdom
PtdIns3P Grip (#G-0302)	Echelon Biosciences Inc., MoBiTec, Göttingen, Germany
PtdIns(4,5)P ₂ Grip (#G-4501)	Echelon Biosciences Inc., MoBiTec, Göttingen, Germany
Molecular size marker	Supplier
GeneRuler™ 100 bp DNA Ladder	Thermo Fisher Scientific, Schwerte, Germany
GeneRuler™ 1 kb DNA Ladder	Thermo Fisher Scientific, Schwerte, Germany

Molecular size marker	Supplier
PageRuler™ Prestained Protein Ladder, 10 to 180 kDa	Thermo Fisher Scientific, Schwerte, Germany
PageRuler™ Unstained Protein Ladder, 10 to 200 kDa	Thermo Fisher Scientific, Schwerte, Germany

6.2.5. Oligonucleotides used in this thesis

Tab. 6.6: Oligonucleotides used for genotyping.

Plant line	Gene / cDNA	Oligonucleotides for genotyping 5´- 3´
<i>pip5k1 pip5k2</i>	<i>PIP5K1</i>	SALK-146728-PIP5K1-for ACTAAAGGGCAATAATCCTTCCACC
		SALK-146728-PIP5K1-rev GCAAATTCTCATGGCCAAGTGGA
	<i>pip5k1</i>	LBa1-SALK-for TGGTTCACGTAGTGGGCCATCG
		SALK-146728-PIP5K1-rev GCAAATTCTCATGGCCAAGTGGA
<i>PIP5K2</i>	<i>PIP5K2</i>	SALK-012487-PIP5K2-for CAGGTTTGATACAATGCACACCAT
		SALK-012487-PIP5K2-rev TGGGAGTCTGATGGAGAAGCTG
	<i>pip5k2</i>	LBa1-SALK-for TGGTTCACGTAGTGGGCCATCG
		SALK-012487-PIP5K2-rev TGGGAGTCTGATGGAGAAGCTG
<i>pCaMV35S::PIP5K2- EYFP</i>	<i>PIP5K2-EYFP</i>	gPIP5K2-for TTAGCTGGCAGGAAACCATTG gVYFP-rev CTTGCCGGTGGTGCAGATGAACTTCAG

Tab. 6.7: Oligonucleotides for qPCRs.

Target gene	Description of oligonucleotides	Oligonucleotides 5' - 3'
<i>UBC10</i> (AT5G53300)	qUBC10-for qUBC10-rev	ACATCATGTAGCGCAGGTCC CCGGAGGGAAATGGATGGTT
<i>PIP5K1</i> (AT1G21980)	qPIP5K1-for qPIP5K1-rev	TAGCTGGCAGGAAACCATCG TGGATAACTGGCTCCTCCTGA
<i>PIP5K2</i> (AT1G77740)	qPIP5K2-for qPIP5K2-rev	CGGTGAGGCTAAGAAACCTGGAG CTTGTCCAGAACTTTTCACTTGGG
<i>PIP5K6</i> (AT3G07960)	qPIP5K6-for qPIP5K6-rev	ATTCTGCAGGCAAGTGGACA TGAATTTCCGGTAGGGGTTCCG
<i>VPS34</i> (AT1G60490)	qVPS34-for qVPS34-rev	GGCGGAGCAGAAAGCCAATA TCGGGAATAGTTGAACCCGC
<i>GCN5</i> (AT3G54610)	qGCN5-for qGCN5-rev	GTGGCTTAAGGGAAGCTGGT GGACATCGCGAGAATCCACT
<i>GH3.3</i> (AT2G23170)	qGH3.3-for qGH3.3-rev (Weiste and Dröge-Laser, 2014)	CATCACAGAGTTCCTCACAAGC GTCGGTCCATGTCTTCATCA
<i>IAA2</i> (AT3G23030)	qIAA2-for qIAA2-rev	TCTACACCTCCTACCAAAACTCAA CTTTGAGAAGCTCGGGGTAGT
<i>IAA5</i> (AT1G15580)	qIAA5-for qIAA5-rev	TCCGCTCTGCAAATTCTGTTC CACGATCCAAGGAACATTTCCCA
<i>IAA19</i> (AT3G15540)	qIAA19-for qIAA19-rev	GGTGATGTACCTTGGGGGATG CCCGGTAGCATCCGATCTTT
<i>EYFP</i>	qEYFP-for qEYFP-rev	CTGAAGTTCATCTGCACCAC GTCGTGCTGCTTCATGTGGTC
<i>mCherry</i>	qmCherry-for qmCherry-rev	CGAGATCAAGCAGAGGCTGA TTCCACGATGGTGTAGTCCT

Tab. 6.8: Oligonucleotides used for cloning.

Vector	cDNA	Oligonucleotides for cloning (5' - 3')
<i>pGEX-6P-1</i>	<i>GCN5</i>	GCN5-Sall-for ATGCGTCGACGCATGGACTCTCACTCTTCCCA
		GCN5-NotI-rev ATGCGCGCCGCCTATTGAGATTTAGCACCAG
	<i>ING1</i>	ING1-Sall-for ATGCGTCGACGCATGTCATTCGCCGAGGAATT
		ING1-NotI-rev ATGCGCGCCGCCTCATCGACCTTCTCTGCTCT
	<i>ING2</i>	ING2-Sall-for ATGCGTCGACGCATGGCTATTGCACGAACTGG
		ING2-NotI-rev ATGCGCGCCGCCTTAGTGTGACTGTGGGAGGA
<i>pMAL-c5G</i>	<i>GCN5</i>	GCN5-NotI-for ATGCGCGCCGCATGGACTCTCACTCTTCCCA
		GCN5-Sall-rev ATGCGTCGACCTATTGAGATTTAGCACCAG
	<i>GCN5₂₁₂₋₃₇₅</i>	GCN5-212-NotI-for ATGCGCGCCGCATGGAGCAAGCAGGACGACT
		GCN5-375-Sall-rev ATGCGTCGACCTATGGCAGCTTTGGATCAA
	<i>GCN5₂₈₄₋₃₇₅</i>	GCN5-284-NotI-for ATGCGCGCCGCATGAGTCAGAAGTTTGGGGA
		GCN5-375-Sall-rev ATGCGTCGACCTATGGCAGCTTTGGATCAA
<i>GCN5_{ILL}</i>		GCN5-NotI-for ATGCGCGCCGCATGGACTCTCACTCTTCCCA
		GCN5-Sall-rev ATGCGTCGACCTATTGAGATTTAGCACCAG
		for introduction of mutation:
		GCN5-ILL-for TTCTGATGGATATTCTTCATCTTTCTGTTATGGT
		GCN5-ILL-rev TACCATAACAGAAAGATGAAGAATATCCATCAGAAG
		GCN5-for ATGGACTCTCACTCTTCCCA
	GCN5-rev CTATTGAGATTTAGCACCAGATT	

Vector	cDNA	Oligonucleotides for cloning (5' - 3')
<i>pMAL-c5G</i>	<i>GCN5^{EDD}</i>	GCN5-NotI-for ATGCGCGGCCGCATGGACTCTCACTCTTCCCA GCN5-Sall-rev ATGCGTCGACCTATTGAGATTTAGCACCAG for introduction of mutation: GCN5-EDD-for TCTGATGGATGAAGATCATGATTCTGTTAT GCN5-EDD-rev ATAACAGAATCATGATCTTCATCCATCAGA GCN5-for ATGGACTCTCACTCTTCCCA GCN5-rev CTATTGAGATTTAGCACCAGATT
	<i>ADA2B</i>	ADA2B-NotI-for ATGCGCGGCCGCATGGGTCGCTCTCGAGGG ADA2B-Sall-rev ATGCGTCGACTTAAAGTTGAGCAATACC
	<i>VPS34</i>	VPS34-NotI-for ATGCGCGGCCGCATGGGTGCGAACGAGTTT VPS34-Sall-rev ATGCGTCGACTCAACGCCAGTATTGAGC
	<i>VPS34¹⁻²¹⁰</i>	VPS34-NotI-for ATGCGCGGCCGCATGGGTGCGAACGAGTTT VPS34-210-Sall-rev ATGCGTCGACTCAAAACAGATGTGAGCTTCC
	<i>VPS34²¹⁰⁻⁸¹⁴</i>	VPS34-210-NotI-for ATGCGCGGCCGCATGTTTGTGGTCATTGAT VPS34-Sall-rev ATGCGTCGACTCAACGCCAGTATTGAGC
<i>pBT3-C-OST4</i>	<i>PIP5K6</i>	OST4-PIP5K6-for ATGCGGCCATTACGGCCCATGTCGGTAGCACACGCAGA OST4-PIP5K6-rev ATGCGGCCGAGGCGGCCGCAGCGTCTTCAACGAAGACCC
	<i>PIP5K9</i>	OST4-PIP5K9-for ATGCGGCCATTACGGCCAATGTCTGGCCTTGACGTACGA OST4-PIP5K9-rev ATGCGGCCGAGGCGGCCCTTGATTTGTTGTTCTGTGAAAT
	<i>GCN5</i>	OST4-GCN5-for ATGCGGCCATTACGGCCCATGGACTCTCACTCTTCCCA OST4-GCN5-rev ATGCGGCCGAGGCGGCCGCTTGAGATTTAGCACCAGATT

Vector	cDNA	Oligonucleotides for cloning (5' - 3')
<i>pBT3-C-OST4</i>	<i>VPS34</i>	OST4-VPS34-for ATGCGGCCATTACGGCCCATGGGTGCGAACGAGTTT
		OST4-VPS34-rev ATGCGGCCGAGGCGGCCGCACGCCAGTATTGAGC
	<i>VPS34₁₋₂₁₀</i>	OST4-VPS34-for ATGCGGCCATTACGGCCCATGGGTGCGAACGAGTTT
		OST4-VPS34-210-rev ATGCGGCCGAGGCGGCCGCAAACAGATGTGAGCTTCC
	<i>VPS34₂₁₀₋₈₁₄</i>	OST4-VPS34-210-for ATGCGGCCATTACGGCCAATGTTTGTGGTCATTGAT
		OST4-VPS34-rev ATGCGGCCGAGGCGGCCGCACGCCAGTATTGAGC
<i>pPR3-N</i>	<i>ADA2B</i>	ADA2B-Sfil-for ATGCGGCCATTACGGCCATGGGTGCGTCTCGAGGGAAGTT
		ADA2B-Sfil-rev ATGCGGCCGAGGCGGCCCTTAAAGTTGAGCAATACCCTT
<i>pEntryA</i>	<i>EYFP-GCN5</i>	pD-GCN5-Ascl-for ATGCGGCGCGCCATGGACTCTCACTCTTCCCA
	<i>EYFP-GCN5_{ILL}</i>	pD-GCN5-NotI-rev ATGCGGCGGCCCTATTGAGATTTAGCACCAGATT
	<i>EYFP-GCN5_{EDD}</i>	

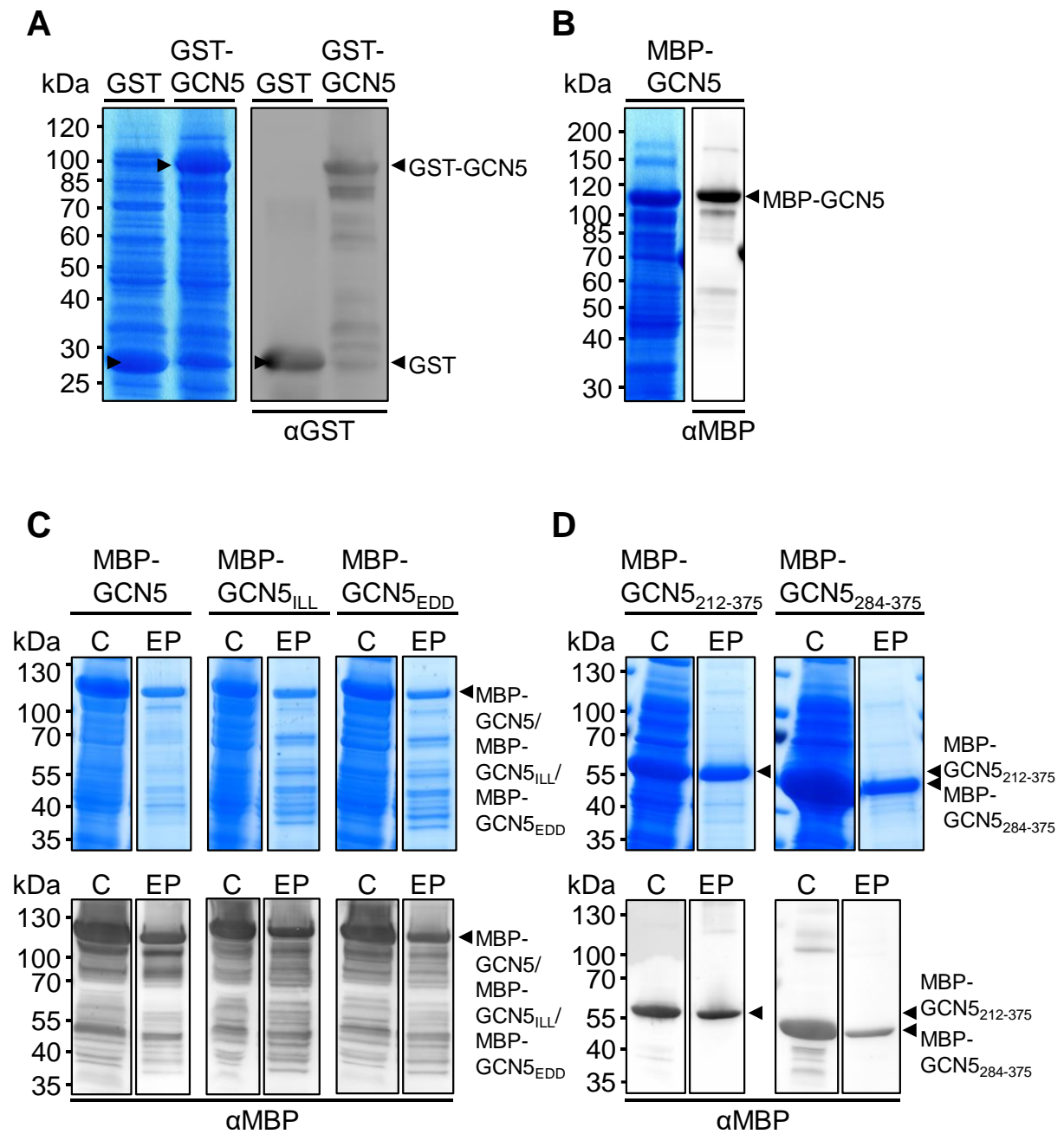
Tab. 6.9: Oligonucleotides used for sequencing.

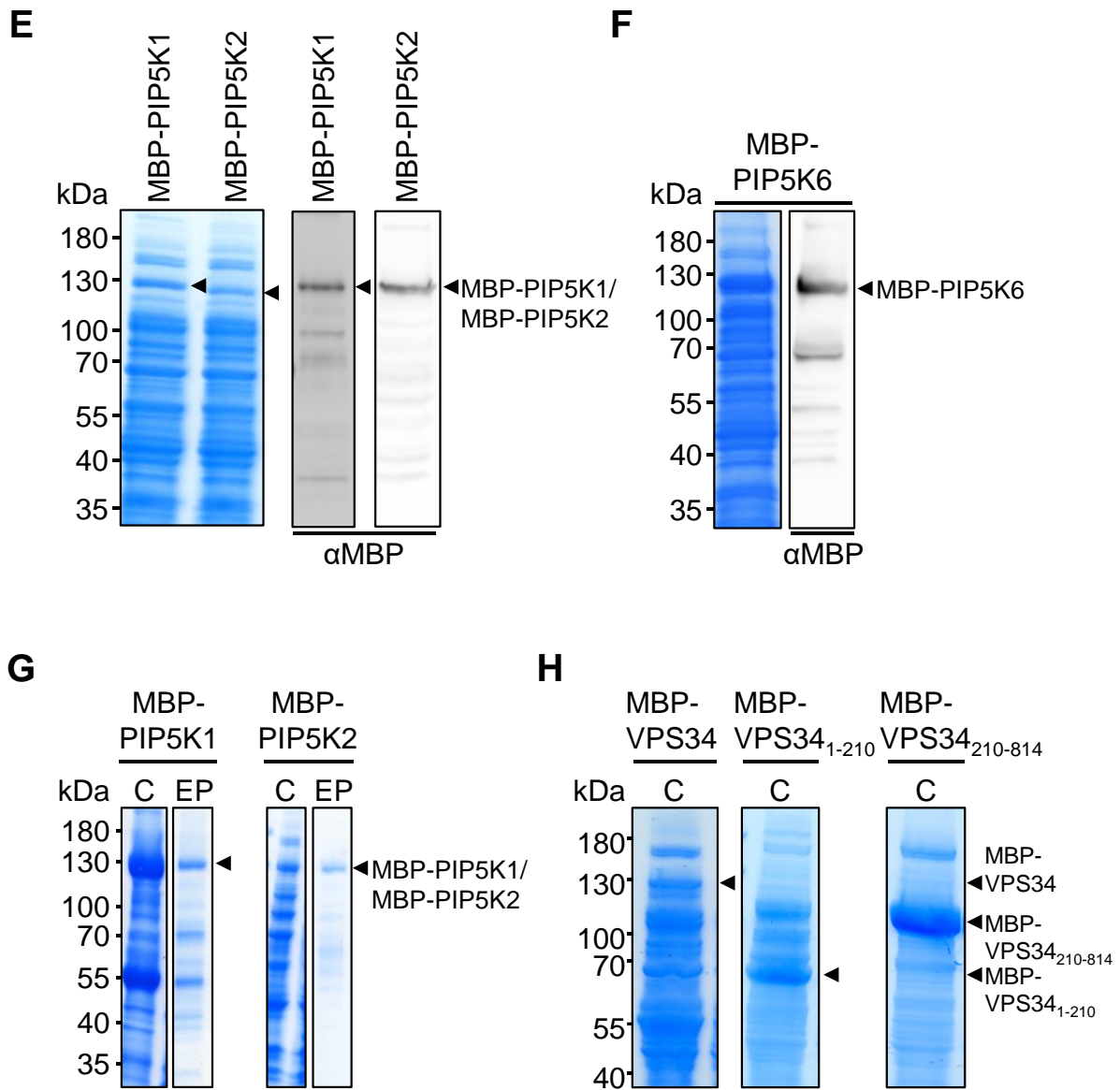
Analyzed sequence	Description of oligonucleotides	Oligonucleotides (5' - 3')
<i>pBT3-C-OST4</i>	pBT3-for	CATGATCATATGGCATGCATG
	pBT3-LexA-rev	ACACCTCTTGTTGCCTGGCCA
<i>pPR3-N</i>	pPR3N-for	ATGCAGATTTTCGTCAAGACTTT
	pPR3N-rev	ATAACTAATTACATGACT
<i>pGEX-6-P1</i>	pGEX-for	GGGCTGGCAAGCCACGTTTGGTG
	pGEX-rev	CCGGGAGCTGCATGTGTGTCAGAGG
<i>pMAL-c5G</i>	pMAL-for	ATGCCGAACATCCCGCAGAT
	pMAL-rev	TTGTCCTACTCAGGAGAGCGTT
<i>pEntryA</i> and <i>pEntryD</i>	35S-for	TATATAAGGAAGTTCATTT
	OCS-rev	TTTACAACGTGCACAACAGAA
	M13-for	CCCAGTCACGACGTTGTAAAACG
	M13-rev	AGCGGATAACAATTTACACACAGG

Analyzed sequence	Description of oligonucleotides	Oligonucleotides (5' - 3')
<i>EYFP</i>	VYFP-for	CTGAAGTTCATCTGCACCACCGGCAAG
	VYFP-rev	CTTGCCGGTGGTGCAGATGAACTTCAG
	HYFP-for	TACCAGTCCGCCCTGAGCAAAGA
	HYFP-rev	TCTTTGCTCAGGGCGGACTGGTA
<i>mCherry</i>	HmCherry-for	CTACGACGCTGAGGTCAAGAC
	HmCherry-rev	GTCTTGACCTCAGCGTCGTAG
<i>GCN5</i> and variants	GCN5-m-for	TGAAGCTTGAGAGCTCTGAT
	GCN5-m-rev	ATCAGAGCTCTCAAGCTTCA
	GCN5-m2-for	TAGAAAGATTATCAAAGT
<i>ADA2B</i>	ADA2B-m-for	AAGAGTTTGACCCTGAATAT
	ADA2b-m-rev	ATATTCAGGGTCAAACCTCTT
<i>PIP5K1</i>	PIP5K1-m1-for	AGTAATATTATGAGGAGTTT
	PIP5K1-m1-rev	AAACTCCTCATAATATACT
	PIP5K1-m2-for	AAAACGGTGAAGAAATCA
	PIP5K1-m2-rev	TGATTTCTTCACCGTTTT
	PIP5K1-m3-for	TGAAGGTA CTGGAGAAG
	PIP5K1-m4-for	CAACACCGCCGCATCAGT
	PIP5K1-m4-rev	ACTGATGCGGCGGTGTTG
<i>PIP5K2</i> and variant <i>PIP5K2 K470A</i>	PIP5K2-m-for	ATTTTGACCCAAGTGAAAA
	PIP5K2-m-rev	TTTTCACTTGGGTCAAAT
	PIP5K2-m2-for	AAGAGATATGCCAACGGAGA
	PIP5K2-m3-for	TTACTATGAAGGTACATGGC
	PIP5K2-m4-for	TATCTCCATTTGTATTGAGA
	PIP5K2-m4-rev	TCTCAATACAAATGGAGATA
	PIP5K2-m5-for	TAGTAATCTCATGAGGAATT
PIP5K2-m5-rev	AATTCCTCATGAGACTACTA	
<i>PIP5K6</i>	PIP5K6-for	ATGTCCGTAGCACACGCAGA
	PIP5K6-rev	TCAAGCGTCTTCAACGAAGA
	PIP5K6-m1-for	TTTGTACTTGT CAGAGAAT
	PIP5K6-m1-rev	ATTCTCTGACAAGTACAAA
	PIP5K6-m2-for	AAAGTTCTTATAAGGATGCT
	PIP5K6-m3-for	TGCCGTCTCAGAAGATGC
	PIP5K6-m4-for	ACCCTTCGACTTCTTCCGG

Analyzed sequence	Description of oligonucleotides	Oligonucleotides (5' - 3')
<i>PIP5K9</i>	PIP5K9-m1-for	CGTGGGATGAGACATGGAAT
	PIP5K9-m2-for	ACGGGTTTTTCGCGCACATCCA
	PIP5K9-m2-rev	ATATAATCAGCTGCATCGAT
	PIP5K9-m3-rev	TAGTTGCCTCAGTAAACCT
	PIP5K9-m4-for	ACAGCACTTAAGATCCCAAT
<i>VPS34</i> and variants	VPS34-m1-for	AGCTGGCAAGGAGCTTGGAT
	VPS34-m1-rev	ATCCAAGCTCCTTGCCAGCT
	VPS34-m2-for	GCAGGAGAATCATCACTCTT
	VPS34-m2-rev	AAGAGTGATGATTCTCCTGC
	VPS34-m3-rev	AGTATATATGTGATCACAGA
<i>ING1</i> and <i>ING2</i>	no specific oligonucleotides within the sequence necessary	

6.2.6. Cell lysates and enriched protein fractions





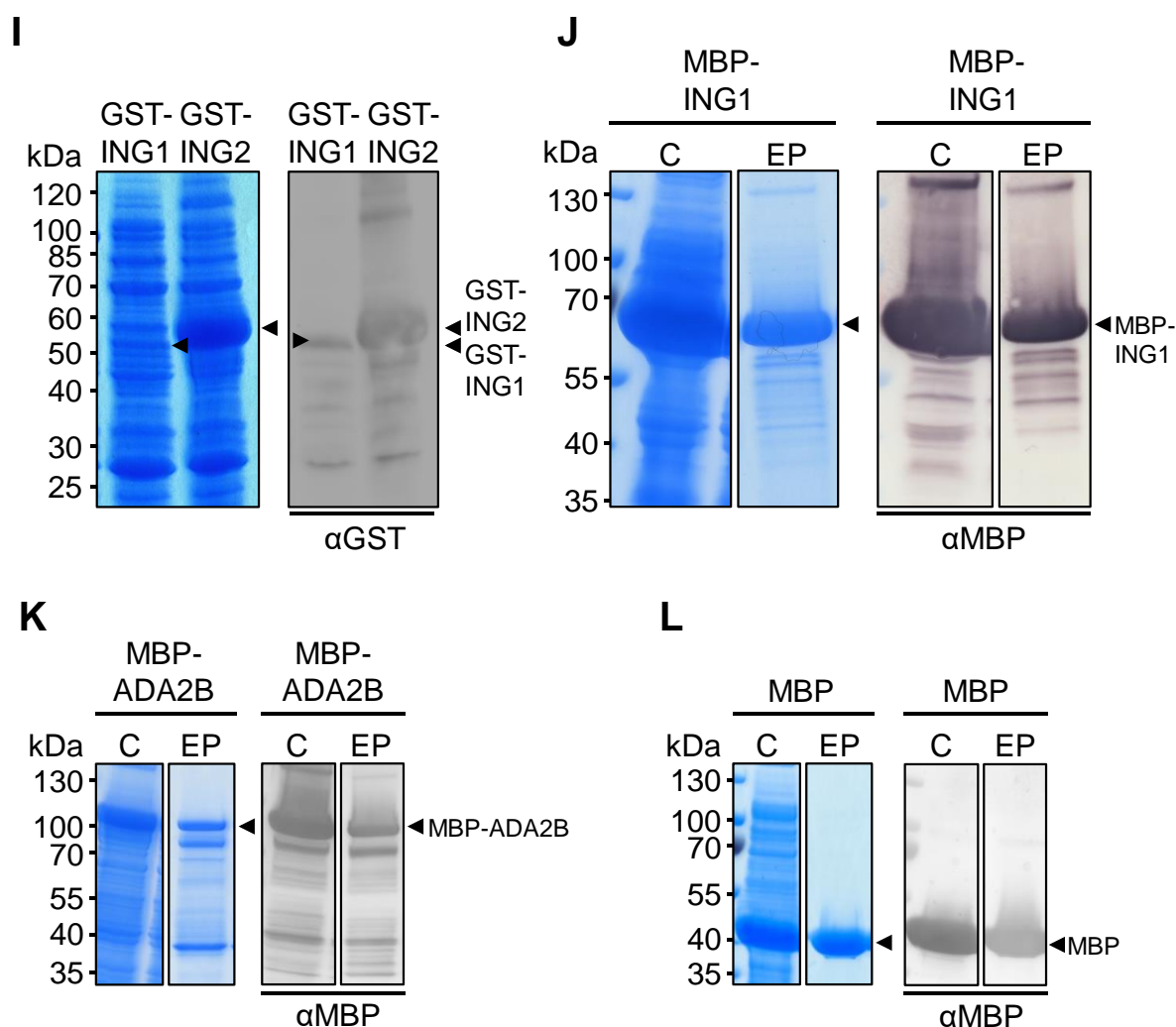


Fig. 6.19: Cell lysates and enriched protein fractions. Proteins were recombinantly expressed in *E. coli* Rosetta2. 10 μ l of protein crude extracts were applied to an SDS-PAGE and were either stained with Coomassie or transferred to a nitrocellulose membrane. Membranes were incubated with primary antisera against GST or MBP. Afterwards, a suitable secondary antibody with a HRP conjugate was applied. Immunodetections were performed via HRP detection. PageRuler™ Unstained Protein Ladder or PageRuler™ Prestained Protein Ladder was used as molecular size marker. To get purified and enriched protein, protein crude extracts of MBP-tagged proteins (C) were purified via affinity chromatography with an amylose matrix. Protein crude extracts and enriched protein fractions (EP) were applied to an SDS-PAGE and were either stained with Coomassie or transferred to a nitrocellulose membrane. Nitrocellulose membranes were incubated with a primary antiserum against MBP epitope and a secondary antibody against mouse with an AP conjugate subsequently. AP detection was performed. PageRuler™ Prestained Protein Ladder was used as molecular size marker. **A**, Protein crude extracts of GST and GST-GCN5 that were used for *in vitro* immuno pull-down assays. **B**, Protein crude extract of MBP-GCN5 that was used for *in vitro* immuno pull-down assays. **C**, Used affinity purified extracts of MBP-GCN5, MBP-GCN5_{ILL} and MBP-GCN5_{EDD} for *in vitro* acetylation assays and liposome sedimentation assays. **D**, Used affinity purified extracts of MBP-GCN5₂₁₂₋₃₇₅ and MBP-GCN5₂₈₄₋₃₇₅ for *in vitro* acetylation assays. **E**, Protein crude extracts of MBP-PIP5K1 and MBP-PIP5K2 that were used for *in vitro* immuno pull-down assays. **F**, Protein crude extract of MBP-PIP5K6 that was used for *in vitro* immuno pull-down assays. **G**, Enriched protein extracts of MBP-PIP5K1 and MBP-PIP5K2 that were used for dot-blot assays. Proteins were enriched by Lennart Schwalgun according to Dejonghe and coworkers (Dejonghe et al., 2016). **H**, Used protein crude extracts of MBP-VPS34, MBP-VPS34₁₋₂₁₀ and MBP-VPS34₂₁₀₋₈₁₄ for *in vitro* immuno pull-down assays and *in vitro* activity assays. **I**, Protein crude extracts of GST-ING1 and GST-ING2 that were used for *in vitro* immuno pull-down assays. **J**, Used

affinity purified extract of MBP-ING1 for liposome sedimentation assays. **K**, Used affinity purified extract of MBP-ADA2B for *in vitro* acetylation assays. **L**, Used affinity purified extract of MBP for liposome sedimentation assays.

Expected molecular sizes of full-length proteins, GST, 26 kDa; GST-GCN5, 89.1 kDa; MBP-GCN5, MBP-GCN5_{ILL}, MBP-GCN5_{EDD}, 105.6 kDa; MBP-GCN5₂₁₂₋₃₇₅, 61.5 kDa; MBP-GCN5₂₈₄₋₃₇₅, 53.1 kDa; MBP-PIP5K1, 128.4 kDa; MBP-PIP5K2, 128.8 kDa; MBP-PIP5K6, 123.9 kDa; GST-ING1, 52.1 kDa; GST-ING2, 56.1 kDa; MBP-ING1, 68.6 kDa; MBP-ADA2B, 98.2 kDa; MBP, 42.5 kDa; MBP-VPS34, 135.8 kDa; MBP-VPS34₁₋₂₁₀, 66.2 kDa; MBP-VPS34₂₁₀₋₈₁₄, 112.3 kDa. Proteins were individually expressed and enriched several times.

6.2.7. Composition of self-cast polyacrylamide gels

Tab. 6.10: Composition of self-cast polyacrylamide gels.

Component	Stock solution	Separation gel	Stacking gel
		10 % (w/v)	5 % (w/v)
Rotiphorese® Gel 30 (37,5:1) (Carl Roth, Karlsruhe, Germany)	30 % (w/v) with 0.8 % (w/v) bisacrylamide	10 % (w/v)	5 % (w/v)
Tris-HCl pH 8.8	1.88 M	370 mM	-
Tris-HCl pH 6.8	625 mM	-	120 mM
ddH ₂ O	-	45 % (v/v)	62 % (v/v)
SDS	10 % (w/v)	0.1 % (w/v)	0.1 % (w/v)
ammonium persulfate (APS)	10 % (w/v)	0.06 % (w/v)	0.09 % (w/v)
N,N,N',N'-tetramethyl-ethylenediamine (TEMED)	~99 % (v/v)	0.01 % (w/v)	0.01 % (w/v)

6.2.8. Primary and secondary antibodies

Tab. 6.11: Primary and secondary antibodies.

Abbreviations: **AB**: Abcam, Cambridge, United Kingdom, **ME**: Merck, Darmstadt, Germany, **NEB**: New England Biolabs Inc., Frankfurt, Germany, **SI**: Sicgen, Cantanhede, Portugal, **TF (IN)**: Invitrogen, now Thermo Fisher Scientific, Schwerte, Deutschland.

Primary antisera					
Epitope	Host	Conjugate	Application	Type	Product No., supplier
anti-GST	goat	-	1:2,000	polyclonal	#27-4577-01, ME
anti-MBP	mouse	-	1:10,000	monoclonal	#E8032S, NEB
anti-GFP	rabbit	-	1:2,000	polyclonal	#A-11122, TF (IN)
anti-mCherry	goat	-	1:2,500	polyclonal	#AB0040-200, SI
anti-H3	rabbit	-	1:5,000	polyclonal	#H0164, ME
anti-H3K9ac	rabbit	-	1:5,000	polyclonal	#ab4441, AB
anti-H3K14ac	rabbit	-	1:5,000	polyclonal	#07-353, ME
Secondary antisera					
Epitope	Host	Conjugate	Application	Type	Product No., supplier
anti-goat	rabbit	HRP	1:7,500	polyclonal	#A5420, ME
anti-goat	rabbit	AP	1:30,000	polyclonal	#A4187, ME
anti-mouse	goat	HRP	1:5,000	polyclonal	#AP130P, ME
anti-mouse	goat	AP	1:30,000	polyclonal	#A3562, ME
anti-rabbit	goat	HRP	1:7,000	polyclonal	#A6154, ME

6.2.9. Specification of software and online tools

Tab. 6.12: Used software and online tools and their applications.

Software	Application	Supplier
Chromas (version 2.6.6)	DNA sequence analysis	Technelysium Pty Ltd, South Brisbane, Australia
EndNote X9.3.3 (Bld 13966)	reference management	Clarivate Analytics, Philadelphia, PA, USA
FusionCapt Advance Solo 7 (version 17.01)	chemiluminescence detection of Western Blots	Vilber Lourmat Deutschland GmbH, Eberhardzell, Germany
ImageJ 1.51s (Fiji)	image processing and analysis	Wayne Rasband National Institutes of Health, USA (http://imagej.nih.gov/ij/), (Schindelin et al., 2012)
LinRegPCR (version 2018.0)	analysis of qPCR data	J. M. Ruijter, Department of Anatomy, Embryology & Physiology, Academic Medical Center, Amsterdam, Netherlands Based on: (Ruijter et al., 2009; Tuomi et al., 2010; Ruijter et al., 2014)
Microsoft Home and Student 2016, Microsoft Office 365 (PowerPoint, Excel, Word)	figures, data analysis, text editing	Microsoft Corporation, Redmond, WA, USA
Quantum-Capt (version 15.15)	detection of UV signals in agarose gels	Vilber Lourmat Deutschland GmbH, Eberhardzell, Germany
R for Windows (version 4.1.0) and R Studio (version 1.4.1106) with multcomp package	ANOVA	R Studio, PBC, Boston, MA, USA (Hothorn et al., 2008) for multcomp
Rotor-Gene Q Series Software (versions 2.1.0 (Build 9) and 2.3.5 (Build 1))	measurement and analysis of qPCR data	Qiagen, Hilden, Germany

Software	Application	Supplier
Spectra Manager for Windows 95/NT (version 1.53.01 (Build 1), including Spectra Analysis and Spectrum Measurement)	CD spectroscopy	JASCO Deutschland GmbH, Pfungstadt, Germany
TINA 2.0 Software	quantification of radiolabeled signals	(Raytest, Straubenhardt, Germany)
ZEN 2.3 SP1 FP3 (black) (version 14.0.18.201)	microscopy	Carl Zeiss, Jena, Germany
Online tool	Application	Supplier
Arabidopsis eFP Browser	elucidating gene expression after auxin treatment	http://bar.utoronto.ca/efp/cgi-bin/efpWeb.cgi?dataSource=Hormone (Winter et al., 2007)
BH-search analyses	identification of basic hydrophobic stretches in amino acid sequences	(Brzeska et al., 2010)
BoxShade (version 3.21)	sequence alignment	K. Hofmann, M. Baron, ExPASy Bioinformatics Resource Portal, SIB Swiss Institute of Bioinformatics, Lausanne, Switzerland
Clustal Omega	sequence alignment	(Madeira et al., 2019)
cNLS Mapper	identification of putative NLS sequences	(Kosugi et al., 2008, 2009a, 2009b)
InterPro	identification of protein domains	European Bioinformatics Institute, Cambridge, United Kingdom, (Blum et al., 2021)
Multalin	sequence alignment	(Corpet, 1988)
NCBI Gene Database	gene sequences for cloning	National Center for Biotechnology Information, U.S. National Library of Medicine, Rockville Pike, Bethesda, MD, USA
NCBI Protein Database	identification of protein domains	National Center for Biotechnology Information, U.S. National Library of Medicine, Rockville Pike, Bethesda, MD, USA

Online tool	Application	Supplier
Primer-BLAST	design of oligonucleotides for qPCR	National Center for Biotechnology Information, U.S. National Library of Medicine, Bethesda, MD, USA (Ye et al., 2012)
PROSITE	identification of protein domains	ExPASy Bioinformatics Resource Portal, SIB Swiss Institute of Bioinformatics, Lausanne, Switzerland (Sigrist et al., 2002, 2013)
ProtParam	calculation of molecular masses of proteins for calculation of mean residue weight ellipticity $[\Theta]_{MRW}$	ExPASy Bioinformatics Resource Portal, SIB Swiss Institute of Bioinformatics, Lausanne, Switzerland (Gasteiger et al., 2005)
SeqNLS	identification of putative NLS sequences	Department of Computer Science and Engineering, University of South Carolina, SC, USA (Lin et al., 2012)

Figures

Fig. 1.1: Arabidopsis PI-kinases.

Fig. 1.2: PIs contribute to several plasma membrane-associated processes.

Fig. 1.3: Arabidopsis PIP5K2 interacts with the nuclear import machinery and contains a functional NLS.

Fig. 1.4: Partial complementation of *pip5k1 pip5k2* double mutant phenotypes upon nuclear-excluded expression of PIP5K2_{AAA}-EYFP.

Fig. 1.5: Different enzymes are involved in epigenetic control.

Fig. 1.6: The composition of the plant SAGA complex.

Fig. 1.7: Domain structure of GCN5.

Fig. 1.8: Increasing auxin levels induce GCN5-regulated transcription.

Fig. 2.1: Histone H3 acetylation levels of *pip5k1 pip5k2* double mutant and PIP5K2-EYFP OE lines.

Fig. 2.2: PIP5K1 and PIP5K2 interact with the histone acetyltransferase GCN5.

Fig. 2.3: GCN5, PIP5K1 and PIP5K2 interact with the epigenetic readers ING1 and ING2 from Arabidopsis.

Fig. 2.4: Overexpression of PI4P 5-kinases reduces auxin-activation of GH3.3.

Fig. 2.5: Overexpression of PI4P 5-kinases reduces auxin-activation of IAA2 and IAA5.

Fig. 2.6: *In vitro* GCN5 acetylation activity.

Fig. 2.7: *In vitro* GCN5 acetylation activity is compromised in presence of PIs.

Fig. 2.8: GCN5 acetylation activity *in vitro* in presence of PIs over time.

Fig. 2.9: Lipid interaction studies of GCN5 and ING proteins with PIs.

Fig. 2.10: GCN5 amino acid sequence contains a putative phospholipid binding site.

Fig. 2.11: Lipid interaction studies of GCN5_{ILL} and GCN5_{EDD}.

Fig. 2.12: *In vitro* acetylation activity of GCN5 and variants.

Fig. 2.13: The VPS34 gene product is active as a PI 3-kinase.

Fig. 2.14: Subcellular localization of VPS34-mCherry in Arabidopsis mesophyll protoplasts.

Fig. 2.15: The PI 3-Kinase VPS34 interacts with GCN5.

Fig. 2.16: Overexpression of VPS34 does not impact auxin-activation of *GH3.3*.

Fig. 2.17: Subcellular localization of GCN5 amino acid substitution variants in Arabidopsis mesophyll protoplasts.

Fig. 3.1: Proposed model of PIs involved in epigenetic control.

Fig. 6.1: Genotypic characterization of *pip5k1 pip5k2* double mutant and *pCaMV35S::PIP5K2-EYFP* OE lines with specific oligonucleotides.

Fig. 6.2: Test for epitope specificity of antisera against different histone H3 acetylation events.

Fig. 6.3: Interaction test of PI4P 5-kinases PIP5K1 and PIP5K2 with histone H3.

Fig. 6.4: GCN5 and ADA2B interact in YTH.

Fig. 6.5: Relative transcript levels of *GH3.3* in mesophyll protoplasts over time.

Fig. 6.6: Basal transcript levels of *GH3.3*, *IAA2* and *IAA5* upon overexpression of PI4P 5-kinases.

Fig. 6.7: Endogenous transcript levels of GCN5 upon transient expression of different PI4P 5-kinases.

Fig. 6.8: Transcript levels of overexpressed PI-kinases and respective controls in protoplasts.

Fig. 6.9: Overexpression of PI4P 5-kinases reduces auxin-activation of *IAA19*.

Fig. 6.10: Enriched proteins used for lipid overlay assays.

Fig. 6.11: Lipid binding studies of PIP grips.

Fig. 6.12: Liposome sedimentation assay of MBP.

Fig. 6.13: BH-search analyses of GCN5_{ILL} and GCN5_{EDD}, ING1, ING2 and MBP.

Fig. 6.14: CD spectroscopy of MBP-GCN5, MBP-GCN5_{ILL}, MBP-GCN5_{EDD} and MBP.

Fig. 6.15: GCN5 and GCN5_{ILL} acetylation activity *in vitro* over time.

Fig. 6.16: Immunodetection of mesophyll protoplasts overexpressing mCherry-tagged VPS34.

Fig. 6.17: Basal GH3.3 transcript levels and endogenous GCN5 transcript levels in protoplasts upon overexpression of VPS34.

Fig. 6.18: Immunodetection of mesophyll protoplasts overexpressing EYFP-tagged GCN5 amino acid substitution variants.

Fig. 6.19: Cell lysates and enriched protein fractions.

Tables

- Tab. 4.1: Media for *E. coli*.
- Tab. 4.2: Media for yeast.
- Tab. 4.3: Plant medium.
- Tab. 4.4: Constructs for recombinant protein expression.
- Tab. 4.5: Constructs for split-ubiquitin-based yeast-two-hybrid assays.
- Tab. 4.6: Transformation vectors for *Arabidopsis* leaf protoplasts.
- Tab. 4.7: Used amounts of protein crude extracts in in vitro immuno pull-down assays.
- Tab. 4.8: In vitro acetylation assay of GCN5.
- Tab. 4.9: Buffers for protoplast preparation.
- Tab. 6.1: Equipment and devices.
- Tab. 6.2: Chemicals used in this study.
- Tab. 6.3: Used Phospholipids.
- Tab. 6.4: Consumables and kits.
- Tab. 6.5: Enzymes, proteins, peptides and molecular size markers.
- Tab. 6.6: Oligonucleotides used for genotyping.
- Tab. 6.7: Oligonucleotides for qPCRs.
- Tab. 6.8: Oligonucleotides used for cloning.
- Tab. 6.9: Oligonucleotides used for sequencing.
- Tab. 6.10: Composition of self-cast polyacrylamide gels.
- Tab. 6.11: Primary and secondary antibodies.
- Tab. 6.12: Used software and online tools and their applications.

Acknowledgements / Danksagung

Vielen, vielen Dank Mareike. Vielen Dank für die fachliche Unterstützung, angefangen bei Vektoren, über Protokolle und gemeinsame Versuche neuer Experimente, bis zu Hilfe bei Postern und Vorträgen, lehrreichen Diskussionen und wertvollem Rat bei der Anfertigung dieser Arbeit. Nicht zu vergessen ist dabei natürlich der Spaß neben der Arbeit mit den vielen amüsanten Gesprächen. Es war eine wunderschöne Zeit mit Dir. Ich durfte so viel von Dir lernen. Vielen Dank, dass ich meine Arbeit zu diesem tollen und interessanten Thema bei Dir anfertigen durfte. Ich bin gespannt, was ich in Zukunft von der AG Nukleus hören werde.

Mein großer Dank gilt auch Ingo. Vielen Dank, dass ich die Möglichkeit bekommen habe, in Deiner Abteilung zu arbeiten und Du die Finanzierung ermöglicht hast. Auch Dir möchte ich danken für wertvolle fachliche Gespräche, neue Impulse und Denkanstöße, auch hinsichtlich dieser Arbeit, aber auch für amüsante Anekdoten und lustige Momente, die ich nicht missen möchte.

Danke Euch beiden, Mareike und Ingo, für zwei besondere Erlebnisse der letzten Jahre. Danke, dass ihr mich nach Galveston mitgenommen habt, wo ich eine tolle Tagung erleben durfte und vielen Dank, dass ihr mir das Shiva gezeigt habt. Ich hätte in beiden Fällen wirklich etwas verpasst.

Danken möchte ich auch der DFG, an deren GRK 2498 „Kommunikation und Dynamik pflanzlicher Zellkompartimente“ (Projektnummer 400681449/GRK2498) ich thematisch assoziiert teilnehmen durfte. Danke an alle Mitglieder des GRKs für das schöne fachliche und persönliche Miteinander.

Mein Dank gilt auch den Gutachtern für Ihre Zeit, die sie sich meiner Dissertation widmen.

Vielen Dank auch an Prof. Dr. Klaus Humbeck, Dr. Xuan Hieu Cao und Charlotte Ost, die mir den ChIP-Assay nähergebracht haben, der in dieser Arbeit leider keine Anwendung mehr fand. Vielen Dank an Dr. Wolfgang Hoehenwarter für die massenspektrometrische Messung.

Danke Christoph, dass Du Dir die Zeit genommen hast, mir die CD-Spektroskopie zu zeigen und vielen Dank an PD Dr. Hauke Lilie, dass ich das Gerät nutzen durfte.

Danke Larissa und Lennart für Eure Unterstützung im Labor. Vielen Dank Lennart, dass ich von Dir ÄKTA-PIP-Kinasen bekommen durfte und vielen Dank Larissa, dass Du mir Vektoren

und MPB-Protein zur Verfügung gestellt hast. Vielen Dank Larissa und Willi für die vielen konstruktiven Diskussionen.

Liebsten Dank an alle meine Kolleginnen und Kollegen, an Willi, Larissa, Lennart, Christoph, Nadine, Monique, Johanna, Johanna, Benita, Julia, Daniel, Katharina, Irene, Praveen, Marta, Feng, Angela, Alex, Marion, Kristin und Martina. Ich hoffe, ich habe niemanden vergessen. Ihr habt meine Promotionszeit unvergesslich gemacht, hattet immer eine helfende Hand, ein offenes Ohr, einen Rat oder einen schlechten Witz parat. Vielen Dank für lebhafte Diskussionen und die schöne Zeit.

Danke an die Studenten, mit denen ich mein Projekt für einige Zeit teilen durfte. Die Arbeit mit Euch hat Spaß gemacht.

Zum Schluss möchte ich meinen Freunden und meiner Familie danken. Danke für Euer Verständnis und Eure Geduld, wenn es im Labor doch mal wieder etwas länger gedauert hat, und für die Aufmunterung, wenn es mal nicht so gelaufen ist, wie es sollte.

Danke Freddy!

Curriculum Vitae

Franziska Daamen

Date of Birth: 16/10/1992
 Place of Birth: Kleve
 Nationality: German

Education

- since 06/2020 **Associated member of RTG 2498**
 Communication and Dynamics of Plant Cell Compartments,
 thematically associated project 10A
- since 03/2017 **PhD**
 Martin Luther University Halle-Wittenberg
 Research group: Nuclear Phosphoinositides (Dr. Mareike Heilmann)
 Department of Plant Biochemistry (Prof. Dr. Ingo Heilmann)
- 10/2014 – 02/2017 **Master of Science in Biochemistry**
 Martin Luther University Halle-Wittenberg
- 10/2011 – 10/2014 **Bachelor of Science in Biochemistry**
 Martin Luther University Halle-Wittenberg
- 2011 **Abitur**
 Collegium Augustinianum Gaesdonck, Goch

Publications and Conferences

Franziska Daamen, Katharina Gerth, Mareike Heilmann (2021) Phosphoinositides modulate auxin-dependent transcription by controlling activity and recruitment of the histone acetyltransferase GCN5 in Arabidopsis. *Molecular Plant*, under review (25/08/2021).

Katharina Gerth, Feng Lin, Franziska Daamen, Wilhelm Menzel, Franziska Heinrich, Mareike Heilmann (2017) Arabidopsis phosphatidylinositol 4-phosphate 5-kinase 2 contains a functional nuclear localization sequence and interacts with alpha-importins. *Plant J.* 92(5):862-878.

Franziska Daamen, Mareike Heilmann (June 2019) The Arabidopsis phosphoinositide kinase PIP5K2 influences transcriptional control by interacting with the histone acetyltransferase GCN5. "Plant Science Student Conference" (PSSC), Leibniz Institute of Plant Biochemistry, Halle (Saale), Germany (poster).

Franziska Daamen, Mareike Heilmann (January 2019) The Arabidopsis phosphoinositide kinase PIP5K2 influences transcriptional control by interacting with the histone acetyltransferase GCN5. Gordon Research Conference "Plant Lipids: Structure, Metabolism and Function", Galveston, Texas, USA (poster).

Franziska Daamen, Mareike Heilmann (January 2019) The Arabidopsis phosphoinositide kinase PIP5K2 influences transcriptional control by interacting with the histone acetyltransferase GCN5. Gordon Research Seminar "Plant Lipids: Structure, Metabolism and Function", Galveston, Texas, USA (poster and talk).

Erklärung

Hiermit erkläre ich, dass ich die vorliegende Dissertation selbständig und ohne fremde Hilfe verfasst habe, keine anderen als die angegebenen Quellen und Hilfsmittel benutzt habe und die den benutzten Werken wörtlich oder inhaltlich entnommenen Stellen als solche kenntlich gemacht habe.

Des Weiteren erkläre ich, bisher keine vergeblichen Promotionsversuche unternommen zu haben und die Dissertation in der gegenwärtigen bzw. in einer anderen Fassung nicht bereits an einer anderen Fakultät vorgelegt zu haben.

Halle (Saale), _____

Franziska Daamen